

**An investigation into the  
contribution of flavin containing  
monooxygenases to the development  
and prevention of thiourea-induced  
pulmonary toxicity in the rat**

Thesis submitted in accordance with the requirements of the  
University of Liverpool for the degree of Doctor of Philosophy

By

Giovanni Pellegrini

November, 2013

## **DECLARATION**

This thesis is the result of my own work. The material contained within this thesis has not been presented, nor is currently being presented, either wholly or in part for any degree or other qualification.

**Giovanni Pellegrini**

This research was carried out in the Department of Pharmacology and Therapeutics, The University of Liverpool.

## Abstract

NR678, a small thiourea-based rodenticide candidate, is lethal to rats when administered orally at relatively small doses (5 and 10 mg/kg) and causes rapid life-threatening respiratory impairment, characterised by severe hydrothorax and pulmonary oedema. However, rats are protected from a normally lethal dose of NR678, after prior exposure to a low dose (0.5 mg/kg). Similar to other molecules containing the thiourea moiety, NR678 is mainly metabolised by flavin containing monooxygenases (FMOs), a class of enzymes involved in the detoxification, or more rarely, bioactivation of N- or S-containing molecules during phase I metabolism. Rat FMO2, the main FMO expressed in the lungs, like the correspondent human isoform, exhibits a genetic polymorphism which may influence the responses of this organ to NR678 and other drugs metabolised by FMOs. The aims of this thesis were to assess the morphological and functional aspects of NR678-induced acute lung injury (ALI) and to investigate the role of the adaptive pulmonary defence response involved in the prevention of the oxidative injury. In addition, the wild rat, which, in contrast to the laboratory rat, possesses a functional pulmonary FMO2, was explored as a possible animal model to evaluate the metabolic and toxicologic consequences of *FMO2* polymorphism in humans. It was shown that pulmonary endothelial cells are the main target of acute NR678 oxidative injury and exhibit ultrastructural alterations, which, coupled with a marked depletion of glutathione (GSH) levels, are likely responsible for the perturbation of pulmonary vascular permeability. The lungs of tolerant animals showed mild and transient changes of the vascular permeability and mildly increased cellularity in the lungs, which was characterised by increased numbers of alveolar macrophages and immature pneumocytes within 24 h after dosing, followed by a rise in the number of mature type II pneumocytes one week later. The microscopic changes resolved by the end of the second week, when rats were found to be again susceptible to a lethal dose of NR678. It was speculated that the adaptive response of the lungs to NR678 could be related to irreversible inhibition of FMOs, rather than increased clearance of the oedema fluid by macrophages and type II pneumocytes, down-regulation of FMOs, evaluated by *in situ* hybridisation and qPCR, or decreased GSH levels. In addition, it was found that the presence of an active FMO2 isoform enhances pulmonary FMO catalytic activity and leads to increased susceptibility to the toxic effects of NR678. In conclusion, the work presented here contributes evidence that *FMO2* polymorphism may be relevant to humans and provides an animal model which can be used to study its implications. NR678 represents an interesting and unique approach to investigate the pathogenesis of ALI and, at the

same time, understanding the defence mechanisms involved in adaptation may bring new insight into potential therapeutic strategies of lung diseases.

## Acknowledgments

Joining a PhD program has been like falling into an enormous debt of gratitude. I have no means to thank here all the friends and colleagues who shared with me their knowledge and gave me support and enthusiasm during these years. I guess the only way to pay them back is to adopt the same attitude in every day of my future professional career.

This experience would not have been possible without the guidance and encouragement of my supervisors, Dr. Dominic Williams, Prof. Anja Kipar and Prof. Kevin Park. I would like to thank them for giving me the opportunity to “go back to school” after a few years spent in Toxicologic Pathology and do this work.

I also want to acknowledge the continuous support I received from Roger Sharple, Sharon Hughes and all the extremely skilled staff working for BASF Pest Control Solutions-UK, which contributed financially to this project. They were excellent guides as well as good friends, who made me feel at home during the frequent visits to their facility.

## Publications

### Papers

**Pellegrini G**, Starkey Lewis PJ, Palmer L, Hetzel U, Goldring CE, Park BK, Kipar A, Williams DP (2013). Intraperitoneal administration of high doses of polyethylene glycol (PEG) causes hepatic subcapsular necrosis and low-grade peritonitis with a rise in hepatic biomarkers. <http://www.ncbi.nlm.nih.gov/pubmed/23831209> doi: 10.1016/j.tox.2013.06.003. [Epub ahead of print]

### Posters

**G Pellegrini**, D Williams, BK Park and A Kipar. Pulmonary defense mechanisms and their potential role in the prevention of thiourea-induced lung toxicity: histopathological and ultrastructural assessment. European Society of Veterinary Pathology/European Society of Toxicologic Pathology (ESVP/ESTP) meeting, 7-9/09/2011, Uppsala, Sweden. Best poster award, ToxPath section, French Society of Toxicologic Pathology.

**G Pellegrini**, A Kipar, BK Park and D Williams. An *in vivo* investigation into thiourea-mediated pulmonary toxicity: a histopathological and ultrastructural assessment. British Society of Toxicology (BTS) autumn meeting, 5-6/09/2011, Nottingham, UK. Commended.

**G Pellegrini**, A Kipar, BK Park and D Williams. From rat poison to personalized drugs: an example of Translational Medicine. Poster day 2012 at the University of Liverpool, 22/03/2012. Best poster award, Health and Life Sciences section.

**G Pellegrini**, PJ Starkey Lewis, L Palmer, U Hetzel, CE Goldring, BK Park, DP Williams and A Kipar. Intraperitoneal administration of high doses of polyethylene glycol (PEG) causes hepatic subcapsular necrosis and low-grade

peritonitis with a rise in hepatic biomarkers. ESTP meeting, 10-12/09/2013, Ghent, Belgium. Awarded the Charles Capen Trainee award.

# Contents

Abstract.....	iii
Acknowledgments .....	v
Publications.....	vi
Contents .....	viii
List of figures .....	xii
List of tables.....	xiv
List of abbreviations .....	xv
<b>CHAPTER 1 INTRODUCTION .....</b>	<b>1</b>
<b>1.1 Need for novel rodenticides .....</b>	<b>2</b>
<b>1.2 Current use and application of thioureas.....</b>	<b>6</b>
<b>1.3 Thiourea-based molecules as rodenticide candidates .....</b>	<b>7</b>
<b>1.4 Tolerance to thiourea(s).....</b>	<b>8</b>
<b>1.5 The role of flavin containing monooxygenases (FMOs) in xenobiotic metabolism .....</b>	<b>9</b>
1.5.1 History of the FMO enzyme family .....	10
1.5.2 Differences from and similarities with cytochrome P450.....	10
1.5.3 Structure of FMOs .....	11
1.5.4 FMO catalytic cycle.....	13
1.5.5 Endogenous and exogenous substrates of FMOs.....	14
1.5.5.1 Nitrogen-containing drugs as FMO substrates .....	15
1.5.5.2 Sulphur-containing drugs as FMO substrates .....	17
1.5.5.3 Endogenous substrates of FMOs.....	19
1.5.6 Tissue- and species-specific differences in the expression of FMOs.....	19
1.5.6.1 FMO expression in humans .....	21
1.5.6.2 FMO expression in mice .....	22
1.5.6.3 FMO expression in rats .....	24
1.5.7 Evaluation of FMO activity in drug development .....	25
<b>1.6 FMO genetic variability.....</b>	<b>26</b>
1.6.1 FMO genetic variants and polymorphism.....	27
1.6.2 <i>FMO2</i> genetic polymorphism.....	29
1.6.3 Modulation of FMO expression.....	31
<b>1.7 Current research on FMOs .....</b>	<b>33</b>
<b>1.8 Aims of this work .....</b>	<b>35</b>



<b>CHAPTER 2 MATERIALS AND METHODS.....</b>	<b>37</b>
<b>2.1 Experimental animal work.....</b>	<b>38</b>
<b>2.2 Experimental procedures .....</b>	<b>39</b>
2.2.1 Post mortem examination .....	41
2.2.1.1 Necropsy, tissue sampling, processing and histology .....	41
2.2.1.2 Immunohistology of the lungs of NR678-treated rats.....	44
2.2.1.3 Transmission electron microscopy of the lung of NR678-treated rats.....	48
2.2.1.4 Determination of the cellular localisation of FMOs in rat tissues by <i>in situ</i> hybridisation (ISH) .....	49
2.2.1.4.1 Preparation of tissue sections for RNA <i>in situ</i> hybridisation .....	49
2.2.1.4.2 Prehybridisation and hybridisation .....	50
2.2.1.4.3 Detection of hybridised probes .....	50
2.2.2 Determination of hepatic and pulmonary glutathione levels and protein concentration in NR678-treated rats .....	51
<b>2.3 Molecular biology.....</b>	<b>53</b>
2.3.1 Extraction of RNA from the lung .....	53
2.3.2 DNase treatment of RNA.....	54
2.3.3 Reverse transcription of RNA into complementary cDNA .....	54
2.3.4 Conventional polymerase chain reaction (PCR) .....	55
2.3.5 Quantitative fluorescence real-time PCR (qPCR) .....	57
2.3.6 Molecular subcloning and synthesis of riboprobes for <i>in situ</i> hybridisation .....	60
2.3.6.1 Ligation of the PCR product .....	60
2.3.6.2 Cloning and transformation of bacteria.....	60
2.3.6.3 Small scale isolation of plasmid DNA (miniprep) .....	61
2.3.6.4 Restriction enzyme digestion and DNA sequencing .....	61
2.3.6.5 Large scale isolation of plasmid DNA (maxiprep) .....	62
2.3.6.6 Preparation of DNA template for RNA transcription .....	63
2.3.6.7 Labelling of the riboprobes with digoxigenin .....	64
2.3.6.8 Dot blot analysis of riboprobes .....	64
2.3.7 Genotyping of rats for <i>FMO2</i> polymorphism.....	65
2.3.7.1 Animals and tissue collection .....	65
2.3.7.2 Extraction of DNA from tissue .....	66
2.3.7.3 Characterisation of <i>FMO2</i> by nested PCR.....	67
<b>2.4 Enzyme assay and metabolic analysis .....</b>	<b>70</b>
2.4.1 Preparation of rat liver and lung microsomes .....	70
2.4.2 Determination of protein content and enzyme activity of liver and lung microsomes .....	71
2.4.3 Incubation of NR678 in rat liver and lung microsomal suspensions .....	72
2.4.4 HPLC method development and validation .....	73
2.4.5 Comparative FMO activity metabolism assay with and without competitive substrate inhibition .....	74
<b>2.5 Statistical analysis .....</b>	<b>75</b>
<b>CHAPTER 3 RESULTS.....</b>	<b>76</b>

<b>3.1</b>	<b><i>In vivo</i> investigation into the acute toxic effects of NR678 and an attempt to elucidate its metabolism <i>in vitro</i> .....</b>	<b>77</b>
3.1.1	Clinical assessment of rats that had received a high dose of NR678 .....	77
3.1.2	Gross post mortem findings in rats that had received a high dose of NR678 .....	79
3.1.3	Cytological and histological findings in rats that had received a high dose of NR678 .....	80
3.1.4	Ultrastructural findings in rats that had received a high dose of NR678 .....	89
3.1.5	Bioanalytical method validation of NR678 and lack of metabolic turnover at HPLC .....	90
<b>3.2</b>	<b><i>In vivo</i> investigation into the pulmonary defence responses involved in the prevention of NR678-induced lung injury.....</b>	<b>95</b>
3.2.1	Clinical assessment of NR678 tolerogenic dose regimen (study 2) .....	95
3.2.2	Assessment of tolerance in NR678-treated rats (study 3) .....	96
3.2.2.1	Changes observed in rats administered a low dose (0.5 mg/kg) of NR678 (group 3) .....	96
3.2.2.1.1	Clinical assessment .....	96
3.2.2.1.2	Gross post mortem findings .....	97
3.2.2.1.3	Histological and immunohistological findings .....	98
3.2.2.1.4	Ultrastructural findings .....	107
3.2.2.2	Changes observed in rats administered a low dose (0.5 mg/kg) of NR678, followed by a high dose (5 mg/kg) 3 h later (group 4).....	112
3.2.2.2.1	Clinical assessment .....	112
3.2.2.2.2	Gross post mortem findings .....	112
3.2.2.2.3	Histological and immunohistological findings .....	112
3.2.2.2.4	Ultrastructural findings .....	116
3.2.2.3	Changes observed in rats after the administration of a high dose (5 mg/kg) of NR678 on day 14 after previous administration of 0.5 mg/kg or 0.5 mg/kg followed 3 h later by 5 mg/kg .....	117
3.2.2.3.1	Clinical assessment .....	117
3.2.2.3.2	Gross post mortem findings .....	118
3.2.2.3.3	Histological findings.....	120
3.2.2.4	Effects of NR678 on hepatic and pulmonary GSH contents <i>in vivo</i> .....	122
<b>3.3</b>	<b>Characterisation of FMO1 and FMO2 expression profiles in untreated rats and rats that had received NR678 .....</b>	<b>123</b>
3.3.1	Determination of cellular localisation of expression of FMO2 in tissues from untreated rats by <i>in situ</i> hybridisation .....	123
3.3.2	Comparative assessment of FMO2 expression by <i>in situ</i> hybridisation in the lungs of control and NR678-treated rats.....	130
3.3.3	Comparative assessment of the levels of FMO1 and FMO2 mRNA in the lungs of control and NR678-treated rats using qPCR .....	132
<b>3.4</b>	<b>Assessment of <i>R. norvegicus</i> as a suitable animal model to investigate the metabolic and toxicological consequences of FMO2 polymorphism in humans.....</b>	<b>134</b>
3.4.1	Detection of FMO2 polymorphism among a wild rat population using a nested PCR method.....	134
3.4.2	Characterisation of FMO2 allelic frequencies in two colonies of laboratory rats (Welsh and Berkshire) using a nested PCR method .....	136
3.4.3	Enzyme assay .....	137
3.4.3.1	Determination of the enzymatic parameters of the S-oxygenation of methimazole carried out by rat liver and lung microsomes .....	137

3.4.3.2	Comparison of the oxygenation of methimazole catalysed by different rat microsomes and enzyme inhibition using NR678.....	140
3.4.4	Characterisation of the <i>in vivo</i> effects of a low dose (0.5 mg/kg) of NR678 administered to rats homozygous for <i>FMO2*1</i> (Welsh rats).....	142
3.4.4.1	Clinical assessment .....	142
3.4.4.2	Gross post mortem findings .....	142
3.4.4.3	Histological findings .....	142
<b>CHAPTER 4 DISCUSSION.....</b>		<b>146</b>
<b>4.1</b>	<b>NR678 as a model of acute lung injury (ALI).....</b>	<b>147</b>
4.1.1	Morphological features and cellular targets of NR678 pulmonary toxicity.....	147
4.1.2	NR678 pulmonary toxicity as a model of drug-induced oxidative stress .....	153
4.1.3	Extra-pulmonary NR678-related effects.....	158
<b>4.2</b>	<b>Morphological characterisation of the adaptive response of the rat lung to sublethal doses of NR678 .....</b>	<b>160</b>
4.2.1	Onset and duration of tolerance to NR678 in the rat lungs.....	160
4.2.2	The morphological characterisation of cell proliferation in the lungs of rats tolerant to NR678 .....	162
4.2.3	An investigation into the mechanisms underlying tolerance to thiourea-based molecules.....	165
<b>4.3</b>	<b>Assessment of <i>R. norvegicus</i> as a suitable animal model to investigate the relationship between <i>FMO2</i> polymorphism in humans and differences in response to thiourea-based drugs .....</b>	<b>169</b>
4.3.1	Metabolic consequences of <i>FMO2</i> polymorphism .....	172
4.3.2	Toxicologic consequences of <i>FMO2</i> polymorphism .....	173
<b>4.4</b>	<b>Potential issues and limitations .....</b>	<b>175</b>
<b>4.5</b>	<b>Concluding remarks .....</b>	<b>180</b>
<b>Appendix I – FMO expression in humans and mice .....</b>		<b>184</b>
<b>Appendix II – Summary of <i>in vivo</i> analyses.....</b>		<b>190</b>
<b>Appendix III – Additional reagents and solutions.....</b>		<b>191</b>
<b>References.....</b>		<b>194</b>

## List of figures

<b>Figure 1.1.</b> Ribbon diagram of the structural domains of the FMO protein.....	13
<b>Figure 1.2.</b> The catalytic cycle of FMOs.....	14
<b>Figure 2.1.</b> Experimental design of the chronotolerance study (study 3).....	41
<b>Figure 2.2.</b> Sketch illustrating the sampling protocol for the lungs.....	43
<b>Figure 2.3.</b> Cell types in the alveoli and their identification based on the expression of cell markers by immunohistology.....	45
<b>Figure 2.4.</b> Gel electrophoresis of miniprep plasmid DNA.....	62
<b>Figure 2.5.</b> Ear punching numbering system to identify rats for genotyping.....	67
<b>Figure 2.6.</b> Nested PCR method for rat <i>FMO2</i> genotyping.....	69
<b>Figure 3.1.</b> Absolute and relative lung weights in rats administered a high dose (5 mg/kg) of NR678.....	79
<b>Figure 3.2.</b> Macroscopic findings in rats administered a high dose (5 or 10 mg/kg) of NR678.....	80
<b>Figure 3.3.</b> Histological demonstration of alveolar and interstitial oedema in the lungs of rats administered a high dose (10 mg/kg) of NR678.....	82
<b>Figure 3.4.</b> Histological and immunohistological demonstration of apoptotic cells within the alveolar lining in rats administered a high dose (5 mg/kg) of NR678.....	83
<b>Figure 3.5.</b> Immunohistological demonstration of type I pneumocytes and endothelial cells in the lungs of rats administered a high dose (5 mg/kg) of NR678.....	85
<b>Figure 3.6.</b> Histological features of the liver of rats administered a high dose (5 mg/kg) of NR678.....	86
<b>Figure 3.7.</b> Histological features of the thymus of rats administered a high dose (10 mg/kg) of NR678.....	88
<b>Figure 3.8.</b> Ultrastructural features of the air-blood barrier in the normal rat lung.....	91
<b>Figure 3.9.</b> Ultrastructural features of the air-blood barrier in the lung of a rat administered a high dose (5 mg/kg) of NR678.....	92
<b>Figure 3.10.</b> Ultrastructural features of the endothelial cell lining in the alveolar capillaries of the lung of a rat administered a high dose (5 mg/kg) of NR678.....	93
<b>Figure 3.11.</b> Overlaid HPLC UV chromatograms of different standard concentrations of NR678 dissolved in methanol.....	94
<b>Figure 3.12.</b> HPLC UV chromatograms of phenylthiourea incubated in rat lung microsomes.....	94
<b>Figure 3.13.</b> Absolute and relative lung weights after the administration of NR678 at a dose of 0.5 mg/kg (LD; group 3) or 0.5 mg/kg, followed 3 h later by 5 mg/kg (LD + HD; group 4).....	97
<b>Figure 3.14.</b> Histological findings in the lungs of rats euthanased at different time points after the administration of NR678 at a dose of 0.5 mg/kg.....	99
<b>Figure 3.15.</b> Immunohistological demonstration of SP-C expressing cells (type II pneumocytes) in the lungs of rats euthanased at 24 h and 7 d after the administration of NR678 at a dose of 0.5 mg/kg (group 3), compared to control rats and rats that had received a high dose (5 mg/kg) of NR678.....	103
<b>Figure 3.16.</b> Immunohistological demonstration of lysozyme-expressing cells (type II pneumocytes and macrophages) in the lungs of rats euthanased at 24 h and 7 d after the administration of NR678 at a dose of 0.5 mg/kg (group 3), compared to control rats and rats that had received a high dose (5 mg/kg) of NR678.....	104
<b>Figure 3.17.</b> Immunohistological assessment of the percentage of cells expressing SP-C and lysozyme in the lungs of rats after the administration of NR678 at a dose of 0.5 mg/kg.....	105
<b>Figure 3.18.</b> Amount of PCNA-positive alveolar cells in the lungs of rats after the administration of NR678 at a dose of 0.5 mg/kg.....	106

<b>Figure 3.19.</b> Immunohistological demonstration of PCNA-positive, proliferating cells in the lungs of a control rat and a rat euthanased 7 d after the administration of NR678 at a dose of 0.5 mg/kg.....	107
<b>Figure 3.20.</b> Ultrastructural features of the lung of rats administered NR678 at a dose of 0.5 mg/kg and euthanased at early time points .....	110
<b>Figure 3.21.</b> Ultrastructural features of the lung of rats euthanased at 24 h and 7 d after the administration of NR678 at a dose of 0.5 mg/kg (group 3), compared to controls.....	111
<b>Figure 3.22.</b> Immunohistological assessment of the percentage of cells expressing SP-C and lysozyme in the lungs of rats after the administration of NR678 at a dose of 0.5 mg/kg, followed by a dose of 5 mg/kg 3 h later .....	115
<b>Figure 3.23.</b> Amount of PCNA-positive alveolar cells in the lungs of rats after the administration of NR678 at a dose of 0.5 mg/kg followed 3 h later by 5 mg/kg.....	116
<b>Figure 3.24.</b> Ultrastructural features in the lungs of a rat (11L-2408) administered NR678 at a dose of 0.5 mg/kg, followed 3 h later by 5 mg/kg and euthanased at 24 h.....	117
<b>Figure 3.25.</b> Macroscopic findings observed at 6 h post administration of a high dose (5 mg/kg) of NR678 on day 14 in rats that had previously received a dose of 0.5 mg/kg, followed 3 h later by 5 mg/kg NR678. ....	119
<b>Figure 3.26.</b> Histological features in the lungs of rats administered a dose of 5 mg/kg of NR678 on day 14 after they had previously received a dose of 0.5 mg/kg (group 3) or 0.5 mg/kg followed 3 h later by 5 mg/kg (group 4).....	121
<b>Figure 3.27.</b> GSH contents in the liver and lung of NR678-treated rats.....	122
<b>Figure 3.28.</b> RNA-ISH for the demonstration of FMO2 mRNA in the male rat brain.....	125
<b>Figure 3.29.</b> RNA-ISH for the demonstration of FMO2 mRNA in the male rat kidney .....	127
<b>Figure 3.30.</b> RNA-ISH for the demonstration of FMO2 mRNA in the male rat liver.....	128
<b>Figure 3.31.</b> RNA-ISH for the demonstration of FMO2 mRNA in the male rat lung .....	129
<b>Figure 3.32.</b> RNA-ISH for the demonstration of FMO2 mRNA localisation in the lungs of male untreated rats compared to those that had received NR678.....	131
<b>Figure 3.33.</b> qPCR analysis showing the levels of relative expression (fold change) of FMO1 (a) and FMO2 (b) in the lungs of rats following exposure to high and low doses of NR678.....	133
<b>Figure 3.34.</b> Characterisation of <i>FMO2</i> by nested PCR in wild caught <i>R. norvegicus</i> .....	135
<b>Figure 3.35.</b> Characterisation of <i>FMO2</i> by nested PCR in two rat colonies (Welsh and Berkshire) housed at BASF Widnes Laboratories. ....	136
<b>Figure 3.36.</b> Effect of methimazole concentration on enzyme velocity in different rat microsomal preparations (Wistar rat liver and lungs and Welsh rat lungs) .....	138
<b>Figure 3.37.</b> Enzyme kinetics of the sulphonylation of methimazole deduced from the Michaelis Menten equation in different rat microsomal preparations .....	139
<b>Figure 3.38.</b> Comparison of methimazole (500 $\mu$ M) oxygenation rates over time (7 min) among different rat microsomal preparations (Wistar rat liver and lungs and Welsh rat lungs). ....	140
<b>Figure 3.39.</b> Inhibitory activity of NR678 on the sulphonylation of methimazole carried out in different rat microsomal preparations.....	141
<b>Figure 3.40.</b> Histological features of alveolar and interstitial oedema in the lungs of Welsh rats that had received a dose of 0.5 mg/kg of NR678, compared to concurrent controls .....	144
<b>Figure 3.41.</b> Histological features of the spontaneous inflammatory changes occurring in the lungs of Welsh rats from study 4, including the controls. ....	145
<b>Figure 4.1.</b> Main mechanisms leading to increased vascular permeability .....	149
<b>Figure 4.2.</b> Scheme of the FMO-mediated S-oxidation of phenylthiourea.....	156
<b>Figure 4.3.</b> Possible mechanisms underlying tolerance to NR678. ....	169
<b>Figure 4.4.</b> Summary of <i>FMO2</i> genotyping results.....	171
<b>Figure 4.5.</b> A system biology approach to the investigation of NR678-induced toxicity and adaptation.....	181

## List of tables

<b>Table 1.1.</b> Novel rodenticide candidates selected for further development during a preliminary screening conducted at BASF Pest Control Solutions.....	5
<b>Table 1.2.</b> Selected examples of drugs which are metabolised by FMOs to a significant extent. ....	21
<b>Table 2.1.</b> List of in vivo animal experiments conducted in this work. ....	38
<b>Table 2.2.</b> Experimental design and animal details of the in vivo studies .....	40
<b>Table 2.3.</b> Alphabetical list of organs and tissues that were examined macroscopically and histologically .....	42
<b>Table 2.4</b> List of special stains carried out for the visualisation of specific tissue components (fibrin and collagen) and the identification of eosinophils .....	44
<b>Table 2.5.</b> Summary of the antibodies and other reagents used for immunohistology .....	47
<b>Table 2.6.</b> Primers used in conventional PCR (for subcloning).....	56
<b>Table 2.7.</b> Thermal cycling conditions of FMO gene PCR amplification for subcloning .....	57
<b>Table 2.8.</b> Primers used in qPCR.....	58
<b>Table 2.9</b> Thermal cycling conditions of target and reference gene qPCR amplification .....	59
<b>Table 2.10.</b> Primers used in nested PCR.....	68
<b>Table 2.11</b> Thermal cycling conditions for the FMO2 gene amplification with a nested PCR (Hugonnard et al., 2004).....	69
<b>Table 2.12.</b> Standard microsomal incubation conditions and optimisation attempts.....	73
<b>Table 3.1.</b> Clinical signs observed in rats administered a high dose (5 or 10 mg/kg) of NR678. Rats were euthanased (E) within 7 h after dosing .....	78
<b>Table 3.2.</b> Summary of the key histological findings in lungs and liver of rats administered a high dose (5 and 10 mg/kg) of NR678 .....	86
<b>Table 3.3.</b> Summary of the key histological findings in the lymphoid tissues of rats administered a high dose (5 and 10 mg/kg) of NR678 .....	88
<b>Table 3.4.</b> Clinical signs observed in rats that had received a low dose (0.5 mg/kg) of NR678, followed by a high dose (5 mg/kg) after 3 h (study 2).....	96
<b>Table 3.5.</b> Summary of the key histological findings in the lungs of rats that had received a low dose (0.5 mg/kg) of NR678 .....	100
<b>Table 3.6.</b> Clinical signs observed in rats administered NR678 at a dose of 0.5 mg/kg, followed 3 h later by a dose of 5 mg/kg (group 4). Rats were eutanased (E) at 24 h (11L-2408 to 11L-2410), 7 d (11L-2411 to 11L-2413) or 14 d (11L-2417 to 11L-2419) after the first dose.....	113
<b>Table 3.7.</b> Summary of the key histological findings in the lungs of rats that had received a low dose (0.5 mg/kg) of NR678, followed 3 h later by a dose of 5 mg/kg.....	113
<b>Table 3.8.</b> Clinical signs observed after the administration of NR678 on day 14 at a dose of 5 mg/kg in rats that had previously received a dose of 0.5 mg/kg (group 3) or 0.5 mg/kg, followed 3 h later by 5 mg/kg (group 4).....	118
<b>Table 3.9.</b> Summary of key histological findings in the lungs after administration of NR678 at a dose of 5 mg/kg on day 14 in rats that had previously received a dose of 0.5 mg/kg (group 3) or 0.5 mg/kg followed 3 h later by 5 mg/kg NR678 (group 4) .....	120
<b>Table 3.10.</b> Summary of the key histological findings in the lungs of Welsh rats administered a low dose (0.5 mg/kg) of NR678 .....	143

# List of abbreviations

## A

AHR, aryl hydrocarbon receptor  
ANTU, alpha-naphthylthiourea  
ANU, alpha naphthyl urea  
AQP-5, aquaporin 5  
ARDS, acute respiratory distress syndrome

## B

BCIP, 5-bromo-4-chloro-3-indolyl phosphate  
BLAST, basic local assignment search tool  
bp, base pair  
BSA, bovine serum albumin

## C

CA1, *cornu Amonis 1*  
CA2, *cornu Amonis 2*  
CA3, *cornu Amonis 3*  
COPR, Control of Pesticide Regulation  
C<sub>q</sub>, cycle of quantification  
CYP, cytochrome P450

## D

d, day(s)  
DAB, diaminobenzidine tetrahydrochloride  
DEPC, diethylpyrocarbonate  
DIG, digoxigenin  
dNTP, deoxyribonucleotide triphosphate  
DTNB, 5-5'-dithiobis[2-nitrobenzoic acid]  
DTT, dithiothreitol

## E

EDTA, ethylenediaminetetraacetic acid  
Eff, efficiency (qPCR)  
EtBr, ethidium bromide

## F

FAD, flavin adenine dinucleotide  
FDA, Food and Drug Administration  
FEPA, Food and Environment Protection Act  
FMO, flavin-containing monooxygenase(s)

## G

GAPDH, glyceraldehyde 3-phosphate dehydrogenase  
GPx, glutathione peroxidase  
GSH, glutathione  
GSSG, oxidised glutathione

## H

h, hour(s)  
H<sub>2</sub>O<sub>2</sub>, hydrogen peroxide  
HD, high dose  
HE, haematoxylin and eosin stain

## I

IARC, International Agency for Research on Cancer  
IH, immunohistology  
ISH, *in situ* hybridisation

## K

KGF, keratinocyte growth factor  
KO, knock-out

## L

LB, Luria-Bertani  
LD, low dose  
LD<sub>50</sub>, median lethal dose  
LLoQ, lower limit of quantification (HPLC)  
LPS, lipopolysaccharide

## M

MgCl<sub>2</sub>, magnesium chloride  
MI, methimazole  
min, minute(s)  
MIQE, Minimum Information for publication of Quantitative real-time PCR Experiments  
MPTP, 1-methyl-4-phenyl-1,2,3,6-tetrahydropyridine  
MTD, maximum tolerated dose

## N

Na<sub>2</sub>S<sub>2</sub>O<sub>4</sub>, sodium dithionate  
NADPH, nicotinamide adenine dinucleotide phosphate  
NBT, nitro blue tetrazolium  
NMD, nonsense mRNA decay  
NO, nitric oxide  
NO<sub>2</sub>, nitrogen dioxide

## P

PAP, peroxidase anti-peroxidase  
PBS, phosphate buffered saline  
PCNA, proliferating cell nuclear antigen

PCR, polymerase chain reaction  
PCT, proximal convoluted tubule  
PEG-200, polyethylene glycol 200  
PFA, paraformaldehyde  
PR, pars recta  
PT, proximal tubule  
PTU, phenylthiourea

## Q

qPCR, quantitative polymerase chain reaction

## R

ROS, reactive oxygen species  
rpm, revolutions per minute  
RT, room temperature

## S

SCC, salt sodium citrate  
sec, second(s)  
SEM, standard error of the mean  
SERM, selective oestrogen receptor modulator  
SNP, single nucleotide polymorphism  
SOD, superoxide dismutase  
SP-C, surfactant protein C

## T

TAE, Tris base, acetic acid, EDTA  
TBS, Tris-buffered saline  
TCDD, 2,3,7,8-tetrachlorodibenzo-p-dioxin  
TE, Tris base, EDTA  
TEM, transmission electron microscopy  
TMA, trimethylamine  
TMAU, trimethylaminuria  
TNB, 5-thio-nitrobenzoic acid

## V

v/v, volume/volume  
V<sub>0</sub>, reaction velocity

## W

w, week(s)  
w/v, weight/volume  
WT, wild type

## X

X-Gal, 5-bromo-4-chloro-3-indolyl β-D-galactopyranoside



# Chapter 1 Introduction

1.1 Need for novel rodenticides

1.2 Current use and application of thioureas

1.3 Thiourea-based molecules as rodenticide candidates

1.4 Tolerance to thiourea(s)

1.5 The role of flavin containing monooxygenases (FMOs) in xenobiotic metabolism

1.6 FMO genetic variability

1.7 Current research on FMOs

1.8 Aims of this work

## 1.1 Need for novel rodenticides

Statutory requirements regulating use, sale, supply and storage of pesticides have been in place in Europe for decades. In Great Britain, the control on pesticides was disciplined under FEPA (British Parliament, Food and Environment Protection Act, 1985) and implemented, one year later, through COPR (Minister of Agriculture, The Control of Pesticide Regulation; amended in 1997). Non-agricultural pesticides, including rodenticides, are regulated by the Health and Safety Executive, which ensures that every rodenticide can be used with a realistic certainty of no harm to human health and without posing unreasonable risks to the environment. Anticoagulant compounds, derived from either 4-hydroxycoumarin (e.g., warfarin, bromadiolone) or indane-1,3-dione (e.g., diphacinone, chlorophacinone), have been employed as rodenticides worldwide for more than fifty years and are still among the most commonly used products for pest control (Watt et al., 2005). The mechanism of action of these molecules is based on the impairment of blood coagulation caused by the inhibition of vitamin K 2,3-epoxide reductase (Ishizuka et al., 2008). Anticoagulant rodenticides, including the more recent “superwarfarins” (brodifacoum, bromadiolone, flocoumafen and difenacoum), are currently regulated within Europe under the Biocidal Products Directive (European Parliament and European Council, 1998). Despite being very effective, several concerns have recently arisen regarding certain technical and regulatory aspects which could compromise the long-term future use of these compounds. Superwarfarins possess long half lives and have shown high levels of environmental persistence (Watt et al., 2005). Because of these undesirable features, coumarin-based rodenticides pose a serious risk of poisoning for non-intended target species and may represent potential dangerous contaminants of the food chain. Furthermore, similarly to certain classes of insecticides, the repeated use of warfarins has caused the onset of drug resistance in several wild rodent species worldwide (Ishizuka et al., 2008). The development of resistance has often been associated with the presence of single nucleotide polymorphisms (SNPs) in the genes of numerous enzymes involved in the metabolism of anticoagulants: specific variations in the DNA sequences coding for these proteins have been linked to increased expression and activity and, in turn, to accelerated detoxification of the rodenticide, including the more potent

superwarfarins (Kohn et al., 2003). Several concerns exist that the overuse of superwarfarins will exponentially increase genetic adaptation, leading to even broader resistance. Hence, research in this field has recently resumed and the development of new and potentially more toxic rodenticides with safer and more selective profiles has been included in the product pipeline of several agrochemical companies.

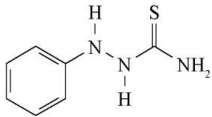
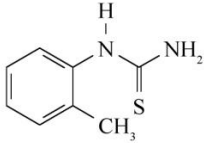
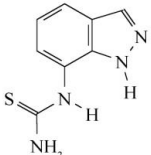
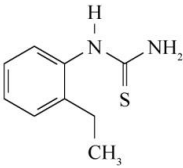
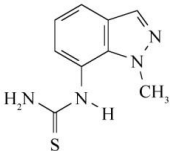
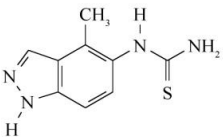
When a new product for pest control is being developed, appropriate studies need to be carried out by the applicants to support safety, efficacy and, where relevant, humaneness of their candidate. While regulations dealing with the later steps of rodenticide development are inevitably tailored to the specific field of rodent control, the earlier discovery phase mimics the analogous developmental process in place for the research on new human and veterinary drug candidates (FEPA and COPR). Potential candidate selection is carried out through preliminary acute toxicity studies, which are then followed by short term multiple dosing oral (*gavage* and diet) toxicity studies. Palatability studies conclude the first stage of rodenticide development, providing a preliminary overview of the manageability, efficacy and mode of action of the new products, which are subsequently refined through the identification of potential rodent resistance, evaluation of consequences on human health and the assessment of poisoning of non target species and environmental impact (Health and Safety Executive, 2012).

In 2008, “BASF Pest Control Solutions-UK” started an extensive screening programme to test several compounds (more than 800 molecules) belonging to different chemical classes and labelled as hazardous or potentially hazardous to human health (personal communication). These molecules were already on the market or were obtained through substitution or addition of small chemical groups to the original structure. The aim of the project was to identify among these screened entities those that were most toxic to rodents and could represent potential rodenticide candidates. The toxicity of these compounds was evaluated using the median lethal dose (LD<sub>50</sub>), i.e. the dose required to cause the death of half the members of the population tested by a fixed time interval (Eaton and Gilbert, 2008), as primary screening method. The efficacy of these molecules was tested on

laboratory rats and mice in dietary oral studies. Briefly, the test article was offered *ad libitum* to five animals for 3 days, with a starting dose of 25 mg/kg. Mortality checks were carried out daily and clinical signs recorded several times during the working hours. When death of more than 50% of the animals occurred, scalar decreasing dosages were tested with similar study design, until a LD<sub>50</sub> range was determined. More than 800 different molecules were screened and reclassified into different groups, according to the LD<sub>50</sub> values obtained: > 1-< 5 mg/kg, ≥ 5-< 10 mg/kg, ≥ 10-< 25 mg/kg and ≥ 25 mg/kg. Six molecules showed an LD<sub>50</sub> between 1 and 5 mg/kg and were selected for further development (**Table 1.1**). All selected molecules contained a thiourea moiety (CH<sub>4</sub>N<sub>2</sub>S), together with phenyl groups or indazole rings in different positions.

The clinical signs recorded in the acute studies in rats given the thiourea-derived compounds (**Table 1.1**) were consistent with severe generalised distress and some of them (rapid breathing, red pigment around nose) suggested selective impairment of the respiratory function. The investigation conducted in this thesis focused on NR678, as it had adequate potency and reasonable manufacturing costs. NR678 is a phenylthiourea with a methyl group substitution in position 6. Rats that had received a dose of 2 mg/kg showed non life-threatening clinical signs including mild piloerection, slight rapid breathing and hunched posture, which resolved within 24 h after dosing. Rats administered a dose of 5 mg/kg instead had decreased motor activity, hunched posture and severe respiratory distress and were euthanased within 8 h after dosing according to humane end points, as defined by the Code of Practice for the Humane Killing of Animals under Schedule 1 (British Parliament, 1986). The estimated LD<sub>50</sub> for NR678 therefore fell between 2 and 5 mg/kg (personal communication).

**Table 1.1.** Novel rodenticide candidates selected for further development during a preliminary screening conducted at BASF Pest Control Solutions. The LD<sub>50</sub> and the clinical signs occurring in Wistar rats after the oral administration of different doses of the six molecules are presented (personal communication).

Molecule ID	Chemical structure	LD <sub>50</sub> (mg/kg)	Clinical signs
NR237		>1, <2	At 1 mg/kg: no clinical signs observed. At 2 mg/kg: splayed gait, half closed eyes, flattened posture, dark eyes, decreased motor activity, severe rapid breathing, piloerection, no food consumption. E
NR678		>2, <5	At 2 mg/kg: mild piloerection, slight rapid breathing, hunched posture. Back to normal between 7-24 h. At 5 mg/kg: severe rapid breathing, piloerection, decreased motor activity, hunched posture, closed eyes, mild oligoemia, red pigment around nose. E
NR713		>2, <5	At 2 mg/kg: mild rapid breathing. Back to normal by 24 h. At 5 mg/kg: severe rapid breathing, piloerection, anaergia, hunched posture, closed eyes, mild oligoemia. E
NR760		>2, <5	At 2 mg/kg: mild rapid breathing. Back to normal between 5-36 h. At 5 mg/kg: severe rapid breathing, piloerection, decreased motor activity, hunched posture, closed eyes, mild phonation. E
NR770		>2, <5	At 2 mg/kg: no clinical signs observed. At 5 mg/kg: severe rapid breathing, piloerection, decreased motor activity, hunched posture, closed eyes, mild oligoemia. E
NR783		>2, <5	At 2 mg/kg: no clinical signs observed. At 5 mg/kg: severe rapid breathing, piloerection, decreased motor activity, hunched posture, closed eyes, mild oligoemia. E

ID: identification. E: euthanasia (culled according to humane end points).

## 1.2 Current use and application of thioureas

Thiourea and its derivatives are manufactured globally on a large scale, as they are extensively used in several industrial applications, including metal cleaning and refinement, the modification of flame retardant resins and the production of copy paper, textile and dyeing auxiliaries and explosives (Ziegler-Skylakakis, 2003). As these numerous appliances may represent important sources of potential human and environmental exposure, the safety of thiourea has been studied extensively in preclinical animal studies. It has been known for a long time that, in several laboratory animal species, a single high (between 10 to 500 mg/kg) dose of thiourea induces severe toxic changes in the lung, characterised by pulmonary oedema and pleural effusion (Dieke et al., 1947). In repeated dose toxicity studies in rodents, the major adverse health effect of this molecule consisted of an inhibitory effect on thyroid function (Mackenzie and Mackenzie, 1943). Histologically, hyperplasia of follicular cells, associated with decreased levels of thyroid hormones, has been a consistent finding in oral (*gavage* or diet) chronic toxicity studies in rodents (Ziegler-Skylakakis, 2003). Altered levels of T3 and T4, alongside morphological changes in the thyroid gland, have been documented also in humans exposed to thiourea at the workplace (Ziegler-Skylakakis, 2003). In carcinogenicity studies conducted more than 50 years ago, administration of thiourea had been related to the development of thyroid follicular neoplasia, at least in rats (Farid, 2004). Genotoxicity of thiourea was assessed using a standard test battery for mutagenicity and the vast majority of assays were negative, ruling out a genotoxic potential for this molecule (Ziegler-Skylakakis, 2003). Accordingly, the International Agency for Research on Cancer (IARC) concluded in 2001 that there was unsatisfactory evidence for the carcinogenicity of thiourea in humans and that the higher incidence of thyroid tumours observed in rats was likely related to a non-genotoxic thyroid tumour induction mechanism, to which the rat, unlike humans, is particularly sensitive (Greaves, 2007a; Ziegler-Skylakakis, 2003). The goitrogenic properties of thiourea have been formerly used in the treatment of thyroid gland hyperactivity (Graves' disease), until this drug was replaced by other molecules, such as methimazole (MI) and propylthiouracil, which still contain the thiourea moiety, but have less severe toxic effects (Franklyn, 2009). Several other drugs currently on the market contain

thiourea within their pharmacophore, including histamine H<sub>3</sub> receptor antagonists [used for the treatment of Alzheimer's disease and schizophrenia (Vollinga et al., 1995)] and non-nucleoside inhibitors of HIV-1 reverse transcriptase (Cantrell et al., 1996). Bone marrow toxicity, characterised by agranulocytosis and reduction in circulating erythrocytes, leukocytes and platelets has been reported in several patients administered thiourea-containing drugs and is the main reason for the withdrawal of some of them (Chang and Morrison, 1979; Forrest et al., 1975; Young and Vincent, 1980). Adverse effects of thiourea-containing drugs, in addition to hypothyroidism and bone marrow toxicity, included also hypersensitivity reactions and hepatotoxicity (Heidari et al., 2013; Onderwater et al., 1998; Woeber, 2002).

### **1.3 Thiourea-based molecules as rodenticide candidates**

As briefly mentioned above, single dose toxicity of thiourea in laboratory rodents and dogs is characterised by severe pulmonary oedema, which is achieved at relatively low doses, in the order of a few milligrams (Ziegler-Skylakakis, 2003). As the acute effects of thiourea are specifically targeting the lungs, thiourea-derived molecules have been used as an experimental model to induce non-inflammatory pulmonary oedema and investigate the physiology and pathogenesis of increased vascular permeability in the lung (Vivet et al., 1983). Besides this, the low LD<sub>50</sub> combined with the low costs of manufacturing, made thiourea an excellent candidate for the development of chemicals for pest control on a commercial basis. Investigation on this subject was mainly conducted during the years surrounding World War II, when the risk of rat-borne epidemics was extraordinarily high and led to the synthesis of alpha-naphthylthiourea (ANTU), an organosulphur compound containing the thiourea moiety and a naphthalene group (Richter, 1945). ANTU was first tested in the early 1940s in Baltimore, Maryland US, which was experiencing in those years unprecedented rat infestations (Keiner, 2005). Since then, several studies aimed to characterise the pathological changes and the mechanism of toxicity of ANTU in rats. The fluid accumulating in the lungs and in the thoracic cavity was seen to contain high levels of protein and was essentially devoid of inflammatory cells (Richter, 1952). Histological and ultrastructural assessment ascribed ANTU-related pulmonary changes to severe perturbation of vascular permeability and injury

to endothelial cells (Cunningham and Hurley, 1972; Meyrick et al., 1972; Rutili et al., 1982; Scott et al., 1990; Vivet et al., 1983). ANTU proved to be an effective rodenticide and it was claimed to have reduced significantly the urban rodent population in the Baltimore trial; however, despite its efficacy, ANTU suffered from several major drawbacks, identified in a survey conducted a few months after its first employment (Keiner, 2005). One of these limitations was that rats that had survived a sublethal dose of the rodenticide were able to withstand subsequent lethal amounts (Dieke and Richter, 1946). Similarly, rats up to 3-4 weeks of age were markedly less susceptible to ANTU-induced pulmonary oedema than older rats (Dieke and Richter, 1946).

## **1.4 Tolerance to thiourea(s)**

The terms “tolerance” and “resistance” are often used interchangeably to indicate the decreased susceptibility of an organism to the effect of toxicants. More accurately, the term “resistance” should be reserved for those adaptive changes which involve the modification of a genetic trait, poorly or not expressed in a population prior to the exposure to the toxicant (Hodgson and Levi, 2001). “Tolerance” instead better applies to individual adaptive responses which do not depend on new genetic tracts acquired through selection, but are based on an acquired physiological state. The rapid development of tolerance on repeated administration at very short space intervals of a drug or poison has been defined as tachyphylaxis or acute tolerance (Cannon, 2007). Numerous studies have attempted to explain the mechanism underlying the decreased responsiveness to ANTU in young rats or animals previously exposed to sublethal doses (Barton et al., 2000; Boyd and Neal, 1976; Van Den Brenk et al., 1976). Interestingly, ANTU induces cross-tolerance to several other molecules which cause lung damage, including noxious gases and bleomycin (Barton et al., 2000). In the same way, other molecules chemically related to ANTU including non-toxic thioureas and certain sulphhydryls are able to elicit the same protective response in the rat lung (Van Den Brenk et al., 1976). As the administration of certain molecules containing iodine was seen to induce tolerance to ANTU, a role for the thyroid gland in the induction of protection was implicated, but immediately excluded following investigation using thyroidectomised rats (Van Den



Brenk et al., 1976). Preliminary experiments undertaken by a group of researchers at the University of California found that the alteration of vascular permeability caused by a high dose of thiourea in the rat lung was associated with increased levels of histamine (Giri et al., 1991a) and suggested that tolerance resulted in reduced plasma concentration of this vaso-active amine (Giri et al., 1991b). More recently, proliferation of epithelial cells in the lung was investigated as a possible mechanism underlying tolerance to ANTU, following the observation that administration of keratinocyte growth factor (KGF) to rats attenuated the pulmonary oedema caused by the rodenticide (Mason et al., 1996). However, the literature in this field has failed to characterise in detail the morphological aspects of the pulmonary proliferative events associated with tolerance and a definitive conclusion on the mechanism underlying the innate and acquired tolerance to thiourea has not been reached. On the other hand, the acute toxicity itself of thiourea-related compounds has not been completely understood. Metabolic activation of thiourea, which mainly occurs through oxidation of the sulphur atom present in the structure, has proven to be an essential condition for the occurrence of lung toxicity (Boyd and Neal, 1976). Activation of the thionocarbonyl moiety is mostly carried out during phase I metabolism by flavin containing monooxygenases (FMOs), of which thiourea is known to be an excellent substrate (Krueger and Williams, 2005).

## **1.5 The role of flavin containing monooxygenases (FMOs) in xenobiotic metabolism**

Biotransformation, the chemical modification of a substance carried out by a living organism, is a key role in the metabolism of those compounds which are not part of the normal biochemical constituents of the body (xenobiotics), such as drugs and poisons (Haschek et al., 2009d). Drug metabolism relies on a complex set of enzymatic pathways responsible for the detoxification of exogenous compounds and is classically divided into two phases. Enzymes responsible for phase I metabolism catalyse oxidative, reductive and hydrolytic reactions and aim to introduce reactive or polar groups into lipophilic xenobiotics to facilitate their conjugation to polar molecules (carried out by phase II metabolic enzymes) and, in turn, their excretion (Kalgutkar et al., 2005). Cytochrome P450 (CYP) is assumed to be the

major enzyme superfamily involved in phase I metabolism (Guengerich, 2001). Oxidative metabolism of xenobiotics, however, is not confined to the P450 monooxygenases and may be carried out by other phase I enzymes, including those belonging to the multi-gene FMO family (Cashman and Zhang, 2006).

### **1.5.1 History of the FMO enzyme family**

FMO was initially discovered in 1964 (Pettit et al., 1964) and was then purified to homogeneity in porcine liver by Dr. Daniel Ziegler and colleagues at the University of Texas in 1971 (Ziegler and Mitchell, 1972). Biochemical properties and metabolic activity toward xenobiotics of the porcine hepatic FMO were characterised in the following years and shown to be very similar to the then recently characterised cytochrome P450 monooxygenase (Ziegler and Poulsen, 1978). However, FMO was demonstrated to be a distinct enzyme with no haem and a single flavin adenine dinucleotide [FAD; (Ziegler and Mitchell, 1972; Ziegler and Poulsen, 1978)]. In the early 1980s, a different FMO was isolated independently by two different research groups from rabbit pulmonary microsomes, providing evidence of the existence of multiple enzymatic forms (Tynes et al., 1985; Williams et al., 1984). It has been proven subsequently that the newly purified FMO isoform (then renamed FMO2) is the major FMO found in the lung of most mammals and has distinct substrate and immunological specificity when compared to the original hepatic isoform (FMO1) purified by Ziegler (Tynes et al., 1985). Since the isolation of the hepatic and pulmonary FMO enzymes, other FMO proteins and genes have been purified and cloned from different tissues in several species. Currently, five functional FMO isozymes, named FMO1 to 5, are known to be expressed in humans and several mammals, including most laboratory species (Krueger and Williams, 2005).

### **1.5.2 Differences from and similarities with cytochrome P450**

The main role of FMOs is considered to be xenobiotic detoxification (Ziegler, 1990). It has been proposed that, similarly to other flavoproteins, FMOs appeared early in the evolutionary process to protect mammals from lipophilic plant-derived nucleophiles present in the diet (Cashman and Zhang, 2006). FMOs, as well as CYP monooxygenases, are able to oxidise a broad spectrum of substrates containing a

nucleophilic heteroatom, such as sulphur and nitrogen and, in some cases, selenium, iodine, phosphorus and even carbon (Cashman, 1995). These include a plethora of endogenous products as well as thousands of synthetic therapeutic drugs, toxicants and carcinogens, which have not necessarily common structural features, apart from most being lipophilic soft nucleophiles. CYP and FMO utilise nicotinamide adenine dinucleotide phosphate (NADPH) and/or nicotinamide adenine dinucleotide (NADH) as reducing agents and catalyse oxidative reactions to incorporate molecular oxygen into the substrate (Krueger and Williams, 2005). Both enzymatic families developed versatile substrate specificity during evolution at the expense of turnover rates (Krueger et al., 2002b). As a consequence, FMOs and CYPs show similar cellular and tissue location, both being present at the highest concentration in the liver and in all tissues most exposed to xenobiotics and involved in detoxification processes (Cashman and Zhang, 2006). CYP-mediated metabolism of heteroatom-containing compounds often results in bioactivation and produces metabolites which are more likely to have toxic or carcinogenic properties, e.g., an epoxide, oxon, or primary aryl *N*-hydroxylamine (Cashman and Zhang, 2006). On the other hand, FMO oxygenation of lipophilic compounds containing heterophilic atoms produces more polar, readily excreted metabolites with reduced pharmacological and toxicological properties. Notable exceptions to this rule have been documented, as FMO itself is able to bioactivate certain molecules. FMO-mediated S-oxygenation of thioureas to a sulfenic acid, which can undergo redox cycling and covalent binding to tissue proteins, is one such example (Cashman and Zhang, 2006).

### **1.5.3 Structure of FMOs**

Similarly to CYP, FMOs are membrane-bound, highly lipophilic enzymes found in the endoplasmic reticulum of several cell types (Cashman and Zhang, 2006). In humans, they are composed of approximately 500 amino acids and have a molecular weight of about 60 KDa (Cashman and Zhang, 2006). Although their 3-dimensional structure has not been completely resolved yet, FMO proteins appear almost identical when evaluated using crystallographic models (Ziegler, 2002). Amino acid identity across different FMO isoform sequences sits around 55% and increases to at least 80% when analogous proteins from different species (human, rabbit, rat and mouse)

are compared (Lattard et al., 2002a). The configurational homology across isoforms is supported by the similarities found between FMO mRNA sequences, such as the presence of a common translation initiation site and numerous repetitive motifs which code for the cofactor (NADPH and FAD) binding sites (Cashman and Zhang, 2006).

A typical FMO enzyme structure consists of a protein dimer composed of identical subunits [Figure 1.1; (Ziegler, 2002)]. The active site of FMO, where the catalytic reactions take place, appears to be a narrow (4.5 Å in diameter) cleft and represents the least conserved region between different flavoproteins. Krueger and Williams (2005) suggest that small variations in the amino acid side chain sequence controlling the access to this channel may account for the differences in antigenicity and physical properties found across FMO members, such as thermolability and inhibition by detergents. To list a few examples, rabbit FMO2 has enhanced thermal stability when compared to porcine FMO1: the former in fact is relatively stable at 45-50°C, especially when NADPH is present, while porcine FMO1 is readily inactivated at these temperatures (Kaderlik et al., 1991; Lawton et al., 1991). Also, antibodies directed against FMO1 do not recognise FMO2 and, at the same time, anti-mouse hepatic FMO1 antibodies for example do not cross react with FMO1 in porcine livers (Krueger and Williams, 2005). This indicates that substrate specificity data or physical properties of a particular FMO family member should be extrapolated carefully across species (Cashman and Zhang, 2006).

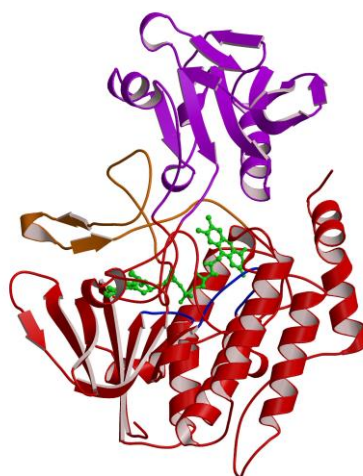


**Figure 1.1.** Ribbon diagram of the structural domains of the FMO protein. FAD coenzyme is depicted in green. Obtained from previously published work (Eswaramoorthy et al., 2006).

### 1.5.4 FMO catalytic cycle

Despite the presence of different species- and tissue-specific isoforms, all FMOs share a unique sequential catalytic cycle, in line with the broad substrate specificity that characterises this class of enzymes (Ziegler, 2002). FMOs activate molecular oxygen through the formation of a C4 $\alpha$  hydroperoxyflavin intermediate (FADOOH), which functions as an oxidising agent for soft nucleophilic molecules gaining access to the active site (Cashman and Zhang, 2006; Krueger and Williams, 2005). This potentially reactive intermediate is preformed in the presence of oxygen and NADPH, but in the absence of a substrate (Cashman and Zhang, 2006). FMOs work therefore like a “cocked gun”: when a potential substrate enters the active site of the flavo-enzyme in its reduced form, it is rapidly oxidised and released (Krueger and Williams, 2005). On the contrary, CYP-catalysed reactions require binding of the substrate early in the cycle, followed by the formation of an unstable intermediate derived from the interaction between O<sub>2</sub> and the ferrous ion contained in the haem group (Cashman and Zhang, 2006). The mechanism of oxygenation of FMO relies on the transfer of two electrons, whereas CYP employs only one (Ziegler, 2002).

The major steps of the catalytic cycle of the FMO may be summarised as follows (**Figure 1.2**):

Step one: The FAD (FAD<sub>ox</sub>) incorporated in the prosthetic group of the enzyme is reduced (FADH<sub>2</sub>) by NADPH through a two electron transfer.

Step two: FADH<sub>2</sub> reacts with molecular oxygen at the 4 $\alpha$  position of the tricyclic ring of the riboflavin to form a flavin hydroperoxide (FADOOH).

Step three: The flavin hydroperoxide intermediate uses one atom of oxygen to oxidise suitable substrates (i.e., containing a soft nucleophilic group) which gain access to the active site (3a), while the other atom of oxygen is incorporated into H<sub>2</sub>O (3b), in order to return the FAD to an oxidised status with the loss of H<sub>2</sub>O and NADP<sup>+</sup>. The binding of NADPH starts a new cycle. Decomposition of the FAD-

intermediate, which represents the regeneration of the enzyme catalytic potential, is slower than the other steps and, in most cases, rate limiting (Ziegler, 2002).

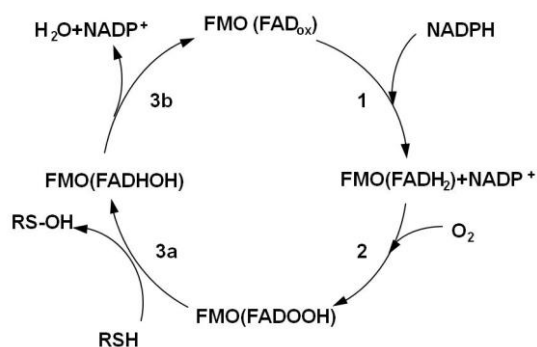


**Figure 1.2.** The catalytic cycle of FMOs. Redrawn from Ziegler, 2002.

Unlike the case with other monooxygenases, the FADOOH intermediate is relatively stable, suggesting that the protein catalytic cleft protects the metabolite from decaying and circumvents the formation of reactive oxygen species [ROS; (Ziegler, 2002)]. The mechanism by which the FMO active site is isolated from the attack of biological reducing agents, such as cysteine and glutathione (GSH), has not been fully elucidated: Cashman (2008) proposes that the configuration of the active site pocket wall and its access channel, low in nucleophilic amino acids which could interact with the electrophilic intermediates formed in the catalytic site or with FADOOH, may represent a likely explanation.

### 1.5.5 Endogenous and exogenous substrates of FMOs

Several nitrogen- and sulphur-containing endogenous substrates and xenobiotics are metabolised by FMOs (see **Table 1.2**), mainly via N- or S-oxygenation (Krueger and Williams, 2005). In order to access the catalytic cleft of the flavo-enzyme, potential substrates must be soft nucleophilic molecules, with specific charge, size and shape limitations, depending on the FMO isoform (Cashman and Zhang, 2006). Uncharged molecules and compounds with a single positive charge are usually excellent substrates, whereas chemical entities containing a negatively-charged or more than one positively-charged group are poorly metabolised or completely excluded from

the FMO active site (Ziegler, 2002). These limitations related to the charge of the substrate are important to avoid unnecessary turnover of numerous endogenous molecules containing a nucleophilic atom (Cashman, 2008). In addition, shape and overall dimensions appear to be major determinants of substrate accessibility to the catalytic pocket, as detailed below (Ziegler, 2002).

FMOs have broad and overlapping substrate specificity, however, several substrate range peculiarities are found within the FMO family and the examples that follow may not apply to all isoforms. FMO1 (except human FMO1) and, to a lesser extent, FMO3 have a wider substrate acceptance range than the other members (Cashman, 2000; Kim and Ziegler, 2000; Krueger and Williams, 2005). FMO2 has the most restricted substrate specificity due to the peculiar steric properties, as demonstrated in experiments using different size tertiary amines and thioureas, which are not metabolised by FMO2 when carrying a side chain shorter than 5 carbons or when bigger than 1,3-diphenylthiourea, respectively (Guo et al., 1992). It has been proposed that the increased substrate selectivity of rabbit FMO2 and its inability to carry out the oxygenation of typical FMO substrates such as imipramine and chlorpromazine may depend on the conformation of the active site of the protein, which is characterised by a narrower access channel, compared to FMO1 (Nagata et al., 1990). Similar restrictions apply to human FMO2 (Henderson et al., 2004a). FMO5 also has a weak catabolic activity against MI, trimethylamine (TMA) or ranitidine, which are all typical FMO substrates, whereas it is reported to S-oxygenate long-chain phenothiazene analogs, n-octalamine and thioethers, which are not normally metabolised by other FMOs (Krueger and Williams, 2005; Motika et al., 2012). Similarly, FMO4 also has a limited substrate range together with low levels of expression (Itagaki et al., 1996).

#### **1.5.5.1 Nitrogen-containing drugs as FMO substrates**

Several nitrogen-containing drugs are excellent substrates of FMOs [(Cashman, 1995); see **Table 1.2**]. Pheniramine and olopatadine (antihistamines), zimelidine (selective serotonin reuptake inhibitor, used as an antidepressant), ranitidine (histamine H<sub>2</sub>-receptor antagonist used as a gastric antacid), itopride (gastroprokinetic agent) and the antiseptic benzydamine are only a few examples of

commonly prescribed drugs for which FMO oxygenation represents a primary metabolic pattern (Krueger and Williams, 2005). Most of these drugs are tertiary amines which are normally metabolised to the correspondent amine oxide by FMO1 and/or FMO3 (Krueger and Williams, 2005). This intermediate typically exhibits less pharmacological and/or toxicological properties than the parent amine or CYP-mediated metabolites obtained through N-dealkylation (Cashman and Zhang, 2006). Several tertiary amines exert their action on the nervous system, such as the antipsychotic compounds imipramine, clozapine, fluoxetine and chlorpromazine or the local anaesthetics bupivacaine and lidocaine; the activity and tissue-specific distribution of FMOs in the nervous system may, therefore, influence the levels of detoxification of these drugs (Bhamre et al., 1995; Cashman and Zhang, 2006). Also in the brain, FMO appears to inactivate through N-oxygenation the neurotoxin 1-methyl-4-phenyl-1,2,3,6-tetrahydropyridine (MPTP), a component of certain pesticides which causes permanent symptoms of Parkinson's disease by destroying dopaminergic neurons in the *substantia nigra* (Cashman and Ziegler, 1986). When MPTP is metabolised instead by monoamine oxidases of glial cells into the toxic cation MPP<sup>+</sup>, it is neurotoxic (Cashman and Ziegler, 1986). In several cases, the N-oxide produced by FMOs is reconverted to the parent form by CYP or other monooxygenases through a mechanism known as retro reduction (Cashman et al., 2008). Although not completely understood, it has been proposed that this mechanism would allow FMOs to temporarily "inactivate" tertiary amines and prolong their action (Krueger and Williams, 2005). Retro reduction has been well characterised by studying the pharmacokinetics of tamoxifen (Krueger and Williams, 2005), a selective oestrogen receptor modulator (SERM) extensively used as adjuvant therapy in breast cancer treatment (Teunissen et al., 2010). This drug is mainly hydroxylated by CYP into a reactive metabolite (4-hydroxytamoxifen) which binds competitively to oestrogen receptors and accounts for the cytostatic activity of the drug on tumours cells (Hemminki et al., 1996). Another important metabolic pathway, although secondary to the previous one, is the conversion of tamoxifen into the correspondent inert amine oxide, which is predominantly carried out by FMO1 and, to a lesser extent, by FMO3 (Krueger et al., 2006). The therapeutic efficacy of tamoxifen may therefore be influenced by the levels of expression of FMO1 and FMO3 in the host tissues and in neoplastic cells and the balance between



bioactivation and detoxification also may vary according to the abundance and genetic polymorphism of CYP and FMO in the target organs (Parte and Kupfer, 2005). Accordingly, it has been argued that the adult human liver, which contains high amounts of CYP and virtually no FMO1, may be at increased risk of developing toxic changes compared to the kidney, where levels of FMO1 approach those of CYP3A4 (Shimada et al., 1994), the most abundant CYP isoform present in the human liver (Guengerich, 2003). Secondary amines, including methamphetamine and propanolol, are turned into the correspondent primary amines by both CYP and FMOs (Krueger and Williams, 2005). Unlike the N-oxygenation of tertiary amines, FMO-mediated metabolism of secondary amines does not always result in detoxification, but may lead to noxious metabolites, such as the neurotoxic N-hydroxy-3,3'-Iminodipropionitrile (Nace et al., 1997) and N-deacetyl ketoconazole (Rodriguez and Miranda, 2000). Secondary N-alkylarylamines are oxygenated by FMOs to metabolites which are considered primarily responsible for the carcinogenic potential of aromatic amines (Vineis and Pirastu, 1997; Ziegler, 1991). Primary amines such as amphetamine and N-octylamine are normally metabolised by FMOs to the correspondent oxymes, which are pharmacologically less active (Krueger and Williams, 2005).

#### **1.5.5.2 Sulphur-containing drugs as FMO substrates**

FMOs readily catalyse the oxygenation of several sulphur-containing drugs, including phenothiazine-derived histamine H<sub>2</sub>-receptor antagonists (cimetidine and ranitidine, the latter is both N- and S-oxygenated by FMOs), thioridazine, theophylline, clindamycin, fenbendazole and MI (Krueger and Williams, 2005). More examples are presented in **Table 1.2**. It has already been mentioned that FMOs normally function as a detoxification system able to transform lipophilic molecules into less toxic hydrophilic compounds. While exceptions to this rule occur very infrequently for N-containing FMO substrates (see paragraph 1.5.5.1), more examples are available of S-oxides produced by FMOs which are more reactive than the parent compounds and potentially harmful. FMO-mediated S-oxygenation of small chemical groups such as sulphides and disulphides, thioethers, thiols and thioureas results in the formation of a sulphoxide, often through an intermediate sulphenic acid (Krueger and Williams, 2005). Sulphenic acids, which can be further

oxidised to sulphinic and sulphonic acids, are extremely reactive electrophiles and are thought to react promptly with the parent drug or with nucleophiles present in the medium, such as GSH or other sulphhydryls to produce disulphides (Mansuy and Dansette, 2011). In line with this, sulphenic acids formed during the *in vitro* and *in vivo* metabolism of thiourea and thioamides, such as thioacetamide or its derivatives (e.g.; the thyrotoxic drugs MI, carbimazol and propylthiouracyl) have been considered to be primarily responsible for the development of the pulmonary and hepatic toxicities associated with the administration of these classes of compounds (Heidari et al., 2013; Henderson et al., 2004b; Krueger and Williams, 2005; Ziegler, 1978). The formation of sulphenic acids has been documented in the metabolism of several other drugs such as the antithrombotic drug Prasugrel and the glitazones (Mansuy and Dansette, 2011); however, as the isolation of these highly reactive intermediates is often unsuccessful due to their lack of stability, not much is known regarding the fate and the toxicologic consequences of sulphenic acids in preclinical species and in humans. Another S-containing drug extensively oxidised by FMOs is ethionamide, a pro-drug antibiotic used as a second choice in the treatment of tuberculosis (Henderson et al., 2008). Ethionamide needs to be converted to the correspondent S-oxide by a mycobacterial FMO in order to exert its therapeutic action (Qian and Ortiz De Montellano, 2006). At the same time, FMO-dependent S-oxygenation of the drug also occurs in the liver (FMO3) and the lung (FMO2) of patients and has been claimed to be the cause of the hepatotoxicity occurring in the 25% of individuals that have to discontinue the treatment (Henderson et al., 2008).

### **1.5.5.3 Endogenous substrates of FMOs**

Similarly to drugs, selected endogenous molecules may also be suitable for FMO turnover. It needs to be said, however, that the definition of “endogenous” has been used somewhat arbitrarily to include chemical entities synthesized exclusively in the body or also xenobiotic and dietary components which undergo conjugation with cysteine, mediated by glutathione S-transferase during phase II metabolism, after which they may be accepted by FMOs (Krueger and Williams, 2005). Biogenic amines such as tyramine (Niwa et al., 2011) and phenethylamine are examples of endogenous amines N-oxygenated by FMOs (mostly FMO3) to trans-oximes, which have little pharmacological activity (Lin and Cashman, 1997). Another example of a typical endogenous substrate of FMOs is represented by the extremely odorous molecule, TMA, which is present in the diet or formed in the gut from the breakdown of choline, carnitine and other dietary components and it is N-oxygenated by FMO3 to the correspondent odourless N-oxide (Lambert et al., 2001). Impairment of FMO-mediated N-oxygenation of TMA is the cause of the genetic disease known as trimethylaminuria (TMAU; Fish-Odour Syndrome), characterized by an excess of TMA in the urine, sweat, and breath of patients (Shephard et al., 2012). Endogenous molecules containing sulphur, such as lipoic acid and cysteamine, are also suitable targets of FMO-oxygenation (Krueger and Williams, 2005). Similarly to S-containing drugs, cysteamine is S-oxygenated to its correspondent disulfide cystamine, which is in turn excreted from the cell. It has been suggested that the action of FMOs prevents cysteamine from accumulating intracellularly and forming hydrogen peroxide (Jeitner and Lawrence, 2001), providing a mean of detoxification and, more speculatively, contributing to the regulation of cellular levels of reducing equivalents (O'connor et al., 2013; Ziegler et al., 1979).

### **1.5.6 Tissue- and species-specific differences in the expression of FMOs**

The expression of the FMO genes across different animal species shows considerable variability. This conflicts with the relatively low number of genes and allelic variants which characterise this family of proteins. Several studies suggest that the expression of FMOs is also influenced by physiological factors, such as species, sex, age and

tissue, cofactor availability and diet (Cashman and Zhang, 2006). A large and growing body of literature has investigated the distribution of FMO isoforms in different animal species (mainly humans, mice, rats, and rabbits), assessing it through different methods, such as RNase protection assays [man (Dolphin et al., 1996) and mouse (Janmohamed et al., 2004)], Western blot analysis (Koukouritaki et al., 2002), quantitative polymerase chain reaction [man (Zhang and Cashman, 2006) and mouse (Siddens et al., 2008)] and *in vitro* microsomal activity tests (Overby et al., 1997). The outcome of these investigations revealed the existence of a marked tissue- and species-specific expression pattern, which may influence the metabolic and toxicologic responses of the organism to the numerous FMO substrates present in the diet and in the environment or that are used as therapeutic drugs in human or veterinary medicine (Krueger and Williams, 2005). Interspecific differences in FMO expression in particular need to be taken into consideration when extrapolating data obtained from laboratory animals to man. We have mentioned already that FMO expression has been reported to be highest in the tissues which are most involved in the metabolism of xenobiotics, such as the liver and the kidney, but also the lung and the small intestine (Cashman et al., 2008). Only limited data are available concerning localisation of FMOs within the brain, where FMO activity toward the numerous biogenic amines present in this tissue is deemed to have an important role in neurotransmission and other essential biological functions (Cashman and Zhang, 2002). FMO proteins have been detected in specific areas of the rat and human brain and are reported to oxygenate typical substrates, including the psychoactive drugs chlorpromazine and imipramine (Bhamre et al., 1995; Bhamre et al., 1993; Kawaji et al., 1995; Kawaji et al., 1994). In a study comparing the expression of FMOs in different areas of the central nervous system of C57BL/6J and SOD1 (G93A) transgenic mice, all FMO genes were detected except *FMO3* (Gagliardi et al., 2011). However, overall FMO mRNA levels observed in the human CNS are extremely low compared to those found in other major organs (approximately 1%), posing the question of what is the actual contribution of FMOs to xenobiotic metabolism in this tissue (Krueger and Williams, 2005).

**Table 1.2.** Selected examples of drugs which are metabolised by FMOs to a significant extent.

Therapeutic category	Drug substrate	Predominant FMO isoforms involved	FMO product	Reference
(Meta)amphetamines	Dimethylamphetamine, Amphetamine	FMO1 (FMO3: ×10 less)	N-oxide	(Lee et al., 2009)
Tobacco alkaloids/ smoking cessation	Nicotine	FMO3	N-oxide	(Benowitz et al., 2009)
Antifungal agents	Voriconazole	FMO1, FMO3	N-oxide	(Yanni et al., 2008)
	Ketoconazole	FMO1-3	N-oxide	(Rodriguez and Buckholz, 2003)
Tricyclic antipsychotic agents	Imipramine, Orphenadrine, Chlorpromazine, Desipramine, Acepromazine, Amitriptylene	FMO1	N-oxide	(Hernandez et al., 2009; Kim and Ziegler, 2000)
Beta blockers	Propranolol	FMO1	N-oxide	(Wu et al., 2004)
Local anaesthetics	Bupivacaine, lidocaine	FMO3	N-oxide	(Wu et al., 2004)
Histamine H <sub>2</sub> -receptor antagonists	Cimetidine Ranitidine	FMO1	S- and N-oxides	(Cashman et al., 1993b; Kim and Ziegler, 2000)
Antihistaminics	Promethazine, Olopatidine, Brompheniramine	FMO1, FMO3	N-oxide	(Cashman et al., 1993a; Clement et al., 1993; Kajita et al., 2002)
Non steroidal antiinflammatory drugs	Sulindac sulphate	FMO1-3	S-oxide	(Xie et al., 2012)
	Benzydamine	FMO1, FMO3	N-oxide	(Stormer et al., 2000)
Insecticides	Aldicarb, Methiocarb, Demeton, Fenthion, Disulfoton, Fonofos, Phorate	FMO1 (less FMO3)	S-oxide	(Furnes and Schlenk, 2005; Henderson et al., 2004a; Leoni et al., 2008; Schlenk et al., 1992)
Antioestrogen compounds	Tamoxifen	FMO1 (much less FMO3)	N-oxide	(Krueger et al., 2006)
Anthelmintics	Albendazole Fenbendazole	Not specified	S-oxide	(Virkel et al., 2004)
Antibiotics	Ethionamide	FMO2, FMO3	S-oxide	(Henderson et al., 2008)
Antithyroid drugs	Methimazole Carbimazole	FMO1-3	S-oxide	(Cashman, 1995)
Gastroprokinetic drugs	Itopride	FMO1, FMO3	N-oxide	(Mushiroda et al., 2000)

### 1.5.6.1 FMO expression in humans

A detailed review of the patterns of tissue distribution and expression of FMOs in humans, which have been fully characterised through qualitative and quantitative assessment, is beyond the scope of this chapter and only the information necessary to understand the importance of animal models in the evaluation of FMO metabolism is provided. A schematic overview of the current knowledge on this subject is presented in **Appendix I**, where the expression of FMOs in humans and mice are compared. FMO3 is the most abundant isoform found in the human adult liver, in contrast to the majority of the species where FMO1 predominates, and it is

recognised as the most important contributor to hepatic FMO-dependent drug and chemical metabolism (Cashman and Zhang, 2006). Hepatic FMO1 and FMO3 exhibit a developmental pattern of expression: FMO1 is present in the foetus but then suppressed 72 hours after birth (Dolphin et al., 1991), whilst FMO3 mRNA is detected only after birth and is found at the highest levels at the end of puberty (Koukouritaki et al., 2002). A similar developmental shift is reported for CYP3A, although the decrease of CYP3A7 occurs in parallel with the increase of CYP3A4 so that the overall hepatic level of CYP3A remains relatively constant at any age (Krueger and Williams, 2005). An issue which has not been fully addressed yet is whether the developmental changes in FMO and CYP expression may influence drug pharmacokinetics and therapeutic outcome in children compared to adults (De Wildt, 2011). FMO activity in fact is deemed to be very low in the liver of neonates, due to the “switch off” of FMO1 expression and the slow rise in FMO3, suggesting that extrahepatic FMO-mediated metabolism of drugs and endogenous substrates may be more relevant in children than in adults (Shephard and Phillips, 2010). Due to the high concentration of FMO1 and the broad substrate specificity of this isoform, the kidney is likely to represent a relevant site of FMO-dependent extrahepatic xenobiotic metabolism (Cashman and Zhang, 2006).

To date, only FMOs 1-3 have been seen to contribute substantially to the metabolism of xenobiotics (Cashman and Zhang, 2006). FMO4 is very unstable and, despite several attempts, its purification has proven to be fastidious and mostly unsuccessful (Lattard et al., 2003). Not much is known, therefore, regarding the involvement of FMO4 in xenobiotic oxygenation. Equally, the contribution of FMO5 to drug metabolism has not been fully elucidated yet, mainly due to a paucity of selective substrates and the peculiar features of this enzyme, which is classified as an FMO based on its primary structure but shows different catalytic cycle and physical properties [e.g. pH dependence; (Jeitner and Lawrence, 2001)]. Nevertheless, the role of FMO5 as an active catalyst of metabolic reactions is currently not deemed important, because of the narrow substrate specificity (see paragraph 1.5.5) and the low activity rate (Krueger and Williams, 2005; Ziegler, 2002).

#### **1.5.6.2 FMO expression in mice**

A key difference in the expression pattern of FMOs between man and mouse is the sex-dependent expression of FMO3 in the liver of the latter. As previously described, FMO3 is expressed in the liver of humans only after birth, in a gender-independent fashion and becomes the predominant FMO isoform in this organ at puberty (see paragraph 0). Interestingly, the liver of the adult male mouse (and dog) lacks FMO3, the expression of which is suppressed at 6 weeks of age, whilst in other murine tissues, levels of FMO3 are comparable between sexes (Cherrington et al., 1998; Falls et al., 1997; Lickteig et al., 2009; Ripp et al., 1999). FMO1 mRNA in mice is present in the liver of both sexes, although at higher levels in females; FMO5 levels on the other hand are comparable between sexes (Falls et al., 1997). FMO mRNA localisation and abundance have been fully characterised in mice (129/SV and C57BL/6J strains) using *in situ* hybridisation (ISH) and RNase protection assays (Janmohamed et al., 2004). According to this study, the distribution of FMO mRNA in the liver follows a lobular pattern: FMO1 and FMO5 mRNA are more abundant in the periportal (centrilobular) hepatocytes and decrease gradually toward the periportal regions. Vice versa, FMO2, FMO3 (female only) and FMO4 mRNA are more copiously present in periportal hepatocytes. According to Janmohamed et al. (2004), all five FMO isoforms are expressed in the mouse kidney, where they are seen to localise primarily in the cortical distal tubules, and to a lesser extent, in the proximal tubules and collecting ducts. In the glomeruli, only FMO1 mRNA is detected. This concurs with the fact that the tubular epithelium is the main site of xenobiotic metabolism in the kidneys and expresses several other enzymes involved in drug bioactivation and detoxification (Lock and Reed, 1998). As stated by Janmohamed, pulmonary FMO mRNA is found in the bronchiolar epithelial cells and in the alveoli: however, the exact cellular localisation of FMOs within the alveolar unit has not been characterised in this paper. All FMO isoforms appear to be present in the murine lung, except FMO4 and all are strongly expressed, apart from FMO2, whose signal is weak. In the brain, cerebral neurons and choroid plexuses are positive for FMO1 and/or FMO5. Janmohamed et al. (2004) compared also mRNA abundance of the different FMOs in the liver and described that FMO5 mRNA is predominant in both sexes, followed by FMO1 in males (5× lower than FMO5) and FMO3 in females (2.5× lower). Levels of FMO2 and FMO4 mRNA in this organ are comparatively much lower than those of the other FMOs. FMO1 was found to be the

most abundant transcript in the lung and kidney, followed by FMO5. Tissue distribution of FMO mRNA in the male and female mouse is depicted in **Appendix I**.

#### **1.5.6.3 FMO expression in rats**

Less information is available concerning the distribution and localisation of FMOs in rat organs and tissues and data concerning the quantitative assessment of mRNA are not available. Evidence of the expression of FMO1 and FMO3 in the rat liver has been shown by different authors (Cherrington et al., 1998; Kimura et al., 1983; Moroni et al., 1995). More recently, FMO1 mRNA bands with similar intensity were detected in liver, kidney and lung using Northern blot analysis (Lattard et al., 2002c). The same manuscript reported the expression of FMO3 mRNA in the liver, the kidneys (stronger signal than the liver) and the lung (negligible expression). In the brain, the signal for FMO mRNA was either very faint (FMO1) or not present at all (FMO3). These results were confirmed using Western blot (Lattard et al., 2002c). FMO4 mRNA has been found by Northern blot or reverse transcription polymerase chain reaction (PCR) in the rat kidney and the small intestine, and, to a lesser extent in the brain and the liver (Lattard et al., 2003). In the rat lung, FMO1 and FMO2 have been detected using Western blot analysis and are likely to represent the only FMO members expressed in this organ at significant levels (Hugonnard et al., 2004). Immunoreactivity of FMO1, FMO3 and FMO4 was studied in the liver and kidney of male animals using immunohistology with custom-made antibodies (Novick et al., 2009). Similarly to the FMO mRNA distribution pattern in the liver of mice, the results suggest that FMO1 and FMO4 are expressed at the highest levels in the centrilobular and periportal areas, respectively. Data on FMO4 expression provided by Novick and co-authors contrast with the low to negligible detection of the correspondent mRNA in the rat liver (Lattard et al., 2003). Rat hepatic FMO3 has been detected with higher intensity in the centrilobular hepatocytes (Novick et al., 2009), whereas in the mouse, the correspondent mRNA was predominantly detected in the periportal areas (Janmohamed et al., 2004). According to Novick, FMO1, FMO3 and FMO4 are all expressed with similar intensity in the renal distal tubules. The brush border of the proximal tubules was strongly positive for FMO1, slightly less for FMO4 and very weakly for FMO3. Glomeruli stained intensely for FMO3



and FMO4 and showed no reactivity for FMO1. No assumption has been made concerning the localisation of FMOs in the rat lung.

### **1.5.7 Evaluation of FMO activity in drug development**

*In vitro* human metabolism studies are routinely conducted at an early phase of preclinical development to identify the metabolic stability of new drug candidates and investigate their most likely metabolic pathways (Cashman, 2008). These studies employ microsomal incubations which are generally carried out with CYP enzyme systems and CYP inhibitors. Screening for FMO oxidative activity against new molecules is also part of the standard test battery, although is not conducted as extensively (Harper and Brassil, 2008). The thermal instability shared by most FMO isoforms, together with the lack of specific inhibitors of FMO activity, has represented a limitation that prevented FMO screening from being conducted on a large scale. Loss of FMO activity during tissue collection or microsome preparation occurs proportionally to the length of time that the tissue remains at an elevated temperature or NADPH-deficient conditions during these procedures (Cashman, 2008). The inhibition of FMO activity is achieved using competitive substrates such as MI or heat inactivation. Differently from CYP, antibodies directed against FMOs are unable to inhibit the catalytic activity of the enzyme and cannot be used in reaction phenotyping studies (Cashman, 2008). Inadequacy of analytical methods used to identify the products of FMO-oxygenation, which at times can be extremely unstable, and the occurrence of retro reduction, as described in paragraph 1.5.5.1, may also have limited the study on FMO contribution to drug metabolism (Shephard and Phillips, 2010). Nowadays, standard assays for FMO oxidative activity are usually limited to the investigation of FMO3 (Cashman, 2008), which, together with FMO5, is the most abundant FMO isoform expressed in adult human liver [(Krueger and Williams, 2005); see paragraph 0]. Recombinant human FMOs, expressed in baculovirus-infected insect cell membranes or cloned by other means, have recently been made available, although most of the metabolic profiling studies conducted in drug development are still carried out using microsomal suspensions (Cashman and Zhang, 2006; Catucci et al., 2012).

## 1.6 FMO genetic variability

FMO enzymes are encoded by the FMO gene family, which is relatively small and probably derived from reduplication of a single ancestral gene, before the evolution of mammals, as demonstrated by the presence of FMO sequences in the genome of several prokaryotic and non-mammalian eukaryotic species (Hernandez et al., 2004). Despite their broad substrate specificity, FMOs are genetically less diverse (five functional members only), when compared to other classes of drug metabolising enzymes (Lawton et al., 1994). Genes encoding CYP enzymes for instance are more numerous (beyond 100 functional genes and pseudogenes) and their expression is characterised by extensive inter-individual variability and polymorphism, which have been associated with different responses to drugs and therapeutic outcomes (Singh et al., 2011). CYP monooxygenase genetic variability is further complicated by the fact that their expression is selectively modulated in response to several environmental influences, including the administration of numerous xenobiotics (Parkinson and Ogilvie, 2008). FMO genes are clustered together on the long arm of chromosome 1 in all species and consist of five functional members (designated *FMO1* through *5*), and, in humans, a sixth pseudogene, which lacks protein-coding ability (Cashman and Zhang, 2006). A second cluster has been discovered also on chromosome 1 and is composed, at least in humans, only of pseudogenes [*FMO6P-11P*; (Krueger and Williams, 2005)].

Recent developments in the identification of the factors affecting FMO gene expression have heightened the need for a more thorough understanding of the molecular mechanisms involved in the control of FMO transcription. The promoter regions regulating this process are not known, with the exception of a few preliminary data collected on human *FMO3* (Klick and Hines, 2007) and the developmental expression of human *FMO1* (Shephard et al., 2007). Future research needs to focus on the identification of the factors implicated in the promotion or inhibition of FMO transcription, which is an essential step for the further understanding of the tissue-specific differences in the distribution of these proteins and the modulation of their expression induced by certain drugs or diseases.

### 1.6.1 FMO genetic variants and polymorphism

The number of known genetic variants of the five FMOs in *Homo sapiens* chromosome 1 ranges from 30 (*FMO4*) to 57 (*FMO3*) and translates into 1 to 19 modifications of the FMO coding region (Cashman, 2002). Despite these considerable numbers, the *in vitro* and *in vivo* consequences of FMO inter-individual variability have not been fully elucidated. Discrepancies in the frequencies of single or multiple FMO alleles in the human FMO genome and their repercussion on enzyme functionality have been best characterised for *FMO3*, due to the direct causative association between small base changes in this gene and TMAU, a human autosomal recessive inherited disease [(Cashman and Zhang, 2006), see paragraph 1.5.5.3]. *FMO3* is selectively involved in the metabolism of TMA, toward which it has the highest activity among FMOs (Li et al., 2011). Several variants in the allelic frequencies of *FMO3* have been documented in different ethnic groups and some of them have been associated with decreased enzyme activity toward reference substrates, such as TMA and benzydamine, and reduced formation of the correspondent N-oxide (Cashman, 2004). Defective metabolism in individuals carrying *FMO3* mutations may cause variable amounts of TMA to accumulate in body fluids and breath, which results in affected individuals displaying an unpleasant odour. The primary and best-known genetic form of TMAU which is detected in the vast majority of cases, is characterised by a restricted number of *FMO3* sequence mutations (i.e., P153L, M66I and E305X) that lead to significant enzymatic dysfunction, build up of unmetabolised urinary TMA and subsequent severe clinical disease (Zhou and Shephard, 2006). On the other hand, transient TMAU has been described in young children and it is likely due to the low levels of *FMO3* found during infancy (Krueger and Williams, 2005). The ratio between TMA and TMA N-oxide in the urine is used as a phenotyping tool in patients challenged with a standard dose of choline and a clinical parameter to evaluate the severity of the disease (Krueger and Williams, 2005). Inherited genetic defects of TMA metabolism have been documented also in certain breeds of chicken (Ward et al., 2009) and dairy cows (Lunden et al., 2002). Decreased function of mutated *FMO3* has also been related to enhanced anticancer activity of sulindac, a cyclooxygenase 2 inhibitor (Cashman and Zhang, 2006). This drug, after being activated by bacteria in the gut

into sulindac sulfide, is converted into an S-oxide and, in turn, to a sulphone by FMO3, and then excreted as such (Xie et al., 2012). Defective FMO3 detoxification has been related to an increase in the circulating levels of sulindac sulfide and therefore to an overall increase in its antineoplastic efficacy. FMO3 genotype and allelic variances were also associated with decreased responses due to increased clearance of the drug olanzapine in schizophrenic patients, where specific symptoms of the disease occurred with higher incidence in individuals carrying certain alleles (Cashman et al., 2008).

Similarly to *FMO3*, several *FMO1* SNPs have been identified in the corresponding human gene (Cashman and Zhang, 2006). Most of these variants encode for identical proteins or generate occasional amino acid substitution with similar amino acids which are unlikely to modify the functionality of the enzyme or have toxicological consequences. This is also supported by the fact that human FMO1 is characterised by limited substrate selectivity compared to FMO1 in other species (Cashman, 2000) and it is expressed mainly in the kidneys and other tissues that possess significantly less metabolic capacity than the human liver (Cashman and Zhang, 2006). However, FMO1 has been proven to represent an important extrahepatic metabolism pathway in humans for certain xenobiotics, such as carbamate and organophosphate thioether pesticides (Furnes and Schlenk, 2005) and further investigation is warranted to rule out a possible contribution of *FMO1* polymorphism to altered responses to drugs in humans, above all in the foetus. In a genetic association study evaluating three enzyme families involved in the metabolism of nicotine, *FMO1* genetic polymorphism has been identified as a risk factor that may contribute to the development of nicotine dependence (Hinrichs et al., 2011).

In addition to SNPs and other rarer types of mutations in the genome, alternative splicing has also been seen to contribute to the generation of FMO variants in several foetal and adult tissues (Cashman and Zhang, 2006). The full length FMO form is generally the most abundant transcript present, except for FMO4 which is fully expressed in human liver and kidney, whilst it is present in the brain as a shorter spliced inactive isoform (Lattard et al., 2003). Due to the paucity of substrates, the proteolytic instability of the expressed protein and the generally low enzymatic

activity, the prediction of changes deriving from the presence of *FMO4* variants, which have been documented though, is challenging and is more likely to be better understood once more information is available regarding the role of this enzyme.

### **1.6.2 *FMO2* genetic polymorphism**

Shortly after being sequenced, human *FMO2* was seen to be highly polymorphic (Dolphin et al., 1998). All Caucasians and Asians genotyped to date have a nonsense mutation in both *FMO2* alleles, characterised by a C (cytosine) → T (thymidine) transition at position 472 of the genomic sequence, leading to the conversion of a glutamine-codon into a premature stop codon (Furnes et al., 2003; Krueger and Williams, 2005). The product of this mutated allele, named *FMO2\*2*, is a truncated 472 amino acid protein that is not active, since it is unable to incorporate FAD (Whetstine et al., 2000). The truncated misfolded protein is catabolised rapidly after synthesis and does not appear to be expressed in the human lung, based on Western blotting, although the correspondent mRNA is present (Hugonnard et al., 2004). Interestingly, approximately 13% to 27% (Cashman and Zhang, 2006; Hugonnard et al., 2004; Krueger and Williams, 2005) of individuals of African-American ethnicity and up to 7% (Cashman and Zhang, 2006) of Hispanic descent possess at least one normal allele (*FMO2\*1*) coding for the full length, enzymatically active protein. Although the data on allelic frequencies reported in the different studies vary substantially, the percentages above should correspond to more than 200 million people worldwide possessing a full length, catalytically active *FMO2* in the lungs and kidneys (Veeramah et al., 2008), both tissues where *FMO2* is expressed at the highest levels (see paragraph 0). Other *FMO2* variants have been detected and are considered of minor importance, as most consist of SNPs of *FMO2\*2*, which codifies for an inactive protein anyway (Krueger et al., 2009).

Interestingly, *FMO2* is also truncated in the laboratory rat, whereas it is intact in the wild rat (Lattard et al., 2002b). In Sprague Dawley and Wistar rats, as in the major part of the human population, *FMO2* encodes a truncated protein of only 432 amino acid residues. Different from humans who carry a single mutation, these rats exhibit a double-deletion, leading to a premature stop codon and a catalytically inactive protein (Hugonnard et al., 2004). In contrast, the *FMO2* isozyme present in the lungs

of *Rattus rattus*, the wild black rat, is a 535 amino acid peptide and is catalytically active. *Rattus norvegicus*, the wild species from which all laboratory rat strains are derived, displays a *FMO2* genetic polymorphism similar to humans and has been proposed as a suitable model to study the implications of *FMO2* allelic variability in the metabolism of drugs catalysed by this isoform (Hugonnard et al., 2004). Hugonnard and co-authors investigated the allelic frequencies of *FMO2\*1* and *FMO2\*2* in a colony of *R. norvegicus* bred in captivity and found that their levels of expression were comparable (48% versus 52%, respectively). *FMO2\*1* appeared indeed to occur with a much higher incidence in *R. norvegicus* than in humans. However, these results might depend on the influence of consanguinity in the specific population of rats examined and no data are available on the frequency of the two alleles in wild rats. *FMO2* is differently expressed in the lung of *R. norvegicus*, according to the correspondent genotype: a 535 amino acid-FMO2 is found at high levels in the lung of homozygotes for the wild-type *FMO2*, while low levels or no protein at all are detected in the lungs of heterozygotes and homozygotes for the mutant *FMO2*, respectively (Hugonnard et al., 2004). In contrast, the inactive 432 amino acid-FMO2 is not present in the lung of *R. norvegicus*, even in the rats carrying only the mutant isoform. According to Hugonnard and co-authors, this is likely due to altered translation or protein instability rather than transcription impairment, because the level of mRNA in the lung is similar in mutant and wild type rats and not influenced by the *FMO2* genotype. Normally, translationally inactive transcripts that contain premature stop codons are eliminated via nonsense mRNA decay (NMD), carried out by exoribonucleases (Alberts et al., 2008). The mechanism by which the mRNA encoding the inactive *FMO2* isoform eludes mRNA degradation is not known. However, mRNA transcripts carrying nonsense mutations which are insensitive to NMD have occasionally been reported (Neu-Yilik et al., 2011), and *FMO2* may represent another example of this poorly characterised anomaly of cellular surveillance pathways.

Only limited knowledge has been gleaned to date regarding the metabolic consequences of *FMO2* polymorphism. FMO-mediated oxidative metabolism in the lung of *R. norvegicus* has been found to be dependent on the *FMO2* genotype (Hugonnard et al., 2004). No assumption has so far been made concerning the

toxicological significance of *FMO2* polymorphism in humans. Individuals with the *FMO2\*1* allele may in fact metabolise xenobiotics differently than individuals with no functional *FMO2* in the lung. Human *FMO2*, for instance, is very active in catalysing the bioactivation of thioureas with low molecular weight and one would predict that individuals expressing the *FMO2\*1* allele would be at enhanced risk of toxicity following exposure (Henderson et al., 2004b). On the other hand, the presence of the *FMO2\*1* allele may protect from the toxic effect of thioether-containing organophosphate pesticides, such as phorate and disulfoton, metabolised by *FMO2* to the correspondent sulfoxide. Organophosphates are instead bioactivated by *CYP* to the oxon, a metabolite that is orders of magnitude more potent in cholinesterase inhibition, and the presence of an active *FMO2* may result in increased detoxification (Henderson et al., 2004a).

### **1.6.3 Modulation of FMO expression**

Unlike the cytochromes P450 and many of the phase II conjugating enzymes, modulation of *FMO* expression has not been fully characterised. Early research on this subject reported that transcription of *FMOs* was predominantly regulated by genetic factors and not markedly influenced by endogenous, dietary or environmental factors (Cashman, 1995). However, there is growing evidence that several variables may influence *FMO* expression and be partly responsible for the different species- and tissue-dependent distribution patterns described in paragraph 1.5.6. It has already been mentioned that insight into the translational and post-translational regulation of the *FMO* genes has started to be gained only in the last few years: however, evidence exists since a long time that age, sex and sex steroids, hormones, nutritional status and circadian rhythms may influence the expression of different *FMO* members in different tissues (Coecke et al., 1998b; Dixit and Roche, 1984; Falls et al., 1997). Testosterone levels influence the expression of *FMOs* in both mice and rats, but in opposite ways. The hormone down-regulates the expression of *FMO3*, and to a lesser degree *FMO1*, *FMO2* and *FMO5* in the mouse liver; castration, on the other hand, leads to up-regulation of these isoforms (Falls et al., 1997; Novick et al., 2010). In contrast, rat *FMO3* activity is enhanced by testosterone, as demonstrated by the increase in *FMO3* activity levels detected during puberty, and reduced after

castration (Lattard et al., 2002a; Lemoine et al., 1991). As a consequence, overall FMO enzymatic activity in rat hepatic microsomal incubations is higher in males than in females (Coecke et al., 1998b). Tissue- and species-specific testosterone-dependent repression of FMO3 in the liver of the mouse has to be taken into consideration when this species is selected to investigate the metabolism of drugs that may represent suitable substrates for this isozyme (Ripp et al., 1999). The female mouse may represent a more reliable animal model to investigate FMO-dependent xenobiotic metabolism in the human liver, which is rich in FMO3 (Cashman, 2008). Oestrogen and progesterone appear less able to influence FMO activity in rodents (Falls et al., 1997), but have been implicated in the modulation of FMO expression in rabbits (Lee et al., 1993) and pigs (Cashman and Zhang, 2006). However, 17  $\beta$ -oestradiol as well as thyroid hormones have been seen to down-regulate the expression of FMOs in co-cultured hepatocytes from male rats (Coecke et al., 1998a; Coecke et al., 1998b). Dixit and Roche (1984) reported higher FMO activity in the liver of fed mice compared to animals starved for 24 hours and in the hepatic microsomes prepared from mice euthanased in the afternoon compared to those euthanased in the morning.

Drugs have also been seen to alter the level of FMO expression in different tissues. Oral administration of 2,3,7,8-tetrachlorodibenzo-p-dioxin (TCDD), a compound acting through the aryl hydrocarbon receptor (AHR), causes long-lasting induction of FMO2 and FMO3 in the liver of C56BL/6J mice (Novick et al., 2010). Additional studies have demonstrated that several other chemical entities binding to AHR, such as methylcholanthrene (Chung et al., 1997; Tijet et al., 2006), consistently upregulate FMO. Nitric oxide, overproduced during inflammatory conditions, was seen to suppress FMO1 transcription in the liver of rats treated with lipopolysaccharide (Park et al., 1999). Administration of the bactericidal antibiotic rifampicin up-regulates the expression of several metabolic enzymes, including FMO4 (Rae et al., 2001). Very recently, paracetamol has been seen to modulate FMO3 levels in the mouse liver (O'connor et al., 2013).

Recently, researchers have shown an increased interest in investigating the association between altered FMO expression and several pathological conditions. In



most cases, the link between FMO down-regulation or over-expression and the disease has not been elucidated; yet, it appears fundamental to know that pharmacokinetics of drugs cleared by FMOs may vary considerably in certain disorders leading to different therapeutic outcomes (Krueger and Williams, 2005). To list only a few examples, up-regulation of FMOs in the central nervous system has been detected in a mouse model of amyotrophic lateral sclerosis (Gagliardi et al., 2011). Patients with atrial fibrillation were found to express significantly increased levels of FMO1 (Kim et al., 2003). Abnormal expression of FMOs has been described in sideroblastic anaemia (Barber et al., 2000) and has been hypothesised in a number of neoplastic conditions (Krueger et al., 2006). Variations of hepatic FMO expression have been described in rodent models of type I and type II diabetes and in humans with type II diabetes (Rouer et al., 1987; Wang et al., 2000). Genetic variations of FMOs have been found to influence the progress of cardiovascular disease in a mouse model of atherosclerosis and hyperlipidaemia (Wang et al., 2011). FMO expression appeared consistently down-regulated in the liver of mice during lipopolysaccharide (LPS) induced systemic inflammation or experimental infection with *Citrobacter rodentium* (Zhang et al., 2009). FMO1 expression and activity were increased in the kidney of rats subjected to hyperosmotic conditions (Rodriguez-Fuentes et al., 2009). Investigations into the relationship between FMO deficiency or over-expression and certain diseases represent a fairly new topic in FMO research which may bring new insights into the therapy and prevention of these conditions.

## **1.7 Current research on FMOs**

Shortly after the first description and isolation of FMOs in the 70s, a considerable amount of literature was published on the structure of these enzymes and their role in phase I metabolism. During the following two decades much more information became available concerning the catalytic mechanism and structure-function relations within the FMO family. General consensus was achieved that FMO contribution to drug metabolism appeared relatively limited compared to CYP. This conclusion was supported by the fact that these proteins were regulated by a small number of genes and their expression was scantily influenced by drugs and endogenous factors (Krueger and Williams, 2005). The advent of new molecular

biology technologies and global gene expression approaches has led to a renewed interest in this subject and to reconsideration of the role attributed to this class of enzymes; indeed more drugs, previously thought to be metabolised exclusively by CYP, have been recognised as suitable substrates for FMOs (Cashman and Zhang, 2006) and several studies have documented a relationship between altered FMO expression levels and the administration of xenobiotics or the occurrence of certain pathological conditions, as detailed already in the previous paragraph.

Toxicological consequences of FMO genetic variability have been poorly addressed, mainly because of the lack of appropriate small animal models with FMO functional activity comparable to humans. We have already mentioned that FMO hepatic metabolism in the adult female mouse resembles that in humans, where FMO3 and FMO5 predominate. For other isoenzymes, such as FMO1 and FMO2, the identification of suitable animal models has proved to be more complicated. Engineered mouse lines that lack the genes encoding for FMO1, FMO2 and FMO4 have been recently developed and used to compare the effect of the antidepressant imipramine, a specific substrate of FMO1, in knockout (KO) and wild-type (WT) animals (Shephard and Phillips, 2010). The lack of FMO1 in KO mice was reported to influence the metabolism of imipramine and lead to behavioural changes: the administration of the drug in fact caused sedation in WT mice as expected, but resulted in severe tremors and spasms in KO mice (Shephard and Phillips, 2010). The authors reported that plasma and tissue concentrations of the parent drugs were increased in KO mice compared to the controls as expected, along with a dramatic reduction in the levels of imipramine N-oxide, the product of FMO1-mediated oxygenation. Interestingly, the amount of desipramine, which results from the CYP-mediated metabolism of imipramine, was increased in the brain of KO mice. The shift from a detoxification pathway represented by FMOs to bioactivation carried out by CYP was considered responsible for the behavioural changes seen in KO mice. Shephard and Phillips (2010) concluded that “studies using a knockout mouse line have identified a more important role for FMO1-mediated metabolism of imipramine than has been predicted from other studies”.

The toxicological consequences of *FMO2* polymorphism in humans are currently unknown. The mouse does not represent an ideal animal model as the levels of FMO2 in this species appear quite low, including in the lung, where FMO2 is instead predominant in other species. The rat in contrast, whose FMO2 is characterised by a genetic polymorphism identical to that occurring in humans, would be an excellent model to reproduce the effects of the different FMO2 genotypes on drug metabolism. Unfortunately, the aggressive behaviour of the wild rat, which is homozygous for the functional *FMO2* allele, limits its use as a laboratory animal and has prevented researchers from investigating this subject in more detail.

## **1.8 Aims of this work**

The work conducted in this thesis aims to investigate the contribution of FMOs to the development and adaptation to the acute pulmonary toxicity of NR678, a phenylthiourea-based rodenticide candidate, in rats. The dissertation seeks to address some of the questions which have so far not been fully answered in the literature concerning the toxicity of thiourea-related molecules and the contribution of FMOs to drug metabolism and adverse drug reactions.

Initially, the research within this thesis focused on the assessment of the target organ toxicity of NR678 and provided a means of investigating the consequences of drug-induced oxidative stress in the lungs. Investigation on the acute toxicity of NR678 allowed to a) identify the morphological changes associated with the increased vascular permeability caused by this molecule in the rat lung and b) determine the cellular targets most exposed to thiourea-related oxidative injury. An attempt was also made to isolate NR678 metabolites using liquid chromatography.

Subsequently, we investigated the development and the morphological characterisation of the adaptive response of the rat lungs to sublethal doses of NR678. The elucidation of the mechanism underlying tolerance to thiourea-related molecules was considered an interesting research field that could bring new insight into the therapeutic approach of pulmonary conditions characterised by increased vascular permeability and oxidative stress, such as acute respiratory distress syndrome (ARDS) or adverse drug reactions (e.g. bleomycin). The questions which

were addressed in this part are: 1) does the administration of low doses of NR678 lead to decreased susceptibility to further lethal doses, similarly to other thiourea-derived molecules?; and 2) is the mechanism of tolerance associated with increased clearance of oedema fluid, increased levels of sulphydryl reducing agents and/or altered expression of FMOs in the rat lungs?

A molecular approach was used to further characterise NR678-induced pulmonary acute toxicity and tolerance, studying the localisation of FMO2 mRNA in the tissues of the rat using a RNA ISH technique. This aimed to provide new insight into the tissue distribution of FMOs in this species, a subject which has not been fully characterised. The expression of FMO1 and FMO2 was then assessed in the lung of tolerant rats by ISH and quantitative PCR (qPCR) to investigate a potential role of these enzymes in the development of tolerance.

The final part of the experimental chapter aimed to address the toxicological implications of *FMO2* polymorphism in humans, by using *R. norvegicus*, whose colonies were available at BASF Pest Control Solutions. *R. norvegicus* was considered a suitable model to explore this topic, because the polymorphism seen in this species represents a natural knockout of *FMO2*. This investigation was conducted using NR678 as a test article, as uncharged small thioureas are known to be excellent substrates of FMO2. Results of this analysis may apply virtually to all molecules which are known to be metabolised by FMO2, including drugs containing a thiourea moiety.

# **Chapter 2 Materials and Methods**

2.1 Experimental animal work

2.2 Experimental procedures

2.3 Molecular biology

2.4 Enzyme assay and metabolic analysis

2.5 Statistical analysis

## 2.1 Experimental animal work

Four studies were conducted, all with oral (*gavage*) administration of the test substance, NR678 [(2,6-dimethyl-phenyl)-thiourea; for detail on the test article, see paragraph 1.1]. All animal experiments were undertaken at the BASF Widnes laboratory, a designated Scientific Procedures Establishment under the Animals (Scientific Procedures) Act (British Parliament, 1986), which implements in the UK the EU Directive 86/609/EEC. The protocols described below were approved by the University of Liverpool Animal Ethics Committee. Details on title, objective and main specifications of these studies are provided in **Table 2.1**. A summary of the main experimental procedures conducted in each study is presented in **Appendix II**.

**Table 2.1.** List of *in vivo* animal experiments conducted in this work.

Study	Study title	Rats		Duration (d)	Objective
		Strain	n.		
1	NR678: single dose acute oral toxicity study in male Wistar rats	Wistar	5	1	To identify the target organs and the toxicological changes induced by a lethal dose of NR678
2	NR678: tolerance development study in male Wistar rats	Wistar	10	7	To determine the development of tolerance to NR678 in rats pre-treated with a low, non-lethal dose and then challenged with a lethal dose
3	NR678: chrono-tolerance study in male Wistar rats	Wistar	36	14	To investigate the morphologic and mechanistic aspects of tolerance to NR678 at different time points post treatment
4	NR678: tolerance development study in male Welsh rats	Welsh	12	2	To determine the development and the patterns of tolerance in a rat strain that expresses a functional pulmonary FMO2 isoform

The time interval between the day of (first) dosing and the day of euthanasia defines the duration of the study. n.: overall number of animals used in the study. d: day(s).

## 2.2 Experimental procedures

For studies 1, 2 and 3, male Wistar rats [age range: 6-7 weeks (w), weight range: 200-250 g] were obtained from Charles River Laboratories (Margate, UK). In study 4, male rats (age range: 10 to 18 w, weight range: 200-300 g) of the so called “Welsh strain”, a warfarin-resistant strain of the Norway rat (*R. norvegicus*), derived from a wild population of rats native to Wales, was used. These rats were from an inbred colony that has been maintained at the BASF Widnes laboratory for several years. The “Welsh strain” was selected as rats from the colony were seen to carry a functional *FMO2* copy in both alleles, according to the genotyping analysis.

All rats were maintained in environmentally controlled rooms with 12 h dark-and-light cycles. They were caged in groups, with tap water and commercial rat food available *ad libitum*. On day 1 (start day of the experiment), prior to dosing with NR678, all animals were weighed and tail-marked. NR678 was formulated on the same day and administered by oral intubation at different doses (**Table 2.2**), while control rats received only the vehicle, which was polyethylene glycol 200 (PEG-200) diluted in black tea. In study 1 (acute single dose toxicity study), three male Wistar rats received a known (see paragraph 1.1) lethal oral dose (10 mg/kg) of NR678 and were euthanased at 6 h post dosing, after they had developed severe clinical signs. Controls (two animals) were culled 8 h after the administration of the vehicle. In study 2, male Wistar rats received an oral dose of 0.5 mg/kg of NR678 and, 3 h later, a dose known to be lethal upon first administration (5 mg/kg of NR678). Clinical signs and mortality were monitored during the following 7 d. The design of the chronotolerance study (study 3) is illustrated in **Table 2.2** and **Figure 2.1**. In study 4, Welsh rats received an oral dose of 0.5 mg/kg of NR678 and were euthanased at 3, 6 and 24 h post dosing.

In all studies, clinical signs were recorded at 0, 0.5, 1, 2, 4, 6 and/or 8 h after dosing and then once or twice daily, until the end of the experiment. They were graded based on their severity, from mild (clinical observation at its least discernible extent) to severe (when the clinical sign caused major distress to the animal and/or impaired normal physiologic functions). Moderate was used to describe intermediate grades.

Any animal that exhibited severe clinical signs such as severe tachypnoea and dyspnoea was constantly monitored and was culled according to the standard operating procedures in force before experiencing severe pain, distress or death.

**Table 2.2.** Experimental design and animal details of the *in vivo* studies. Study 1: single dose acute toxicity study. Study 2: tolerance development study in Wistar rats. Study 3: chronotolerance study. Study 4: tolerance development study in Welsh rats.

### Study 1

Group	Treatment	Dose (mg/kg)	n.	Euthanasia	Animal ID
1	Vehicle	-	2	8 h	10L-1245, 10L-1246
2	NR678	10	3	6 h	10L-1247 to 10L-1249

### Study 2

Group	Treatment	Dose (mg/kg)	n.	Euthanasia	Animal ID
1	NR678	0.5 (time 0) + 5 (3h)	5	7 d	10L-4742 to 10L-4746

### Study 3

Group	Treatment	Dose (mg/kg)	n.	Euthanasia	Animal ID
1	Vehicle	-	3	24 h	11L-2402 to 11L-2404
2	NR678	5	3	6 h	11L-2405 to 11L-2407
3	NR678	0.5	3	3 h	11L-2420 to 11L-2422
			3	6 h	11L-2423 to 11L-2425
			3	24 h	11L-2426 to 11L-2428
			3	7 d	11L-2429 to 11L-2431
			3	14 d	11L-2435 to 11L-2437
		0.5 (time 0) + 5 (d 14)	3	14 d	11L-2432 to 11L-2434
4	NR678	0.5 (time 0) + 5 (3 h)	3	24 h	11L-2408 to 11L-2410
			3	7 d	11L-2411 to 11L-2413
			3	14 d	11L-2417 to 11L-2419
		0.5 (time 0) + 5 (3 h) + 5 (d 14)	3	14 d	11L-2414 to 11L-2416

### Study 4

Group	Treatment	Dose (mg/kg)	n.	Euthanasia	Animal ID
1	Vehicle	-	3	24 h	12L-2251 to 12L-2253
2	NR678	0.5	3	3 h	12L-2254 to 12L-2256
3			3	6 h	12L-2257 to 12L-2259
4			3	24 h	12L-2260 to 12L-2262

Animal ID (identification) refers to the case numbering system used by the Histology Laboratory, Veterinary Laboratory Services, School of Veterinary Science, University of Liverpool, where the tissue samples were processed for the histological examination. n: total number of animals in the group.



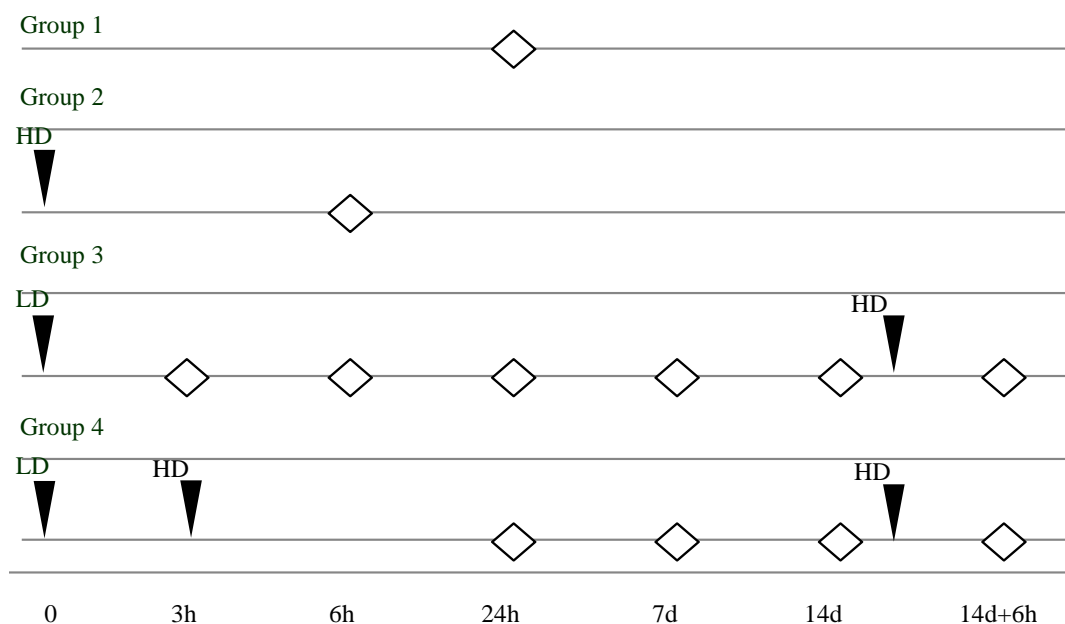


**Figure 2.1.** Experimental design of the chronotolerance study (study 3). Rats ( $n = 36$ ) were divided in 4 groups according to the treatment received. Group 1: vehicle control; group 2: oral NR678 administration at a dose of 5 mg/kg (high dose, HD); group 3: oral NR678 administration at a dose of 0.5 mg/kg (low dose, LD); group 4: oral NR678 administration of LD, followed after 3h by the HD. Rats were euthanased at different time points (3 rats per time point; diamonds). Separate cohorts of rats from both groups 3 and 4 were challenged on day 14 with the HD. Arrowheads represent the time of dosing (with LD or HD).

## 2.2.1 Post mortem examination

### 2.2.1.1 Necropsy, tissue sampling, processing and histology

For euthanasia, rats were anaesthetised with carbon dioxide ( $\text{CO}_2$ ), followed by exsanguination. Body weights were collected at necropsy to allow calculation of organ to body weight ratios. A complete necropsy, including a thorough external and internal gross post mortem examination was performed on each rat. Blood was sampled from the abdominal *vena cava*, using a 5 mL syringe connected to a butterfly intravenous cannula (23 G). Any fluid that was present in the thoracic cavity of treated animals (study 1) was aspirated through a syringe, quantified and cytological specimens prepared, stained with May Grunwald Giemsa and examined. Liver, lung and brain from each rat of study 3 were weighed after exenteration. Representative samples of the organs and tissues listed in **Table 2.3** from all animals

and, when present, any tissue exhibiting a macroscopic abnormality were fixed in 4% buffered paraformaldehyde (PFA) for histological examination. Further samples of brain, heart, liver, lung, kidney and/or spleen were rapidly frozen in liquid nitrogen and stored at -80°C for further analyses (glutathione measurements and RNA isolation).

**Table 2.3.** Alphabetical list of organs and tissues that were examined macroscopically and histologically.

Adrenal glands (cortex and medulla) <sup>a</sup>	Mammary gland
Aorta (thoracic)	Optic nerves
Bone and joint (femoral-tibial joint)	Pancreas <sup>a</sup>
Bone marrow (sternum)	Peripheral nerve (sciatic)
Brain <sup>a, b, c</sup>	Pituitary gland
Caecum	Prostate gland
Colon	Salivary gland (submandibular)
Duodenum	Seminal vesicles
Epididymides	Skeletal muscle (thigh, diaphragm)
Oesophagus	Skin
Eyes	Spinal cord (cervical and lumbar)
Gut associated lymphoid tissue	Spleen <sup>a, b</sup>
Harderian gland	Stomach (forestomach and glandular)
Heart <sup>a, b</sup>	Testes
Ileum	Thymus <sup>a, b</sup>
Jejunum	Thyroid/parathyroid glands
Kidneys <sup>a, b</sup>	Tongue
Liver <sup>a, b, c</sup>	Trachea
Lungs <sup>a, b, c</sup>	Urinary bladder
Lymph nodes (mandibular and mesenteric)	

All tissues listed (except the femoro-tibial joint) were processed and examined histologically in study 1. a: Organs and tissues processed for histological examination in study 3. b: organs and tissues processed for histological examination in study 4. c: organs weighed in study 3.

According to the literature published on the acute toxicity of thiourea, the main pathological changes following the administration of the thiourea-based molecule NR678 were expected in the lungs (Ziegler-Skylakakis, 2003). In order to achieve optimal fixation and preservation of the lung, a specific fixation and sampling protocol was developed and applied (**Figure 2.2**), taking into consideration the known literature on the methods for routine lung fixation in rodents. Lungs were

exenterated and fixed through gentle intratracheal instillation of PFA in all studies, except study 1, which represented the initial full pathological screening. Instillation of the broncho-alveolar unit with fixative washes out the cells located within the alveolar lumen and alters their original distribution, confounds the presence and the quantification of pulmonary fluid and may lead to damage and rupture of the thin alveolar septa (Braber et al., 2010; Renne et al., 2001). However, early fixation of the lower broncho-alveolar tract allows clear identification of pulmonary cell types and eliminates several artefacts associated with a crushed, non inflated lung parenchyma (Renne et al., 2001). Precautions were taken to avoid over-inflation and thereby artefactual emphysematous changes.

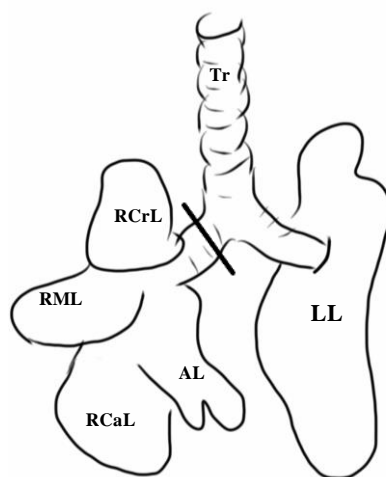


**Figure 2.2.** Sketch illustrating the sampling protocol for the lungs (ventral view). Light and electron microscopy were performed on the left (LL) and the right cranial (RCrL) lobes, respectively. The remaining right lobes (RML: right median lobe, RCaL: right caudal lobe, AL: accessory lobe) were snap frozen in liquid nitrogen and stored at  $-80^{\circ}\text{C}$ . In study 3, the right hilus was ligated (line) and the right lobes were dissected free from the bronchi and vessels and removed. The wet weight of the whole right lung was then recorded. Tr: trachea.

After 48 h fixation in PFA, the selected (**Table 2.3**) organs and tissues from all rats were trimmed, dehydrated in graded alcohol and routinely paraffin wax embedded. Sections ( $3\text{-}5\ \mu\text{m}$  thick) were prepared, mounted on glass slides, deparaffinised in xylene, rehydrated through graded alcohols and stained with haematoxylin and eosin (HE) for the histological examination. In addition, a range of routine special stains for the demonstration of fibrin and eosinophils were performed on consecutive

sections from the lungs of all animals from study 1 (**Table 2.4**). The Masson Trichrome stain was applied for the visualisation of collagen fibres in the lungs of selected animals from studies 1 and 3 (**Appendix II**). All stains were performed by the technicians in the Histology Laboratory, Veterinary Laboratory Services, School of Veterinary Science, University of Liverpool, according to routine staining protocols. Appropriate control tissues were stained alongside to monitor the conditions and the quality of the staining procedure.

**Table 2.4** List of special stains carried out for the visualisation of specific tissue components (fibrin and collagen) and the identification of eosinophils.

Special stain	Target	Staining pattern
<b>Martius Scarlet Blue</b>	Fibrin	Muscle and fibrin: red. Nuclei: brown/black. Collagen: blue. Erythrocytes: yellow
<b>Phosphotungstic acid-haematoxylin</b>	Fibrin	Nuclei, erythrocytes, fibrin: blue. Cytoplasm: pink to brown red. Collagen: brown-pink
<b>Fraser Lendrum</b>	Eosinophils and fibrin	Fibrin, keratin, some cytoplasmic granules: orange/red. Collagen: green
<b>Masson Trichrome</b>	Collagen	Nuclei: black. Muscle, cytoplasm: red. Collagen: blue to green

The histological findings were classified with standard pathological nomenclature and severities were graded on a scale of 1 to 5 as slight, mild, moderate, marked or severe with “slight” applied when the finding was the least extent discernible and “severe” the greatest extent possible. Microscopic findings that are not usually graded were listed as present. The findings were reviewed by Prof. Anja Kipar, Dr.med.vet.habil., Dipl. ECVP, MRCVS.

### **2.2.1.2 Immunohistology of the lungs of NR678-treated rats**

For the characterisation of the cell types populating the alveolar unit (**Figure 2.3**) and to determine the presence of apoptotic and proliferating cells in alveoli, immunohistology (IH) was employed.

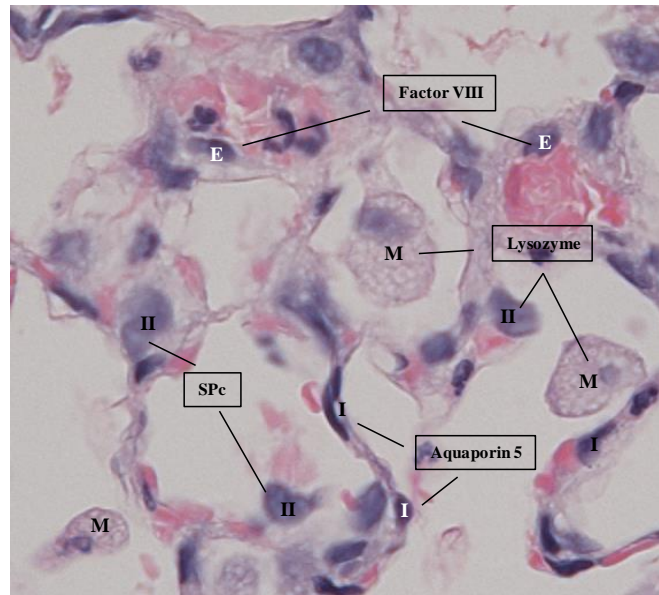


**Figure 2.3.** Cell types in the alveoli and their identification based on the expression of cell markers by immunohistology (boxed). E: endothelial cells; M: macrophages; I: type I pneumocytes; II: type II pneumocytes.

A rabbit polyclonal antibody reacting with rat aquaporin 5 (AQP-5) was used as a specific marker of type I pneumocytes. AQP-5 is a water channel protein involved in membrane osmotic water permeability and is found on the apical membranes of glandular epithelium in the airways, in the salivary glands and in type I pneumocytes of several species (Raina et al., 1995). Surfactant protein C (SP-C), a small hydrophobic protein found in the lamellar bodies of type II pneumocytes (Beers and Lomax, 1995), was employed as a selective marker for type II pneumocytes (Kasper and Singh, 1995). Lysozyme is an antibacterial peptide found in several secretions (tears, sweat, saliva) and in the lysosomal granules of leukocytes (Mitchell and Cotran, 2007a). Rat alveolar macrophages are strongly positive when stained with immunohistological methods for the detection of lysozyme (Klockars and Osserman, 1974). However, in the rat, lysozyme is also synthesised by type II pneumocytes, which is in contrast to man, where the protein can be detected in the cytoplasm of submucosal glandular epithelial cells, but not in type II pneumocytes (Singh et al., 1988). Endothelial cells were identified using immunohistology for von Willebrand factor (factor VIII-related antigen), which is expressed in specific cytoplasmic organelles known as Weibel-Palade bodies. This antigen is considered a sensitive marker of normal and activated endothelial cells (Zhang et al., 2010). Apoptotic cells

were labelled using an antibody against cleaved caspase 3, an executioner caspase of the apoptotic cascade (Mitchell and Cotran, 2007b). Proliferating cell nuclear antigen (PCNA) is a protein expressed in the nucleus of cells during DNA synthesis and in the cytoplasm during mitosis; it was used in this work as a marker of cell proliferation (Whitfield et al., 2006). IH was performed on PFA-fixed and paraffin-embedded lung sections, using the peroxidase anti-peroxidase (PAP) method, as previously described (Kipar et al., 1998). Briefly, sections were deparaffinised in xylene ( $2 \times 5$  min) and rehydrated in decreasing concentrations of ethanol ( $2 \times 3$  min washes in 100% ethanol, followed by  $1 \times 3$  min wash in 96% ethanol). Endogenous peroxidase was inactivated by incubation at room temperature (RT) for 30 min with 0.5% (v/v) hydrogen peroxide dissolved in methanol. Sections were washed twice with Tris-buffered saline (TBS, 0.1 M Tris-HCl with 0.9% NaCl, pH 7.4) and underwent antigen retrieval by incubation with 10 mM citrate buffer [0.9% (v/v) 0.1 M citric acid and 1% (v/v) 0.1 M sodium acetate] at pH 4.0 or 6.0 or with protease. Slides were then washed with TBS and incubated with 50% swine serum in TBS (10% rat serum for PCNA) for 10 min at RT to prevent any non-specific binding of the antiserum. Subsequently, sections were incubated for 15–18 h at 4°C with the primary antisera, followed by incubation with secondary antisera at RT for 30 min and a final 30 min incubation with rabbit or mouse PAP (1:100 in TBS) at RT (**Table 2.5**). Between each incubation step, slides were washed with TBS. Sections were then incubated for 10 min at RT with 0.05% 3,3'-diaminobenzidine tetrahydrochloride (DAB) and 0.01% H<sub>2</sub>O<sub>2</sub> in 0.1 M imidazole buffer (0.1 M imidazole, 0.1 M HCl pH 7.1), washed  $3 \times$  in TBS and  $1 \times$  in distilled water and counterstained for 1 min with Papanicolaou's haematoxylin (Merck, Darmstadt, Germany; 20 mL in 400 mL distilled water), followed by rinsing for 5 min in tap water and dehydration in ascending alcohols, clearing in xylene, coverslipping and mounting. All immunohistological stains were performed by Ms Valerie Tilston, research technician at Histology Laboratory, Veterinary Laboratory Services, School of Veterinary Science, University of Liverpool.

**Table 2.5.** Summary of the antibodies and other reagents used for immunohistology.

Antibody	Antigen retrieval	Block	Primary antibody dilution	Secondary antibody dilution	Detection
<b>Caspase 3</b> (Cell Signaling 9664)	Citrate pH 6.0	20% ss in TBST	1:50 in 20% ss in TBST	Swine anti Rabbit IgG 1:100 in 20% ss in TBST (Dako Z0196)	PAP Rabbit 1:20 in 20% ss in TBST (Covance SMI)
<b>PCNA</b> (Dako M0879)	Citrate pH 4.0	10% rat serum in TBST	1:100 in TBST	Rat anti Mouse 1:100 in TBST (Jackson Immuno Research 415-005-166)	PAP Mouse 1:500 in TBST (Jackson Immuno Research)
<b>Aquaporin 5</b> (Abcam ab78486)	None	20% ss in TBST	1:100 in 20% ss in TBST	Swine anti Rabbit 1:100 in 20% ss in TBST	PAP Rabbit 1:20 in 20% ss in TBST
<b>Factor VIII</b> (Dako A0082)	Protease	ss:TBST 1:2	1:1000 in 20% ss in TBST		
<b>SP-C</b> (Santa Cruz sc-13979)	None	20% ss in TBST	1:50 in TBST		
<b>Lysozyme</b> (Dako A0099)	Protease	ss:TBST 1:2	1:1000 in 20% ss in TBST		

ss = swine serum. TBST = 1× TBS Buffer + 0.05% Tween 20

An attempt was made to quantify the number of alveolar macrophages and type II pneumocytes in the lung of rats from study 3. This was done based on the number of SP-C expressing cells, which are known to be type II pneumocytes (Kasper and Singh, 1995). Cells that expressed lysozyme were identified in the alveolar lumen (alveolar macrophages) and lining the alveoli (type II pneumocytes and macrophages). Cell counts were performed as follows. Each stained slide was placed on the optical photomicroscope (Nikon Eclipse 80i, Kingston upon Thames, UK) and examined with the 40 × objective (400-fold magnification). Ten fields were selected (five fields from each lung section on the slide), avoiding areas at the periphery of the section or regions containing large bronchial and vascular structures, to examine comparable numbers of alveoli. Immuno-stained cells for both SP-C and lysozyme, as defined above, were calculated as a percentage of the total cells counted in each field. For the quantification of PCNA-positive proliferating cells in the lung of rats from study 3, twenty random fields (ten fields from each lung section on the slide) were evaluated at the 40 × magnification and the PCNA proliferative index was expressed as the average number of positive cells/field. Occasional positive cells other than alveolar lining cells, such as bronchial or bronchiolar epithelial cells,

endothelial cells in arteries and veins as well as inflammatory cells were not included in the counts.

### **2.2.1.3 Transmission electron microscopy of the lung of NR678-treated rats**

From selected rats (one rat/group; study 3), approximately 1 cm<sup>3</sup> samples of lung tissue were rapidly removed from the cranial right lobe (see figure **Figure 2.2**), placed in approximately 2 mL of 2.5% glutaraldehyde in 0.1 M sodium cacodylate buffer (pH 7.4) and sliced with a stainless steel razor blade into 1-2 mm<sup>3</sup> cubes. These specimens were fixed in glutaraldehyde at 4°C and subsequently processed for transmission electron microscopy (TEM) by Ms Marion Pope, Electron Microscopy Unit, Veterinary Laboratory Services, School of Veterinary Science, University of Liverpool. Briefly, specimens were washed in 0.1 M sodium cacodylate buffer and fixed in 1% osmium tetroxide in phosphate buffer/distilled water for 90 min. After rinsing in distilled water, specimens were stained with 2% uranyl acetate in 0.69% maleic acid for 90 min and dehydrated in ascending concentrations of ethanol, followed by acetone. Tissues were subsequently infiltrated with resin (TAAB Laboratories Equipment Ltd, Aldermaston, UK) in acetone at concentrations of 30%, 70% and 100% (w/v) for 1 h each. The specimens were transferred into polyethylene embedding capsules filled with fresh 100% resin, where they were left overnight for the polymerisation step. Semi-thin sections (1 µm) were prepared from resin-embedded blocks using an ultramicrotome (Reichert-Jung Ultracut; Munich, Germany) with a diamond knife (Diatome Ltd.; Biel, Switzerland), then stained with toluidine blue and examined under the light microscope, to choose areas of interest (those exhibiting the main findings identified in the HE stained sections) for the preparation of ultrathin sections. Ultrathin sections (60 nm) were prepared with a diamond knife, mounted on copper grids, stained with Reynold's lead citrate and examined with a transmission electron microscope (Philips EM208S, Cambridge, UK).



#### **2.2.1.4 Determination of the cellular localisation of FMOs in rat tissues by *in situ* hybridisation (ISH)**

*In situ* hybridisation (ISH) was undertaken to investigate the distribution and localisation of FMO mRNA in the tissues of untreated rats from studies 3 and 4. Among the riboprobes prepared for FMO1 to 5, only the riboprobe complementary to the mRNA of FMO2 yielded satisfactory signals. Once optimised, RNA-ISH was used to compare the localisation of FMO2 mRNA between control rats and those receiving NR678 (5 mg/kg and 0.5 mg/kg) in study 3. Details on the synthesis of RNA probes for RNA-ISH are provided in paragraph 2.3.6.

##### **2.2.1.4.1 Preparation of tissue sections for RNA *in situ* hybridisation**

Sections (3-5  $\mu\text{m}$ ) from PFA-fixed, paraffin wax-embedded tissues were mounted on slides and deparaffinised in xylene (2  $\times$  for 5 min), then washed twice in 100% ethanol (5 min), once for 5 min in 96% ethanol in diethylpyrocarbonate (DEPC) water and once in 70% ethanol in DEPC water (5 min). Slides were then rinsed for 5 min in DEPC water and transferred into a nuclease-free coplin jar containing DEPC water (1 min). They were then washed in 1  $\times$  phosphate buffered saline (PBS, VWR International; Lutterworth, UK) for 5 min and incubated for 20 min in 0.2 M HCl at RT to reduce cross-linking of proteins. Proteolysis was continued with two 30 min washes with 2  $\times$  salt sodium citrate (SCC, VWR International) plus 5 mM EDTA at 50°C and exact 15 min incubation at 37°C with proteinase K solution [1 M Tris, 0.1 M CaCl<sub>2</sub>, DEPC water, proteinase K (Roche; Burgess Hill, UK)]. The proteinase K concentration was determined empirically and varied from 1 to 5  $\mu\text{g}/\text{mL}$ ; for the final FMO2 RNA-ISH, a concentration of 2  $\mu\text{g}/\text{mL}$  was used. The reaction was stopped by washing the slides in 0.2% (v/v) glycine in PBS at RT for 5 min. Sections were post-fixed in 4% PFA at RT for 4 min and then washed twice in 1  $\times$  PBS for 1 min and once in 1  $\times$  PBS plus 5 mM magnesium chloride (MgCl<sub>2</sub>) for 15 min. In order to reduce the background and inactivate RNases, slides were immersed in 0.25% (v/v) acetanhydride in 0.1 M triethanolamine (pH 7.5, VWR International) for 10 min and then rinsed twice in 1  $\times$  PBS at RT for 1 min each and then once for 15 min.

#### 2.2.1.4.2 Prehybridisation and hybridisation

As a prehybridisation step, sections were incubated for 1 h at 52°C in prehybridisation buffer, the composition and preparation of which are detailed in **Appendix III**. Hybridisation was carried out by covering each section with 40 µL of the appropriate digoxigenin-labelled riboprobe, diluted 1:200, 1:100 or 1:50 (final concentration of FMO2 riboprobe: 1:200) in hybridisation buffer mix (see **Appendix III**). Once the hybridisation solution was added, the sections were covered with hydrophobic gel-bond film and sealed with rubber glue (Fix-O-Gum; Marabu, Bucks, UK) to prevent evaporation, then placed in a hybridisation chamber and incubated overnight at 37°C or 52 °C (37°C for the FMO2 riboprobe). The coverslip was then removed and the sections were returned to a coplin jar, where they underwent a series of stringent post-hybridisation washes [2 × 15 min wash in 6 × SCC with 45% (v/v) formamide at 42°C; 2 × 5 min wash in 2 × SCC at RT; 2 × 15 min wash in 0.2 × SCC at 50°C] to remove unbound probes.

#### 2.2.1.4.3 Detection of hybridised probes

After equilibration in Buffer 1 (see **Appendix III**) for 1 min, non-specific binding was blocked by incubation with blocking solution [2% (v/v) sterile normal sheep serum (Sigma), 0.3% (v/v) Triton X-100 in Buffer 1] at RT for 30 min. For the demonstration of probe bound to tissue mRNA, slides were incubated in alkaline phosphatase-coupled anti-digoxigenin antibody (anti-DIG-AP Fab fragments, Roche; 1:200 in blocking solution) for 2 h at RT. They were then washed twice in Buffer 1 at RT for 15 min and equilibrated for 2 min at RT in Buffer 3 (see **Appendix III**). Finally, sections were incubated at RT in the dark with staining solution, composed of Buffer 3, three SIGMAFAST™ BCIP®-NBT tablets [containing 0.15 mg/mL of 5-bromo-4-chloro-3-indolyl phosphate (BCIP) and 0.30 mg/mL of 4-nitro tetrazolium chloride (Nitro blue tetrazolium, NBT)] and 0.05% (w/v) levamisole. The development of the signal was monitored regularly using a microscope and the reaction was stopped after 4 to 8 h by submerging the sections in Buffer 4 (see **Appendix III**) for 10 min and subsequent rinsing in nuclease-free water for at least 5 min. The sections were counterstained for 10 sec using Papanicolaou's haematoxylin diluted 1:20 in distilled water (see paragraph 2.2.1.2) before mounting

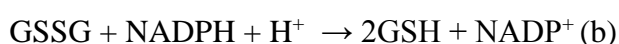
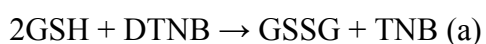
with glycer-gel (Dako; Ely, UK) and coverslipped. The slides were left to dry in the dark until microscopic examination. Positive hybridisation resulted in a dark brown-black cytoplasmic precipitate. Intensity of the signal was defined as weak (light brown granular staining that could however be clearly differentiated from background staining) or strong (diffuse intense dark brown-black cytoplasmic staining, often obscuring the nucleus); intermediate degrees were classified as moderate. A probe with known hybridisation pattern was included in each run to confirm the correct performance of the protocol. For this purpose, a DIG-labelled probe complementary to murine herpesviral tRNA, which has been optimised in our laboratory, was selected. Control tissues included cell pellets obtained from viral cultures or sections of lungs and upper airways from mice infected with the virus.

FMO2 RNA-ISH was applied to sections from liver, lung, kidney and brain of control rats from studies 3 and 4. In each run, sections were hybridised with the FMO2 antisense probe and with the correspondent FMO2 sense probe. The expression of FMO2 mRNA in the lungs of control rats and those receiving NR678 (5 mg/kg and 0.5 mg/kg) was compared in a single run, where the lungs of all animals from study 3, except those challenged on day 14 with a dose of 5 mg/kg of NR678, were hybridised with the FMO2 antisense riboprobe; the sense probe was applied to the lung sections of one animal/ each endpoint (1/3 rats). The staining reaction in this run was stopped in all sections at 5 h after the start of the incubation.

### **2.2.2 Determination of hepatic and pulmonary glutathione levels and protein concentration in NR678-treated rats**

Total (oxidised and reduced) glutathione and protein amounts were determined in the liver and the lungs of all animals in study 3. Briefly, approximately 50 mg of liver tissue (right lateral lobe) or 200 mg of lung tissue (right caudal lobe) was homogenised in 200  $\mu$ L 6.5% (w/v) 5-sulfosalicylic acid and 800  $\mu$ L GSH stock buffer (143 mM  $\text{NaH}_2\text{PO}_4$  and 6.3 mM EDTA in distilled water, pH 7.4), using a manual glass homogeniser. The homogenates were incubated on ice for 10 min and then pelleted through centrifugation at 20,000 g for 5 min. The supernatant was collected and 1 mL of 1 M NaOH was added to each protein pellet and incubated at

60°C for 1 h. Samples were then stored at -80°C until the Lowry assay was carried out. The supernatant was used for the GSH assay which represented modified, previously published methods (Owens and Belcher, 1965; Vandeputte et al., 1994). It is based on the addition of 5-5'-dithiobis[2-nitrobenzoic acid] (DTNB, Ellman's Reagent) to the sample which triggers a chemical reaction in which GSH is constantly recycled (see below). DTNB reacts with thiols, including reduced GSH, leading to their oxidation to a disulphide (GSSG or GS-TNB) with the stoichiometric formation of 5-thio-nitrobenzoic acid (TNB). The latter is a chromophore, whose rate of formation can be detected at 412 nm with a spectrophotometer and is proportional to the sum of GSH and GSSG present. The GS-TNB or GSSH are subsequently reduced to GSH by the highly specific enzyme glutathione reductase, in the presence of NADPH, releasing a second TNB molecule and recycling the GSH (Rahman et al., 2006). The principle of the colorimetric determination of GSH levels using DTNB is exemplified as follows:



In the presence of NADPH, glutathione reductase re-converts GSSG (or the GSH adduct GS-TNB) into the reduced form (GSH; b). This in turn reduces DTNB to TNB (a). The formation of TNB is evaluated by measuring the absorbance at 412 nm (Anderson, 1985).

For the assay, 20 µL of supernatant diluted 1:10 and 1:20 or GSH standards (0-80 nM/mL) were added in duplicate to a 96-well microplate, followed by the addition of 20 µL GSH stock buffer to neutralise the pH. 200 µL of daily assay reagent (1 mM DTNB, 0.34 mM NADPH in GSH stock buffer) was added to each well. This was followed by an exact 5 min incubation at RT. The enzymatic reaction described above was initiated by the addition of 50 µL GSH reductase (6.96 U/mL in GSH stock buffer). GSH formation was followed at 412 nm for 2.5 min in a MRX microplate reader (Dynotech Laboratories, Billingham, UK). All reagents were covered in aluminium foil to protect them from light. Soluble protein levels were measured using the Lowry assay (Lowry et al., 1951), which is based on the

reactivity of the protein N terminus with divalent cupric ions under alkaline conditions. Monovalent  $\text{Cu}^+$  and the aromatic protein residues cause the reduction of a phenol reagent (Folin and Ciocalteu's phenol reagent, Sigma), resulting in differential, protein concentration dependent colour intensity, which can be measured at 750 nm. 50  $\mu\text{L}$  of the liver and lung protein pellet dissolved in NaOH or standard bovine serum albumin (BSA) dilutions (1-200  $\mu\text{g}/\text{mL}$ ) were added in duplicate to a 96-well clear plate, together with 50  $\mu\text{L}$  Lowry reagent (0.5 mL 1% copper sulphate, 0.5 mL 2% sodium potassium tartrate, 10 mL sodium carbonate in 0.5 M NaOH). 150  $\mu\text{L}$  of Folin reagent (1:10 in water) was added to each well. After incubating at RT for 30 min, the absorbance was read at 750 nm with a MRX microplate reader.

## **2.3 Molecular biology**

### **2.3.1 Extraction of RNA from the lung**

Total RNA was extracted from the lung right lobes of all animals from studies 3 and 4 that had been stored at  $-80^{\circ}\text{C}$ . Approximately 50-100 mg of tissue was placed in RNase-free 2 mL Eppendorf tubes and 200  $\mu\text{L}$  of Trizol Reagent (Sigma) was added to each sample. Tissues were homogenised thoroughly using disposable RNase-free Eppendorf micropestles. After the addition of further 800  $\mu\text{L}$  of Trizol Reagent, the samples were incubated for 5 min at RT to facilitate precipitation of non-RNA cellular components. 200  $\mu\text{L}$  of 100% chloroform was added to each sample, followed by vigorous shaking by hand for 15 sec and vortexing for 15 sec. The tubes were left to incubate for 2-3 min at RT and then centrifuged at  $12,000 \times g$  for 15 min at  $4^{\circ}\text{C}$  to allow separation of the mixture into different phases, the uppermost of which being a colourless aqueous layer, containing the RNA. The aqueous phase was transferred, without disturbing the interphase, into a new 2 mL Eppendorf tube and 500  $\mu\text{L}$  of isopropyl alcohol was added to precipitate the RNA from the solution. The mixture was incubated at RT for 10 min until a white top layer had formed and then centrifuged for 10 min ( $13,000 \times g$ ,  $4^{\circ}\text{C}$ ). The supernatant was carefully removed without disturbing the gel-like pellet of precipitated RNA and 1 mL of chilled 75% ethanol was added to the pellet which was then spun for 5 min ( $7,500 \times g$ ,  $4^{\circ}\text{C}$ ). The supernatant was again discarded and the pellet air-dried for 5-10 min. Finally, the

pellets were dissolved in 44  $\mu\text{L}$  (or multiples for the most concentrated samples) of RNase-free water. An aliquot of the resultant RNA from each sample was quantified using a NanoDrop spectrophotometer (Labtech International; Uckfield, UK) and the RNA either stored at  $-80^{\circ}\text{C}$  or subjected to DNase treatment.

### **2.3.2 DNase treatment of RNA**

Rigorous DNase treatment was performed on RNA samples on the same day or the day after RNA isolation, using a DNA-free DNase kit [Life Technologies Ltd. (Ambion®); Paisley, UK] according to the manufacturer's instructions. Briefly,  $10 \times$  DNase buffer and 0.5  $\mu\text{L}$  of DNase I were added to the tubes containing the isolated RNA, proportionately to the volume of the RNA solution (44  $\mu\text{L}$  or multiples). Samples were incubated at  $37^{\circ}\text{C}$  for 20 min in a water bath, followed by addition of further 0.5  $\mu\text{L}$  of DNase I and further incubation at  $37^{\circ}\text{C}$  for 20 min. Afterwards, 1/10 of the volume of DNase inactivation reagent was added to each tube, which was then incubated at RT for 2 min while it was mixed frequently. The tubes were centrifuged at  $10,000 \times g$  for 1.5 min and the resultant RNA was transferred to new RNase-free 500  $\mu\text{L}$  tubes. An aliquot of RNA from each tube was quantified using the NanoDrop spectrophotometer. All RNA samples with a ratio of adsorption at 260 nm vs 280 nm ( $A_{260}/280$ ) between 1.9 and 2.1 were deemed suitable for reverse transcription, whereas samples with ratio values outside this range were discarded. The integrity of total RNA was assessed running an aliquot of the RNA (selected samples only) on agarose gel stained with SYBR® Safe DNA Gel Stain (Life Technologies, Paisley, UK). Sharp, clear 28S and 18S RNA bands, with the former twice as intense as the 18S band, were considered a reliable indicator of RNA integrity (Bustin et al., 2009).

### **2.3.3 Reverse transcription of RNA into complementary cDNA**

The Improm-II Reverse Transcriptase kit (Promega; Southampton, UK) was used for the synthesis of cDNA from isolated and DNase-treated RNA. A starting volume equivalent of 2.5  $\mu\text{g}$  RNA and 1.0  $\mu\text{L}$  of Oligos (dT16) were added to RNase-free water (25  $\mu\text{L}$  reaction) and heated at  $70^{\circ}\text{C}$  for 5 min on a heating block to promote their annealing to the 3' end of any polyadenylated RNA molecule and its priming

for cDNA synthesis. Afterwards, the tubes were immediately stored on ice and 10  $\mu$ L  $5 \times$  RT buffer, 8  $\mu$ L  $MgCl_2$  (25 mM), 1  $\mu$ L dNTP mix (10 mM), 2.5  $\mu$ L reverse transcriptase enzyme and nuclease-free water were added to make up a total volume of 50  $\mu$ L. The solutions were incubated in a thermal cycler using the following conditions: 25°C for 5 min, 42°C for 60 min and 70°C for 15 min. The resultant cDNA was diluted by adding 200  $\mu$ L nuclease-free water to each sample to achieve a final concentration of 10 ng/ $\mu$ L. cDNA samples were stored at -20°C until they were used in the PCR. Control reactions were run in parallel in order to reveal the presence of contaminating templates (negative control, no template) or to verify the absence of contaminating DNA template (negative reaction, no reverse transcriptase).

### **2.3.4 Conventional polymerase chain reaction (PCR)**

PCR was used for the amplification of the cDNA. The PCR products then served as templates for the synthesis of RNA probes for RNA-ISH (molecular subcloning, see paragraph 2.3.6). In addition, conventional PCR was used to test the specificity of the primers and optimise the efficiency of the amplification prior to performing qPCR. In addition, a nested PCR method was employed for the characterisation of *FMO2* (see paragraph 2.3.7.3). The list of the primers used for cloning purposes is provided in **Table 2.6**. Primer pair sequences were designed using Primer3Web, Version 3.0.0, a free online primer designing tool (Rozen and Skaletsky, 2000). The basic local assignment search tool (BLAST) search engine (Altschul et al., 1990) was used to test the specificity of the primers against the whole rat genome database. The following parameters were taken into consideration for primer selection whenever possible: primer length [18-23 base pairs (bp)], desired product length (350-450 bp), melting temperature (between 52°C and 65°C), GC content (40-65%) and the lack of secondary structures (hairpins, self and cross primer dimers) and cross homology. Primer pair sequences for *FMO2* were obtained from Hugonnard et al. (2004).

**Table 2.6.** Primers used in conventional PCR (for subcloning).

Primer name	NCBI reference sequence	Primer Sequence 5' → 3'	Melting t°C	GC %	Product length (bp)
<b>FMO1 forward</b>	NM_012792.1	GATGACCTCCTGACCTCG	60.9	61.1	401
<b>FMO1 reverse</b>		GGGGTTGGGTGTCTCTGG	65.7	66.6	
<b>FMO2 forward</b>	NM_144737.2	TCAAAGACCCTAAACTGGCTGTG	60.7	47.8	282
<b>FMO2 reverse</b>		AGGCGGTGATGGAGAAAAGTG	60.6	52.3	
<b>FMO3 forward</b>	NM_053433.2	TGCCATCCCCACAACCGACCTG	67.0	63.6	449
<b>FMO3 reverse</b>		ACAAAGCAATGAGCACTGGAACA	61.5	43.4	
<b>FMO4 forward</b>	NM_144561.2 (variant 2)	GGACGGAGCCAGAAATGCCA	62.8	60	364
<b>FMO4 reverse</b>		GCCTTGCTTTATGACAACCTGCCCT	65.7	52	
<b>FMO5 forward</b>	NM_144739.1	GGACAGCCAGCGTCATAC	57.8	61.1	370
<b>FMO5 reverse</b>		AGTGAAGCGGGAGCATTG	60.3	57.8	

Reactions were carried out using the GoTaq® Flexi DNA Polymerase kit (Promega). The PCR mixture contained: 5 µL of 10 × green or colourless (for cloning) buffer, 4 µL of 25 mM MgCl<sub>2</sub>, 1 µL of 10 mM dNTPs, 0.25 µl GoTaq® DNA Polymerase (5 u/µl), 2 µL of both upstream and downstream primers (10 µM stock), 10 µL (100 ng) of template cDNA and nuclease-free water to a final volume of 50 µL. Master mixes were prepared in a dedicated cabinet, which was decontaminated prior to each use by UV irradiation. The reaction conditions for each target gene amplified for cloning purpose are reported in **Table 2.7**. Annealing temperatures were optimised for each primer pair based on the melting temperatures. To ensure that all 3' ends of the product were adenylated and to optimise the cloning reaction (see paragraph 2.3.6.1), the final extension step was prolonged to 10 min.



**Table 2.7.** Thermal cycling conditions of FMO gene PCR amplification for subcloning.

Step	t°C	Time (min)	Number of cycles
Initial denaturation	94	2	1
Denaturation	94	0.5	35
Annealing	63 except FMO5 (59) and FMO2 (60.6)	1	
Extension	72	1	
Final extension	72	10	1
Soak	4	indefinite	1

To check whether the PCR generated the anticipated amplicon, PCR products were separated by agarose gel electrophoresis and visualised with ethidium bromide (EtBr) or the SYBR® Safe DNA Gel Stain (Sigma). Samples (10 µL) were mixed with 5 × New England Biolab (Herts, UK) loading buffer (only when colourless GoTaq® Flexi buffer was used) and loaded into agarose gels, composed of 1.5% (w/v) agarose, TAE buffer (40 mM Tris-base, 20 mM glacial acetic acid and 1 mM EDTA) and 0.1 µg/mL nucleic acid stain (EtBr or SYBR® Safe DNA Gel Stain). Products were electrophoresed at 70 or 120 V (depending on the size of the gel) in a horizontal electrophoresis tank (BioRad; Hemel Hempstead, UK), filled with TAE buffer. The size of the amplicons obtained was compared with the bands generated by 100 bp or 1 Kb DNA ladders (New England Biolab). Gels were examined for band detection under UV light and digital images taken. PCR products producing a single, discrete band of the expected size were considered to reflect a satisfactorily optimised PCR amplification.

### **2.3.5 Quantitative fluorescence real-time PCR (qPCR)**

The qPCR experiments were carried out following MIQE guidelines (Bustin et al., 2009) and using an Opticon Monitor 2 real time PCR machine (MJ research, Biorad). The analysis was conducted on the pulmonary cDNA of all rats from study 3, except for the two cohorts challenged on day 14 with the high dose of NR678. Reactions were carried out in 200 µL transparent plastic thin-walled tube strips. The set-ups

included 14.2  $\mu\text{L}$  master mix (SYBRGreen JumpStart Taq ReadyMix, Sigma, see **Appendix III**), 0.4  $\mu\text{L}$  upstream and downstream primers (10  $\mu\text{M}$ ) for the genes of interest and 5  $\mu\text{L}$  of cDNA (10 ng/ $\mu\text{L}$ ), to a final reaction volume of 20  $\mu\text{L}$ . Target gene (*FMO1* and *FMO2*) primer sequences (**Table 2.8**) were designed using the Beacon Designer 3.0 software (Premier Biosoft, Palo Alto, CA, USA), following the same criteria as those used for conventional PCR primer selection, except for a different desired amplicon length (50-150 bp). Two reference gene (*GAPDH*; glyceraldehyde 3-phosphate dehydrogenase) primer pairs (primer sets GAPDH1 and GAPDH2) were selected in order to match the annealing temperatures of *FMO1* and *FMO2* primer pairs and maximise the efficiency within the same run. Both reference gene primer sets were obtained from previously published sequences. Set 1 was from published work (Myers et al., 2010), whereas set 2 was available online (Shinegene Molecular Biotech, 2012). No-reverse transcription and no-template negative controls were included in each run.

**Table 2.8.** Primers used in qPCR.

Primer name	NCBI reference sequence	Primer Sequence 5' $\rightarrow$ 3'	Melting $t^{\circ}\text{C}$	GC%	Product length (bp)
<b>FMO1 forward</b>	NM_012792.1	GATGACCTCCTGACCTCG	60.9	61.1	142
<b>FMO1 reverse</b>		CTCCTTCCCACCTTTCCTG	59.8	55.5	
<b>FMO2 forward</b>	NM_144737.2	TCAAAGACCCTAAACTGGCTGTG	60.7	47.8	103
<b>FMO2 reverse</b>		ATGGCATTCTGGCTCCTTC	67.5	55	
<b>GAPDH1 forward</b>	NM_017008	CCCATCACCATCTCCAGGAG	67.9	57.1	285
<b>GAPDH1 reverse</b>		GTTGTCATGGATGACCTTGGC	66.6	52.3	
<b>GAPDH2 forward</b>		TGGAGTCTACTGGCGTCTT	60.1	52.6	138
<b>GAPDH2 reverse</b>		TGTCATATTTCTCGTGGTTCA	60.6	38.0	

The thermal cycling parameters for target and reference gene qPCR reactions are reported in **Table 2.9**. The optimal annealing temperature for each reaction was assessed in a single experiment testing a range of annealing temperatures above and

below the calculated melting temperature of the primers. A melting curve analysis step was added at the end of each single run in order to assess the presence of unintended double stranded DNA products.

**Table 2.9** Thermal cycling conditions of target and reference gene qPCR amplification.

Step	t C°	Time	Number of cycles
Initial denaturation	94	10 min	1
Denaturation	94	30 sec	35
Annealing	60 (FMO1 and GAPDH2) 63.5 (FMO2 and GAPDH1)	30 sec	
Extension	72	30 sec	
Primer dimer melt off	75	1 sec	
Plate reading	-	-	
Final extension	72	5 min	1
Melting temperature	65-95 (increment 0.2/sec)		1
Soak	4	indefinite	1

Results were evaluated using the Opticon Monitor software v.3.1.32 (MJ Research, Biorad), normalised against the reference gene according to the formula below (Pfaffl, 2001) and analysed statistically (one-way ANOVA).

$$ratio = \frac{Eff(target)^{\Delta Cq Target (Control-Treated)}}{Eff(reference)^{\Delta Cq Reference (Control-Treated)}}$$

The difference in C<sub>q</sub> (cycle of quantification) values ( $\Delta C_q$ ) between target and reference genes was calculated in control samples and then compared to that obtained from different treatment groups ( $\Delta \Delta C_q$ ). The formula accounted for the different efficiencies (Eff) between target and reference genes.

### **2.3.6 Molecular subcloning and synthesis of riboprobes for *in situ* hybridisation**

Riboprobes were synthesised in an *in vitro* transcription reaction using the FMO DNA template obtained from a commercially available ribovector plasmid.

#### **2.3.6.1 Ligation of the PCR product**

The first step of the cloning method was the direct insertion of the Taq-polymerase PCR-amplified FMO fragments into a plasmid vector, containing vaccinia virus topoisomerase I (TOPO cloning). Ligation of the PCR product into the pCRII-TOPO vector (Life Technologies Ltd.) was carried out as follows: 4  $\mu\text{L}$  of fresh (same day) PCR product (FMO1 to 5) was incubated for 10 min at RT with 1  $\mu\text{L}$  salt solution (1.2 M NaCl, 0.06 M  $\text{MgCl}_2$ ) and 1  $\mu\text{L}$  vector (10 ng/ linearised plasmid DNA), which were both supplied with the kit. The reaction tube was kept on ice until transformation.

#### **2.3.6.2 Cloning and transformation of bacteria**

The plasmid containing the ligated amplicon was then transferred to bacteria in a process known as transformation. The insertion of new genetic material into competent *Escherichia coli* (Top 10 One Shot Cells, Life Technologies Ltd.) was carried out by adding the cloning reaction product (2  $\mu\text{L}$ ) to the cells (50  $\mu\text{L}$ ), thawed on ice. The samples were gently mixed, incubated on ice for 30 min, heat shocked at 42°C for exactly 30 sec and placed on ice for 5 min. Then, 800  $\mu\text{L}$  of Luria-Bertani (LB) medium containing 50  $\mu\text{g}/\text{mL}$  ampicillin was added to the tubes. The cells were incubated at 37°C for 45 min at 200 rpm in an orbital shaker. A 100  $\mu\text{L}$  aliquot of each sample was plated on LB agar. The remaining culture was centrifuged at  $2,000 \times g$  for 5 min and 100  $\mu\text{L}$  of the sediment was plated as well. LB agar plates, containing 100  $\mu\text{g}/\text{mL}$  ampicillin and 40  $\mu\text{L}$  5-bromo-4-chloro-3-indolyl  $\beta$ -D-galactopyranoside (X-Gal, Sigma) were incubated at 37°C overnight. Up to six white to light blue colonies, representing bacteria with ampicillin resistance and successful ligation of the PCR product, were added each to 10 mL tubes with 50  $\mu\text{g}/\text{mL}$  ampicillin and incubated at 37°C at 200 rpm in an orbital shaker overnight. 250  $\mu\text{L}$

of the culture was added to 750  $\mu\text{L}$  60% (v/v) glycerol and stored at  $-80^{\circ}\text{C}$ , while the remaining broth was used for plasmid DNA extraction.

### **2.3.6.3 Small scale isolation of plasmid DNA (miniprep)**

In order to test the efficacy of the cloning reaction, a small amount of plasmid DNA was extracted from the bacterial broth and sequenced. The tubes containing the culture broth were centrifuged ( $4,000 \times g$ , 10 min) and the supernatant discarded. Pellets were resuspended in 200  $\mu\text{L}$  glucose solution (**Appendix III**) until all clumps were dissolved and the solution transferred to 1.5 mL Eppendorf tubes which were incubated at RT for 5 min. 400  $\mu\text{L}$  of denaturation solution (**Appendix III**) was added to the tubes, which were gently mixed until the solution became viscous and slightly clear. After incubation on ice (exactly 5 min), 300  $\mu\text{L}$  of neutralisation solution (**Appendix III**) was added, followed by further incubation on ice for 5 min. The tubes were centrifuged ( $20,000 \times g$ , 7 min) and the supernatant transferred to new tubes. DNA precipitation was initiated with the addition of 500  $\mu\text{L}$  isopropyl alcohol, followed by 15 min incubation on ice and centrifugation at  $20,000 \times g$  for 5 min. The pellet was air-dried for 10 min, and then 200  $\mu\text{L}$  TE buffer (pH 8.0) and 100  $\mu\text{L}$  7.5 M sodium acetate was added and the solution mixed until the pellet was completely dissolved. This was followed by incubation on ice for 15 min, centrifugation at  $20,000 \times g$  for 5 min and addition of 600  $\mu\text{L}$  100% ethanol to the supernatant after it had been transferred into a new tube. The vials were incubated at  $-20^{\circ}\text{C}$  for 1 h and then spun at  $20,000 \times g$  for 10 min. The resulting pellet (plasmid DNA) was air-dried for 10 min, then resuspended in 100  $\mu\text{L}$  TE buffer and stored at  $4^{\circ}\text{C}$ .

### **2.3.6.4 Restriction enzyme digestion and DNA sequencing**

Plasmid DNA was linearised by restriction endonuclease digestion to confirm the successful insertion of the PCR product. Three separate reactions were set up, using two different restriction enzymes, *Bam*HI and *Xho*I (New England Biolabs), which cut at specific recognition sites situated on opposite ends of the PCR product insert loci in the plasmid. For each reaction, 2  $\mu\text{L}$  plasmid DNA was added to 2  $\mu\text{L}$  of the appropriate  $10 \times$  restriction enzyme buffer, 0.2  $\mu\text{L}$  of  $100 \times$  BSA, 1  $\mu\text{L}$  RNase A with no (uncut), one (single cut) or two (double cut) restriction enzymes (1  $\mu\text{L}$  each)

and made up to a total volume of 20  $\mu$ L with nuclease-free water. The reaction mix was incubated at 37°C for 1 h and the resulting products were visualised on an agarose gel. Successful transformation was considered to have occurred when the product visualised on the agarose gel obtained through double digestion appeared clearly smaller than the one formed by the single cut (**Figure 2.4**). Samples of the miniprep plasmid DNA deemed to carry the insertion were sent to a sequencing laboratory (Beckman Coulter Genomics; Takeley, UK) and sequences obtained from the laboratory were compared to those published for the genes of interest using BLAST.

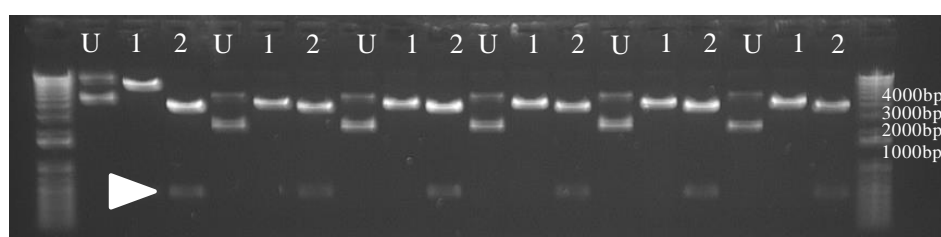


**Figure 2.4.** Gel electrophoresis of miniprep plasmid DNA. Uncut (U) or linearised DNA (FMO4 in this specific example) cut with one or both restriction enzymes were visualised on an electrophoresis gel. The lane for plasmid DNA which had been cut with both endonucleases (2) is appreciably distinct from lane 1, which corresponds to single cut DNA (1). The different band size is due to the presence of the PCR insert, which is eliminated from the plasmid sequence by the double cut (arrowhead).

### 2.3.6.5 Large scale isolation of plasmid DNA (maxiprep)

Large quantities of plasmid DNA were obtained from the samples which were successfully sequenced using QIAGEN Plasmid Maxi Kit (Qiagen; Manchester UK). Composition of the buffers contained in this kit is reported in **Appendix III**. Either 5  $\mu$ L of glycerol stock or a single colony were added to 10 mL LB broth containing 50  $\mu$ g/mL ampicillin and incubated at 37°C in an orbital rotator for 4-8 h, until the solution became cloudy. The prestarter culture was then put in a 2 L flat-bottomed flask with 400 mL LB broth containing 50  $\mu$ g/mL ampicillin and incubated overnight at 37°C in an orbital shaker. After centrifugation (6,000  $\times$  g, 5 min), the bacterial pellet obtained was resuspended with 10 mL Buffer P1, lysed through the addition of 10 mL Buffer P2, followed by gentle mixing and incubation at RT for exactly 5 min.

Neutralisation was carried out with the addition of 10 mL Buffer P3, followed by incubation on ice for 20 min and two centrifugations ( $20,000 \times g$ , 15 min,  $4^{\circ}\text{C}$ ). The supernatant was then added to a Qiagen-tip 500 that had been equilibrated with Buffer QBT, and allowed to decant by gravity flow. The DNA linked to the tip special filter was washed twice with 30 mL Buffer QC and finally eluted with 15 mL Buffer QF. Plasmid DNA isolation from the eluate was obtained through the addition of 10.5 mL isopropanol and centrifugation ( $15,000 \times g$ , 15 min,  $4^{\circ}\text{C}$ ), followed by addition of 5 mL 70% ethanol to the supernatant and further centrifugation ( $15,000 \times g$ , 10 min). The resulting pellet was air-dried, resuspended with 500  $\mu\text{L}$  TE buffer and a sample of DNA quantified using the NanoDrop spectrophotometer.

#### **2.3.6.6 Preparation of DNA template for RNA transcription**

The DNA template obtained from the maxiprep extraction was prepared for the generation of RNA transcripts. 5  $\mu\text{g}$  plasmid DNA extracted from the maxiprep was linearised in two separate reactions, using 5  $\mu\text{L}$  *Bam*H1 or *Xho*I endonucleases, 5  $\mu\text{L}$  of  $10 \times$  restriction enzyme buffer, 0.5  $\mu\text{L}$  of  $100 \times$  BSA and nuclease-free water up to a total volume of 50  $\mu\text{L}$ . *Bam*H1 and *Xho*I generated the sense and the antisense probes, respectively, for all FMOs, except for FMO3. The reaction mix was incubated at  $37^{\circ}\text{C}$  for 2 h. To remove salts and protein, an equal volume of phenol:chloroform:isoamyl alcohol (25:24:1) was added to the DNA template. After vigorous vortexing and centrifugation ( $20,000 \times g$ , 1 min), the upper aqueous layer was transferred into a new tube without disturbing the underlying organic phase and the steps were repeated once more with phenol:chloroform:isoamyl alcohol (25:24:1) and then once with chloroform:isoamyl alcohol (24:1). Precipitation of DNA was carried out with 1/10 volume of 3 M sodium acetate and  $3 \times$  volume of ice-cold 100% ethanol, followed by incubation at  $-20^{\circ}\text{C}$  for at least 1 h and centrifugation at  $20,000 \times g$  for 10 min. The supernatant was discarded and the same steps were repeated with 70% alcohol. The pellet was then dissolved in 30  $\mu\text{L}$  nuclease-free water.

### **2.3.6.7 Labelling of the riboprobes with digoxigenin**

Standard RNA labelling was carried out with a RNA labelling kit (Roche), using digoxigenin-11-UTP as the label molecule. 1 µg of purified template DNA (each sense and anti-sense) was added to an RNase-free vial with nuclease-free water up to a volume of 13 µL and subsequently mixed with 2 µL of 10 × transcription buffer, 1 µL protector RNase inhibitor, 2 µL of 10 × NTP labelling mixture (10 mM ATP, CTP, GTP, 6.5 mM UTP, 3.5 mM digoxigenin-11-UTP) and 2 µL SP6 (anti-sense probe for all FMOs, except FMO3) or T7 (sense probe for all FMOs, except FMO3) RNase polymerase. The mixture was incubated at 37<sup>0</sup>C for 2 h. Any remaining DNA template was removed by adding 2 µL DNase I to the sample, which was incubated at 37<sup>0</sup>C for 15 min. The reaction was stopped by the addition of 2 µL of 0.2 M EDTA. 1 µL 1 mg/mL of yeast tRNA (Roche) was added to the DNase digested probes, and the RNA was precipitated by addition of 1/10 volume of 3 M sodium acetate (pH 5.2) and 2.5 × volume of 100% ethanol. The vials were incubated at -80<sup>0</sup>C for 30 min and then centrifuged at maximum speed for 20 min. The supernatant was discarded and the pellet was washed with 70% ethanol, followed by centrifugation at maximum speed for 5 min at RT. The supernatant was carefully removed, the pellet air-dried for 10 min and then resuspended in 45 µL of nuclease-free water. Alkaline hydrolysis was used to shorten selected probes (FMO1, FMO3 and FMO5) to 200 bp when no signal was detected with the originally designed, longer probes. 5 µL of 0.4 M sodium bicarbonate (NaHCO<sub>3</sub>)/0.6 M sodium carbonate (Na<sub>2</sub>CO<sub>3</sub>) at pH 10.2 was added to the probe and incubated at 60<sup>0</sup>C for an exact number of minutes depending on the probe (not done for the FMO2 probe). The mixture was neutralised by adding 5 µL of 3 M sodium acetate (NaAc; pH 4.6) and the previous ethanol precipitation and wash step was repeated. The pellet was air-dried for 10 min and then resuspended in 50 µL nuclease-free water.

### **2.3.6.8 Dot blot analysis of riboprobes**

A dot blot analysis was carried out to determine empirically the concentration of the newly synthesised probes. For this purpose, the probes were diluted 10 × in 10 µg/mL yeast tRNA (Roche) and 5 µL of each of the five serial dilutions prepared spotted onto a Hybond N+ membrane (Amersham Biosciences; Little Chalfont, UK)



and allowed to dry before cross linking using a UV Stratalinker (Stratagene; Cambridge, UK). The membrane was then incubated on a shaker in washing buffer (0.1 M maleic acid, 0.15 M NaCl, pH 7.5, 0.3% v/v Tween 20) for 2 min and placed in blocking solution (10 × blocking solution in maleic acid buffer) for 30 min, followed by incubation with the sheep polyclonal anti-digoxigenin antibody also used in the RNA-ISH [Anti-DIG-AP (Roche), 1:5000 in blocking solution] for 30 min. After being rinsed twice with washing buffer for 15 min, the membrane was incubated for 3 min in detection buffer (0.1 M Tris HCl, 0.1M NaCl, pH 9.5) and then placed in the dark without shaking in 10 mL of staining buffer, made with one SIGMAFAST™ BCIP®-NBT tablet dissolved in water. The signal developed over the following hour and the reaction was stopped by placing the membrane in 50 mL TE buffer for 5 min.

### **2.3.7 Genotyping of rats for *FMO2* polymorphism**

A nested PCR was carried out to investigate wild rats and different laboratory rat strains for a polymorphism in *FMO2* and to discriminate between mutant and wild-type alleles.

#### **2.3.7.1 Animals and tissue collection**

Genotyping analysis was conducted in two phases, in the first part, the aim was to characterise the frequency of truncated and full-length *FMO2* alleles in wild rats, whereas the objective of the second part was to determine the allelic frequencies of this gene in laboratory rat strains derived from a common wild rat ancestor.

A total of 35 wild male and female rats captured in the North-West of England were examined. Four of these [two each *R. norvegicus* (brown rat) and *R. rattus* (black rat)], identified on the basis of morphological features, i.e. size, shape of the ears and length of the tail, were trapped in Cheshire by a professional exterminator commissioned by the BASF Widnes laboratories. Animals were euthanased with CO<sub>2</sub>, followed by exsanguination. A complete post mortem examination was performed on each rat and representative samples of liver, lung, kidney, heart, brain, spleen and thymus were fixed in formalin and routinely processed for histological examination to assess the general health of the rats. Two aliquots of the organs listed

above and from the tail were stored at -20°C and -80°C. The remaining 31 rats (all *R. norvegicus*) had been trapped in the Liverpool urban area as part of the PhD project of Kieran Pounder (Department of Integrative Biology, University of Liverpool) to examine the prevalence of hantaviruses and Ljungan virus in wild rodents. Rats had been anaesthetised with isoflurane immediately after trapping and killed by cervical dislocation. Organ samples had been collected shortly after euthanasia and stored at -80°C and samples of lungs or liver were kindly provided for this project.

The second part of the analysis was conducted on two colonies of laboratory rats (named Welsh and Berkshire), which have been maintained at the BASF Widnes laboratories for several years. Both colonies were generated by the mating of wild and laboratory rat ancestors and subsequent brother/sister mating for several generations. Animals (12 male and 12 female Welsh rats and 13 male Berkshire rats) were identified through ear punching, which also allowed the collection of an adequate tissue sample for the DNA analysis (Cinelli et al., 2007). Briefly, a small circle (approximately 1 mm diameter) of external ear tissue was collected using an ear punch, which was cleaned and disinfected between animals to minimise the risk of infection and DNA contamination. Each rat was identified with a unique code obtained from the initials of the gender and group (MW: male Welsh; FW: female Welsh; MB: male Berkshire), followed by a number assigned depending on the number and position of the hole/notches (**Figure 2.5**).

### **2.3.7.2 Extraction of DNA from tissue**

DNA was extracted from all captured wild rats (33 *R. norvegicus* and 2 *R. rattus* specimens) and from the first 5 rats/gender in both Welsh and Berkshire colonies. DNA was also obtained from three laboratory rats (Wistar strain), which belonged to the control group of study 3. Isolation of total DNA was carried out using the QIAamp DNA Mini Kit (Qiagen). Most solutions used in this procedure are proprietary components of the kit and information regarding their actual composition has not been made available, unless specified. Briefly, approximately 20 mg of tissue (lung, liver or ear) were weighed, cut into small pieces and placed in a 1.5 mL tube with 180 µL of ATL Buffer (tissue lysis buffer).

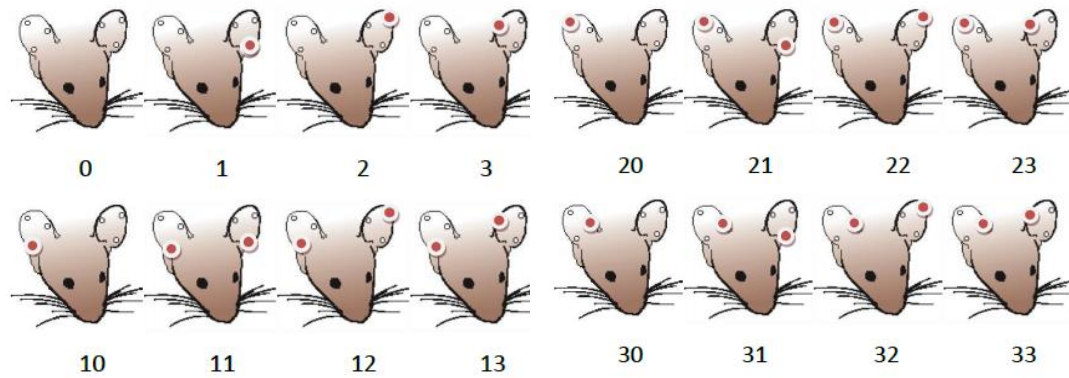


**Figure 2.5.** Ear punching numbering system to identify rats for genotyping. According to the number and position (medial, central or lateral region of the left or right external ear) of the holes, rats were assigned a unique identification number. Image (mouse head drawing) source: National Institutes of Health, courtesy of [www.theodora.com/rodent\\_laboratory](http://www.theodora.com/rodent_laboratory), used with permission.

Complete lysis of samples was obtained by the addition of 20  $\mu\text{L}$  of proteinase K [ $> 600$  milli absorbance units (mAU), contained in the kit] and an overnight incubation at  $56^\circ\text{C}$ . 200  $\mu\text{L}$  of AL Buffer (lysis buffer) was added to the tubes, followed by incubation at  $70^\circ\text{C}$  for 10 min, after which 200  $\mu\text{L}$  of ethanol was added. The mixture was applied to a QIAamp Mini spin column and centrifuged at  $6,000 \times g$  for 1 min. The column was washed and centrifuged, once with 500  $\mu\text{L}$  Buffer AW1 ( $6,000 \times g$  for 1 min) and twice with 500  $\mu\text{L}$  Buffer AW2 ( $20,000 \times g$  for 3 min). DNA was extracted eluting the column twice with 200  $\mu\text{L}$  AE Buffer (10 mM Tris-Cl and 0.5 mM EDTA; pH 9.0), followed by incubation at RT for 10 min and centrifugation at  $6,000 \times g$  for 1 min. DNA concentrations and quality were evaluated with a NanoDrop spectrophotometer. Samples with A260/280 ratio between 1.6 and 1.8 were deemed suitable for PCR amplification. DNA samples were stored at  $-20^\circ\text{C}$  until further use.

### 2.3.7.3 Characterisation of *FMO2* by nested PCR

Frequencies of *FMO2* alleles were determined using a nested PCR technique, modified from Hugonnard et al. (2004), that allowed efficient targeting of the point mutation which differentiates the truncated *FMO2* allele from its full length counterpart. The nested PCR was conducted with all DNA samples extracted as

specified above. Samples of DNA derived from Wistar rats and *R. rattus* were used as positive controls, since these animals are known to be homozygous for the mutated (*FMO2\*2*) and the full-length (*FMO2\*1*) *FMO2*, respectively (Hugonnard et al., 2004).

Both amplifications were carried out using the GoTaq® Flexi DNA Polymerase kit (Promega) and primer pairs designed from *R. norvegicus* and *R. rattus FMO2* gene sequences were obtained from Hugonnard et al., 2004 (**Table 2.10**).

**Table 2.10.** Primers used in nested PCR. Primers used in the first amplification were FMO2F1 (forward) and FMOR1 (reverse). In the second amplification step, a common forward primer (FMO2F2) was used together with two reverse primers, targeting the mutant truncated (FMO2R2m) or the wild full-length (FMO2R2w) *FMO2* sequence.

Primer name	Gene bank accession number	Primer Sequence 5' → 3'	Melting t C°	GC %	Product length (bp)
FMO2F1	AF458414	CGCTTGCCTTCGGAGACG	61.1	66.7	1313
FMO2R1		TCTGGGTGAGGATGGCATTC	59.5	55.0	
FMO2F2		CACGAGCATTTGCATCAATACCTG	58.0	45.8	236
FMOR2m		ATCTGGCTCTGGCTTTCCAA	59.3	50.0	
FMO2R2w		CTGGCTCTGGCTTTCCC	55.0	61.1	

Exactly 100 ng of genomic DNA was amplified with 2 µL of the correspondent upstream (FMO2F1) and downstream (FMO2R1) primers (10 µM stock) and 5 µL of 10 × green buffer, 4 µL of 25 mM MgCl<sub>2</sub>, 1 µL of 10 mM dNTPs, 0.25 µl GoTaq® DNA Polymerase (5 u/µl) and nuclease free water to a final volume of 50 µL. The second amplification was carried out using 1 µL of the amplification product of the first PCR and the same mixture as above, divided in two tubes, one for each reverse primer (FMO2-R2m and FMO2-R2w, recognising specifically the mutant or the full length *FMO2*, respectively; see **Figure 2.6**). The conditions of amplification were identical to those previously described by Hugonnard et al. (2004; **Table 2.11**).

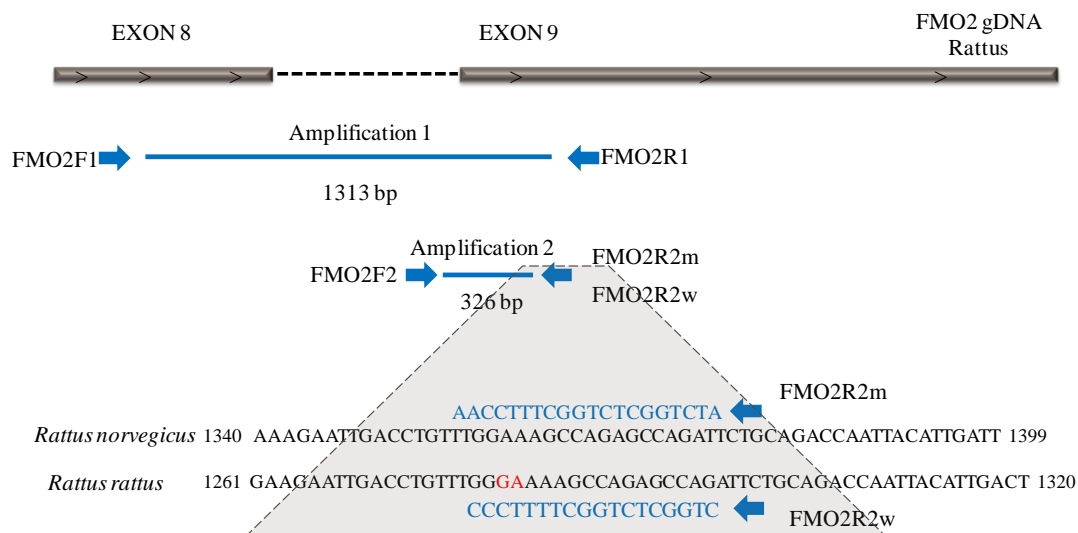


**Figure 2.6.** Nested PCR method for rat *FMO2* genotyping. Genomic DNA (gDNA) was first amplified with a primer pair (FMO2-F1 and -R1) that generates a 1313 bp amplicon (spanning exons). The second amplification was conducted with a common forward primer (FMO2-F2) and two different downstream primers (FMO2-R2m and FMO2-R2w) that anneal to either the mutant or wild-type FMO2 sequence, respectively. The double mutation targeted by the specific reverse primers is displayed in red. Modified from Hugonnard et al. (2004).

**Table 2.11** Thermal cycling conditions for the *FMO2* gene amplification with a nested PCR (Hugonnard et al., 2004).

a) Parameters of the first amplification.

Step	t °C	Time	Number of cycles
Initial denaturation	94	3 min	1
Denaturation	94	20 sec	35
Annealing	62	30 sec	
Extension	72	90 sec	
Final extension	72	5 min	1
Soak	4	indefinite	1

b) Parameters of the second amplification.

Step	t °C	Time	Number of cycles
Initial denaturation	94	2 min	1
Denaturation	94	20 sec	21
Annealing	70 (mutant) 64 (wild)	30 sec	
Extension	72	30 sec	
Final extension	72	5 min	1
Soak	4	indefinite	1

## **2.4 Enzyme assay and metabolic analysis**

All chemicals and reagents mentioned in this section were obtained from Sigma; Poole, UK, unless otherwise specified.

### **2.4.1 Preparation of rat liver and lung microsomes**

Rat liver and lung microsomes were prepared as described (Gill et al., 1995; Philpot et al., 1975). Briefly, liver and lung were removed from twelve adult male Wistar rats (age range: 6-8 w, weight range: 150-170 g), obtained from Charles River Laboratories (Margate, UK) and used as control animals in other studies conducted in our laboratory based on the specifications detailed above (gender, age, weight, euthanasia, no treatment). Liver and lung microsomes were also prepared from eight Welsh male rats, different from those used in study 4. Due to the thermal lability of several FMO isoforms (Krueger and Williams, 2005), organs were rapidly chilled after removal and procedures such as homogenisation and centrifugation were carefully monitored to avoid raises in temperature which can lead to inactivation and loss of FMO activity. Livers and lungs were rinsed with ice-cold 0.067 M phosphate buffer (pH 7.4), containing 1.15% (v/w) KCl. Lung lobes were carefully separated from connective tissue and major bronchi. Pooled specimens of liver and lung were chopped with scissors and homogenised with both manual and motor-driven (Kinematica Polytron PT3000, Phillip Harris, Manchester, UK) tissue homogenisers in ice-cold buffered KCl ( $3 \times$  the volume of the tissue). This was followed by differential centrifugation, using an Optima L-60 preparative ultra centrifuge (Beckman-Coulter; High Wycombe, UK). With the first spin, conducted at  $10,000 \times g$  for 25 min at  $4^{\circ}\text{C}$ , sedimentation of unbroken cells, nuclei and mitochondria was achieved, while the second spin at  $105,000 \times g$  for 65 min at  $4^{\circ}\text{C}$  precipitated the microsomal component. A further centrifugation with the same parameters was conducted on the microsomal pellet resuspended in the same buffer. Finally, the pellet was dissolved in phosphate buffer without KCl, split into 1 mL aliquots and stored at  $-80^{\circ}\text{C}$ .

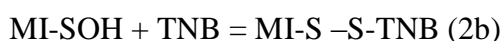
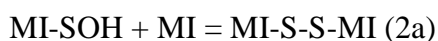
## 2.4.2 Determination of protein content and enzyme activity of liver and lung microsomes

Hepatic microsomal cytochrome P450 activity was measured according to a previously described method (Omura and Sato, 1964). Briefly, microsomes were diluted in phosphate buffer without KCl at a concentration of 1 mg/mL and divided in two cuvettes. A few grains of sodium dithionate ( $\text{Na}_2\text{S}_2\text{O}_4$ ) were added to both in order to reduce iron contained in the haem group of cytochrome P450 from the ferric ( $\text{Fe}^{3+}$ ) to the ferrous ( $\text{Fe}^{2+}$ ) form.  $\text{CO}_2$  was then gassed through the sample cuvette only, at one bubble/second speed for 1 min. Levels of the haemoprotein were measured calculating the difference spectrum between the reference and the sample cuvettes at 450-490 nm, corrected for an extinction coefficient of 91 mM/cm. Values obtained were  $> 0.3$  nmol/mg protein. Concurrently, the protein content of the microsomes was measured by the Lowry assay (Lowry et al., 1951), using BSA as a standard (see paragraph 2.2.2).

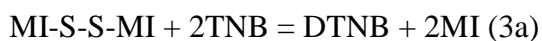
Liver and lung microsomal FMO activity was evaluated by measuring the S-oxygenation of MI, a rather specific substrate for FMO enzymes, through a spectrophotometric method, as described by Dixit and Roche (1984). The MI assay method, used to evaluate FMO activity in whole cell homogenates or subfractions, is based on the high affinity of MI for the FMO active site, by which it is metabolised to the correspondent sulphoxide (1) in the presence of oxygen and NADPH:



The sulphoxide reacts with the parent molecule (2a) or TNB (2b) to produce a disulphide:



The disulphide is able to oxidise TNB to DTNB, with the formation of one (3a) or two (3b) molecules of MI:



When dithiothreitol (DTT), a strong reducing agent, is added to the standard reaction (without MI), it converts all DTNB to TNB. The disappearance of TNB, converted back to DTNB after the addition of MI, is measured at 412 nm with a spectrophotometer.

A standard reaction mixture (final volume: 1 mL) was set up for each pool of microsomes, containing 0.1 M tricine/KOH (pH 8.3), 0.06 mM DTNB, 0.02 mM DTT, 0.1 mM NADPH and 100 mg of microsomal protein. The reactions were incubated at 37°C in an optical polystyrene spectrophotometer cuvette and the substrate-independent rate of oxygenation was monitored at 412 nm for 3 min. Subsequently, MI (1 mM) was added and the rate of decrease of optical density was recorded for 5 min. In a set of experiments, microsomes were previously heated at 55°C to inhibit FMO activity and investigate the contribution of P450 to the oxygenation of MI.

### **2.4.3 Incubation of NR678 in rat liver and lung microsomal suspensions**

Liver and lung microsomes were incubated with NR678 at 37°C, for up to 1 h. Standard reactions were carried out in a final volume of 1 mL phosphate buffer, pH 7.4, containing 1 mg/mL rat hepatic microsomal protein, NR678 (500 µM), MgCl<sub>2</sub> (5 mM), with or without the addition of NADPH (1 mM). As no NR678 turnover was detected using this set-up, step-by-step modifications to the conditions described above were introduced, including changes in the reagent type and concentration, temperature, pH and incubation times, as shown in **Table 2.12**.



**Table 2.12.** Standard microsomal incubation conditions and optimisation attempts.

Incubation parameters		Standard	Modifications
Reagents and cofactors	MgCl <sub>2</sub>	5 mM	500 µM-20 mM
	NADPH	1 mM	500 µM-5 mM Or replaced with NADPH-regenerating system (0.5 mM NADP <sup>+</sup> ; 5 mM glucose-6-phosphate; 1.5 U glucose-6-phosphate dehydrogenase)
	Microsomal protein (rat liver)	1 mg/mL	0.5-20 mg/mL Or replaced with rat lung microsomes or mouse liver microsomes
	NR678	500 µM	50 µM-100 mM Dissolved in distilled water or methanol
	FAD	-	0.5-5 mM
	GSH	-	0.5-5 mM
	Incubation conditions	Incubation temperature	37°C
Incubation time		15 min	30 sec – 1 h
pH		7.4	7.0-8.9

The reaction was stopped by the addition of an equal volume of ice-cold acetonitrile. Samples were then cooled at -20°C for 2 h, centrifuged (4°C, 10 min, 2200 rpm) and the supernatant was gassed to dryness using N<sub>2</sub>. Samples were resuspended in 200 µL methanol (50%), centrifuged again (4°C, 5 min, 2200 rpm) and the supernatant was analysed by high-performance liquid chromatography (HPLC). Phenylthiourea, (PTU) whose chromatographic trace has been previously characterised (Henderson et al., 2004b), was used as a positive control to test the ability of the *in vitro* system to catalyse S-oxygenation of thiourea-related molecules. Incubations prepared without NR678 or without the microsomal proteins were included in each run. Samples were prepared at least in triplicate.

#### 2.4.4 HPLC method development and validation

Analysis was performed using the Dionex Summit HPLC system (Dionex Corporation, Sunnyvale, CA, USA). The samples were resolved with a Gemini-NX

5 $\mu$ m C18 (250 mm by 4.60 mm, Phenomenex; Macclesfield, UK). The mobile phase consisted of methanol and distilled water. A sample aliquot of 50  $\mu$ L was injected into the column and eluted at different flow rates (0.8-1.1 mL/min). A gradient of 10% to 60% methanol was set up for 20 min, maintaining 60% methanol for 5 min, and finally reverting to 10% over 5 min. The analytes were detected by a UVD170S UV detector (Dionex) at 240 nm or 254 nm. Method validation was carried out in accordance with guidelines set out by the FDA (Food and Drug Administration, 2001). Parameters evaluated throughout this process included accuracy, precision, stability, sensitivity and reproducibility. Stability of the analytes was investigated after long-term (frozen at -20°C) and short-term (RT) storage, and after several freeze and thaw cycles. A calibration curve was generated using a blank sample, a zero sample (containing the internal standard phenylthiourea) and six different concentrations (0.001 mM to 10 M) of NR678 (5 samples/each), covering the expected range, including the lowest limit of quantification (LLoQ).

#### **2.4.5 Comparative FMO activity metabolism assay with and without competitive substrate inhibition**

FMO activities of the different microsomal pools (Wistar rat liver and lung and Welsh rat lung) were compared, using the MI assay (see paragraph 2.4.2). Differences in absorbance, i.e. the rate of formation of DTNB, were recorded at 412 nm with a spectrophotometer at four consecutive 1 min intervals following the addition of MI to the incubations. The reaction rate (reaction velocity,  $V_0$ ) was expressed as nmol per min per mg of microsome protein, after conversion of the mean difference in optical density ( $\Delta$ OD) into nmol, using the molar absorption coefficient for DTNB at 37°C (Eyer et al., 2003). Enzyme kinetics were determined using nine scalar concentrations (ranging from 5  $\mu$ M to 1 mM) of the substrate, and were calculated by plotting  $V_0$  as a function of the ratio between  $V_0$  and the substrate (S) concentration (Eadie–Hofstee diagramme). The data sets were analysed by GraphPad Prism version 6.00 for Windows (GraphPad Software, La Jolla California USA, [www.graphpad.com](http://www.graphpad.com), demo version) with a non linear regression method which fits the Michaelis-Menten equation. The experiments were conducted in triplicate. Once the kinetic parameters were determined, FMO activity against MI over time

(7 min) was compared among the different microsomal incubations, selecting a single substrate concentration (500 mM). The experiment was conducted in triplicate, at three different days. Negative controls, omitting the microsomal protein or MI, or composed exclusively of buffer, were included in each run. Enzyme inhibition was investigated, repeating the same experiment with the addition of NR678 (500  $\mu$ M).

## **2.5 Statistical analysis**

Statistical analysis was applied to data sets obtained from study 3 and was conducted using StatsDirect statistical software (StatsDirect Ltd, Altrincham, UK). The normality for each data subset was tested using the Shapiro-Wilk test. As normality was indicated, parametric one-way analysis of variance (ANOVA) was applied, followed by the Dunnett multiple component test. Statistical evaluation was conducted on mean organ weights (paragraph 2.2.1.1), IH cell counts (paragraph 2.2.1.2), GSH liver and lung measurements (paragraph 2.2.2) and relative expression of pulmonary FMO1 and FMO2 mRNA (paragraph 2.3.5). All results were expressed as mean  $\pm$  standard deviation or standard error of the mean (SEM). Statistical significance was set at  $p < 0.05$ .

# Chapter 3 Results

3.1 *In vivo* investigation into the acute toxic effects of NR678 and an attempt to elucidate its metabolism *in vitro*

3.2 *In vivo* investigation into the pulmonary defence responses involved in the prevention of NR678-induced lung injury

3.3 Characterisation of FMO1 and FMO2 expression profiles in untreated rats and rats that had received NR678

3.4 Assessment of *R. norvegicus* as a suitable animal model to investigate the metabolic and toxicological consequences of *FMO2* polymorphism in humans

### **3.1 *In vivo* investigation into the acute toxic effects of NR678 and an attempt to elucidate its metabolism *in vitro***

Data from several sources have shown that the lungs represent the main target for the acute toxic effect of thiourea (reviewed in Ziegler-Skylakakis, 2003) and selected thiourea-related molecules, such as phenylthiourea (Greaves, 2007d; Scott et al., 1990) and the rodenticide ANTU (Dieke et al., 1947; Dieke and Richter, 1946; Meyrick et al., 1972). Fatal pulmonary oedema and pleural effusion have been described consistently across several laboratory animal species, including mice, rats and dogs, following the oral administration of high doses (Ziegler-Skylakakis, 2003). We hypothesised that NR678, a phenylthiourea derivate that has been investigated as a potential rodenticide candidate (see paragraph 1.1), might exert its lethal effect in a similar way and therefore carried out a single dose acute toxicity study (study 1) in which rats received by oral *gavage* a known lethal dose (10 mg/kg) of NR678. All rats succumbed within a few hours of administration of the compound, showing dyspnoea and gross and post mortem findings consistent with severe pulmonary oedema and hydrothorax. These findings were further investigated as part of study 3 (tolerance study), where a cohort of 3 rats received NR678 at a dose of 5 mg/kg. The results obtained from this animal cohort are included in this section as they are consistent with the acute dose-limiting toxicity of NR678 (DL<sub>50</sub> of NR678 was within 2 to 5 mg/kg; see paragraph 1.1). An attempt was also made to isolate the metabolite(s) of NR678 using rat liver and lung *in vitro* microsome systems.

#### **3.1.1 Clinical assessment of rats that had received a high dose of NR678**

All rats receiving NR678 at a dose of 10 mg/kg (study 1) were electively euthanased starting at 6 h after dosing, due to severe, worsening clinical signs. Clinical signs were first observed at 2 h after dosing, when rat 10L-1248 showed hunched posture and decreased motor activity (**Table 3.1**). At 3 h, animals 10L-1248 and 10L-1249 exhibited mild laboured and rapid breathing, respectively. These clinical observations, suggestive of respiratory distress, increased in severity (from mild over moderate to severe) within the following hours and were consistently observed in all

treated animals. At 6-7 h after dosing, the severity of the respiratory clinical signs prompted elective euthanasia. Additional clinical signs included half closed eyes and piloerection. Most animals were not eating or drinking from 3 h after dosing onwards. Animals that had received a dose of 5 mg/kg (study 3) developed similar clinical signs, but later (at about 4 h after dosing) and with generally lower severity. One rat (11L-2406) exhibited only mild clinical signs (piloerection and hunched posture) and was euthanased at the end of the experiment (7-8 h post dosing). Dehydration was observed in two animals at 7 h after dosing. The hydration status was checked empirically by pinching up the skin over the neck, which should relax without delay into its normal position in normally hydrated animals. The vehicle-control rats from both studies did not develop any clinical signs and were euthanased immediately after the necropsies of animals dosed with NR678 were completed (> 7 h post dosing).

**Table 3.1.** Clinical signs observed in rats administered a high dose (5 or 10 mg/kg) of NR678. Rats were euthanased (E) within 7 h after dosing.

Rat ID	9 am	930 am	10 am	11 am	12 pm	1 pm	2 pm	3 pm	330 pm	4 pm
11L-2405	NR678 5 mg/kg	NCSO	NCSO	NCSO	NCSO	HP, DMA, PE, LB(2)	HP, DMA, PE, LB(2)	HP, DMA, PE, LB(2)	HP, DMA, PE, LB (3), DH. E	-
11L-2406	NR678 5 mg/kg	NCSO	NCSO	NCSO	NCSO	NCSO	NCSO	PE	PE, HP	PE, HP. E
11L-2407	NR678 5 mg/kg	NCSO	NCSO	NCSO	NCSO	HP, DMA, PE	HP, DMA, PE, LB(2)	HP, DMA, PE, LB (2)	HP, DMA, PE, LB (3), DH. E	-
10L-1247	NR678 10 mg/kg	NCSO	NCSO	NCSO	NCSO	HP, DMA, PE, RB (1)	HP, DMA, PE, RB (2)	HP, DMA, PE, RB (2)	HP, DMA, PE, RB (2)	HP, DMA, PE, RB (3) .E
10L-1248	NR678 10 mg/kg	NCSO	NCSO	HP, DMA	HP, DMA, PE, LB (1)	HP, DMA, PE, LB (2), HCE	HP, DMA, PE, LB (2), HCE	HP, DMA, PE, LB (2), HCE	HP, DMA, PE, LB (3), HCE. E	-
10L-1249	NR678 10 mg/kg	NCSO	NCSO	NCSO	RB(1)	HP, DMA, PE, LB (2)	HP, PE, LB (3), HCE	HP, PE, LB (3), HCE.	-	-

ID: identification. NCSO: no clinical signs observed; HP: hunched posture; DMA: decreased motor activity; PE: piloerection; RB: rapid breathing (tachypnoea); LB: laboured breathing (dyspnoea); HCE: half-closed eyes; DH: dehydration. Numbers in brackets indicate the severity of tachypnoea and dyspnoea (mild: 1, moderate: 2 and severe: 3).

### 3.1.2 Gross post mortem findings in rats that had received a high dose of NR678

In rats that had received NR678 at a dose of 5 mg/kg, the absolute and relative (to body and to brain) weights of the lungs (right lobes) were measured and compared to those of the controls. An approximately 20% increase in mean absolute and relative to brain lung weights (**Figure 3.1**) was observed in treated rats, which was not statistically significant .

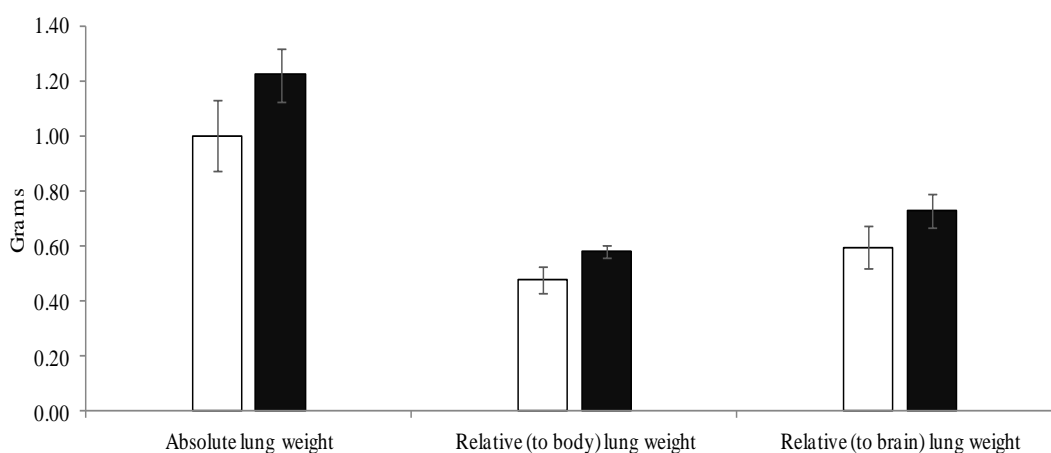


**Figure 3.1.** Absolute and relative lung weights in rats administered a high dose (5 mg/kg) of NR678. Treated rats: black bars. Control rats: white bars. Data are presented as mean  $\pm$  standard deviation for n=3. Relative to body weights were calculated according to the formula: (absolute lung weight/body weight)  $\times$ 100.

NR678-treated rats, regardless of the dose (5 or 10 mg/kg), all exhibited a pleural effusion (hydrothorax), represented by the presence of 3 to 6 mL of clear, transparent fluid. The lungs were uncollapsed and generally showed diffuse dark red discoloration and wet appearance, consistent with pulmonary hyperaemia and oedema (**Figure 3.2**). The amount of blood collected from the abdominal vena cava shortly after euthanasia was consistently lower in treated animals than in the controls (approximately 1.5-2.5 mL vs. 3.5-5 mL) and the blood of the treated animals appeared darker and more viscous, indicating dehydration. In addition, treated animals exhibited relatively small prostate glands and seminal vesicles and a

distended stomach (due to the presence of a large amount of ingesta). The significance of these findings is not clear, but it is most likely that they are indirect effects of the primary, toxic pulmonary changes. Food impaction in the stomach may have been caused by reduced amounts of water in the gastric content due to dehydration together with decreased gastric motility related to the deteriorating health. Reduction in size of the male genital accessory glands is a common finding in rodents during debilitating conditions (Greaves, 2007c) and may have been caused again by dehydration and consequent reabsorption of water from glandular secreta.

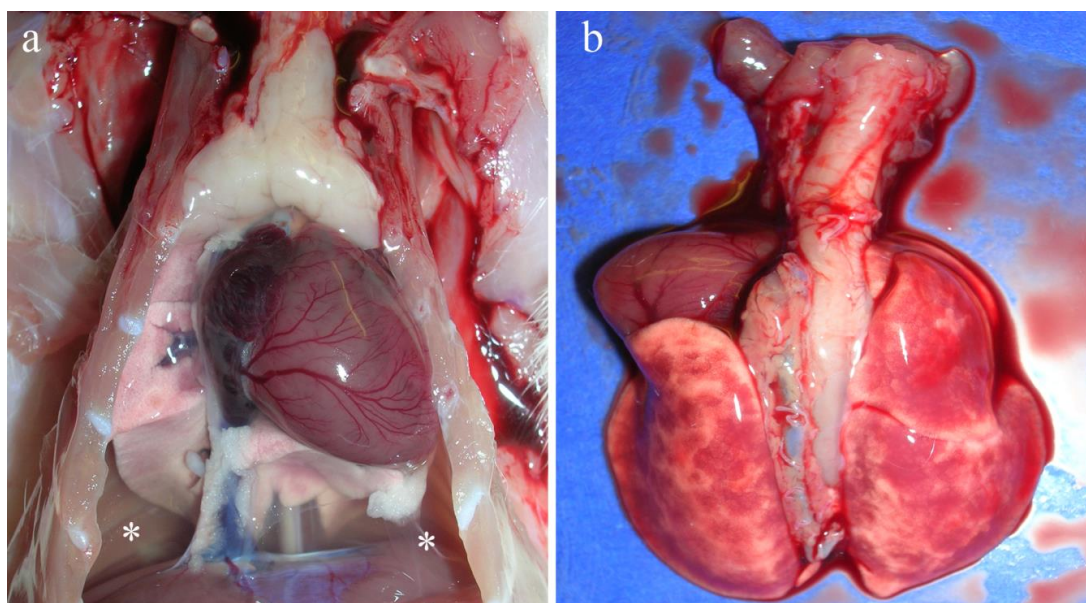


**Figure 3.2.** Macroscopic findings in rats administered a high dose (5 or 10 mg/kg) of NR678. (a) Rat 10L-1248 (10 mg/kg of NR678, euthanased at 6 h post dosing). The pleural cavity contains a moderate amount of clear fluid (\*). (b) Rat 11L-2405 (5 mg/kg of NR678, 6 h post dosing). The lungs appear wet and exhibit mottled to diffuse red discolouration.

### **3.1.3 Cytological and histological findings in rats that had received a high dose of NR678**

The cytological specimens prepared from sediments of the thoracic fluid of rats receiving 10 mg/kg exhibited low cellularity. They showed occasional individualised, non reactive mesothelial cells within a moderately proteinaceous background, suggesting the fluid was a transudate.



The histological changes observed in NR678-treated rats were restricted to the lungs and liver. Compared to control rats (**Figure 3.3a,c**), the main histological feature in the lung of treated animals was a multifocal alveolar oedema, characterised by the presence of moderate to high amounts of eosinophilic, homogenous or faintly granular material filling the alveolar lumen (**Figure 3.3b**). Alveoli located immediately beneath the pleura were most intensely affected. Similar proteinaceous material was diffusely present in the interstitium surrounding bronchi and blood vessels (interstitial oedema; **Figure 3.3d**). Lymphatic vessels were dilated and contained large amounts of similar eosinophilic material. Pulmonary blood vessels and capillaries appeared markedly dilated and engorged with red blood cells (hyperaemia). The alveolar and interstitial fluid did not stain positive for fibrin using special stains (MSB Trichrome, PTAH and Fraser-Lendrum). NR678-induced microscopic changes were not dose-related as they occurred with similar incidence and severity in both treatment groups. However, rat 11L-2406 that had been given NR678 at a dose of 5 mg/kg and had shown less severe clinical signs (**Table 3.1**), also exhibited less intense pulmonary alveolar oedema (graded as mild), whereas the remaining treated animals all had moderate or marked alveolar oedema. Several treated rats also exhibited mild changes in the alveoli, represented by scattered cells showing dark condensed and fragmented nuclei (**Figure 3.4a, b**). These cells, which were most likely consistent with endothelial cells, type I or, less frequently, type II pneumocytes, based on their morphology and location within the alveolus, were shown to undergo apoptosis based on their expression of cleaved caspase 3 (**Figure 3.4d**). Increased numbers of macrophages, characterised by abundant eosinophilic foamy cytoplasm, were present within the alveoli of treated rats. They were mainly found within the alveolar lumen (**Figure 3.4a**). In both treated groups (5 and 10 mg/kg), these cells often exhibited increased cytoplasmic eosinophilia and karyolysis (necrosis).

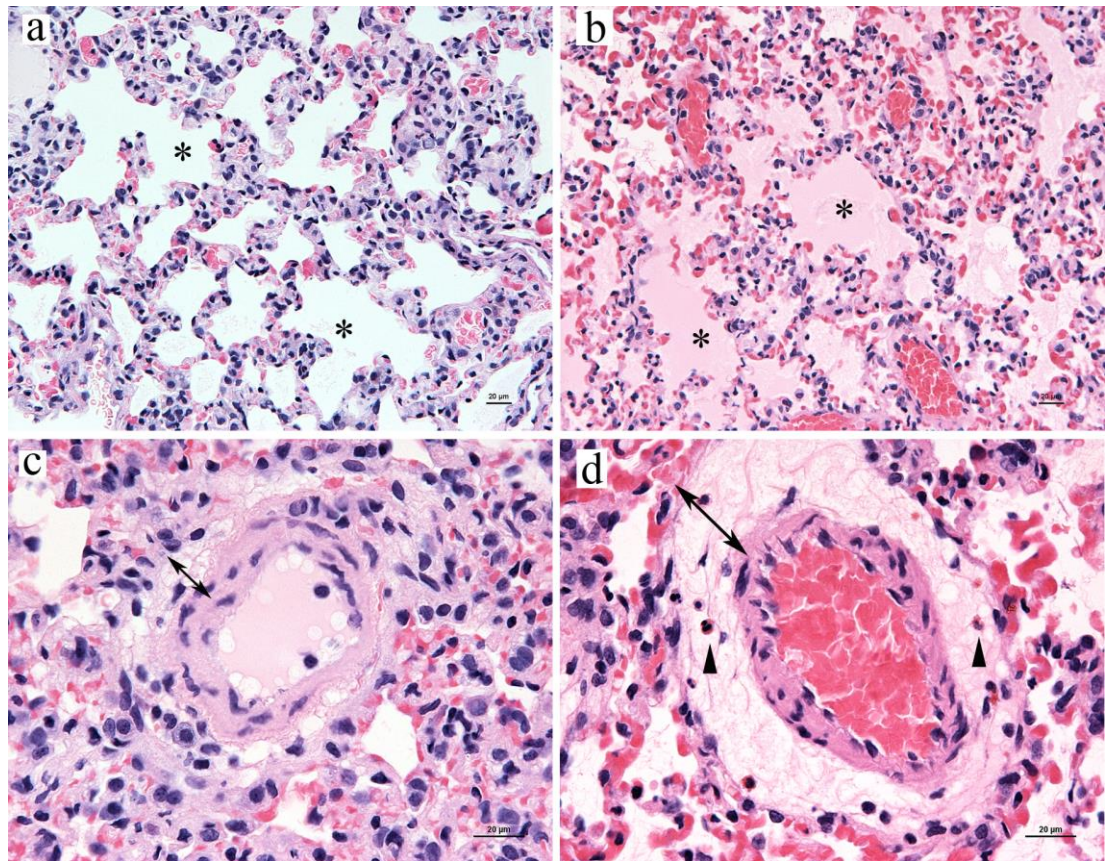


**Figure 3.3.** Histological demonstration of alveolar and interstitial oedema in the lungs of rats administered a high dose (10 mg/kg) of NR678. (a) Rat 10L-1246 (control, euthanased at 8 h post dosing). The alveolar lumen (\*) is empty. (b) Rat 10L-1247 (10 mg/kg of NR678, 7 h post dosing). Alveolar lumina (\*) contain abundant faintly eosinophilic homogenous proteinaceous fluid. Small vessels and alveolar capillaries are engorged with erythrocytes (hyperaemia). (c) Rat 10L-1246 (control). There is virtually no separation between the outline of an artery (double-headed arrow: perivascular space) and the adjacent parenchyma. (d) Rat 10L-1247 (10 mg/kg of NR678, 6 h after dosing). The perivascular space (double-headed arrow) is markedly distended due to the presence of fluid (interstitial oedema). Scattered eosinophils (arrowheads) are present in the expanded perivascular space. HE stain. Bars: 20  $\mu$ m. Lung tissue was fixed by immersion in formalin, without previous instillation.

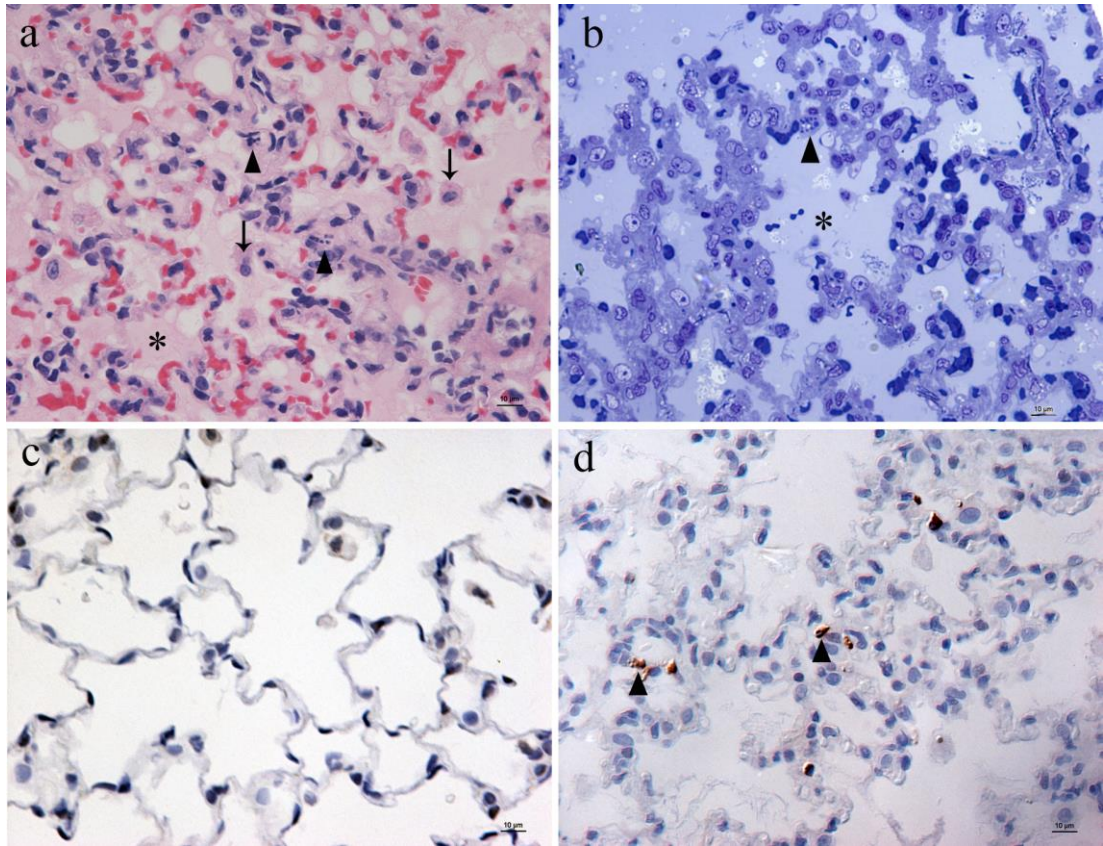


**Figure 3.4.** Histological and immunohistological demonstration of apoptotic cells within the alveolar lining in rats administered a high dose (5 mg/kg) of NR678. (a and b) Rat 11L-2405 (5 mg/kg of NR678, euthanased at 6 h post dosing). (a) Scattered cells lining the alveoli show nuclear condensation and fragmentation (arrowheads). The alveolar lumen (\*) contains proteinaceous fluid and alveolar macrophages (arrows). HE stain. (b) Alveoli filled with proteinaceous fluid (\*) and apoptotic lining cells (arrowhead) are seen in more detail in semithin sections stained with Toluidine blue. (c and d). Immunohistology for cleaved caspase 3. (c) In the control animal (11L-2402, 24 h post dosing), no positive cells are found. (d) In the treated rat (11L-2405), alveolar cell death is via apoptosis, as indicated by the presence of occasional alveolar cells (likely type I and II epithelial and vascular endothelial cells; arrowheads) expressing cleaved caspase 3. Peroxidase anti-peroxidase method, rabbit anti-human cleaved caspase 3, Papanicolaou's haematoxylin counterstain. Bars: 10  $\mu$ m.

Staining for aquaporin 5 to highlight type I pneumocytes confirmed the presence of a continuous alveolar lining (**Figure 3.5a,b**). Apart from the scattered apoptotic changes mentioned above, endothelial cells did not exhibit evident morphological changes and immunohistological staining for the endothelial cell marker von Willebrand factor (factor VIII-related antigen) confirmed the presence of an intact, non activated endothelial cell lining of blood vessels (**Figure 3.5c,d**).

Histological changes in the liver of treated animals were represented by scattered individual necrotic centrilobular hepatocytes, surrounded by a few mononuclear inflammatory cells, mainly lymphocytes and macrophages. No evidence of single cell necrosis was detected in the control rats (**Figure 3.6a**). Dying hepatocytes were characterised by increased cytoplasmic eosinophilia and dark condensed nuclei (**Figure 3.6b**) and did not express cleaved caspase 3 (data not shown), suggesting necrosis as the main mechanism of death rather than apoptosis. In the control livers, the centrilobular and midzonal hepatocytes exhibited a clear rarefied cytoplasm (**Figure 3.6a**) consistent with the accumulation of a moderate amount of glycogen. Diffuse glycogen loss was evident in all treated animals (**Figure 3.6b**), as suggested by the condensed, homogeneously eosinophilic cytoplasm of the centrilobular and midzonal hepatocytes in these rats. This finding is likely a consequence of the decreased food consumption observed in treated rats which was seen from 3 h post dosing onwards.

The incidence and severity of microscopic changes in the lungs and liver of NR678-treated rats are shown in **Table 3.2**.



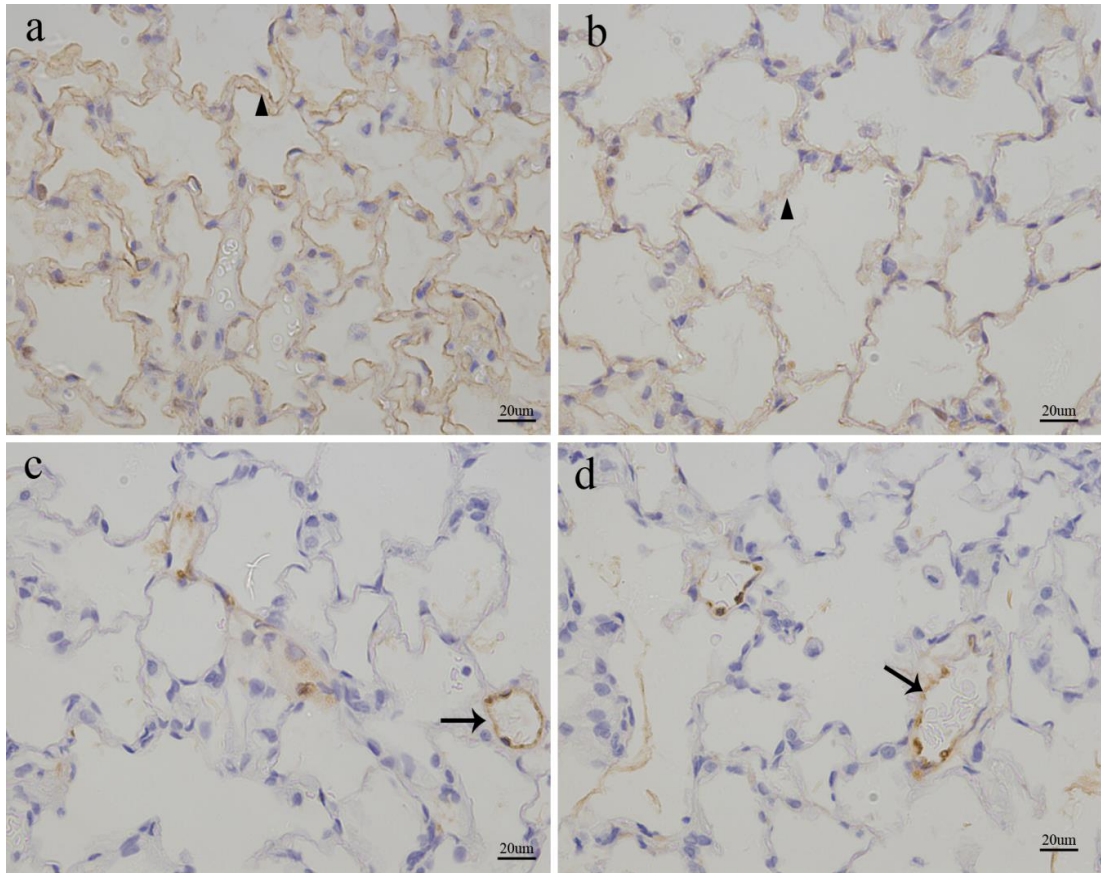


**Figure 3.5.** Immunohistological demonstration of type I pneumocytes and endothelial cells in the lungs of rats administered a high dose (5 mg/kg) of NR678. (a and b) Immunohistology for aquaporin 5. (a) Rat 11L-2402, (control, euthanased at 24 h post dosing). Aquaporin 5-positive type I pneumocytes form a continuous layer (arrowhead). (b) Rat 11L-2405 (5 mg/kg of NR678, 6 h post treatment). Like in the control animal, aquaporin 5-positive type I pneumocytes form a continuous layer. Peroxidase anti-peroxidase method, rabbit anti-rat aquaporin 5, Papanicolaou's haematoxylin counterstain. (c and d) Immunohistology for factor VIII-related antigen. (c) Rat 11L-2402. The endothelial lining (arrow) consists of a continuous layer of flat cells. (d) Rat 11L-2405. Like in the control animal, the endothelial lining is represented by a continuous layer of flat cells. Peroxidase anti-peroxidase method, rabbit anti-human factor VIII, Papanicolaou's haematoxylin counterstain). Bars: 20  $\mu$ m.

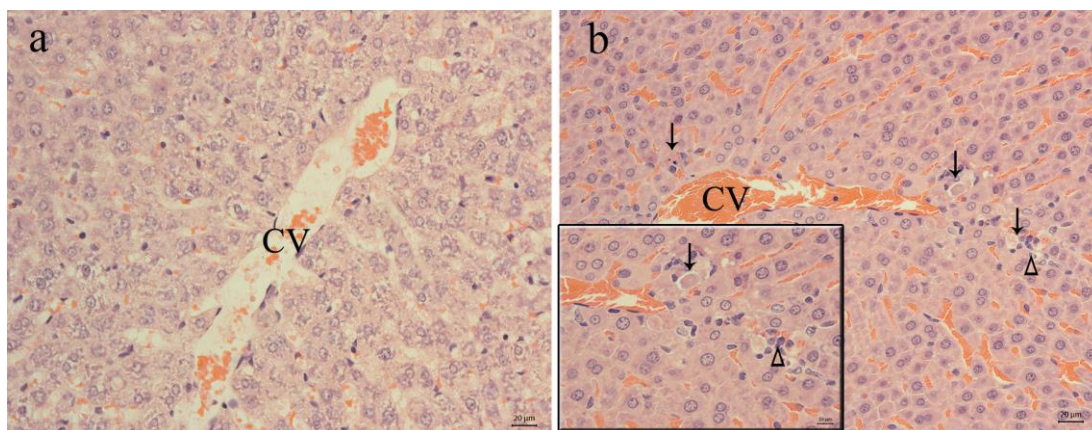


**Figure 3.6.** Histological features of the liver of rats administered a high dose (5 mg/kg) of NR678. (a) Rat 11L-2402 (control, euthanased at 8 h post dosing). The centrilobular hepatocytes are all viable and show abundant clear rarefied cytoplasm, consistent with the accumulation of glycogen. (b) Rat 11L-2405 (5 mg/kg of NR678, 6 h post dosing). Scattered necrotic hepatocytes (arrows), characterised by increased cytoplasmic eosinophilia and nuclear pyknosis, are observed in a centrilobular area, surrounded by occasional mononuclear inflammatory cells (open arrowhead). Hepatocytes have a homogeneous eosinophilic cytoplasm, indicating that they are devoid of glycogen. CV: centrilobular vein. HE stain. Bars: 20 µm. Inset: 10 µm.

**Table 3.2.** Summary of the key histological findings in lungs and liver of rats administered a high dose (5 and 10 mg/kg) of NR678.

NR678 dose (mg/kg)	Histological findings			
	Lungs			Liver
	Alveolar and interstitial oedema	Increased alveolar macrophages	Alveolar cell apoptosis	Single hepatocyte necrosis
5	3/3 (2.7)	3/3 (1.5)	2/3 (1.0)	3/3 (1.3)
10	3/3 (3.6)	3/3 (2)	2/3 (1.5)	3/3 (1.6)

Results are expressed as number of animals showing the histological finding/number of animals per group. The average severity of each finding (in brackets) was calculated by summing the severity grades and dividing the total by the number of animals affected by that finding. Severities of histological findings were graded on a scale of 1 to 5 as slight, mild, moderate, marked or severe.

NR678-related microscopic changes were observed also in the lymphoid organs. In control animals, lymphatic tissues (thymus, spleen, mesenteric lymph nodes and gut-associated lymphoid tissue) generally exhibited only rare apoptotic cells, mostly consistent with lymphocytes. In the thymus, apoptotic lymphocytes were mostly observed within the cortex (**Figure 3.7a,b**); the spleen and lymph nodes showed moderately sized primary lymphoid follicles with very occasional apoptotic lymphocytes in the centre. The number of apoptotic lymphocytes was increased in the lymphoid tissues of treated rats. In animals administered a dose of 10 mg/kg, lymphocyte apoptosis was mainly seen in the cortex of the thymus (marked severity; **Figure 3.7c,d**) and in the lymphoid follicles of the mesenteric lymph nodes; low or moderate numbers of apoptotic lymphocytes were also observed in the splenic white pulp (lymphoid follicles, marginal zone and periarteriolar lymphoid sheaths) and in the lymphoid follicles of the gut-associated lymphoid tissue. In addition, scattered apoptotic lymphocytes were also detected in the lamina propria of duodenum, jejunum and ileum. Mild to marked lymphocytic apoptosis was also present in the spleen (white pulp) and the thymus (cortex) of rats given a dose of 5 mg/kg; the remaining lymphoid organs were not examined in this cohort. The incidence and severity of microscopic changes in the lymphatic tissues of NR678-treated rats are shown in **Table 3.3**.

In addition, both control and treated animals occasionally exhibited slight to mild interstitial infiltration by eosinophils around the main pulmonary vessels and bronchi. Eosinophils were moderately increased in number in the lungs of rat 10L-1247 dosed with 10 mg/kg of NR678, where they infiltrated the interstitium surrounding small calibre vessels. These findings were not NR678-related effects because they were distributed randomly among groups or their appearance was similar to findings detected in controls from this and other studies using rats from the same strain and supplier (study 3).



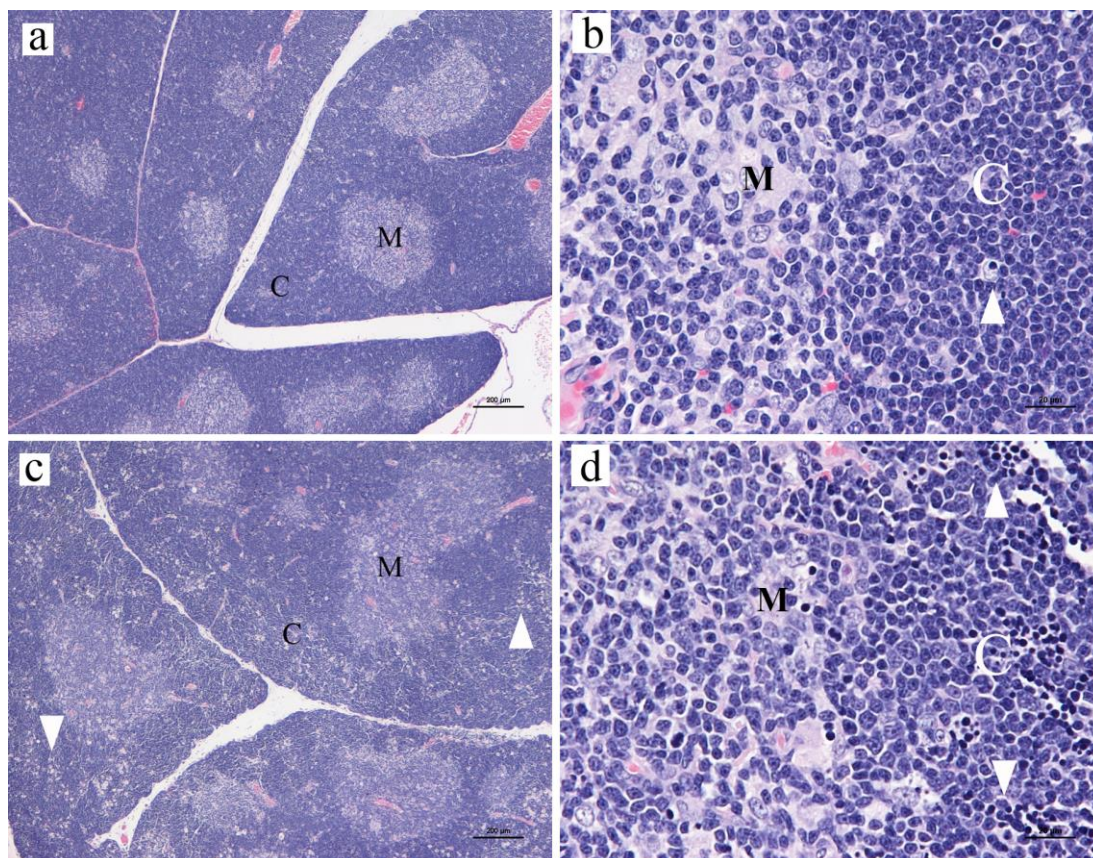


**Figure 3.7.** Histological features of the thymus of rats administered a high dose (10 mg/kg) of NR678. (a and b) Rat 10L-1245 (control, euthanased at 7 h post dosing). (a) The thymus has a normal microscopic appearance with clear distinction between cortex (C) and medulla (M). (b) Apoptotic lymphocytes (arrowhead), characterised by a dark condensed nucleus, are extremely rare in the thymic cortex. (c and d) Rat 10L-1247 (10 mg/kg of NR678, 7 h post dosing). (c) The thymic cortex exhibits decreased cellularity. (d) In the cortex, numerous apoptotic lymphocytes are seen. HE stain. Bars: 200 µm (a and c) and 20 µm (b and d).

**Table 3.3.** Summary of the key histological findings in the lymphoid tissues of rats administered a high dose (5 and 10 mg/kg) of NR678.

NR678 dose (mg/kg)	Lymphocytic apoptosis			
	Thymus	Spleen	Mesenteric lymph nodes	Gut-associated lymphoid tissue
5	3/3 (4.0)	3/3 (2.3)	NE	NE
10	3/3 (4.0)	3/3 (2.0)	1/3 (4.0)	3/3 (2.3)

Results are expressed as number of animals showing the histological finding/ number of animals per group. The average severity of each finding (in brackets) was calculated by summing the severity grades and dividing the total by the number of animals affected by that finding. NE: not examined. Severities of histological findings were graded on a scale of 1 to 5 as slight, mild, moderate, marked or severe.



### **3.1.4 Ultrastructural findings in rats that had received a high dose of NR678**

Since the light microscopic examination of the lung did not provide any evidence of overt vascular damage as a cause for the observed marked pulmonary oedema, an ultrastructural examination was undertaken.

Examination of a control animal confirmed the normal lung morphology in rats of this age group (**Figure 3.8**). Alveolar capillaries were lined by one continuous layer of endothelial cells (unfenestrated endothelium; **Figure 3.8a,b**). The amount of cytoplasm displayed by the endothelial cells varied according to the topographical distribution of the capillary (**Figure 3.8b**). Endothelial cells exhibited abundant cytoplasm and therefore appeared thick at the interface with the pulmonary interstitium and contained a moderate amount of organelles and caveolae. The cytoplasm of the endothelial cells opposing the alveolar lumen appeared markedly attenuated and almost devoid of organelles and intercellular junctions. A thin, 10-15 nm continuous electron-dense rim (basement membrane) was visible beneath the endothelium, separating it from the pneumocytes (**Figure 3.8c**). The endothelial cells opposing the type I alveolar epithelial cells, from which they are separated by the basement membrane, form the alveolar-capillary (air-blood) barrier, through which gases are exchanged (Gil, 2011; Meyrick, 1990).

In the lungs of the rat euthanased at 6 h after the administration of NR678, the general architecture of the alveolar unit was preserved and comparable to that of the control animal (**Figure 3.9a**). However, sub-endothelial or endothelial cytoplasmic bleb formation was detected within the alveolar capillaries (**Figure 3.9a,b,c**). The blebs appeared to result from the separation of the cytoplasm of the endothelial cell from the underlying basal lamina (subendothelial bleb; **Figure 3.9b**) or to have developed within the cytoplasm itself. Blebs ranged from 100 nm to 1  $\mu$ m in diameter and had a segmental distribution, being more frequent in the thin portion of the alveolar-capillary unit. They usually contained material that, due to its electron density being similar to that in the capillary lumen, was interpreted as proteinaceous material consistent with plasma. In addition, the endothelial lining appeared

multifocally discontinuous (**Figure 3.9c**). This finding was characterised by an irregular endothelial cell surface and occasional gap formation, often in areas adjacent to the intercellular junctions. In proximity to the gaps within or between endothelial cells, the alveolar lumen contained proteinaceous material with an electron-density similar to that of plasma (alveolar oedema; **Figure 3.9d**). Similarly, collagen fibres in the interstitium were separated by analogous proteinaceous material (interstitial oedema). Endothelial cells often appeared swollen (**Figure 3.9d**) and showed rarefaction or swelling of organelles and caveolae (**Figure 3.10a**) as well as formation of round electron-dense bodies (**Figure 3.10c**), interpreted as aggregates of RNA (Meyrick et al., 1972). Rarely, endothelial cells exhibited signs of irreversible injury, characterised by nuclear pyknosis and fragmentation (interpreted as apoptotic cells, **Figure 3.10d**). Ultrastructural evidence of cell death was not detected in other cell types, suggesting that those alveolar cells that were identified as apoptotic in the HE stained sections and due to their expression of cleaved caspase 3 (**Figure 3.4**) were almost exclusively endothelial cells. A few binucleated endothelial cells were also observed (**Figure 3.10d**).

### **3.1.5 Bioanalytical method validation of NR678 and lack of metabolic turnover at HPLC**

NR678 was found to elute at 16.2 min (**Figure 3.11**). A calibration curve was generated (concentrations: 0.001–5 mM; **Figure 3.11 inset**) and the LLoQ was determined to lie between 0.005 and 0.01 mM. Mean test values were within 10% of the actual value when different replicates (accuracy) and batches (precision) were run. NR678 gave consistent elution times and total absorbance values when it was stored at different temperatures (RT, 4°C and -20°C) for different amounts of time (6 h, 24 h, 48 h and 7 d) or after freeze and thaw cycles. In both liver and lung rat microsomal suspensions, no discernible metabolite of NR678 was detected at either low or high concentrations. HPLC analysis of liver and lung microsomal incubations of the reference standard PTU revealed a single metabolic peak (**Figure 3.12**), presumably consistent with PTU-sulphenic acid as previously described (Henderson et al., 2004b).

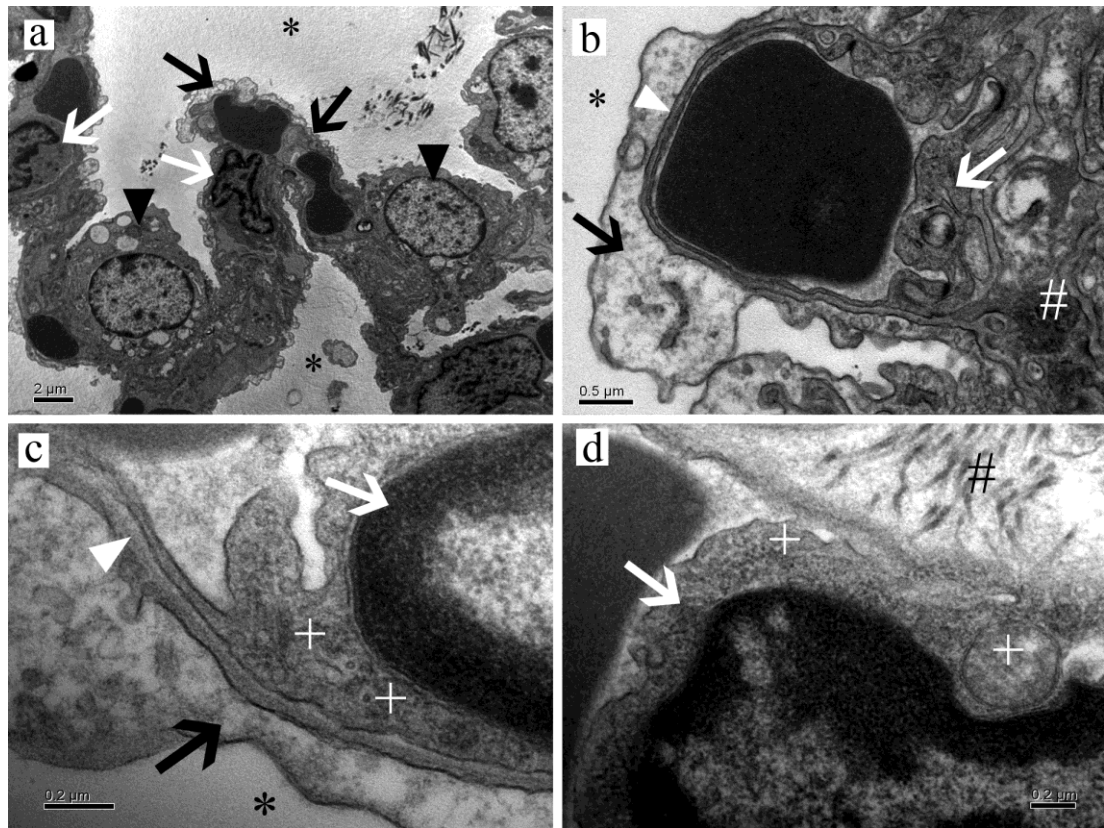


**Figure 3.8.** Ultrastructural features of the air-blood barrier in the normal rat lung. Rat 11L-2402 (Control, euthanased at 8 h post dosing). (a) The alveolar lumen (\*) is lined by type I (black arrows) and type II (black solid arrowheads) pneumocytes and contains capillaries lined by endothelial cells (white arrows). (b) Type I pneumocytes (black arrow) are separated from the underlying capillary endothelial cells by a fused continuous basal lamina (white arrowhead). Endothelial cells are flat where they interact with type I pneumocytes, whereas they are thicker (white arrow indicates endothelial cell cytoplasm) at the interface with the alveolar interstitium (#). (c) Closer view of the air-blood barrier. The basement membranes of the type I pneumocyte (black arrow) and the endothelial cell (white arrow) are fused and form a single layer (white arrowhead). The cytoplasm of both cell types contains a small quantity of organelles (+). (d) Closer view of a portion of an endothelial cell (white arrow) opposing the interstitium (#). Rough endoplasmic reticulum and mitochondria are seen within the cytoplasm (+).

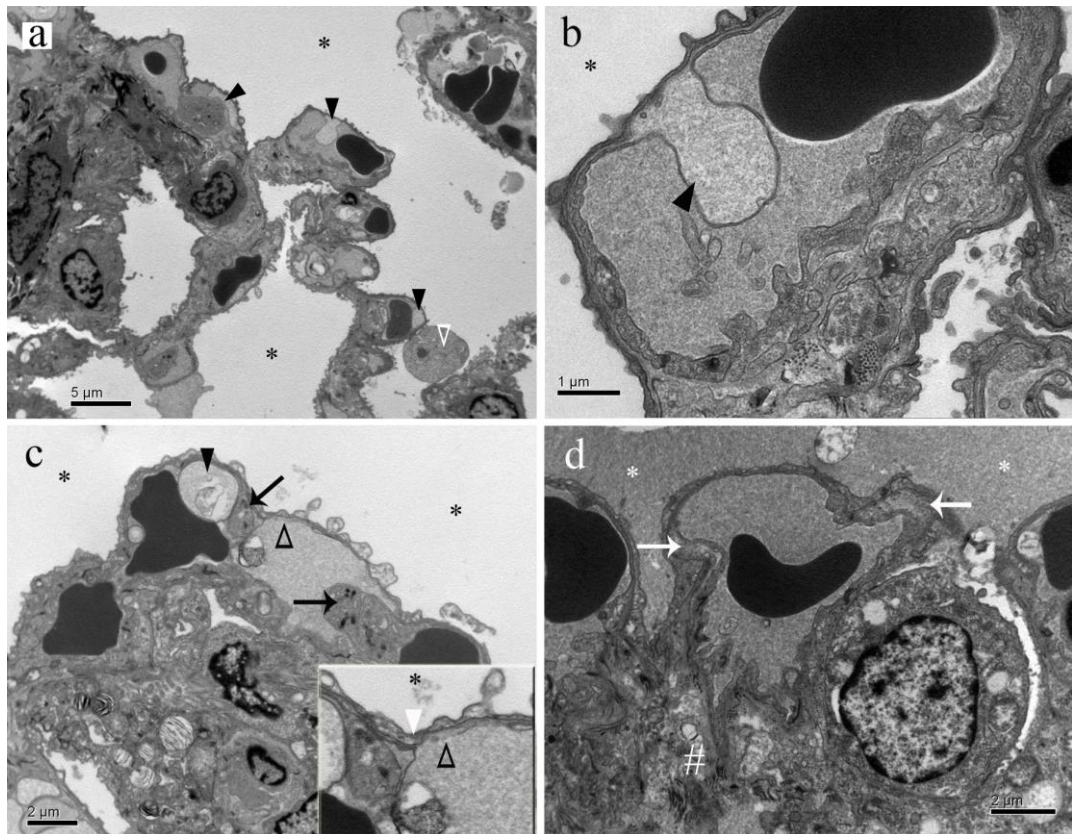


**Figure 3.9.** Ultrastructural features of the air-blood barrier in the lung of a rat administered a high dose (5 mg/kg) of NR678. Rat 11L-2405 (euthanased at 6 h post dosing). (a) The architecture of the alveolar unit is preserved, however, endothelial cells appear partially detached from the basement membrane and protrude into the capillary lumen to form up to 1  $\mu\text{m}$  blebs (solid black arrowheads). A degenerate macrophage (open white arrowhead) is seen within the alveolar lumen (\*). (b) Closer view of a subendothelial bleb. The cytoplasm of the endothelial cell is separated from the underlying basement membrane, forming a 1  $\mu\text{m}$  in diameter cleft (solid black arrowhead). (c) The endothelial lining appears multifocally discontinuous and exhibits occasional gaps (open black arrowhead). Endothelial cells with a fragmented nucleus (apoptosis; solid black arrow) are observed infrequently. Inset: gap formation (open black arrowhead) occurs in the vicinity of the cellular junction (solid white arrowhead) (d) The alveolar lumen (\*) is filled with granular proteinaceous material similar to the material present in the capillary lumen (plasma). Similar material multifocally expands the air-blood barrier (white arrows) and the interstitium (#).

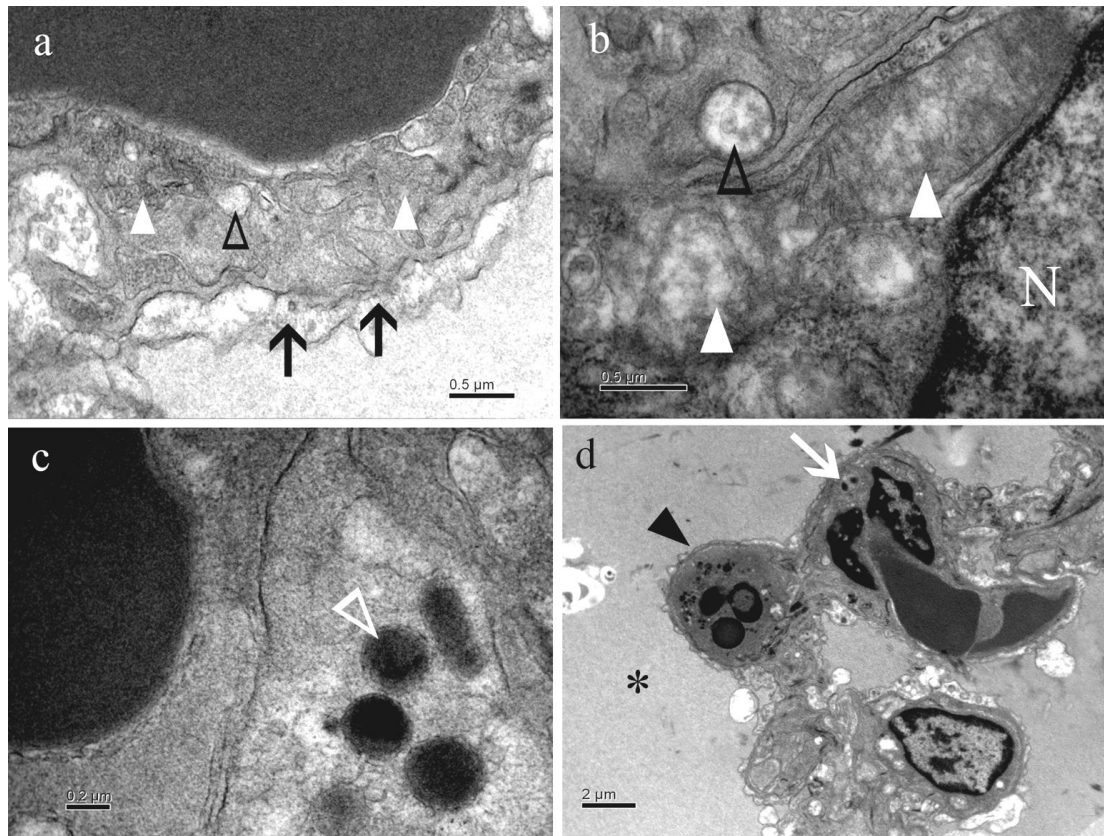


**Figure 3.10.** Ultrastructural features of the endothelial cell lining in the alveolar capillaries of the lung of a rat administered a high dose (5 mg/kg) of NR678. Rat 11L-2405 (ethanased at 6 h post dosing). (a) The basement membrane is multifocally discontinuous (black arrows). The cytoplasm of the endothelial cell is distended and contains swollen mitochondria (solid white arrowheads) and dilated caveolae (open black arrowheads). (b) Closer view of the cytoplasm of an endothelial cell (N; nucleus) exhibiting swollen mitochondria (solid white arrowheads) and dilated caveolae (open black arrowheads). (c) Multifocal round or oval electron dense aggregates (open white arrowhead) are seen within the cytoplasm of an endothelial cell. (d) Occasional apoptotic (solid black arrowhead) and binucleated (white arrow) endothelial cells are seen. The adjacent alveolar lumen is filled with granular proteinaceous fluid (\*).

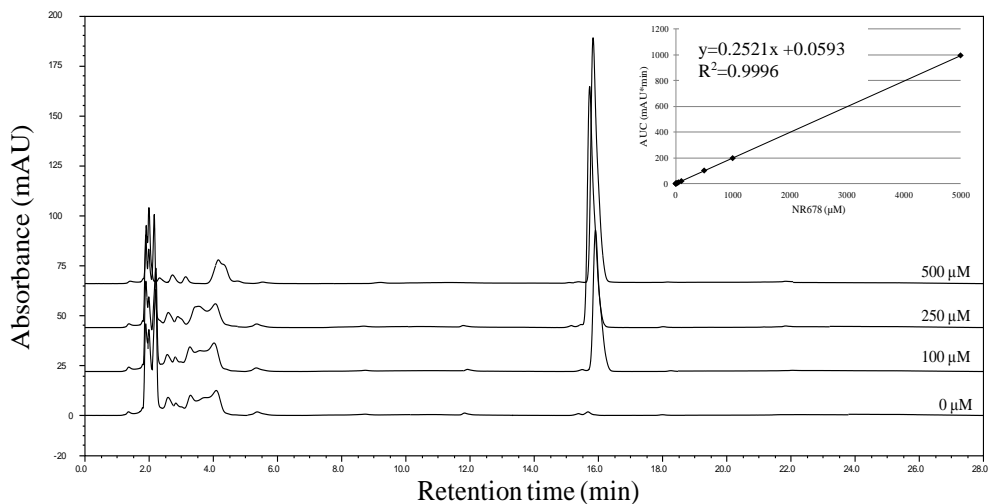


**Figure 3.11.** Overlaid HPLC UV chromatograms of different standard concentrations of NR678 dissolved in methanol. Inset: linear calibration curve. The mobile phase is methanol and distilled water at a flow rate of 0.9 mL/min. UV: 230 nm.

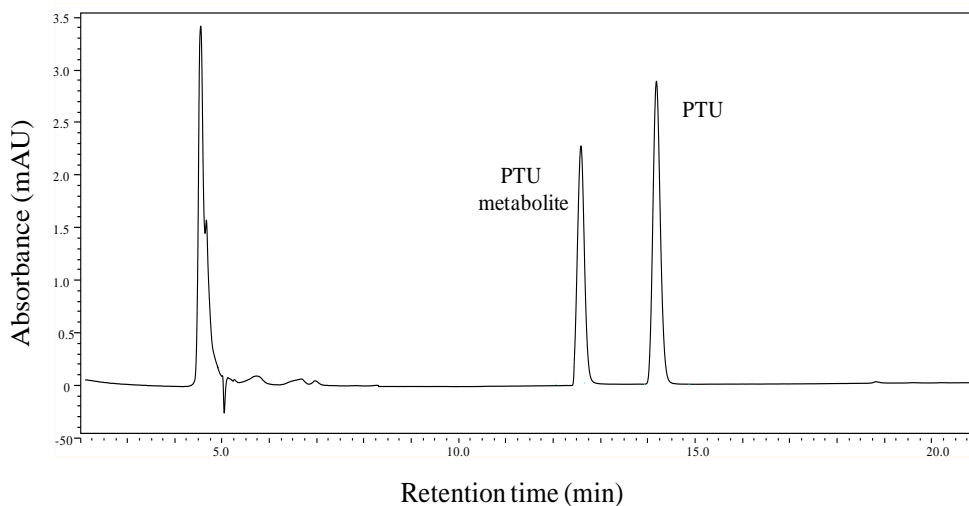


**Figure 3.12.** HPLC UV chromatograms of phenylthiourea incubated in rat lung microsomes. A single metabolite peak is discernible at approximately 12.7 min. The mobile phase is methanol and distilled water at a flow rate of 0.9 mL/min. UV: 230 nm.

## **3.2 *In vivo* investigation into the pulmonary defence responses involved in the prevention of NR678-induced lung injury**

As mentioned before, the administration of low non-lethal doses of the thiourea-based rodenticide ANTU to rats resulted in the development of tolerance to normally lethal doses (Barton et al., 2000; Dieke and Richter, 1946; Van Den Brenk et al., 1976). In order to investigate whether this was also the case for NR678, a pilot study (study 2) was undertaken in which rats received a low dose (0.5 mg/kg) of NR678, followed 3 h later by a dose that had been previously shown to be lethal (5 mg/kg, see paragraph 1.1). Rats did not succumb to the high dose, suggesting they had developed the expected tolerance. Subsequently, a more extensive study (study 3) was carried out to investigate the morphological changes associated with the development of tolerance to NR678 over a period of 14 d. This study comprised rats that received the low dose alone (group 3) and rats administered the low dose, followed 3 h later by the high dose (group 4).

### **3.2.1 Clinical assessment of NR678 tolerogenic dose regimen (study 2)**

In study 2, five rats received NR678 at a dose of 0.5 mg/kg, followed, after 3 h, by a dose of 5 mg/kg. All rats survived until the end of the study (day 7). No clinical signs were observed after the administration of the LD, within the 3 h prior to administration of the HD. The first clinical signs were evident at 3-4 h after the administration of the HD, when rat 10L-4742 exhibited mildly decreased motor activity (**Table 3.4**). On day 2, all rats showed mild clinical signs, including decreased motor activity, piloerection, hunched posture and rapid breathing. Two rats still exhibited mild rapid breathing and piloerection during the morning of day 3, but recovered completely by midday. After this, no clinical signs were observed until the end of the experiment. Animals gained weight during the study (data not shown) and showed normal food consumption. The clinical observations described in these animals are suggestive of minor respiratory distress and mild general illness, when compared with the clinical signs of severe respiratory distress seen after the

administration of the HD alone (see paragraph 3.1.1 and **Table 3.1**). The resolution of these signs within less than 48 h confirms the development of tolerance.

**Table 3.4.** Clinical signs observed in rats that had received a low dose (0.5 mg/kg) of NR678, followed by a high dose (5 mg/kg) after 3 h (study 2). Euthanasia (E) was performed on day 7.

Rat ID	Day 1				Day 2			Day 3			Days 4 to 7
	930am	12pm	3pm	430pm	8am	12pm	3pm	9am	12pm	3pm	
10L-4742	NCSO	NCSO	DMA	DMA	DMA, PI, HP, RB (1)	DMA, PI, HP, RB (1)	DMA, PI, HP, RB (1)	RB (1)	NCSO	NCSO	NCSO. E
10L-4743	NCSO	NCSO	NCSO	NCSO	DMA	DMA	DMA	NCSO	NCSO	NCSO	NCSO. E
10L-4744	NCSO	NCSO	NCSO	NCSO	NCSO	SL	SL	NCSO	NCSO	NCSO	NCSO. E
10L-4745	NCSO	NCSO	NCSO	NCSO	DMA, PI, HP, RB (1)	DMA, PI, HP, RB (1)	DMA, PI, HP, RB (1)	PI, RB (1)	NCSO	NCSO	NCSO. E
10L-4746	NCSO	NCSO	NCSO	NCSO	DMA	DMA, SL	DMA, SL	NCSO	NCSO	NCSO	NCSO. E

NCSO: no clinical signs observed; HP: hunched posture; DMA: decreased motor activity; PI: piloerection; RB: rapid breathing (tachypnoea); SL: salivation; ID: identification. Numbers in brackets indicate the severity of tachypnoea (mild: 1).

### 3.2.2 Assessment of tolerance in NR678-treated rats (study 3)

In study 3, rats received the low dose of NR678 (group 3) or, as in study 2, the low dose followed by the high dose after 3 h (group 4) and were culled at different time points (see **Table 2.2** and **Figure 2.1**). The results obtained from these two groups were compared with those of rats administered the vehicle (controls, group 1) or the high dose (group 2).

#### 3.2.2.1 Changes observed in rats administered a low dose (0.5 mg/kg) of NR678 (group 3)

##### 3.2.2.1.1 Clinical assessment

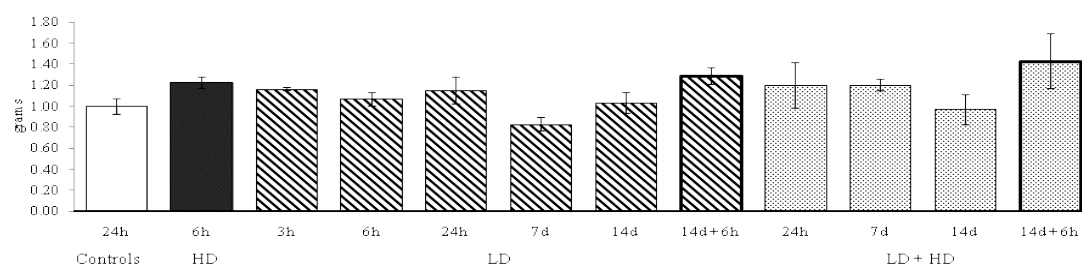
All rats survived until the end of the study (day 14). No clinical signs were recorded in these animals at any time point.



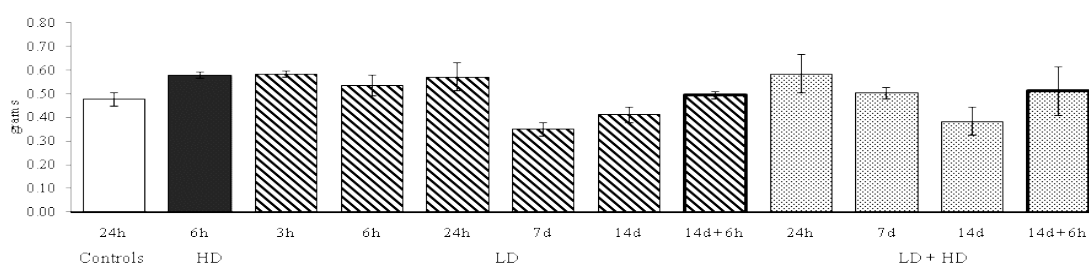
### 3.2.2.1.2 Gross post mortem findings

There was no evident difference in lung weights (right lobes only) between rats that had received a dose of 0.5 mg/kg of NR678 (group 3) and control animals (**Figure 3.13**). There were no relevant gross findings in these rats.

#### (a) Absolute lung weights



#### b) Relative to body lung weights [(absolute lung weight/body weight) × 100]



#### (c) Relative to brain lung weights

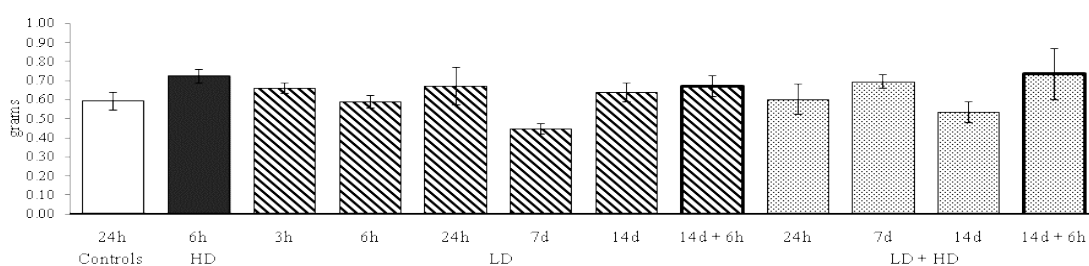


**Figure 3.13.** Absolute and relative lung weights after the administration of NR678 at a dose of 0.5 mg/kg (LD; group 3) or 0.5 mg/kg, followed 3 h later by 5 mg/kg (LD + HD; group 4). Group 3 and 4 rat cohorts challenged with a dose of 5 mg/kg of NR678 on day 14 and euthanased 6 h later are highlighted (bold outlines). Data are presented as mean  $\pm$  standard deviation for n=3. Data from the controls (group 1) and rats administered 5 mg/kg (HD; group 2) are reported here for comparison purposes.

### 3.2.2.1.3 Histological and immunohistological findings

The histological changes observed in rats that had received a dose of 0.5 mg/kg of NR678 (group 3) were restricted to the lungs. No relevant changes were found in the other organs examined microscopically, i.e. liver, kidneys, heart, brain, spleen and thymus.

In the lungs, there was no evidence of alveolar and interstitial oedema, as it was seen with the acute pulmonary toxicity of NR678 observed in rats administered a dose of 5 mg/kg (group 2; see paragraph 3.1.3.). Rats that had received a dose of 0.5 mg/kg of NR678 exhibited slight to mild type II pneumocyte hyperplasia; histological evidence of it was first seen at 24 h (**Figure 3.14b**). Pneumocyte hyperplasia was most obvious at day 7 post dosing (**Figure 3.14c**) and no longer present on day 14 (**Figure 3.14d**). Type II pneumocyte hyperplasia was characterised by a diffuse mild thickening of the alveolar septa due to the presence of large cuboidal cells with abundant pale eosinophilic cytoplasm and a large round euchromatic nucleus with a single prominent nucleolus. Most of these cells were located at the junction between alveolar septa (alveolar “corners”) and were confirmed to be type II pneumocytes by their expression of SP-C, as shown by IH. Similarly to rats administered a high dose of NR678 (5 or 10 mg/kg; see **Table 3.2**), increased numbers of macrophages (graded slight to mild) were present free in the alveolar lumen. Only occasional macrophages, characterised by an average diameter of 15 µm and homogenous eosinophilic cytoplasm, were seen in the control animals (**Figure 3.14a**); in treated rats, alveolar macrophages were more numerous and larger (up to 30 µm diameter), with abundant finely vacuolated clear cytoplasm (**Figure 3.14b**). The increase in macrophages was pronounced in all animals at the early time points (3, 6 and 24 h), whereas it was less frequently observed (one rat of three), and if, then only with a slight degree, at 7 and 14 d after dosing.

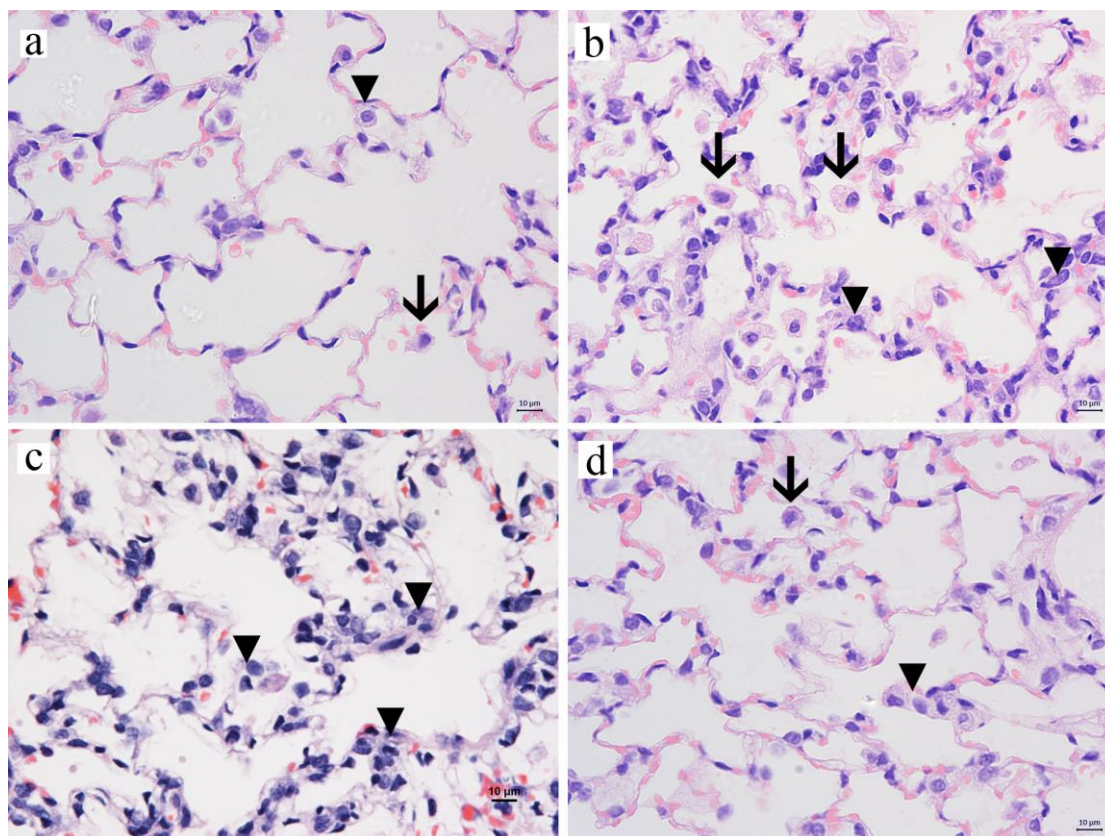


**Figure 3.14.** Histological findings in the lungs of rats euthanased at different time points after the administration of NR678 at a dose of 0.5 mg/kg. (a) Rat 11L-2402 (control, euthanased at 24 h). Thin alveolar septa are shown, lined by type I and type II (arrowhead) alveolar epithelial cells. Occasional macrophages (arrow) are seen free in the alveolar lumen. (b) Rat 11L-2428 (0.5 mg/kg of NR678, 24 h). Alveolar septa are thickened by increased numbers of cells, several of which exhibit morphological features consistent with type II pneumocytes (arrowheads). The number of macrophages present in the alveolar lumina (arrows) is increased. Macrophages are large (up to 30 µm in diameter) and foamy. (c) Rat 11L-2429 (0.5 mg/kg of NR678, 7 d). Increased numbers of type II pneumocytes are evident. Only very few macrophages are noted, similarly to controls. (d) Rat 11L-2436 (0.5 mg/kg of NR678, 14 d). The numbers of macrophages within the alveolar lumina and type II pneumocytes are comparable to those in the control animals. HE stain. Bars: 10 µm.

Histological findings in rats receiving a dose of 0.5 mg/kg of NR678 are summarised in **Table 3.5**.

**Table 3.5.** Summary of the key histological findings in the lungs of rats that had received a low dose (0.5 mg/kg) of NR678 (group 3).

Group	Dose (mg/kg)	Time of death post treatment	Histological findings			
			Alveolar and interstitial oedema	Increase in alveolar macrophages	Type 2 pneumocyte hyperplasia	Alveolar cell apoptosis
1	0	24 h	0/3	0/3	0/3	0/3
2	5	6h	3/3 (2.6)	3/3 (2)	0/3	2/3 (1.5)
3	0.5	3 h	0/3	3/3 (1.6)	0/3	0/3
		6 h	0/3	3/3 (2)	0/3	0/3
		24 h	0/3	3/3 (2)	2/3 (1)	0/3
		7 d	0/3	1/3 (1)	3/3 (1.3)	0/3
		14 d	0/3	1/3 (1)	0/3	0/3

Results are expressed as number of animals showing the histological finding/ number of animals per group. The average severity of each finding (in brackets) was calculated by summing the severity grades and dividing the total by the number of animals affected by that finding. Data from the controls (group 1) and rats administered the high dose (group 2) are reported here for comparison purposes.

A Masson Trichrome stain for the detection of collagen was performed on the lungs of selected rats euthanased on days 7 and 14 after dosing. This did not provide evidence of increased amounts of collagen in these animals when compared to the controls (results not shown).

An attempt to confirm the increased numbers of type II pneumocytes and macrophages seen histologically was conducted using IH for SP-C and lysozyme. Staining for SP-C antigen in control animals consisted of a faint brown granular cytoplasmic reaction; the positive granules within the cytoplasm are likely consistent with immunolabelled lamellar and multivesicular bodies which represent the cellular storage compartment of mature SP-C (Conkright et al., 2001). These granules were generally low in number (one to three per cell) and were predominantly seen in the perinuclear cytoplasm (**Figure 3.15a**). In the treated animals, a similar granular pattern of positivity was observed, although the staining intensity appeared generally stronger, the granules were more numerous and often tended to coalesce forming a crescent-shaped brown area around the nucleus, in particular in the lungs of rats euthanased on day 7 (**Figure 3.15d**). Rare immune-stained cells were detected within the alveolar lumen and were interpreted as desquamated type II pneumocytes or as

macrophages containing SP-C as a result of surfactant degradation (Fehrenbach, 2001). The vast majority of cells that were free in the alveolar lumen did not express SP-C and were consistent with alveolar macrophages (**Figure 3.15b,c**). In the lungs of the control animals, the lysozyme expression was seen in numerous cells lining the alveoli, several of which had the morphology of type II pneumocytes, and in cells present in the alveolar lumen (interpreted as alveolar macrophages; **Figure 3.16a**). The latter generally exhibited a stronger staining intensity than type II pneumocytes, which was due to the presence of numerous cytoplasmic dark-brown dense granules [likely consistent with lysosomes, where lysozyme is mainly stored (Gibson and Phadke, 1994)], in addition to the diffuse light brown cytoplasmic staining that was seen in all positive cells. In treated rats, lysozyme-expressing alveolar cells consistent with type II pneumocytes were similar in size and morphology to those of control animals, but alveolar macrophages generally appeared larger as seen also with histology and exhibited a stronger staining (**Figure 3.16b,c**).

In order to corroborate the histological results, the SP-C- and lysozyme-positive cell populations were counted separately in all treated groups (expressed as the average proportion of total cells present in the field/10 fields) and compared to those found in the control lungs. In the latter, type II pneumocytes expressing SP-C represented approximately 7% of total cells in the alveolar unit field (**Figure 3.17a**). Type II pneumocyte hyperplasia observed histologically (see **Table 3.5**) was confirmed by the statistical analysis, which demonstrated a highly significant ( $p < 0.001$ ) increase (compared to controls) in the proportion of cells expressing SP-C in rats euthanased on day 7 after dosing, where type II pneumocytes represented approximately 18% of the total cells in the alveolar unit (**Figure 3.17a**). No significant differences were found at earlier time points, including in rats euthanased at 24 h after the administration of NR678, in contrast to the histopathological results (see **Table 3.5**). The proportions of SP-C labelled type II pneumocytes in rats euthanased on day 14 were still slightly higher than in control rats, although no statistical significance was observed. On the other hand, in the lungs of the control animals, lysozyme positive cells represented approximately 16% of the total alveolar cells (**Figure 3.17b**), and those within the alveolar lumen (free alveolar macrophages) were detected and represented less than 2% of total cells per field (**Figure 3.17c**). Accordingly,

lysozyme-positive alveolar lining cells accounted for approximately 14% of all cells in the alveolar unit (**Figure 3.17d**), half of which may be assumed to represent type II pneumocytes, according to SP-C immunohistology (7%; see **Figure 3.17a**). A time-dependent increase in the total number of lysozyme positive cells was detected in treated rats (**Figure 3.17b**). The proportion of positive cells progressively increased from as early as 3 h after dosing (approximately 19% of total cells) until day 7. The increase was statistically significant at the 6 h ( $p < 0.05$ ) and day 7 ( $p < 0.01$ ) time points (22% and 23% of total cells, respectively). The rats euthanased on day 14 exhibited scores similar to the controls (17%). Already at 3 h after the administration of the LD, the percentage of macrophages free in the lumen of the alveoli was twice as high as in the controls (approximately 4% of total cells, see **Figure 3.17c**). The increase was statistically significant ( $p < 0.01$ ) at the 6 h and 24 h time points, where macrophages in the alveolar lumen represented approximately 6% of the total cells. From 24 h onwards, the number of desquamated macrophages decreased progressively (4.3% at day 7) to reach at day 14 levels similar to controls (2.3%). The proportion of lysozyme-positive cells lining the alveoli was only slightly increased or similar to that of controls (approximately 14% of total cells in the alveolar unit) in treated rats euthanased at early time points (3, 6 and 24 h) after dosing (**Figure 3.17d**). These data paralleled those obtained at these time points with the SP-C staining, suggesting that the increase in cellularity observed in the early stage of NR678-induced pulmonary injury mainly represents a raise in the numbers of alveolar macrophages. On day 7, rats exhibited a significant ( $p < 0.05$ ) increase in the proportion of lysozyme-expressing alveolar cells, accounting for approximately 18% of all cells. The results obtained from the SP-C staining in rats euthanased at this time point suggested that the lysozyme-containing alveolar cells are mostly type II pneumocytes. At the 14 d time point, percentages of lysozyme-positive alveolar cells were decreased to approximately 15%.



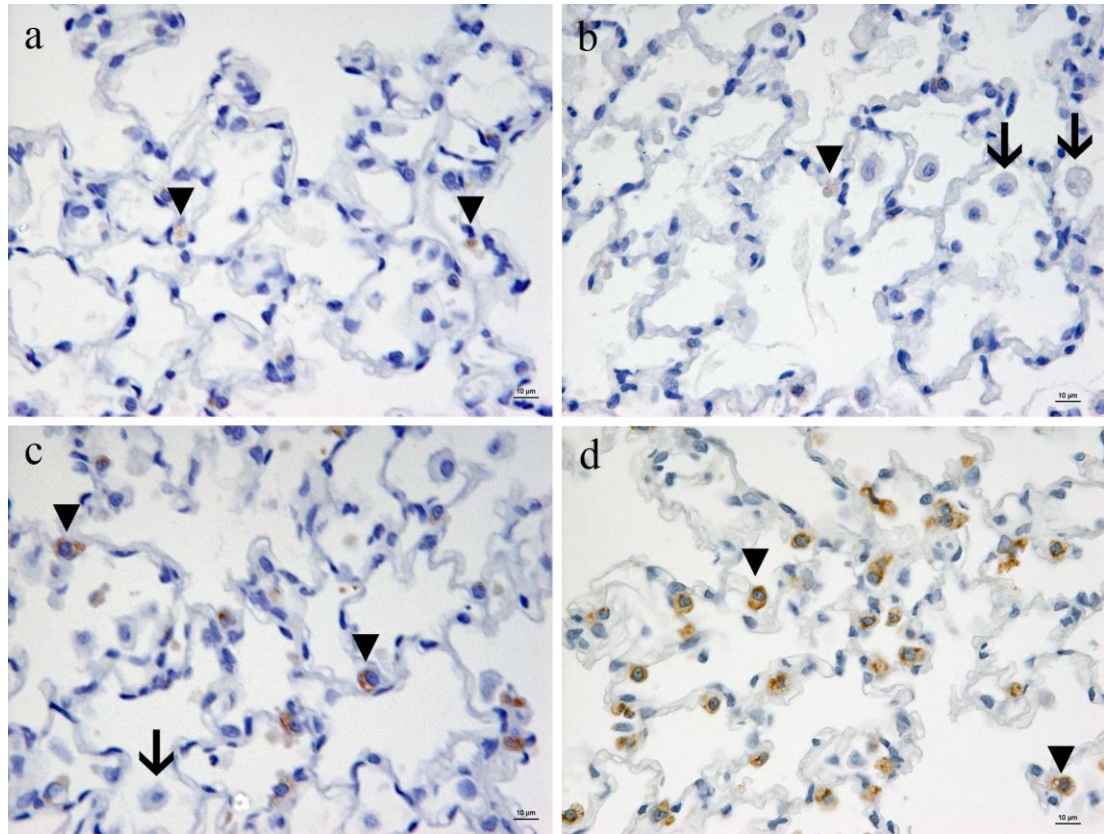


**Figure 3.15.** Immunohistological demonstration of SP-C expressing cells (type II pneumocytes) in the lungs of rats euthanased at 24 h and 7 d after the administration of NR678 at a dose of 0.5 mg/kg (group 3), compared to control rats and rats that had received a high dose (5 mg/kg) of NR678. (a) Rat 11L-2403 (control, euthanased at 24 h). Scattered type II pneumocytes in the alveolar wall are seen, they are identified based on their morphology in combination with the expression of SP-C (arrowheads). Type II pneumocytes exhibit localised faint cytoplasmic staining. (b) Rat 11L-2405 (5 mg/kg of NR678, 6 h). The number of SP-C positive type II pneumocytes is comparable to those of the controls. Numerous large cells (arrows) that do not express SP-C are present within the alveolar lumen (consistent with alveolar macrophages). (c) Rat 11L-2428 (0.5 mg/kg of NR678, 24 h). Alveoli exhibit numbers of SP-C positive type II pneumocytes similar to the controls or only slightly increased. (d) Rat 11L-2430 (0.5 mg/kg of NR678, 7 d). The number of SP-C positive cells is increased. Type II pneumocytes can be identified based on their strong perinuclear granular cytoplasmic staining. Peroxidase anti-peroxidase method, rabbit anti-human SP-C, Papanicolaou's haematoxylin counterstain. Bars: 10 µm.

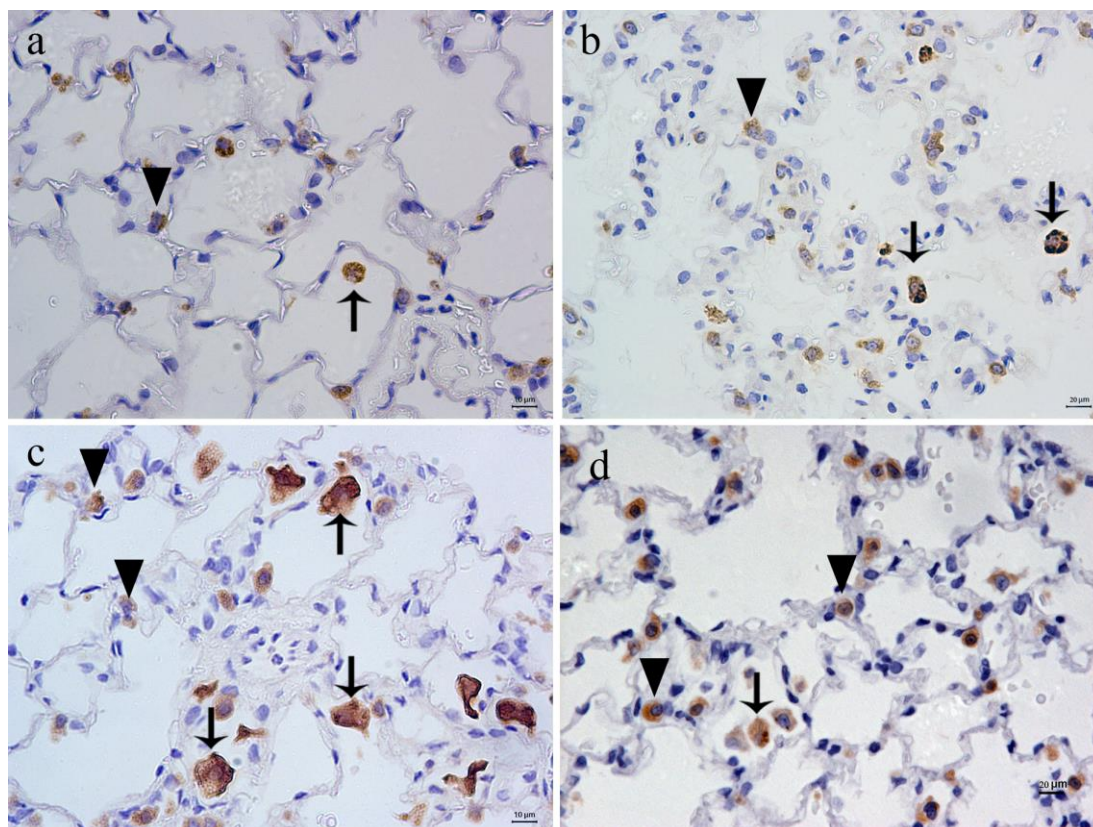


**Figure 3.16.** Immunohistological demonstration of lysozyme-expressing cells (type II pneumocytes and macrophages) in the lungs of rats euthanased at 24 h and 7 d after the administration of NR678 at a dose of 0.5 mg/kg (group 3), compared to control rats and rats that had received a high dose (5 mg/kg) of NR678. (a) Rat 11L-2402 (control, euthanased at 24 h). Numerous lysozyme-positive cells are seen lining the alveoli (type II pneumocytes; arrowhead). Only scattered positive cells are seen within the alveolar lumen (alveolar macrophages; arrow). (b) Rat 11L-2405 (5 mg/kg of NR678, 6 h). Lysozyme-positive cells within the alveolar lumen (alveolar macrophages) are slightly increased in number compared to controls and exhibit strong granular cytoplasmic staining. (c) Rat 11L-2428 (0.5 mg/kg of NR678, 24 h). Alveolar macrophages are clearly increased in number and are larger than those in the controls. They also exhibit a stronger staining intensity than type II pneumocytes. (d) Rat 11L-2431 (0.5 mg/kg of NR678, 7 d). Lysozyme-positive cells lining the alveoli are more numerous than in the control lungs. Peroxidase anti-peroxidase method, rabbit antibody against human lysozyme, Papanicolaou's haematoxylin counterstain. Bars: 20  $\mu$ m.



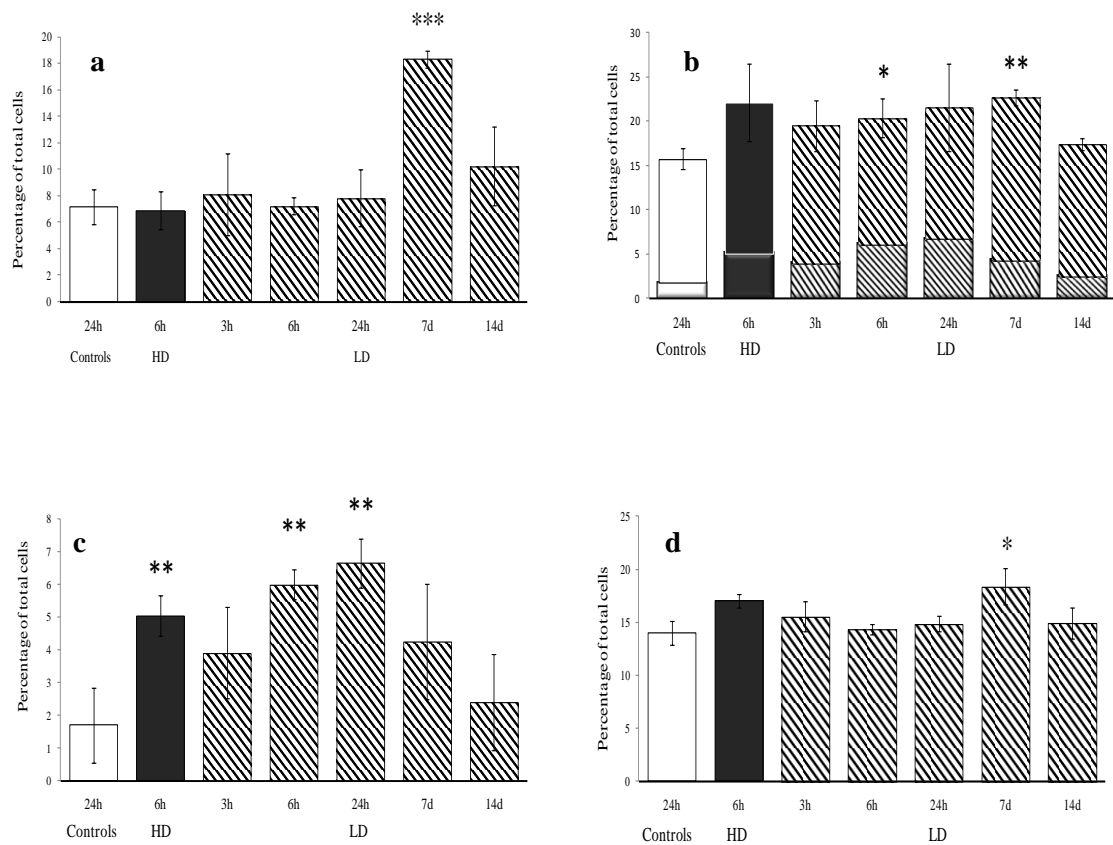


**Figure 3.17.** Immunohistological assessment of the percentage of cells expressing SP-C and lysozyme in the lungs of rats after the administration of NR678 at a dose of 0.5 mg/kg (LD; group 3). (a) Percentages of total cells expressing SP-C (type II pneumocytes). (b) Percentages of total cells expressing lysozyme, including both free alveolar macrophages (bottom bar) and alveolar lining cells (top bar). Error bars refer to the overall percentage of lysozyme positive cells. (c) Percentages of cells within the alveolar lumen expressing lysozyme (alveolar macrophages). (d) Percentages of alveolar cells expressing lysozyme (macrophages and type II pneumocytes). Data are presented as mean percentage of positive cells/total cells/field/animal  $\pm$  standard deviation for n=3. \* p < 0.05, \*\* p < 0.01, \*\*\* p < 0.00 (ANOVA, Dunnett's multiple comparison test). Data from the controls (group 1) and rats administered 5 mg/kg (HD; group 2) are reported here for comparison purposes.

In an attempt to assess whether the treatment initiated proliferation of cells in the alveoli, IH for PCNA was performed. In control animals, PCNA expression in alveolar lining epithelial cells was either rare or not detected at all (**Figures 3.18** and **3.19a**). Similarly, treated rats euthanased at early time points (3, 6 and 24 h) showed negligible PCNA expression (**Figure 3.18**). However, at day 7 post dosing, a distinct statistically significant ( $p < 0.01$ ) increase in PCNA-positive, proliferating cells was observed (**Figures 3.18** and **3.19a**). Based on their morphology, many PCNA-positive, alveolar lining cells were identified as type II pneumocytes (**Figure 3.19b**, inset). By day 14, the number of PCNA-positive alveolar cells had decreased to levels similar to those in controls (**Figure 3.18**).

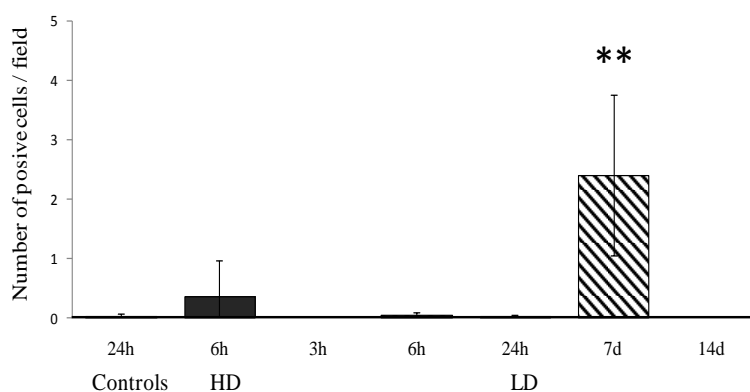


**Figure 3.18.** Amount of PCNA-positive alveolar cells in the lungs of rats after the administration of NR678 at a dose of 0.5 mg/kg (LD; group 3). Data are presented as average number of positive cells /field/animal  $\pm$  standard deviation for  $n=3$ . \*\*  $p < 0.01$  (ANOVA, Dunnett's multiple comparison test). Data from the controls (group 1) and rats administered 5 mg/kg (HD; group 2) are reported here for comparison purposes.

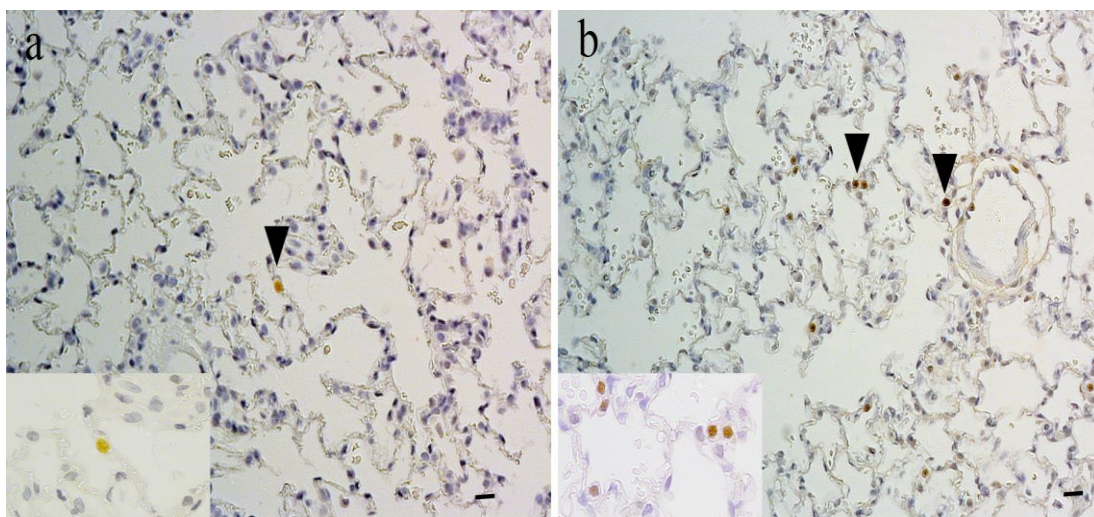


**Figure 3.19.** Immunohistological demonstration of PCNA-positive, proliferating cells in the lungs of a control rat and a rat euthanased 7 d after the administration of NR678 at a dose of 0.5 mg/kg (group 3). (a) Rat 11L-2402 (Control, 24 h). Rare positive cells (arrowhead) are seen in the alveolar lining. Inset: higher magnification, demonstration of the homogenous nuclear staining, representing the presence of PCNA in the nucleus. (b) Rat 11L-2429 (0.5 mg/kg of NR678, 7 d). Several PCNA-positive alveolar lining cells are present. Inset: higher magnification to highlight the positive cells. Peroxidase anti-peroxidase method, mouse antibody against rat PCNA, Papanicolaou's haematoxylin counterstain. Bars: 50  $\mu$ m.

#### 3.2.2.1.4 Ultrastructural findings

TEM was carried out on the lungs of individual rats representative of animals euthanased at different time points after the administration of NR678 at a dose of 0.5 mg/kg (group 3). The ultrastructural findings were compared with those obtained from the control animal and those of the acute toxicity study (see paragraph 3.1.4) to confirm and characterise the pulmonary changes that develop in rats in response to a tolerogenic dose of NR678.

In rats administered NR678 at a dose of 0.5 mg/kg, endothelial cell alterations were observed at early time points (3, 6 and 24 h) in combination with the occurrence of increased numbers of alveolar macrophages (at 6 and 24 h; **Figure 3.20**). Endothelial cell changes were represented by the formation of variably-sized blebs in the endothelial cells lining the alveolar capillaries, which were identical to those described in rats that had received the high dose of NR678 (group 2, see paragraph

3.1.4), but less frequently observed. At 3 h post dosing, blebs were only occasionally seen (**Figure 3.20a**), at 6 h, they were observed in several endothelial cells (**Figure 3.20b**), and at 24 h, they were only very rarely found (**Figure 3.20c,d**). They were not detected at later time points (7 and 14 d post dosing). As in animals receiving the high dose, the blebs appeared to be produced by the separation of the endothelial cell from the underlying basement membrane or to develop within the cytoplasm of the endothelial cell itself and were filled with proteinaceous material showing an electron-density similar to that of plasma. Further changes, like those observed after administration of the high dose (discontinuous endothelial lining, gap formation between endothelial cells, endothelial cell degeneration or necrosis; see paragraph 3.1.4.) were not present.

Consistently with the histological and immunohistological findings, increased numbers of alveolar macrophages were obvious in rats euthanased at 6 and, especially, 24 h after dosing. Ultrastructurally, alveolar macrophages were generally characterised by an irregular, mostly triangular or polygonal shape and a variable size (up to 30  $\mu\text{m}$  in diameter). They were found free in the alveolar lumen or, more often, adhered to the surface of the alveolar lining (**Figure 3.20c,d**). They possessed small pseudopods that appeared to make contact with the alveolar epithelial cell and a variety of cytoplasmic organelles such as mitochondria, endoplasmic reticulum and lysosomes that showed no alteration.

In rats euthanased at 24 h and 7 d post dosing, mature type II pneumocytes were more frequent than in control rats and animals examined early after treatment. Mature type II alveolar epithelial cells in control rats appeared as cuboidal cells scattered in the alveolar epithelium, with a preferential location at the alveolar corners (**Figure 3.21a**). Their cytoplasm contained lamellar bodies, tightly packed concentric membrane lamellae, surrounded by an outer membrane, varying in size from 100 nm to 2  $\mu\text{m}$  (average diameter: 1  $\mu\text{m}$ ). More often, lamellar bodies appeared as round empty cytoplasmic vesicles containing only a few disarranged electron dense lamellae [likely the consequence of suboptimal fixation; (Williams, 1990); **Figure 3.21a**]. The luminal surface of type II pneumocytes was covered by short microvilli. Numerous mitochondria and rough endoplasmic reticulum (**Figure**

**3.21a**), as well as small amounts of smooth endoplasmic reticulum were seen in the cytoplasm. The morphology of mature type II pneumocytes was identical in control and treated animals, but in treated rats at the 7 d time point, they contained an increased number of lamellar bodies that often coalesced and reached a diameter of up to 3  $\mu\text{m}$  (**Figure 3.21d**). Undifferentiated cells with morphological features normally seen in either type I or type II pneumocytes were found with increased frequency in rats euthanased at 24 h and 7 d post dosing (**Figure 3.21c,d**). These cells were characterised by a large oval to elongated, sometimes slightly indented, electron lucent nucleus with finely stippled chromatin and a small amount of cytoplasm, devoid of lamellar bodies or other organelles, except for endoplasmic reticulum. They were interpreted as immature pneumocytes, as previously described (Adamson and Bowden, 1974; Evans et al., 1975). Such immature pneumocytes were very rare in the controls animals (**Figure 3.21b**), where up to 3 cells/ultrathin section were found. In rats at 24 h and still at 7 d they post treatment, they were seen in almost every alveolar unit.

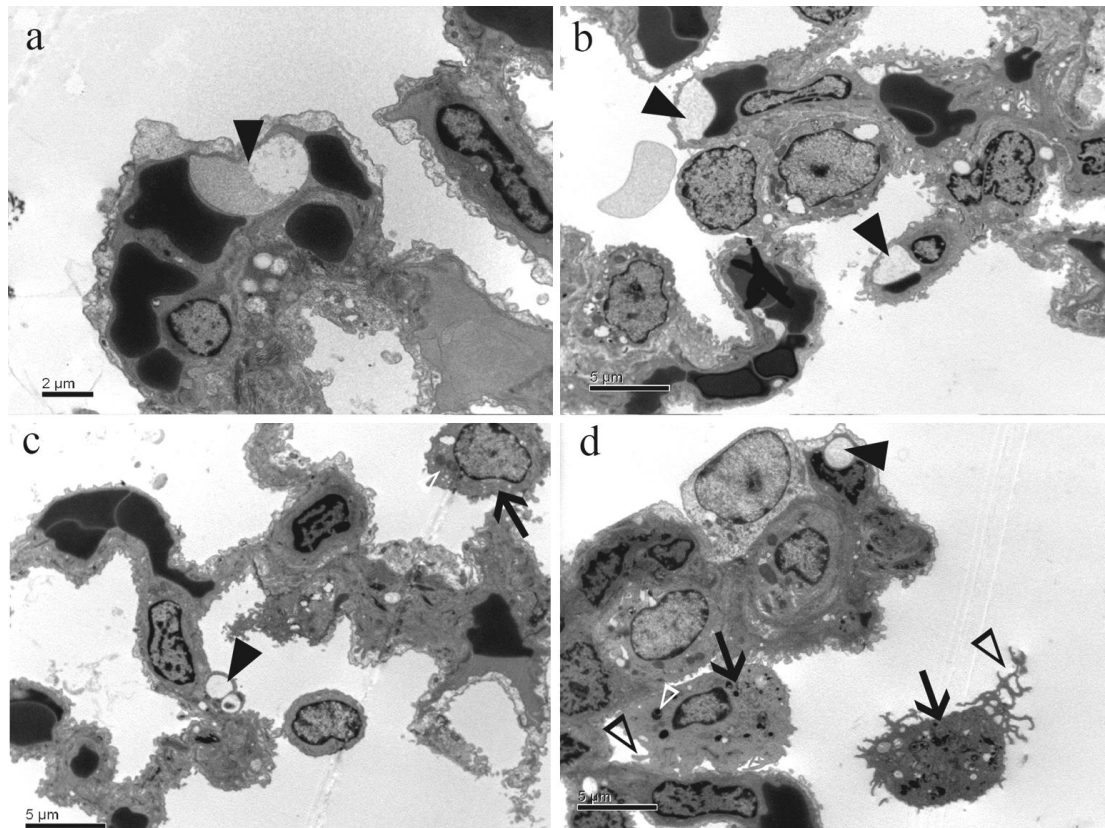


**Figure 3.20.** Ultrastructural features of the lung of rats administered NR678 at a dose of 0.5 mg/kg and euthanased at early time points. (a) Rat 11L-2420 (euthanased at 3 h). An endothelial cell within the alveolar capillary appears to separate from the underlying basement membrane forming a large bleb (solid arrowhead). The bleb is partially filled with electron dense granular material. (b) Rat 11L-2424 (6 h). Endothelial blebs are frequently observed within the alveolar capillaries (arrowheads). (c and d) Rat 11L-2427 (24 h). Individual capillary endothelial cells with bleb formation. Increased numbers of macrophages (arrows) are present free in the alveolar lumen or in contact with the alveolar epithelial cells. Open black arrowheads: pseudopods of the alveolar macrophages. Open white arrowheads: lysosomes within the alveolar macrophages.

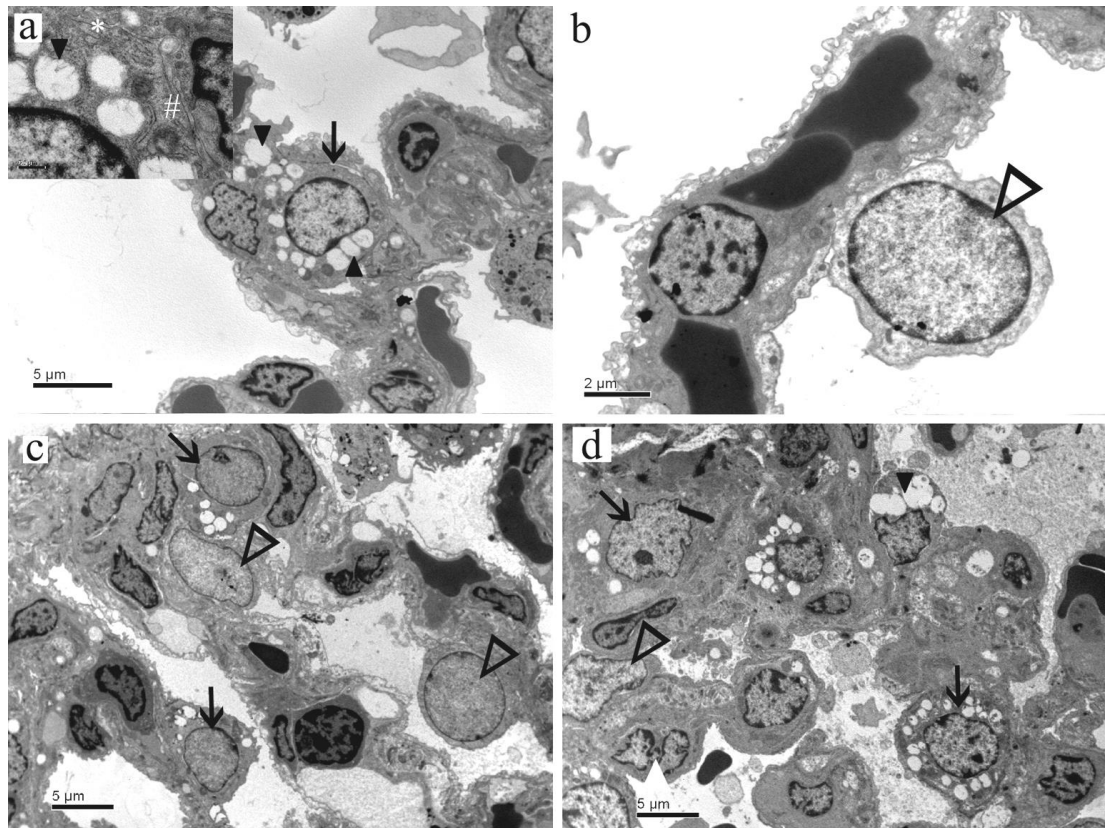


**Figure 3.21.** Ultrastructural features of the lung of rats euthanased at 24 h and 7 d after the administration of NR678 at a dose of 0.5 mg/kg (group 3), compared to controls. (a and b) Rat 11L-2402 (control, euthanased at 24 h). (a) A typical type II alveolar epithelial cell (arrow) protruding into the alveolar lumen and containing multiple, variably-sized lamellar bodies (solid arrowheads). Inset: the detail of a portion of the cytoplasm of the type II pneumocyte is shown. In addition to the lamellar bodies, rough endoplasmic reticulum (\*) is seen. Note the junctional complex (#) with a neighbouring cell. (b) An immature type II pneumocyte precursor cell (“intermediate cell”; open arrowhead) protrudes into the alveolar lumen. It is characterised by scant cytoplasm and a large electron lucent nucleus containing low amount of granular chromatin. (c) Rat 11L-2427 (0.5 mg/kg of NR678, 24 h). Numerous immature pneumocytes (open arrowheads) are present in the alveolar unit, together with mature type II pneumocytes (arrows). (d) Rat 11L-2430 (0.5 mg/kg of NR678, 7 d). Numerous mature type II pneumocytes (arrows) are present and often contain several enlarged lamellar bodies (solid arrowhead).

### **3.2.2.2 Changes observed in rats administered a low dose (0.5 mg/kg) of NR678, followed by a high dose (5 mg/kg) 3 h later (group 4)**

#### **3.2.2.2.1 Clinical assessment**

All rats that had received a low dose of NR678 followed 3 h later by the high dose survived until the end of the study (up to day 14), but exhibited mild clinical signs consistent with minor respiratory distress (dyspnoea) and mild general illness (piloerection, hunched posture and decreased motor activity; **Table 3.6**). These clinical observations were similar to those observed in animals administered the high dose alone (group 2, see paragraph 3.1.1 and **Table 3.1**), though far less intense. They were also transient and observed only on days 1 and 2 post treatment. One rat (11L-2408) remained asymptomatic until the scheduled time of euthanasia (24 h post treatment).

#### **3.2.2.2.2 Gross post mortem findings**

There was no evident difference in lung weights (right lobes only) between the challenged rats from group 4 and the controls (**Figure 3.13**). The only significant macroscopic finding was observed in rat 11L-2410, euthanased at 24 h after dosing. This animal exhibited 3 mL of clear fluid in the thoracic cavity (moderate hydrothorax), similar to, though less marked than animals treated with the high, lethal dose alone (see paragraph 3.1.2).

#### **3.2.2.2.3 Histological and immunohistological findings**

The histological changes observed in the challenged rats were restricted to the lungs and were consistent with those detected in rats that had received a dose of 0.5 mg/kg of NR678 without challenge. However, one rat (11L-2410), euthanased at 24 h post dosing, exhibited mild alveolar and interstitial oedema and mild apoptosis of alveolar lining cells, most likely consistent with endothelial cells (**Table 3.7**). This animal had also shown clinical signs of moderate dyspnoea (**Table 3.6**) and moderate hydrothorax at the gross examination.



**Table 3.6.** Clinical signs observed in rats administered NR678 at a dose of 0.5 mg/kg, followed 3 h later by a dose of 5 mg/kg (group 4). Rats were euthanased (E) at 24 h (11L-2408 to 11L-2410), 7 d (11L-2411 to 11L-2413) or 14 d (11L-2417 to 11L-2419) after the first dose.

Rat ID	Day 1				Day 2		Day 3 to 6	Day 7	Day 8 to 13	Day 14
	9 am	12 pm	3 pm	4 pm	9 am	3 pm		9 am		9 am
11L-2408	LD	NCSO, HD	NCSO	NCSO	NCSO.E	-	-	-	-	-
11L-2409	LD	NCSO, HD	PI, HP, LB (1)	PI, HP, LB (1)	HP, LB (1). E	-	-	-	-	-
11L-2410	LD	NCSO, HD	PI, HP, LB (2)	PI, HP, DMA, LB (2)	HP, LB (2). E	-	-	-	-	-
11L-2411	LD	NCSO, HD	PI, HP	PI, DMA, HP	HP, LB (1)	PI, HP, LB (1)	NCSO	NCSO. E	-	-
11L-2412	LD	NCSO, HD	NCSO	PI	NCSO	PI, HP, LB(1)	NCSO	NCSO. E	-	-
11L-2413	LD	NCSO, HD	NCSO	NCSO	NCSO	PI, HP LB (1)	NCSO	NCSO. E	-	-
11L-2417	LD	NCSO, HD	NCSO	NCSO	PI, HP, LB (1)	NCSO	NCSO	NCSO	NCSO	NCSO. E
11L-2418	LD	NCSO, HD	NCSO	NCSO	PI, HP, LB (1)	NCSO	NCSO	NCSO	NCSO	NCSO. E
11L-2419	LD	NCSO, HD	PI, LB (1)	PI, LB (1)	HP, LB (1)	PI, HP, LB (1)	NCSO	NCSO	NCSO	NCSO. E

ID: identification; NCSO: no clinical signs observed; HP: hunched posture; DMA: decreased motor activity; PE: piloerection; LB: laboured breathing (dyspnoea); LD: low dose (0.5 mg/kg); HD: high dose (5 mg/kg). Numbers in brackets indicate the severity of dyspnoea (mild: 1, moderate: 2).

**Table 3.7.** Summary of the key histological findings in the lungs of rats that had received a low dose (0.5 mg/kg) of NR678, followed 3 h later by a dose of 5 mg/kg (group 4).

Group	Dose (mg/kg)	Time of death post treatment	Histological findings			
			Alveolar and interstitial oedema	Increase in alveolar macrophages	Type 2 pneumocyte hyperplasia	Alveolar cell apoptosis
1	0	24 h	0/3	0/3	0/3	0/3
2	5	6h	3/3 (2.6)	3/3 (2)	0/3	2/3 (1.5)
4	0.5 + 5 (3 h later)	24 h	1/3 (2)	3/3 (3)	2/3 (1.3)	1/3 (2)
		7 d	0/3	2/3 (1.5)	3/3 (2)	0/3
		14 d	0/3	2/3 (1)	1/3 (1)	0/3

Results are expressed as number of animals showing the histological finding/ number of animals per group. The average severity of each finding (in brackets) was calculated by summing the severity grades and dividing the total by the number of animals affected by that finding. Data from the controls (group 1) and rats administered the high dose (group 2) are reported here for comparison purposes.

Similar to rats administered 0.5 mg/kg of NR678 (group 3), increased numbers of alveolar macrophages and type II pneumocytes were observed histologically in the lungs of the challenged rats. SP-C immunohistology revealed a significant ( $p < 0.05$ ) increase (14.1% of total alveolar cells) in type II pneumocytes at 7 d after dosing, which doubled the number observed in the control rats (7.1%; **Figure 3.22a**). Percentages decreased, reaching values similar to those of untreated rats, in animals euthanased on day 14. Accordingly, the average proportion of lysozyme positive cells was significantly increased at 24 h ( $p < 0.001$ ) and 7 d ( $p < 0.05$ ) after dosing (approximately 24% of the total cells), compared to that observed in the controls (16%; **Figure 3.22b**). On day 14, the proportion of alveolar macrophages and type II pneumocytes expressing lysozyme had decreased to 19%, suggesting some degree of recovery. Similarly to rats receiving a dose of 0.5 mg/kg of NR678, the increases in lysozyme-positive alveolar cells were mainly represented by alveolar macrophages at 24 h (**Figure 3.22c**), whilst those seen at 7 d mostly consisted of type II pneumocytes lining the alveolar wall and macrophages (**Figure 3.22d**). An increase of PCNA-positive pneumocytes, although not statistically significant, was observed in animals euthanased at 7 d after dosing (**Figure 3.23**), with a pattern similar to that observed in animals administered the low dose of NR678 (**Figure 3.18**).

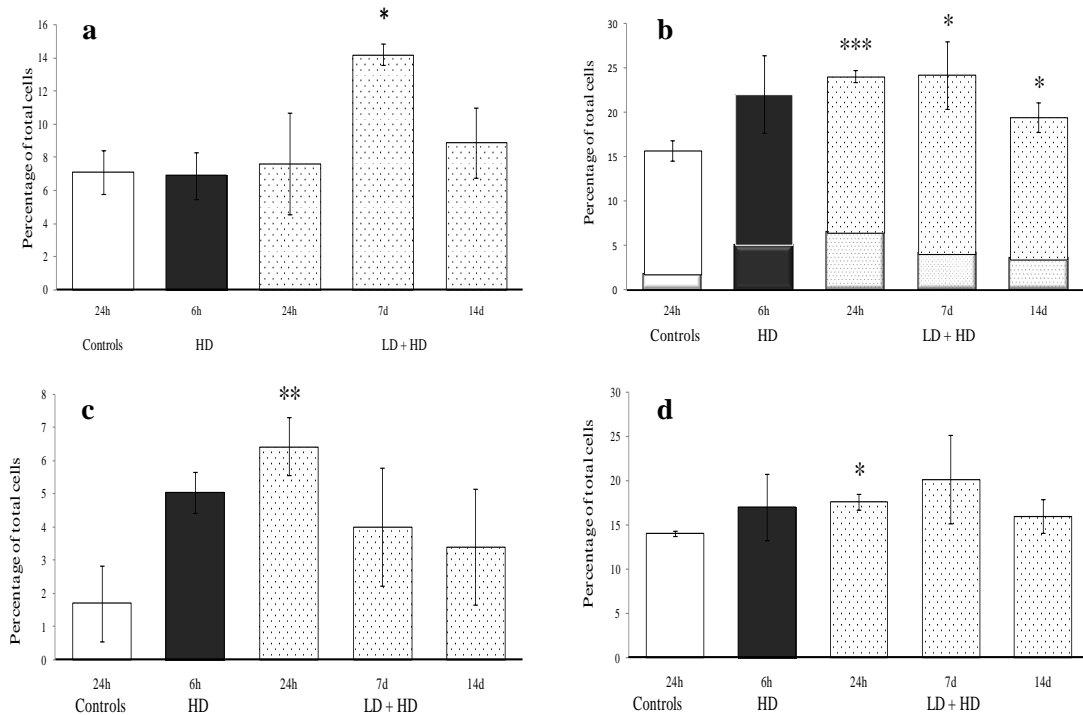


**Figure 3.22.** Immunohistological assessment of the percentage of cells expressing SP-C and lysozyme in the lungs of rats after the administration of NR678 at a dose of 0.5 mg/kg, followed by a dose of 5 mg/kg 3 h later (LD + HD; group 4). (a) Percentages of total cells expressing SP-C (type II pneumocytes). (b) Percentages of total cells expressing lysozyme, including both alveolar macrophages (bottom bar) and alveolar lining cells (top bar). Error bars refer to the overall percentage of lysozyme positive cells. (c) Percentages of cells in the alveolar lumen expressing lysozyme (alveolar macrophages). (d) Percentages of alveolar lining cells expressing lysozyme (macrophages and type II pneumocytes). Data are presented as mean percentage of positive cells/total cells/field/animal  $\pm$  standard deviation for n=3. \*  $p < 0.05$ , \*\*  $p < 0.01$ , \*\*\*  $p < 0.001$  (ANOVA, Dunnett's multiple comparison test). Data from the controls (group 1) and rats administered 5 mg/kg (HD; group 2) are reported here for comparison purposes.

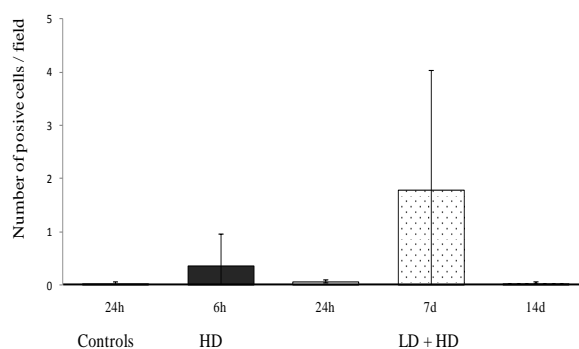


**Figure 3.23.** Amount of PCNA-positive alveolar cells in the lungs of rats after the administration of NR678 at a dose of 0.5 mg/kg followed 3 h later by 5 mg/kg (LD + HD; group 4). Data are presented as average number of positive cells/field/animal  $\pm$  standard deviation for n=3. Data from the controls (group 1) and rats administered 5 mg/kg (HD; group 2) are reported here for comparison purposes.

#### 3.2.2.2.4 Ultrastructural findings

The ultrastructural findings in rats that had received a dose of 0.5 mg/kg of NR678 followed by 5 mg/kg were similar to those described for the other groups. However, the changes in the endothelial cells of rats euthanased at 24 h (**Figure 3.24**) were more pronounced than in rats administered NR678 at a dose of 0.5 mg/kg and euthanased at the same and earlier time points (3 and 6 h; see paragraph 3.2.2.1.4). Endothelial blebs were frequent (**Figure 3.24a,b**), whilst endothelial gap formation was rarely detected. In several fields, the alveolar lumen contained proteinaceous material consistent with plasma (alveolar oedema; **Figure 3.24a**). Different from rats that had received the high, lethal dose alone (see paragraph 3.1.4), there was no evidence of endothelial cell injury, such as swelling, degeneration or death. Additional ultrastructural findings consisted of an increase in alveolar macrophages (at 24 h post dosing) and type II pneumocytes (at 24 h and 7 d) and are identical to those described in animals that had received only the low dose of NR678 (see paragraph 3.2.2.1.4)

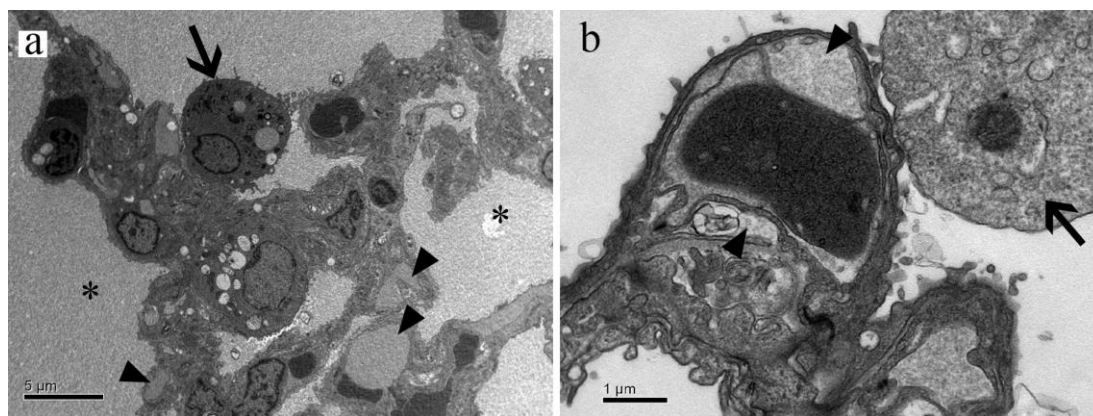


**Figure 3.24.** Ultrastructural features in the lungs of a rat (11L-2408) administered NR678 at a dose of 0.5 mg/kg, followed 3 h later by 5 mg/kg and euthanased at 24 h. (a) Several endothelial blebs (solid arrowheads) are observed within the alveolar capillary. The alveolar lumen (\*) is filled by granular proteinaceous material. (b) Close-up of an endothelial defect showing the multifocal separation of the thin cytoplasm of the endothelial cell from the underlying basement membrane (solid arrowheads). Arrows: alveolar macrophages.

### 3.2.2.3 Changes observed in rats after the administration of a high dose (5 mg/kg) of NR678 on day 14 after previous administration of 0.5 mg/kg or 0.5 mg/kg followed 3 h later by 5 mg/kg

In an attempt to determine whether animals previously dosed with NR678 exhibited prolonged decreased susceptibility to a lethal dose of the compound, two cohorts of rats that had previously been administered NR678 at a dose of 0.5 mg/kg (group 3) or 0.5 mg/kg followed by 5 mg/kg 3 h later (group 4) received a further dose of 5 mg/kg in the morning of day 14 post initial treatment.

#### 3.2.2.3.1 Clinical assessment

After the challenge on day 14, all rats that had previously received a dose of 0.5 mg/kg of NR678 (group 3) exhibited moderate dyspnoea (**Table 3.8a**). Also, two of three animals that had previously received a dose of 0.5 mg/kg of NR678, followed after 3 h by 5 mg/kg (group 4) exhibited mild dyspnoea, whereas the remaining rat (11L-2415) had no symptoms (**Table 3.8b**). Overall, the clinical signs were less severe than in animals that had received the high, lethal dose alone (see **Table 3.1**). In particular the animals from group 4 challenged on day 14 showed only minor clinical signs. Also, challenge with the high dose on day 14 post initial

treatment resulted in more severe clinical signs (**Table 3.8a**) than challenge after only 3 h (see paragraph 3.2.1 and **Table 3.4** and **Table 3.6**).

**Table 3.8.** Clinical signs observed after the administration of NR678 on day 14 at a dose of 5 mg/kg in rats that had previously received a dose of 0.5 mg/kg (group 3) or 0.5 mg/kg, followed 3 h later by 5 mg/kg (group 4).

a) Clinical signs in rats administered NR678 at a dose of 0.5 mg/kg (day 1, at 9 am) and challenged in the morning of day 14 with 5 mg/kg

Rat ID	Day 1				Day 2		Day 3 to 13	Day 14			
	9 am	12 pm	3 pm	4 pm	9 am	3 pm		9 am	12 pm	2 pm	4 pm
11L-2432	LD	NCSO	NCSO	NCSO	NCSO	NCSO	NCSO	NCSO, HD	PI, HP, DMA, LB (2)	PI, HP, DMA, LB (2)	PI, HP, DMA, LB (2). E
11L-2433	LD	NCSO	NCSO	NCSO	NCSO	NCSO	NCSO	NCSO, HD	NCSO	PI, HP, DMA, LB (2)	PI, HP, DMA, LB (2). E
11L-2434	LD	NCSO	NCSO	NCSO	NCSO	NCSO	NCSO	NCSO, HD	PI, HP, DMA,	PI, HP, DMA, LB (2)	PI, HP, DMA, LB (2). E

b) Clinical signs in rats administered NR678 at a dose of 0.5 mg/kg (day 1, at 9 am), followed by 5 mg/kg at 12 pm and re-challenged in the morning of day 14 with 5 mg/kg

Rat ID	Day 1				Day 2		Day 3 to 13	Day 14			
	9 am	12 pm	3 pm	4 pm	9 am	3 pm		9 am	12 pm	2 pm	4 pm
11L-2414	LD	NCSO, HD	PI, LB (1)	PI, HP, DMA, LB (1)	NCSO	NCSO	NCSO	NCSO, HD	PI, HP, LB (1)	PI, HP, LB (1)	HP, DMA, LB (1). E
11L-2415	LD	NCSO, HD	NCSO	NCSO	NCSO	NCSO	NCSO	NCSO, HD	NCSO	NCSO	NCSO. E
11L-2416	LD	NCSO, HD	NCSO	NCSO	NCSO	NCSO	NCSO	NCSO, HD	PI, HP, DMA	PI, HP, LB (1)	HP, DMA, LB (1). E

ID: identification; NCSO: no clinical signs observed; HP: hunched posture; DMA: decreased motor activity; PE: piloerection; LB: laboured breathing (dyspnoea); E: euthanasia; LD: low dose; HD: high dose. Numbers in brackets indicate the severity of dyspnoea (mild: 1, moderate: 2).

### 3.2.2.3.2 Gross post mortem findings

The two cohorts challenged with a high dose of NR678 on day 14 after initial treatment with NR678 at a dose of 0.5 mg/kg (group 3) or 0.5 mg/kg, followed after 3 h by 5 mg/kg NR678 (group 4) exhibited an increase in absolute lung weights and/or lung weights relative to brain weights (**Figure 3.13a,c**), whereas the lung weights relative to body lung weights were unchanged (**Figure 3.13b**). These weight increases resembled those observed in rats that had received the high, lethal dose of

NR678 alone (**Figure 3.1**). The lung weight increases, however, were not statistically significant (p: 0.0045).

All rats in the group 3 cohort challenged on day 14 after initial treatment with a dose of 0.5 mg/kg of NR678 exhibited a moderate to severe hydrothorax, represented by accumulation of clear fluid (3-5 mL) in the thoracic cavity, moderate diffuse pulmonary hyperaemia and oedema, characterised by diffuse dark red discolouration and wet appearance of the lungs, and slight dilation of the stomach due to impacted ingesta. The same gross findings occurred with similar incidence in the group 4 cohort challenged with the high dose of NR678 on day 14, i.e. all three rats exhibited moderate to severe hydrothorax (3-6 mL of clear fluid; **Figure 3.25**), moderate diffuse hyperaemia of the lungs and slight distention of the stomach with ingesta in one rat.

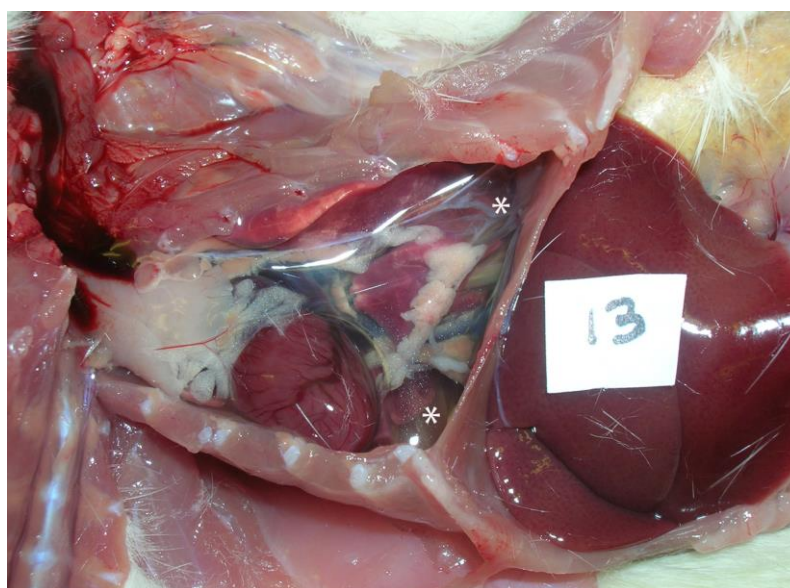


**Figure 3.25.** Macroscopic findings observed at 6 h post administration of a high dose (5 mg/kg) of NR678 on day 14 in rats that had previously received a dose of 0.5 mg/kg, followed 3 h later by 5 mg/kg NR678 (group 4; rat 11L-2414). The thoracic cavity contained 3 mL of clear fluid (\*), consistent with moderate hydrothorax. The lungs exhibit diffuse dark red discolouration, representing moderate hyperaemia. The label in the picture refers to the original animal number.

### 3.2.2.3.3 Histological findings

The histological changes observed in rats challenged on day 14 with a lethal dose of NR678 were restricted to the lungs. Pulmonary oedema was seen histologically in all rats (**Table 3.9** and **Figure 3.26**), with similar incidence and severity as in rats receiving the high dose alone (see **Figure 3.3**). Like rats from group 2, the animals challenged with the high dose on day 14 exhibited slightly increased numbers of alveolar macrophages and slight apoptosis of alveolar endothelial cells.

**Table 3.9.** Summary of key histological findings in the lungs after administration of NR678 at a dose of 5 mg/kg on day 14 in rats that had previously received a dose of 0.5 mg/kg (group 3) or 0.5 mg/kg followed 3 h later by 5 mg/kg NR678 (group 4).

Group	Dose (mg/kg) (day 1)	Dose (mg/kg) (day 14)	Time of death after last treatment	Histological findings		
				Alveolar and interstitial oedema	Increased alveolar macrophage	Alveolar cell apoptosis
2	5	-	6 h	3/3 (2.6)	3/3 (2)	3/3 (1.3)
3	0.5	5	6 h	3/3 (2.6)	2/3 (1)	2/3 (1)
4	0.5 + 5 (3 h later)	5	6 h	3/3 (3)	1/3 (1)	1/3 (1)

Results are expressed as number of animals showing the histological finding/ number of animals per group. The average severity of each finding (in brackets) was calculated by summing the severity grades and dividing the total by the number of animals affected by that finding. Data for rats administered a dose of 5 mg/kg (group 2) are reported here for comparison purposes.



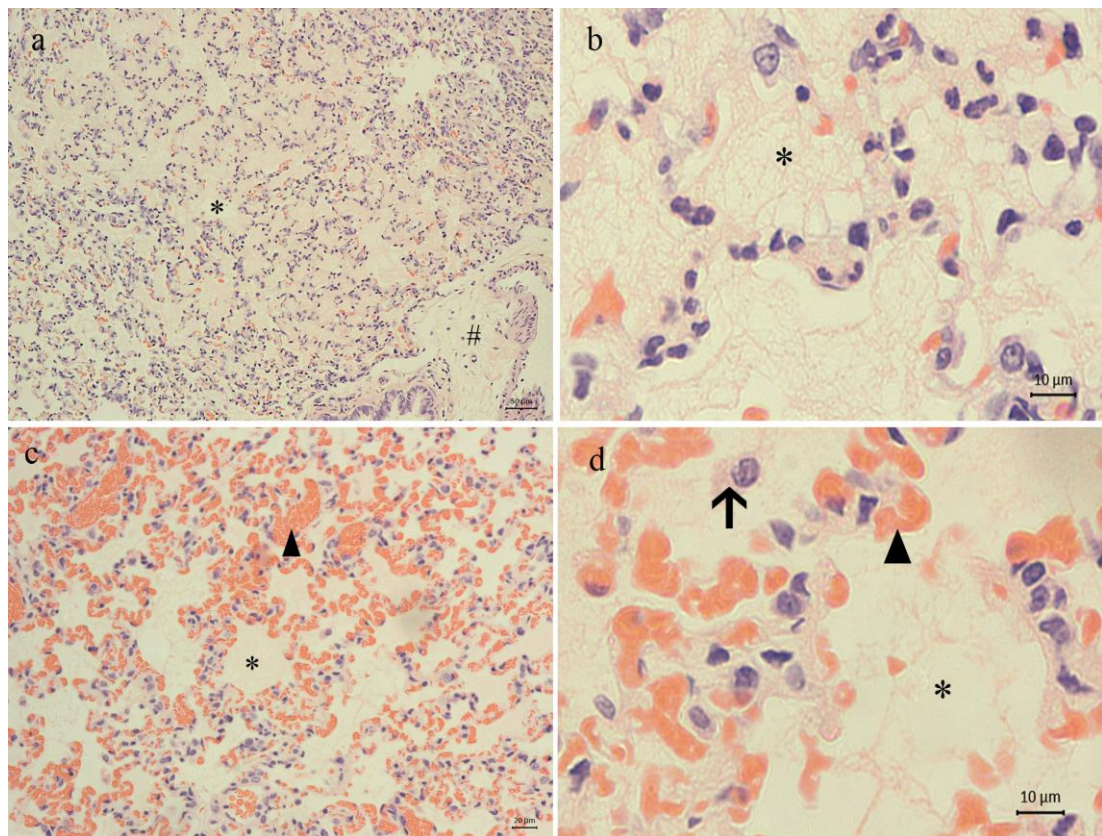


**Figure 3.26.** Histological features in the lungs of rats administered a dose of 5 mg/kg of NR678 on day 14 after they had previously received a dose of 0.5 mg/kg (group 3) or 0.5 mg/kg followed 3 h later by 5 mg/kg (group 4). (a and b) Rat 11L-2414 (group 4, rechallenged on day 14 with 5 mg/kg of NR678 and euthanased 6 h later). (a) Multifocally, alveoli are filled with a large amount of faintly eosinophilic material (\*; alveolar oedema). The interstitial space surrounding bronchi and vessels is markedly expanded (#; interstitial oedema). Bar: 50  $\mu$ m. (b) Higher magnification of an area where the alveolar units contain eosinophilic material arranged in a meshwork of fibrils (\*, consistent with fibrin). Bar: 10  $\mu$ m. (c and d) Rat 11L-2435 (group 3, challenged on day 14 with 5 mg/kg of NR678 and euthanased 6 h later). (c) There is a low amount of homogeneous to fibrillar eosinophilic material within alveolar lumina (\*, alveolar oedema). Alveolar capillaries and small calibre veins are filled with erythrocytes (solid arrowheads; moderate to marked diffuse hyperaemia). Bar: 20  $\mu$ m (d) Higher magnification of (c). Arrow: alveolar macrophage. HE stain. Bar: 10  $\mu$ m.

### 3.2.2.4 Effects of NR678 on hepatic and pulmonary GSH contents *in vivo*

GSH levels were measured in the liver and lung of all rats in study 3, including those challenged on day 14 with the high dose of NR678. In the liver of rats administered the high dose alone (group 2) and in the two cohorts of rats that had received the high dose of NR678 on day 14, GSH levels were reduced to approximately 70% of those measured in the control rats (**Figure 3.27a**). Hepatic GSH levels in rats that had been administered the low dose of NR678 without challenge were generally lower than those observed in the controls. No meaningful differences were seen in rats administered a dose of 0.5 mg/kg of NR678 followed by 5 mg/kg 3 h later compared to control rats.

The levels of pulmonary GSH in rats that had received the high dose and in the cohorts challenged on day 14 were reduced to approximately 10% of those measured in the controls (**Figure 3.27b**). Lung GSH levels in rats administered the low dose or the low dose followed by the high dose 3 h later were generally comparable or moderately lower than those observed in the controls.

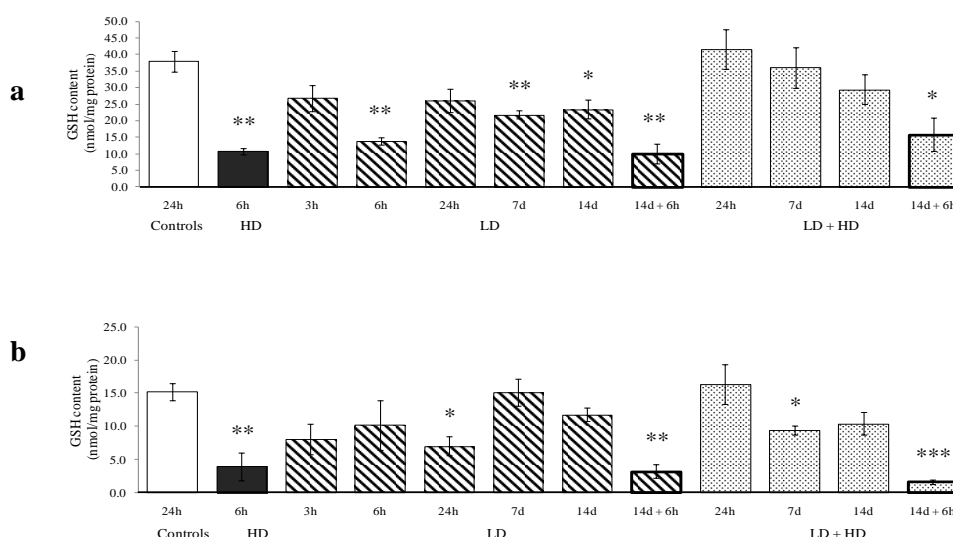


**Figure 3.27.** GSH contents in the liver and lung of NR678-treated rats. Hepatic (a) and pulmonary (b) GSH levels are shown in rats administered the high dose (HD, 5 mg/kg; group 2) of NR678, the low dose alone (LD, 0.5 mg/kg; group 3) or the low dose, followed 3 h later by the high dose (LD + HD; group 4). Group 3 and 4 rat cohorts challenged with the high dose on day 14 and euthanased 6 h later are highlighted (bold outlines). Data are presented as mean  $\pm$  standard deviation for n=3. \* p < 0.05 \*\* p < 0.01 \*\*\* p < 0.001 (ANOVA, Dunnett's multiple comparison test).

### **3.3 Characterisation of FMO1 and FMO2 expression profiles in untreated rats and rats that had received NR678**

Compared to other species, available data concerning the distribution of FMO isoforms in the rat are scant and focus predominantly on the expression of FMO1 and FMO3 in the liver and kidneys [(Novick et al., 2009); see paragraph 1.5.6.3]. In the rat lung, FMO1 and FMO2 are the predominant FMO isoforms, as shown by Western blot analysis (Hugonnard et al., 2004). However, no research has been conducted to identify the cells expressing these proteins or the correspondent mRNA in this organ. Our main interest was to characterise the localisation of FMO2 mRNA in the rat lungs as a mean to assess the potential role of FMO2 in the onset of the acute toxic effect of thiourea-based molecules and in the development of tolerance. Thus, in this chapter, we investigate the expression profile of FMO2 in untreated male Wistar and Welsh rats using isoform-specific antisense RNA probes, as detailed in paragraph 2.2.1.4.3. We show that FMO2 mRNA is present in selected cell types in the brain, liver, kidneys and, to the highest extent, in the lungs. We use RNA-ISH to compare the tissue- and cell-specific expression of FMO2 in the lungs of untreated rats with that observed in rats that had received NR678, either at high (5 mg/kg) or tolerogenic (0.5 mg/kg) doses. In addition, we explore the potential role of FMO1 and FMO2 in the development of thiourea-related toxicity and tolerance comparing the mRNA levels of these two isoforms in the lungs of control and treated rats using a qPCR technique, as described in paragraph 2.3.5.

#### **3.3.1 Determination of cellular localisation of expression of FMO2 in tissues from untreated rats by *in situ* hybridisation**

RNA-ISH was applied to sections from liver, lung, kidney and brain of control rats from study 3 (male Wistar rats) and study 4 (male Welsh rats). As no meaningful difference was noted in the expression of FMO2 in the different tissues between the two strains, the results that are subsequently described apply to both. In all tissues, a positive signal resulted in a black or dark brown cytoplasmic precipitate. A hybridisation signal was occasionally detected in sections hybridised with the

correspondent FMO2 sense RNA probe; however, this was generally weak and limited to specific anatomic locations, as described below.

In a transverse section of the brain taken at the level of the transition between the diencephalon and the mesencephalon, a moderate to strong signal was observed in the cerebral cortex, mostly in the superficial laminae, and the hippocampus (**Figure 3.28a**). Cortical neurons (**Figure 3.28b**) exhibited a strong diffuse uniform cytoplasmic signal, whilst in the hippocampus the signal intensity varied among the different layers: neurons located in layers CA2 and CA3 [*Cornu Amonis* 2 and 3 (Witter and Amaral, 2004)] were intensely positive, whilst only occasional positive neurons with a signal of moderate intensity were observed in layer CA1 and in the *gyrus dentatus* (**Figure 3.28a,c**). Scattered ependymal cells lining the choroid plexus showed a moderately intense signal (**Figure 3.28d**). No expression of FMO2 mRNA was observed in the endothelial cells of the meningeal vessels (**Figure 3.28b**). Similarly to the results obtained by RNA-ISH in mice (Janmohamed et al., 2004), there was no evidence of FMO2 expression in astrocytes. In the brain sections hybridised with the sense probe, cortical neurons exhibited a weak/moderate signal, whilst no signal was detected in the hippocampus (data not shown).

In the kidneys, FMO2 mRNA localised predominantly to the proximal tubules (PT) in the outer cortex and in the collecting ducts (**Figure 3.29**). The apical portion of the PT epithelial cells exhibited a diffuse light brown cytoplasmic precipitate, whilst a more intense signal was present at their luminal brush border (**Figure 3.29a,b**). However, overall only a small proportion of the PTs, approximately corresponding to 30% of PTs in the section, exhibited FMO2 mRNA expression. The reason for the lack of a uniform staining pattern is unknown, but it is possible that the presence of FMO2 is limited to specific portions of the PT. The PT, which can be recognised in HE stained sections because the epithelial cells exhibit a brush border, is divided in a convoluted portion (PCT), which begins at the urinary pole of the glomerulus and a straight part (pars recta, PR), predominantly located at the junction between cortex and medulla (Haschek et al., 2009b).

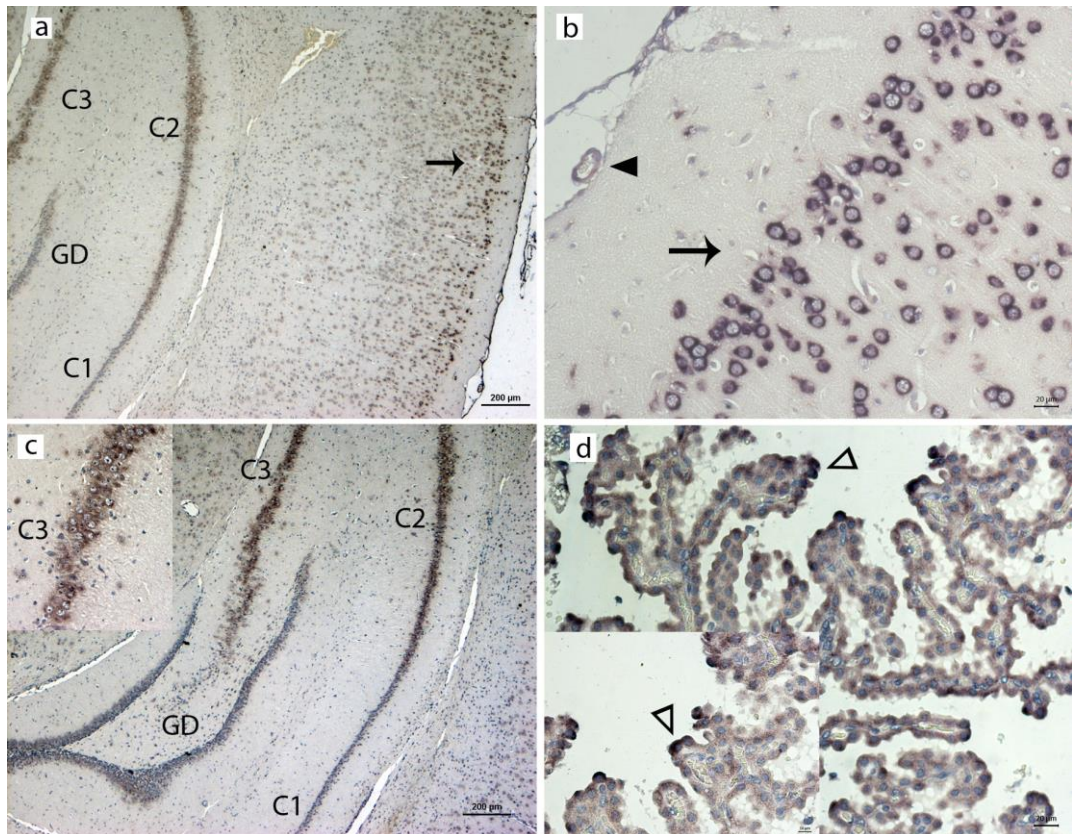


**Figure 3.28.** RNA-ISH for the demonstration of FMO2 mRNA in the male rat brain. Rat 11L-2404 (control, euthanased at 24 h). (a) An intensely dark brown precipitate in the cytoplasm of cortical (arrow) and hippocampal neurons represents the positive signal; in the hippocampus, FMO2 mRNA expression is mainly seen in neurons in the CA2 and CA3 layers, and to a lesser extent, in the CA1 layer and the *gyrus dentatus* (GD). Bar: 200  $\mu\text{m}$ . (b) Higher magnification (bar: 20  $\mu\text{m}$ ) of the positive cortical neurons in the superficial laminae. The endothelial cells lining a meningeal vessel (solid arrowhead) are negative (c) Hippocampus, highlighting of FMO2 mRNA expression in the CA2 and CA3 layers. Inset: detail of the positive neurons in CA3. (d) Scattered positive cells expressing FMO2 in the choroid plexus (open arrowheads; bar: 20  $\mu\text{m}$ ). Inset: higher magnification (bar: 10  $\mu\text{m}$ ). Paraffin-embedded tissue sections, antisense probe for mRNA encoding FMO2, Papanicolaou's haematoxylin).



In several species, including humans, non human primates and laboratory rodents, the PT comprises three different segments (P1, P2 and P3): P1 is the short initial tract continuous to the Bowman epithelium, which is thought to possess the highest rate of metabolic activity; P2 is the largest part and consists of the more distal part of the PCT, whilst segment P3 (approximately corresponding to the PR) starts at the level of the outer stripe of the medulla and ends at the loop of Henle (Haschek et al., 2009b). The cortical location and the distribution of positive cells may suggest that FMO2, like other metabolic enzymes, is mostly expressed in the P1 segment. Collecting ducts in the inner medulla and in the papilla exhibited a strong diffuse cytoplasmic signal (**Figure 3.29c,d**), whereas weak or no FMO2 mRNA expression was observed in the distal tubules and the glomeruli, respectively (**Figure 3.29a**). Pelvic urothelial cells generally exhibited a strong signal; however, a moderately to strongly intense dark brown precipitate was observed in the same location in sections hybridised with the sense probe (**Figure 3.29e, f**), despite abundant stringent attempts at clearing the supposedly non-specific reaction. Accordingly, the signal in the pelvic epithelium was not considered as specific and further interpretation avoided.

In the liver, FMO2 mRNA was detected in the cytoplasm of bile duct epithelial cells, with a moderate signal intensity (**Figure 3.30a,b**). No discernible signal was observed for FMO2 mRNA in the hepatocytes. Kupffer cells and endothelial cells did not exhibit any positive signal. Also, no signal was observed in the liver sections hybridised with the sense probe (negative controls).

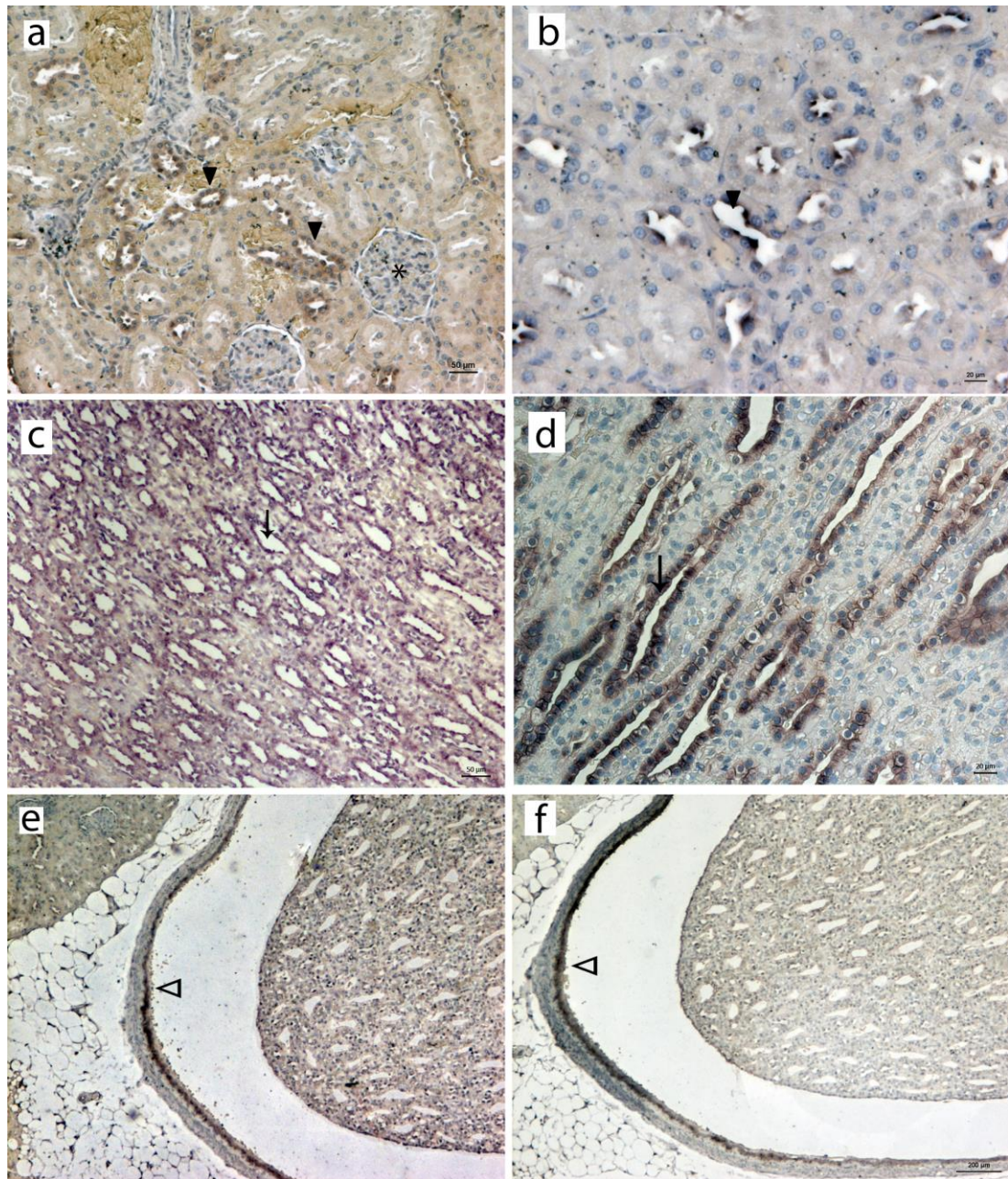


**Figure 3.29.** RNA-ISH for the demonstration of FMO2 mRNA in the male rat kidney. Rat 11L-2404 (control, euthanased at 24 h). (a) Positive scattered proximal tubules in the renal cortex (arrowheads). Glomeruli (\*) are negative. Bar: 50  $\mu\text{m}$ . (b) Higher magnification of the positive tubules (bar: 20  $\mu\text{m}$ ). (c) Epithelial cells lining the collecting ducts exhibit a strong positive cytoplasmic signal (arrow). Bar: 50  $\mu\text{m}$ . (d) Higher magnification of the positive collecting ducts (bar: 20  $\mu\text{m}$ ). (e) The urothelium of the renal pelvis shows an intense diffuse cytoplasmic signal. (f) Sections incubated with the sense probe (supposed negative controls) exhibit a diffuse cytoplasmic signal of the renal pelvic urothelium similar to that obtained with the antisense probe after the same incubation time (bar: 200  $\mu\text{m}$ ). Paraffin-embedded tissue sections, antisense (sense: f) probe for mRNA encoding FMO2, Papanicolaou's haematoxylin).



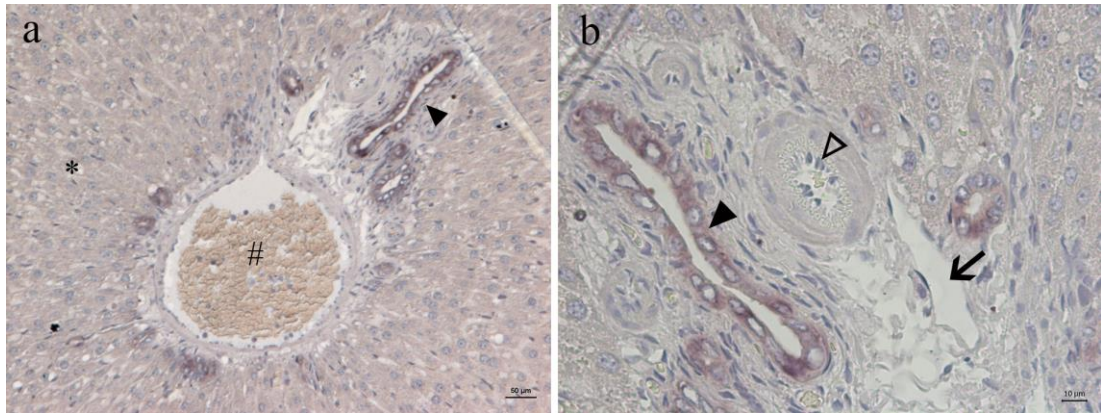


**Figure 3.30.** RNA-ISH for the demonstration of FMO2 mRNA in the male rat liver. Rat 11L-2404 (control, euthanased at 24 h). (a) The bile duct epithelial cells (solid arrowhead) exhibit a positive signal of moderate intensity. No signal is detected in the hepatocytes and in the endothelial cells lining the periportal vascular structures. Bar: 50  $\mu\text{m}$ . (b) Higher magnification. Bar: 10  $\mu\text{m}$ . Vein: #; artery: open arrowhead; and lymphatic vessel: arrow. Paraffin-embedded tissue sections, antisense probe for mRNA encoding FMO2, Papanicolaou's haematoxylin.

In the lungs, FMO2 mRNA localised to the bronchiolar epithelium and to the alveolar unit (**Figure 3.31a**), with a variable distribution pattern. Nonciliated bronchiolar epithelial cells (Clara cells), identified on the sections by their dome shape and the lack of cilia, exhibited an intense signal in the apical portion of their cytoplasm (**Figure 3.31b,c**). In the rat, Clara cells are mainly seen in the more distal bronchioles and, in particular, in the terminal bronchioles (Jeffery and Reid, 1975). Accordingly, FMO2 positive cells had the same distribution pattern, while large bronchioles and bronchi exhibited only scattered or no positive cells, respectively, indicating that the ciliated respiratory epithelium does not express FMO2. Within the alveolar unit, type II pneumocytes exhibited strong signals, represented by a diffuse cytoplasmic precipitate that often obscured the nucleus (**Figure 3.31d,e**). Moderate FMO2 mRNA expression was observed in cells lining the alveoli/alveolar capillaries (**Figure 3.31e**). These cells displayed a small amount of cytoplasm, but could not be fully identified based on their morphology. However, they are likely consistent either with endothelial cells and/or type I pneumocytes. Alveolar macrophages showed an intense diffuse cytoplasmic signal (**Figure 3.31e**). In addition, endothelial cells lining small and mid calibre pulmonary vessels were also found to be positive (**Figure 3.31f**), a result which differed from that seen in venous and arterial endothelial cells in any other tissues.



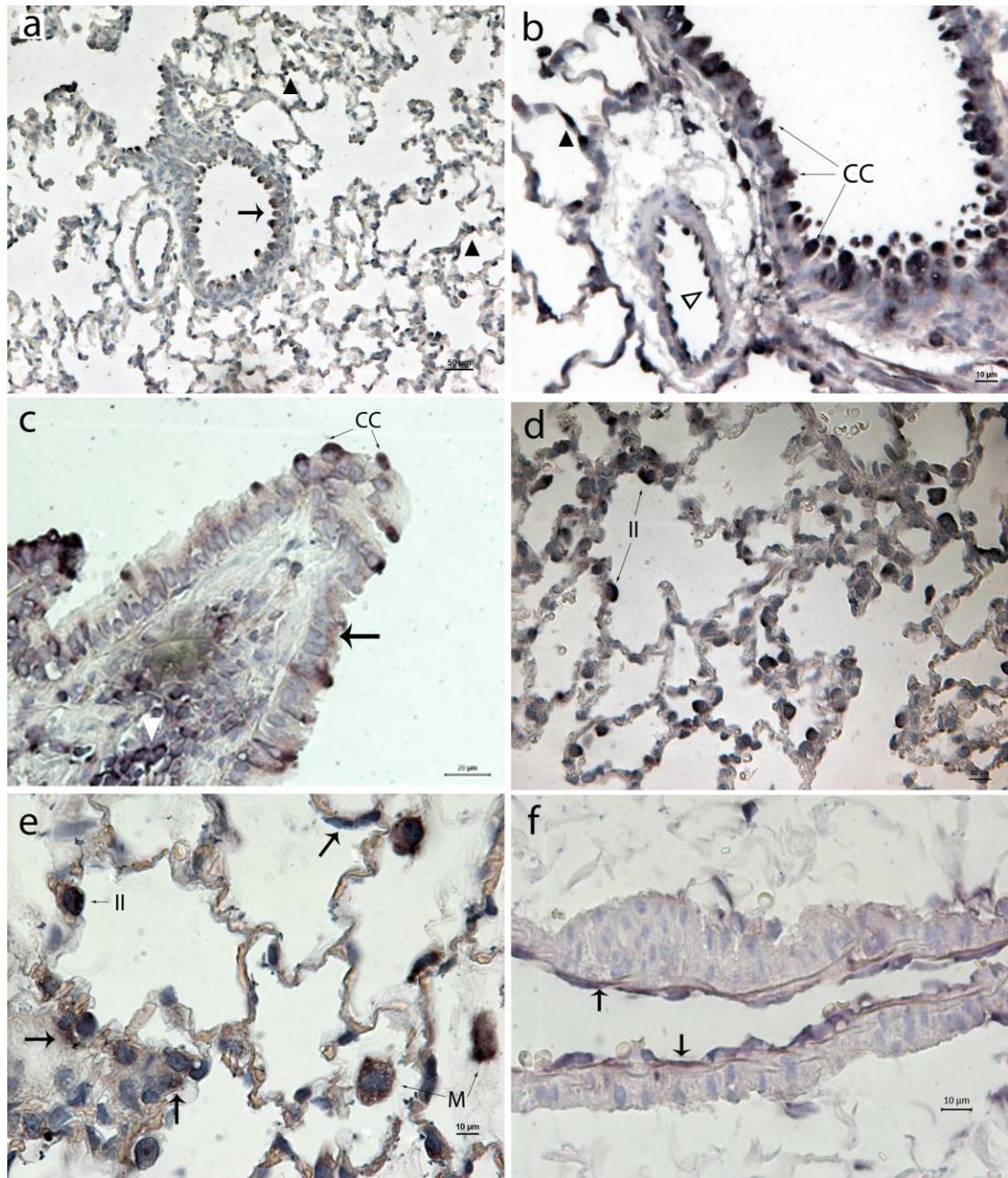


**Figure 3.31.** RNA-ISH for the demonstration of FMO2 mRNA in the male rat lung. Rat 11L-2404 (control, euthanased at 24 h). (a) Positive bronchiolar epithelial lining cells (arrow) and scattered cells within the alveolar septa (solid arrowheads). Bar: 50  $\mu$ m. (b). A strong signal is detected in the distal bronchioles, in cells with a morphology consistent with Clara cells (CC). Endothelial cells (open arrowhead) are also positive. Bar: 10  $\mu$ m (c) More proximal bronchioles exhibit only scattered intensely positive cells (CC), whilst the vast majority of the lining cells (ciliated respiratory epithelium; arrow) are negative. Mononuclear inflammatory cells within the lamina propria (white solid arrowhead) express FMO2 mRNA. Bar: 20  $\mu$ m. (d) Within the alveolar septa, FMO2 mRNA is expressed predominantly by type II pneumocytes (II). Bar: 50  $\mu$ m. (e) Alveolar macrophages (M) exhibit diffuse intense signal. Scattered cells within the alveolar unit (type I pneumocytes or endothelial cells; arrows) express FMO2. Bar: 10  $\mu$ m. (f) Detail of a mid-sized artery lined by positive endothelial cells (arrows). Bar: 10  $\mu$ m. Paraffin-embedded tissue sections, antisense probe for mRNA encoding FMO2, Papanicolaou's haematoxylin.

### **3.3.2 Comparative assessment of FMO2 expression by *in situ* hybridisation in the lungs of control and NR678-treated rats**

In order to identify potential changes in the degree and distribution of the pulmonary FMO2 mRNA expression in rats that had received a high dose (5 mg/kg) or a tolerogenic dose (0.5 mg/kg) of NR678, lungs of all animals from study 3 were examined by RNA-ISH. Similarly to the controls, FMO2 mRNA in treated rats localised predominantly to Clara cells, type II pneumocytes and alveolar macrophages. This distribution pattern was observed in all treatment groups (group 2: 5 mg/kg of NR678; group 3: 0.5 mg/kg; and group 4: 0.5 mg/kg, followed by 5 mg/kg after 3 h) and at all end points (3, 6 and 24 h, 7 and 14 d). However, in line with the increases in type II pneumocytes and alveolar macrophages observed after dosing (see paragraphs 3.2.2.1.3 and 3.2.2.2.3), the cells expressing FMO2 in the alveolar unit of the lungs of treated animals were generally more numerous than in the controls. No difference was noted in the number of bronchiolar cells expressing FMO2. Although not characterised quantitatively, the increases of FMO2-positive alveolar cells in treated animals can be summarised as follows:

- In rats treated with a high dose of NR678 (group 2), numerous cells within the alveolar lumen expressed FMO2. These were interpreted as alveolar macrophages, which, according to the histological and immunohistological results, were moderately increased in this group compared to the controls (**Figure 3.32b**).
- In the lungs of rats administered a low dose (0.5 mg/kg) of NR678 (group 3), no difference in the expression of FMO2 was found at the 3 and 6 h end points, compared to the controls. In rats euthanased at 24 h and 7 d post dosing, there was an evident increase in the number of FMO2 positive cells within the alveolar unit, predominantly consistent with type II pneumocytes and alveolar macrophages (**Figure 3.32c**). At the 24 h end point, the large intra-alveolar macrophages observed at HE exhibited an intensely positive signal for FMO2 mRNA. In the lungs of rats euthanased at 24 h and 7 d after dosing, cells with a morphology consistent with type II pneumocytes exhibited variable amounts of FMO2 mRNA. Type II pneumocytes, characterised by a large amount of cytoplasm, contained an intense dark brown



diffuse precipitate. At the 14 d end point, there was no appreciable difference in the FMO2 expression compared to the controls.

- Similarly to rats that had received a low dose (0.5 mg/kg) of NR678, animals administered a low dose of NR678 followed by a high dose (5 mg/kg) 3 h later (group 4) exhibited an evident increase in the number of alveolar cells containing FMO2 mRNA at the 24 h and the 7 d end points. FMO2 expression at 14 d post dosing was comparable to the controls.

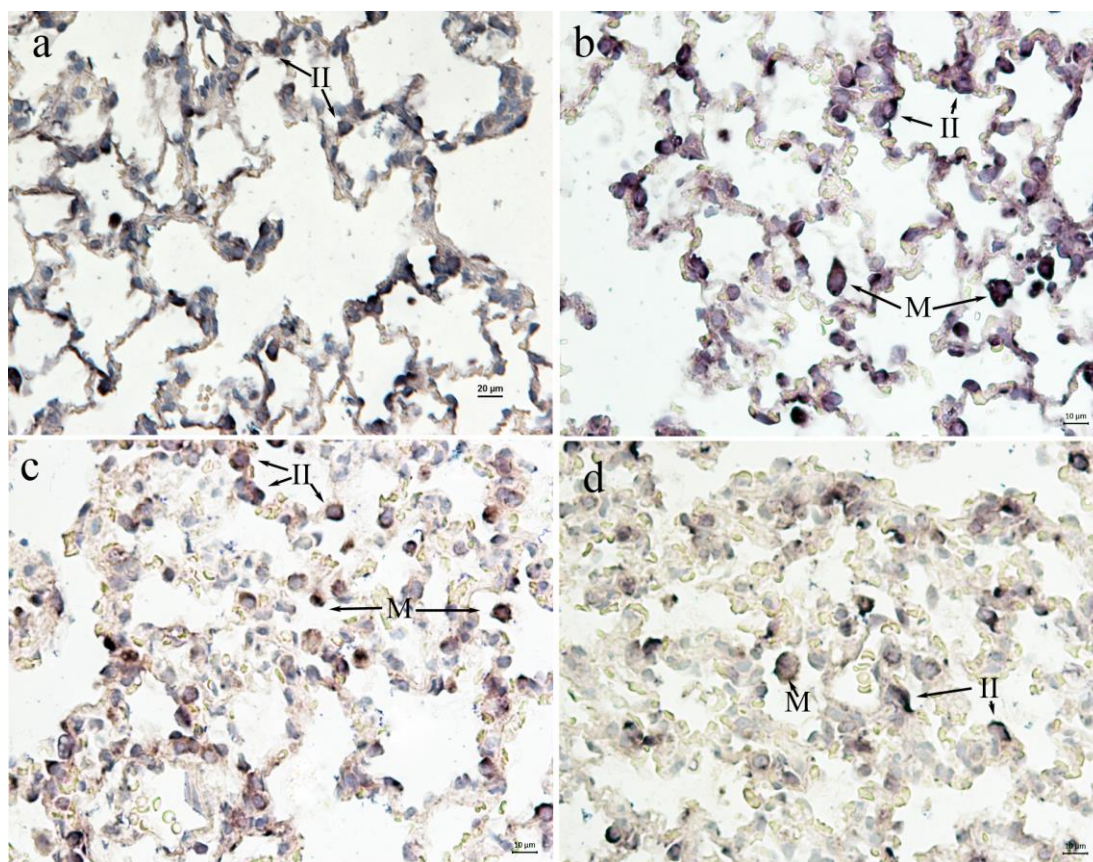


**Figure 3.32.** RNA-ISH for the demonstration of FMO2 mRNA localisation in the lungs of male untreated rats compared to those that had received NR678 (a) Rat 11L-2404 (control, euthanased at 24 h). Numerous alveolar lining cells, predominantly consistent with type II pneumocytes (II) express FMO2. Bar: 20 µm. (b). Rat 11L-2405 (5 mg/kg of NR678, 6 h). The numerous desquamated alveolar macrophages (M) present in the section express FMO2 mRNA. Bar: 10 µm (c). Rat 11L-2427 (0.5 mg/kg of NR678, 24 h). Increased numbers of FMO2-labelled type II pneumocytes (II) and alveolar macrophages (M) are evident. (d) Rat 11L-2429 (0.5 mg/kg of NR678, 7 d). Positive cells are mildly increased in number compared to the controls. Bar: 50 µm. Paraffin-embedded tissue sections, antisense probe for mRNA encoding FMO2, Papanicolaou's haematoxylin.

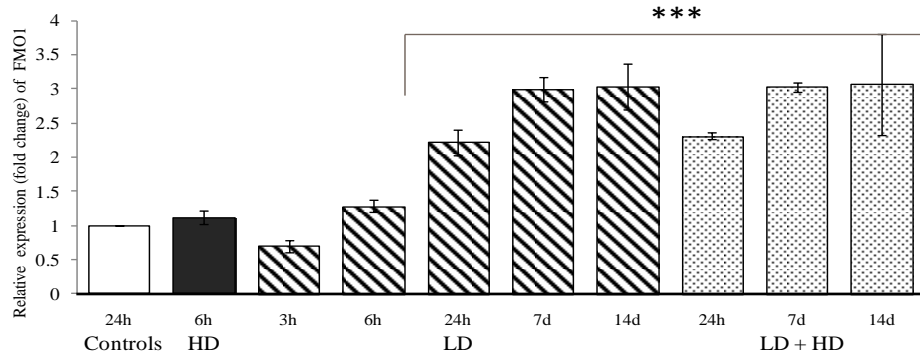
### 3.3.3 Comparative assessment of the levels of FMO1 and FMO2 mRNA in the lungs of control and NR678-treated rats using qPCR

qPCR was used to quantify the FMO1 and FMO2 transcription in the lungs of rats from study 3 (see paragraph 2.3.5), which allowed the comparison of the pulmonary FMO1 and FMO2 mRNA levels from animals that had received a lethal (5 mg/kg; group 2) or a tolerogenic (0.5 mg/kg; groups 3 and 4) dose of NR678 with those of control rats.

In treated rats euthanased at  $\geq 24$  h, regardless of the dose administered, FMO1 mRNA levels were significantly increased (**Figure 3.33a**). In rats that had received the low dose of NR678 or the low dose followed 3 h later by the high dose, FMO1 transcription was increased by 2.2- and 2.3-folds respectively after 24 h, with further elevation by 3.0 fold for both after 7 d. After 14 d from the administration of NR678, an approximately  $3 \times$  increase of the FMO1 mRNA levels compared to the controls was still observed. mRNA levels were unchanged compared to controls in rats euthanased at 6 h that had received the high dose (group 2) or the low dose (group 3) of NR678. In rats given the low dose and euthanased after 3 h, FMO1 mRNA was reduced by 0.3-fold; however, the decrease was not statistically significant ( $p: 0.05$ ).

In all treated animals, including those euthanased at the earliest end points (3 and 6 h), FMO2 mRNA levels were significantly ( $p < 0.001$ ) higher than in controls (**Figure 3.33b**). The amount of FMO2 transcripts in the lungs of treated animals tended to increase progressively with time, independent of the dose of NR678 that had been administered. In the lungs of rats administered the low dose (group 3), FMO2 mRNA levels were increased by approximately 2.3-fold compared to controls at 3 h, with further increase to  $2.8 \times$  at 6 h,  $4.1 \times$  at 24 h,  $4.7 \times$  at 7 d and  $6.5 \times$  at 14 d. In rats administered the low dose of NR678, followed 3 h later by the high dose (group 4), the levels of FMO2 mRNA elevated by 2.2-fold at 24 h and 4.8-fold at 7 d, after which they did not increase further ( $4.6 \times$ ) at the 14 d end point.

**a) FMO1**



**b) FMO2**

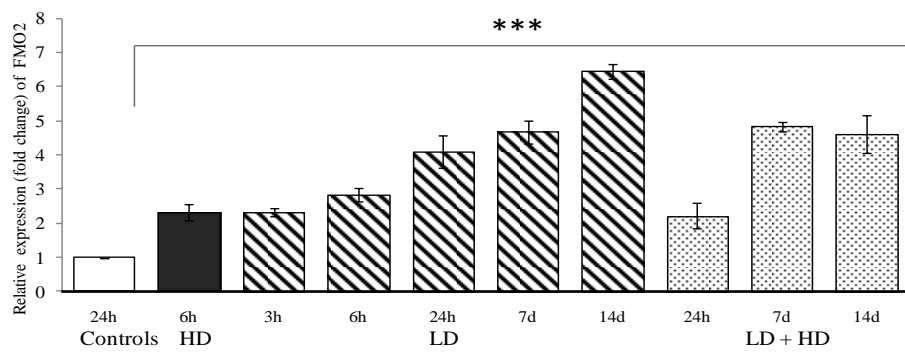


**Figure 3.33.** qPCR analysis showing the levels of relative expression (fold change) of FMO1 (a) and FMO2 (b) in the lungs of rats following exposure to high and low doses of NR678. Data are presented as mean  $\pm$  standard errors for 3 different experiments. \*\*\*  $p < 0.001$  (ANOVA, Dunnett's multiple comparison test).

### **3.4 Assessment of *R. norvegicus* as a suitable animal model to investigate the metabolic and toxicological consequences of *FMO2* polymorphism in humans**

It has already been mentioned that human *FMO2* is highly polymorphic (Dolphin et al., 1998) and encodes for a truncated inactive protein in all the Caucasians and Asians genotyped to date (Furnes et al., 2003; Krueger et al., 2002b). However, in a small proportion of individuals of African-American and Hispanic ethnicities, the gene is not mutated and an enzymatically active protein is expressed in several tissues, especially in the lungs, where *FMO2* is most abundant (Cashman and Zhang, 2006; Hugonnard et al., 2004; Krueger and Williams, 2005). A similar polymorphism occurs in rats, where the *FMO2* gene has been shown to encode for a shorter inactive protein in laboratory strains, but not in wild rats (Lattard et al., 2002b). A genetic polymorphism for *FMO2* has been demonstrated in *R. norvegicus* (Hugonnard et al., 2004), the wild ancestor of laboratory rat strains. Accordingly, *R. norvegicus* may represent a suitable model to study metabolic and toxicological consequences of *FMO2* polymorphism in humans.

In this study, we investigate the distribution of *FMO2* allelic frequencies in a population of wild rats trapped in the Liverpool urban area and in two colonies of rats (Welsh and Berkshire rats) housed at the BASF Pest Control Solutions facility. Subsequently, we show that the lungs of rats expressing a functional *FMO2* have increased metabolic activity towards small thiourea-based molecules and are at increased risk of developing the acute toxic effects of NR678, when compared to the lungs of rats possessing the truncated isoform.

#### **3.4.1 Detection of *FMO2* polymorphism among a wild rat population using a nested PCR method**

Genomic DNA was extracted from the liver or lungs of 33 wild rats (*R. norvegicus*), trapped in Cheshire (n = 2) or in the Liverpool urban area (n = 31). *FMO2* polymorphism in these animals was characterised using the nested PCR method described by Hugonnard et al. (2004; see paragraph 2.3.7.3).

The first PCR amplification generated in all animals an amplicon with an approximate size of 1300 bp (**Figure 3.34a**). These PCR products were re-amplified using a common upstream primer (FMO2-F2) and two different downstream primers (FMO2-R2m and FMO2-R2w), which recognise specifically the mutant or the full length *FMO2*, respectively (see paragraph 2.3.7.3). Subsequent visualisation of the PCR products by agarose gel electrophoresis yielded sharp, single bands of approximately 300 bp (**Figure 3.34b**) and provided the following results: (1) a single band with FMO2-R2m and none with FMO2-R2w; (2) a single band with FMO2-R2w and none with FMO2-R2m; and (3) a single band with each reverse primer. Rats were therefore classified as homozygous for the mutant *FMO2* (1; n = 4, 12.1%), homozygous for the full length *FMO2* (2; n = 17; 51.1%) or heterozygous (3; n = 13, 36.4%). The allelic frequencies for *FMO2*\*1 (full length form) and *FMO2*\*2 (mutated inactive form) in the wild population of rats examined in the present study were 69.7% and 30.3%, respectively.

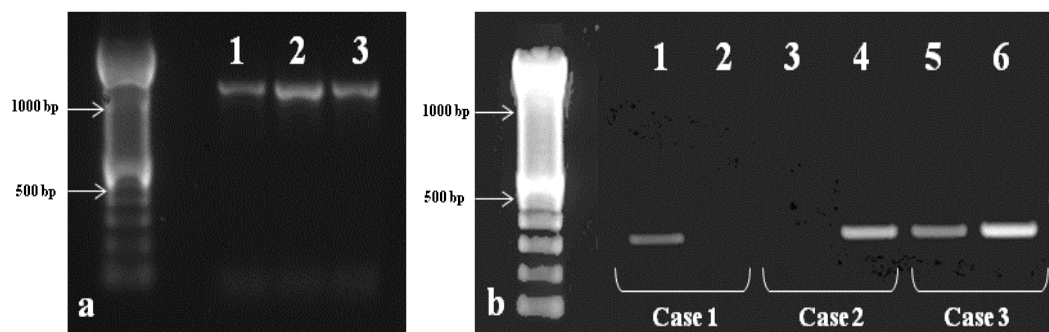


**Figure 3.34.** Characterisation of *FMO2* by nested PCR in wild caught *R. norvegicus*. (a) The product of the first PCR amplification, carried out using FMO2-F1 and FMO2-R1 primers, generated a fragment of approximately 1300 bp in size. Each lane is loaded with a different sample. (b) In case 1 (rats homozygous for the mutant form), a fragment of approximately 300 bp was amplified using the primer pair FMO2-F2/FMO2-R2m (lane 1) and none using FMO2-F2/FMO2-R2w (lane 2). In case 2 (rats homozygous for the full length form), no amplification was detected using the primer pair FMO2-F2/FMO2-R2m (lane 3), while a fragment of approximately 300 bp was recognised using the primer pair FMO2-F2/FMO2-R2w (lane 4). In heterozygous rats (case 3), both FMO2-F2/FMO2-R2m and FMO2-F2/FMO2-R2w generated the expected amplicon.

### 3.4.2 Characterisation of *FMO2* allelic frequencies in two colonies of laboratory rats (Welsh and Berkshire) using a nested PCR method

*FMO2* genotyping analysis by the same nested PCR method was carried out in two colonies of laboratory rats (Welsh and Berkshire), that had been established at the BASF Widnes laboratories several years ago by cross breeding of wild rats with laboratory rats. Genotyping aimed to establish whether a *FMO2* polymorphism was present in these two populations of rats. 37 rats (12 male and 12 female Welsh rats, 13 male Berkshire rats) were available for genotyping. DNA extraction and analysis of 5 rats/gender from each the Welsh and Berkshire colonies did identify all 15 animals homozygous for *FMO2\*1* (**Figure 3.35**). This result was deemed adequate to confirm the lack of *FMO2* polymorphism in these colonies, and no further analysis was conducted in the remaining rats.

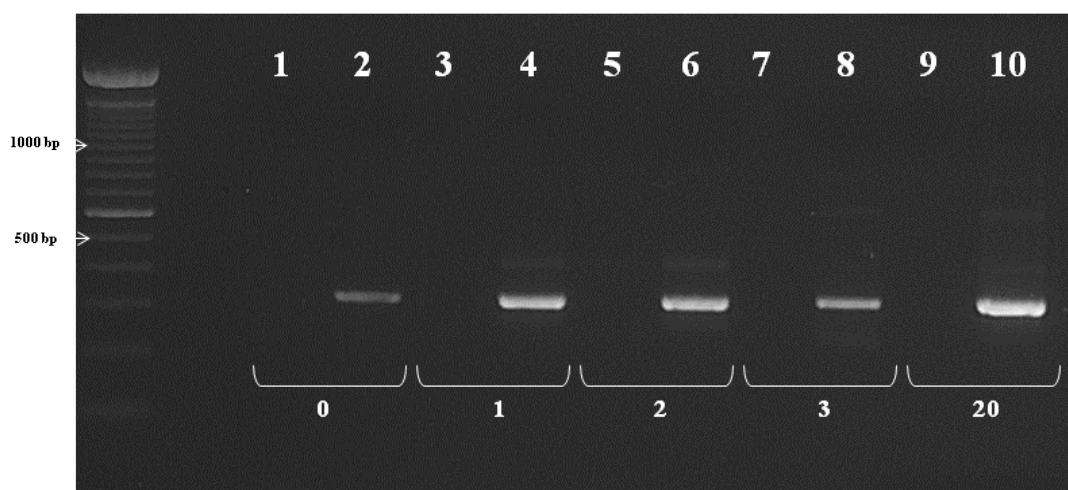


**Figure 3.35.** Characterisation of *FMO2* by nested PCR in two rat colonies (Welsh and Berkshire) housed at BASF Widnes Laboratories. Only the results from the first five genotyped males (identified as 0, 1, 2, 3 and 20 based on ear punching) of the Welsh rat colony are shown. An approximately 300 bp-sized band is amplified using FMO2-F2/FMO2-R2w (even lanes). No amplification product is seen using FMO2-F2/FMO2-R2m (odd lanes).



### 3.4.3 Enzyme assay

We hypothesized that the presence of a functional FMO2 in the rat lungs may lead to different metabolic activities towards molecules which undergo FMO-mediated oxygenation. In order to prove this, we analysed FMO-dependent S-oxygenation of MI in liver and lung microsomes following the method described by Dixit and Roche (1984) and compared the catalytic properties of FMOs between pulmonary microsomes prepared from Welsh (homozygous for *FMO2\*1*) and Wistar (homozygous for *FMO2\*2*) rats.

#### 3.4.3.1 Determination of the enzymatic parameters of the S-oxygenation of methimazole carried out by rat liver and lung microsomes

The oxidation of MI catalysed by FMOs was first investigated in three different microsomal pools (Wistar rat liver and lungs, Welsh rat lungs) using nine scalar concentrations of the substrate (ranging from 5  $\mu$ M to 1 mM) and measuring the reaction velocity ( $V_0$ ; see paragraph 2.4.5). MI S-oxidase activity was observed in all three microsomal preparations (**Figure 3.36**). MI oxidation in liver and lung microsomes that were previously heated at 55°C to inhibit FMO activity was negligible, confirming that the reaction is mainly conducted by FMOs (data not shown).

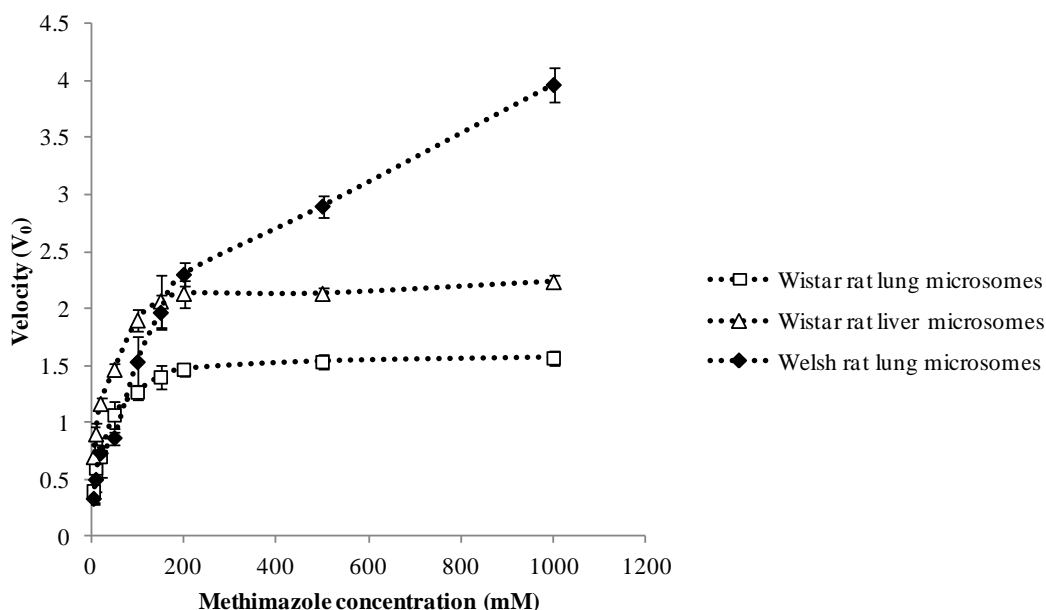
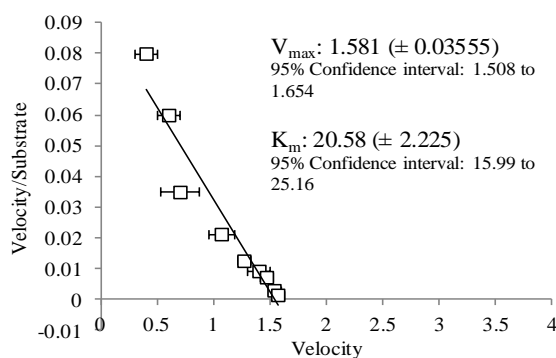


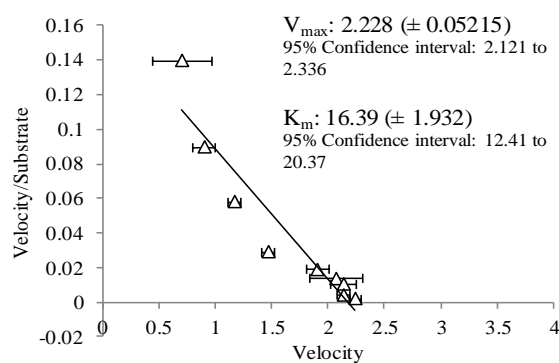
**Figure 3.36.** Effect of methimazole concentration on enzyme velocity in different rat microsomal preparations (Wistar rat liver and lungs and Welsh rat lungs). Reaction velocity, obtained by reading of the optical density at 412 nm, is plotted against MI concentration. Data are presented as mean  $\pm$  standard deviation of three independent measurements.

The data obtained were plotted using an Eadie-Hofstee diagram (**Figure 3.37**) and the kinetic parameters were calculated for each microsomal pool. The Eadie-Hofstee graphical representation of the enzymatic reaction of the Wistar rat liver (**Figure 3.37a**) and lung (**Figure 3.37b**) microsomes consisted of a straight line, suggesting that oxygenation of MI in these preparations was predominantly a monophasic reaction. In Welsh rat lung microsomes (**Figure 3.37c**), two distinct kinetic components were involved in the oxygenation of MI. The  $V_{\max}$  (1.875 nmol/min/mg) and  $K_m$  (34.22  $\mu\text{M}$ ) of the first enzyme were similar to those (1.581 nmol/min/mg and 20.58  $\mu\text{M}$ , respectively) seen in the monoenzymatic reaction of the Wistar rat lungs. The second kinetic component exhibited high activity also at the lowest substrate concentrations, as demonstrated by the  $V_{\max}$  (4.605 nmol/min/mg) and the  $K_m$  (215.9  $\mu\text{M}$ ), which were respectively 2.5 $\times$  and 6 $\times$  higher than those of the first phase.

a) Wistar rat lung microsomes



b) Wistar rat liver microsomes



c) Welsh rat lung microsomes

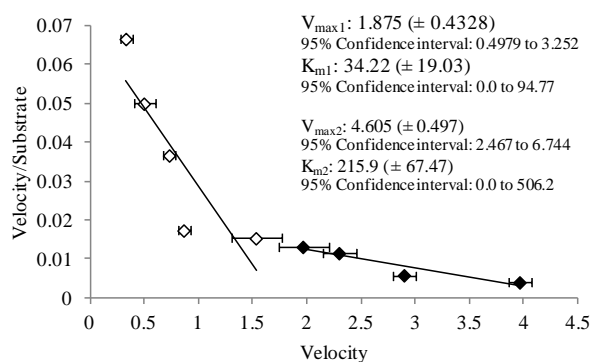


**Figure 3.37.** Enzyme kinetics of the sulphonylation of methimazole deduced from the Michaelis-Menten equation in different rat microsomal preparations. (a) Wistar rat lung microsomes (b) Wistar rat liver microsomes and (c) Welsh rat lung microsomes. Reaction velocity is plotted in an Eadie-Hofstee diagram against the ratio between velocity and substrate concentration. Data are presented as mean  $\pm$  standard deviation obtained from three different measurements.  $V_{\max}$ : maximum velocity of the reaction.  $K_m$ : Michaelis-Menten constant.

### 3.4.3.2 Comparison of the oxygenation of methimazole catalysed by different rat microsomes and enzyme inhibition using NR678

Catalytic activities were further investigated in Wistar and Welsh rat microsomes monitoring the change in absorbance at 412 nm for 7 min after the addition of a single concentration (500 mM) of MI to the incubations (**Figure 3.38**). Formation of DNTB measured at 7 min after the addition of MI was highest in Welsh rat lung microsomes, followed by Wistar rat liver microsomes. S-oxygenation of MI catalysed by Wistar rat lung microsomes instead was approximately  $2 \times$  slower than that carried out by the Welsh rat lung microsomal preparations.

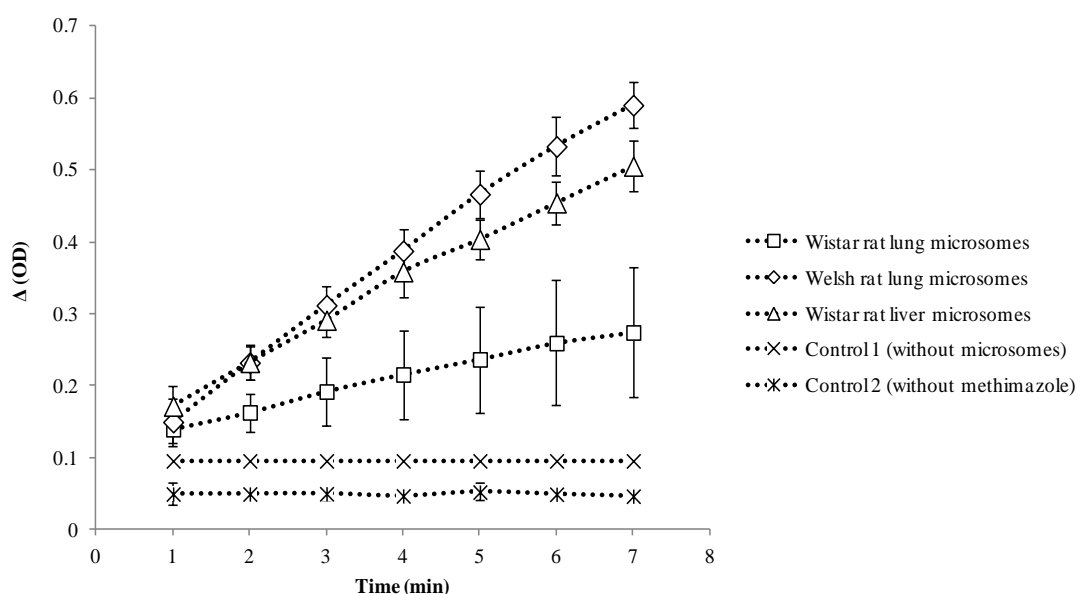
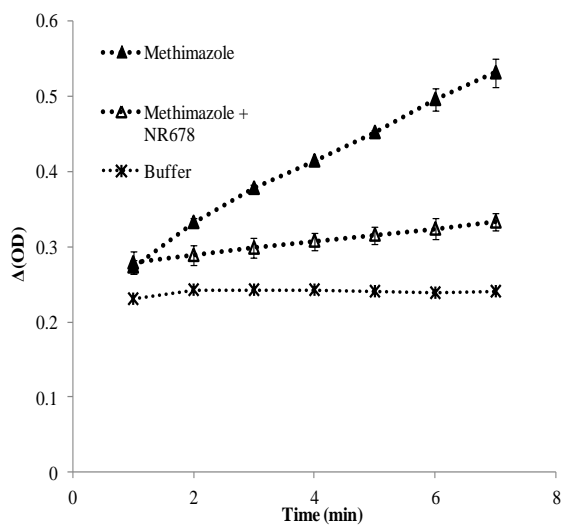


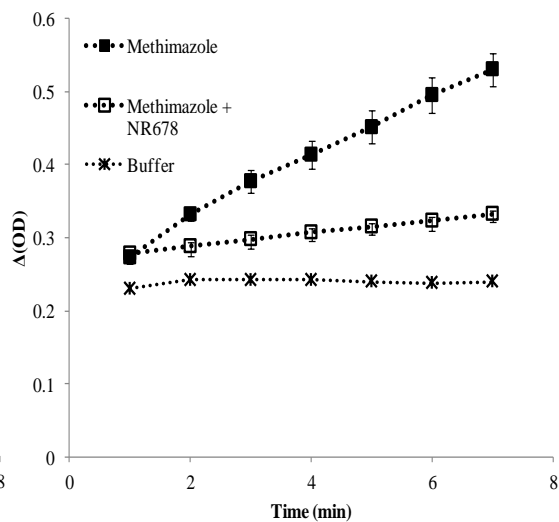
**Figure 3.38.** Comparison of methimazole (500 mM) oxygenation rates over time (7 min) among different rat microsomal preparations (Wistar rat liver and lungs and Welsh rat lungs). Difference in absorbance ( $\Delta OD$ ) is plotted against time (7 min). Data are presented as mean  $\pm$  standard deviation for  $n=9$  (three different measurements obtained from three independent experiments).

The experiment above was repeated with 500 mM of NR678 added to the incubations and comparing the curves obtained to those generated by incubations containing only MI or buffer. Non competitive inhibition of NR678 occurred in all three microsomal preparations (**Figure 3.39**).

**a) Wistar rat lung microsomes**



**b) Wistar rat liver microsomes**



**c) Welsh rat lung microsomes**

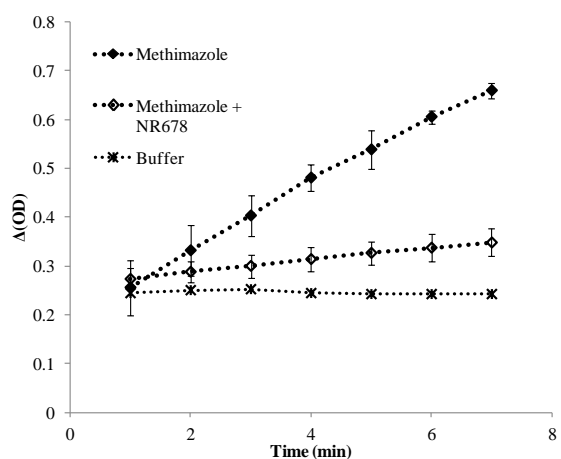


**Figure 3.39.** Inhibitory activity of NR678 on the sulphonylation of methimazole carried out in different rat microsomal preparations. (a) Wistar rat lung microsomes (b) Wistar rat liver microsomes and (c) Welsh rat lung microsomes. Difference in absorbance ( $\Delta(OD)$ ) is plotted against time (7 min). Data are presented as mean  $\pm$  standard deviation obtained in three independent measurements.

### **3.4.4 Characterisation of the *in vivo* effects of a low dose (0.5 mg/kg) of NR678 administered to rats homozygous for *FMO2\*1* (Welsh rats)**

The general increase of FMO activity toward the test molecule observed in the Welsh rat lungs compared to the Wistar strain may result in increased susceptibility of this organ to the toxic effects of NR678. In order to confirm this hypothesis, the Welsh rat colony genotyped as described above was used in a toxicity study (study 4), where male Welsh rats received a dose of 0.5 mg/kg of NR678 and were euthanased at 3, 6 and 24 h after dosing. The objective of the study was to assess drug-related morphological changes and compare the development and dynamics of tolerance in rats homozygous for *FMO2\*1* (Welsh) with those obtained from Wistar rats (homozygous for *FMO2\*2*) in study 3; for this reason, the selected dosage and time points in study 4 were identical to those employed in the low dose group of study 3.

#### **3.4.4.1 Clinical assessment**

All rats administered a dose of NR678 of 0.5 mg/kg survived until the scheduled euthanasia. Most animals were asymptomatic, however, two rats (12L-2257 and 12L-2258) exhibited mild or moderate dyspnoea, respectively, together with piloerection and decreased motor activity, starting at 5 h after dosing. Both rats were euthanased at the scheduled time point (6 h). Another animal (12L-2262) showed mild dyspnoea and decreased motor activity at 6 h post dosing. These symptoms were no longer present on the following day at the time of scheduled euthanasia (24 h).

#### **3.4.4.2 Gross post mortem findings**

The two rats that had shown mild dyspnoea (scheduled euthanased at 6 h after dosing), exhibited mild hydrothorax (characterised by the presence of 1.5 mL clear fluid in the thoracic cavity) and moderate diffuse hyperaemia in the lungs. No macroscopic findings were observed in the remaining rats.

#### **3.4.4.3 Histological findings**

The histological changes observed in Welsh rats that had received a dose of 0.5 mg/kg of NR678 (study 4) were restricted to the lungs (**Table 3.10**). The main

histological finding was a moderate or marked alveolar and interstitial oedema (**Figure 3.40**), which had similar features to that observed in Wistar rats receiving a high dose (5 and 10 mg/kg; see paragraph 3.1.3). Pulmonary oedema occurred in rats euthanased at 3 h (1/3 animals) and 6 h after dosing (2/3 animals) and was not detected in the three rats euthanased at 24 h. Scattered apoptotic cells (severity: slight) were present in the alveolar lining in one rat euthanased at the 3 h time point. A mild or moderate increase in the number of alveolar macrophages occurred in all rats euthanased at 3 and 6 h post treatment and in 1/3 rats at 24 h. This finding had been seen previously in Wistar rats receiving NR678 at low (see paragraph 3.2.2.1.3) and high (see paragraph 3.1.3) doses.

**Table 3.10.** Summary of the key histological findings in the lungs of Welsh rats administered a low dose (0.5 mg/kg) of NR678 (study 4).

Group	NR678 dose (mg/kg)	Time of death post treatment	Histological findings		
			Alveolar and interstitial oedema	Increased alveolar macrophage	Alveolar cell apoptosis
1	0	24 h	0/3	0/3	0/3
2	0.5	3 h	1/3 (4)	3/3 (2.6)	1/3 (1)
3		6 h	2/3 (3.5)	3/3 (2)	0/3
4		24 h	0/3	1/3 (2)	0/3

Results are expressed as number of animals showing the histological finding/ number of animals per group. The average severity of each finding (in brackets) was calculated by summing the severity grades and dividing the total by the number of animals affected by that finding.

In addition to the treatment-related findings described above, there was evidence of an inflammatory reaction in the lungs of the Welsh rats (**Figure 3.41**), with an incidence and severity that was similar in all different groups, including the controls. This was represented by a slight to moderate multifocal perivascular and interstitial granulomatous inflammatory infiltration, composed of lymphocytes, fewer macrophages and plasma cells and occasional neutrophils, with scattered multinucleated giant cells; and moderate to severe proliferation of the bronchus-associated lymphoid tissue (BALT). These findings were considered spontaneous, i.e. not treatment related, and were likely caused by an infectious agent affecting the Welsh rat colony, which is conventionally, rather than barrier, -maintained. Although serological tests were not undertaken in these animals or other animals in the colony and the specific aetiologic agent involved in the inflammatory process could not be

identified, such histological lesions, in particular the BALT hyperplasia and the lymphocytic-dominated inflammatory infiltrate, are highly suggestive of the early stage of *Mycoplasma pulmonis* infection (Percy and Barthold, 2007; Schoeb et al., 2009).

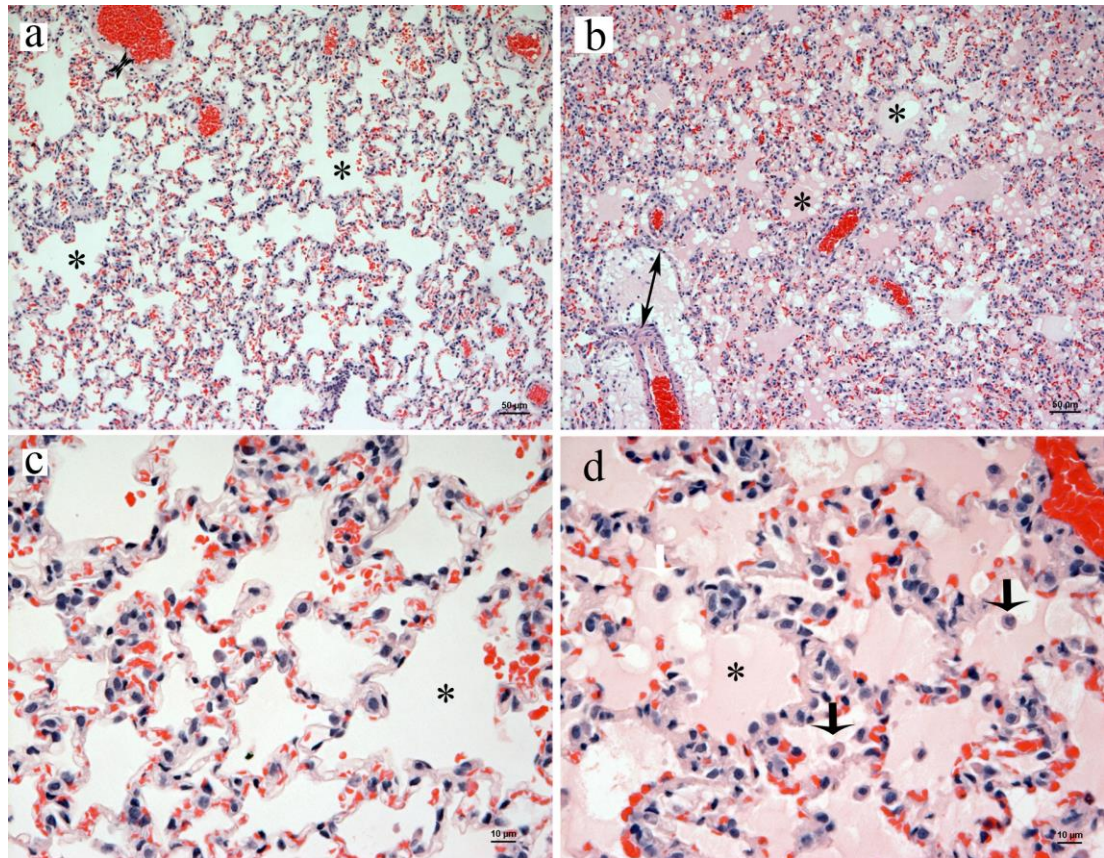


**Figure 3.40.** Histological features of alveolar and interstitial oedema in the lungs of Welsh rats that had received a dose of 0.5 mg/kg of NR678, compared to concurrent controls. (a) Rat 12L-2251 (control, euthanased at 24 h post dosing). The alveolar lumen (\*) is filled with air and appears as a clear space. There is virtually no separation between the outline of vessels (double-headed arrow: perivascular space) and the adjacent parenchyma. (b) Rat 12L-2257 (0.5 mg/kg of NR678, 6 h after dosing). Alveolar lumina (\*) contain abundant eosinophilic homogenous proteinaceous fluid. The perivascular space (double-headed arrow) is markedly distended by the presence of fluid (interstitial oedema). (c) Rat 12L-2251. Closer view of the normal alveoli. (d) Rat 12L-2257. Higher magnification of the pale eosinophilic proteinaceous fluid filling the alveoli. There is an increased number of macrophages within the alveolar lumen (arrows).



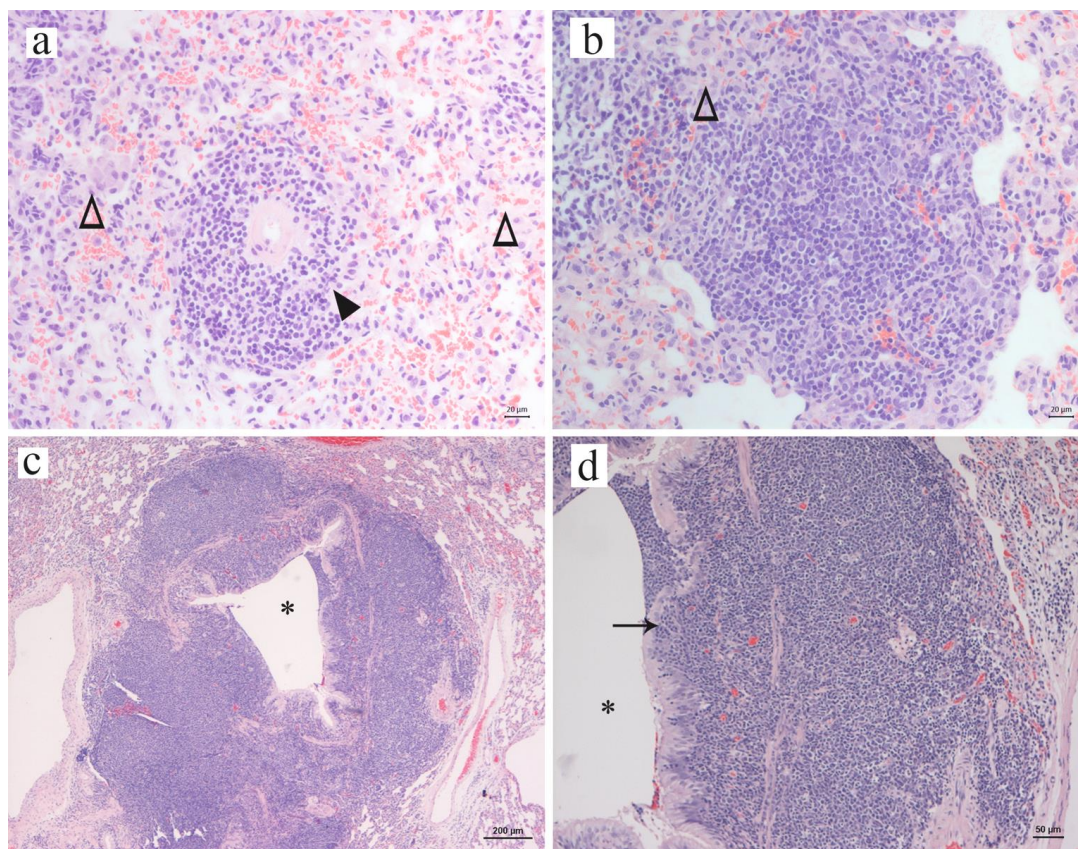


**Figure 3.41.** Histological features of the spontaneous inflammatory changes occurring in the lungs of Welsh rats from study 4, including the controls. (a) Rat 12L-2260 (0.5 mg/kg of NR678, euthanased at 24 h post dosing). There is a periarteriolar aggregate of lymphocytes (solid arrowhead) and a more diffuse interstitial infiltration of mononuclear cells (open arrowheads), composed predominantly of macrophages, with fewer lymphocytes and plasma cells (bar: 20  $\mu$ m). (b, c and d) Rat 12L-2253 (control, 24 h post dosing). (b) Closer view of the inflammatory infiltrate in a control animal. Macrophages (open arrowhead) are large and characterised by abundant eosinophilic cytoplasm (bar: 20  $\mu$ m). (c) Surrounding a bronchus (\*), there is a large accumulation of lymphocytes, consistent with hyperplasia of BALT (bar: 200  $\mu$ m). (d) At higher magnification, lymphocytes infiltrate the bronchial wall and there is marked lymphocytic exocytosis in the epithelium (arrow). Bar: 50  $\mu$ m.

# Chapter 4 Discussion

4.1 NR678 as a model of acute lung injury (ALI)

4.2 Morphological characterisation of the adaptive response of the rat lung to sublethal doses of NR678

4.3 Assessment of *R. norvegicus* as a suitable animal model to investigate the relationship between *FMO2* polymorphism in humans and differences in response to thiourea-based drugs

4.4 Potential issues and limitations

4.5 Concluding remarks

The results presented in chapter 3 focused on three main subjects: 1) the investigation of the acute toxicity of the thiourea-related rodenticide candidate NR678 in the rat lung, as an example of drug-induced oxidative stress in this organ, 2) the characterisation of the morphological adaptive changes occurring in the rat lungs in response to sublethal doses of NR678 and 3) the preliminary assessment of the possible metabolic and toxicological implications of *FMO2* polymorphism in rats as a model of the human polymorphism. Following this order, we will interpret here the results of the experiments, discussing their main limitations alongside their implications for future research.

## **4.1 NR678 as a model of acute lung injury (ALI)**

In the first part of this work, we assessed the acute target organ toxicity of a single oral dose of NR678 in the rat. The compound was administered at two different doses, 5 or 10 mg/kg, which both exceeded the maximum tolerated dose (MTD) determined in the preliminary LD<sub>50</sub> studies conducted at BASF Pest Solutions.

### **4.1.1 Morphological features and cellular targets of NR678 pulmonary toxicity**

NR678-treated rats developed severe respiratory clinical signs, including tachypnoea and dyspnoea within 6 h post dosing, prompting elective euthanasia (see paragraph 3.1.1). The cause of the clinical signs was a multifocal rather than diffuse, moderate to marked alveolar and interstitial pulmonary oedema with hydrothorax (see paragraphs 3.1.2-3), which confirmed that NR678, as several other thiourea derivatives, is a potent selective pulmonary toxicant in rats at a dosage of  $\geq 5$  mg/kg. Pulmonary oedema was considered the cause of moribundity of the rats, in concurrence with the increased pressure exerted on the lung by the severe hydrothorax (compression atelectasis). Hypoxaemia resulting from impairment of gas exchange in flooded and compressed alveoli, coupled with the depression of blood volume caused by the shunting of considerable amounts of fluid from the vascular to the extracellular compartments, may explain the rapidly-establishing moribundity of NR678-treated rats. Interestingly, fluid accumulation in the lung, even in episodes of severe pulmonary oedema, is rarely uniform (Mirza et al., 2011),

but occurs with a multifocal distribution pattern, as in NR678-treated rats, where only patchy alveolar areas were affected, mostly beneath the pleura. The reason for the lack of an uniform distribution of alveolar oedema is unknown and may be related to a highly efficient, rat-specific mechanism of fluid drainage from the alveolar and interstitial parenchyma to the pleural compartment, mediated by the lymphatic system (Vivet et al., 1983). This would explain the severe extent of pleural effusion in the absence of diffuse alveolar flooding. These findings are consistent with the acute pulmonary toxicity previously reported for molecules containing a thiourea moiety (Dieke and Richter, 1946; Richter, 1945; Richter, 1946), including the thiourea-based compound ANTU, marketed to fight rat-borne epidemics during World War II [(Keiner, 2005); see paragraph 1.3]. These molecules have been extensively used as a means to investigate the pathogenesis and mechanisms of acute pulmonary oedema in several animal species (Haschek et al., 2009e; Hurley, 1978; Vivet et al., 1983). However, the mechanism leading to pulmonary oedema is not completely understood yet.

Injury to the pulmonary parenchyma may be directed to a specific cell type, most often endothelial cells and type I pneumocytes, or target several cell types indiscriminately (Haschek et al., 2009e). Injury of type I pneumocytes following the administration of ANTU has been described only after the administration of very high doses (Smith, 1986). Accordingly, it is unlikely that the epithelial compartment represents a primary target of NR678 toxicity. In NR678-treated rats, the pulmonary architecture was well preserved and no alteration of the alveolar lining epithelium integrity was observed when lung sections were stained with an antibody against AQP-5, a water channel protein constitutively present on the membrane of type I pneumocytes (see paragraph 3.1.3). Scattered apoptotic cells lining the alveoli of rats given NR678 were positive for cleaved caspase 3 by IH and most were identified as endothelial cells at ultrastructural examination (paragraph 3.1.4). Sporadic pneumocytic apoptosis may have been caused by hypoxia following alveolar flooding by extravasated fluid and consequent impairment of gas exchange (Martin et al., 2005), rather than being a direct effect of the drug.

Oedema in NR678-treated rats is likely to be related to the primary effacement of endothelial cells, as supported by the histological and ultrastructural changes. Pulmonary vascular endothelium comprises one of the largest capillary networks of the body and, among several other functions, it plays a major role in regulating lung fluid balance and solute transport, in response to a plethora of physiologic and pathologic stimuli (Haschek et al., 2009e). Increased permeability of the vascular endothelium has been classically ascribed to two different mechanisms, namely 1) the loss of integrity of endothelial cells by direct or immune cell-mediated damage or 2) the increased function of the transport pathways, both across the endothelial cell (transcellular pathway) or between neighbouring cells (paracellular pathway), as depicted in **Figure 4.1** (Chiang et al., 2011; Mitchell and Cotran, 2007a).

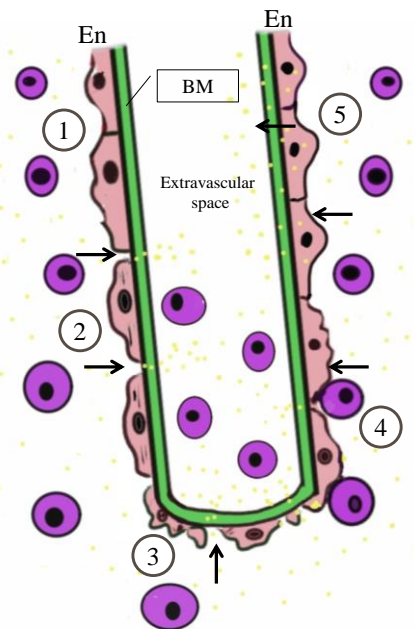


**Figure 4.1.** Main mechanisms leading to increased vascular permeability. (1) In the absence of pathological stimuli, the vascular endothelium, composed of a monolayer of endothelial cells (En) separated from the extravascular space by a continuous basement membrane (BM), is semipermeable to plasma proteins (yellow dots) and leukocytes (purple cells). (2) Increased vascular permeability may occur following contraction of endothelial cells resulting in widened intercellular spaces (paracellular pathway). (3) Direct damage to endothelial cells, causing degeneration and necrosis, is responsible for disruption of the vascular barrier and fluid leakage into the interstitium. (4) Endothelial injury may be also mediated by inflammatory cells, resulting in a similar outcome. (5) Movement of fluid and macromolecules into the extravascular space may occur via the transcellular pathway, characterised by albumin-mediated vesicular transport of solutes and proteins through the endothelial cell. Modified from Mitchell and Cotran, 2007a.

Direct injury to endothelial cells (**Figure 4.1**, 3 and 4) has been described as a cause of pulmonary oedema in numerous pathological conditions, including physical injury (burns), sepsis and several vasculitides with different aetiologies (Mitchell and Cotran, 2007a). This may have occurred in NR678-treated rats as well, which exhibited ultrastructural subcellular alterations in the endothelium, such as rearrangement and rarefaction of cytoplasmic organelles and the formation of endothelial and subendothelial blebs (see paragraph 3.1.4). However, the integrity of the pulmonary endothelial cell layer was not affected in NR678-treated rats, as confirmed by IH for factor VIII-related antigen (see paragraph 3.1.3) and the frequency of truly degenerate or apoptotic endothelial cells observed in the ultrathin sections (see paragraph 3.1.4) was too low to justify a substantial alteration of vascular permeability. This suggests that direct damage to endothelial cells may have contributed only to a minor extent to NR678-induced increased vascular permeability. Immune-mediated endothelial cell injury was also excluded, as there was no evidence of increased numbers of neutrophils and/or lymphocytes, targeting the endothelium.

Movement of fluid through the transcellular pathway (**Figure 4.1**, 5) is mediated by an active process of transcytosis, whereby albumin-filled uncoated vesicles are transported from one side to the other in the endothelial cell (Mitchell and Cotran, 2007a). This is probably a minor way of fluid exchange compared to the paracellular pathway (**Figure 4.1**, 4), in which connections between adjacent endothelial cells widen and let fluid, proteins, and/or cells pass through the gap. There was no evidence of increased formation of transcytotic vesicles in rats receiving NR678, which should not be confused with the blebs seen in the endothelial cells using TEM (see paragraph 3.1.4). Similar endothelial and subendothelial blebs have been described ultrastructurally in several models of lung oedema (Lopez et al., 1988) and their significance is unknown.

There was strong evidence that paracellular gap formation may represent the most plausible explanation of the increased permeability associated with NR678 administration, as supported by the presence of ultrastructural intercellular gaps between the pulmonary capillary endothelial cells (see paragraph 3.1.4). This is a

common pathway employed by endothelial cells to permit paracellular transport, in which they dramatically modify their shape as a consequence of rearrangement and contraction of the actin-based anchor filament system (Chiang et al., 2011). A variety of bioactive agonists (e.g.; histamine and thrombin), cytokines (TNF- $\alpha$  and IL-1 $\beta$ ), growth factors (VEGF) and mechanical stress itself are known to influence different components of the cytoskeletal system of the endothelial cell (Mitchell and Cotran, 2007a). Inflammatory mediators act through the activation of several protein kinase C isoforms, which in turn control the phosphorylation of actin and its linking proteins at the cell-to-cell junction (Lum and Malik, 1994). Phosphorylation causes a rearrangement of the cytoskeletal proteins leading ultimately to retraction of the microtubular system, the rounding-up of the cell and the widening of intercellular gaps. Opening of the intercellular gaps does not only occur in response to physiological conditions, but can also be elicited by different types of pathological insults, such as oxidative injury, which is the most likely event leading to disruption of the microfilaments and microtubules of endothelial cells in NR678-induced lung damage (Hinshaw et al., 1986).

Though the consequences of free radical damage on individual pulmonary cell types may be extremely variable (Smith, 1986), selective damage to endothelial cells and increased vascular permeability have been observed with a number of drugs causing oxidative stress. Bleomycin-induced acute lung endothelial injury is probably one of the best examples of the above, although not as extensively characterised as the more commonly described chronic findings of bleomycin pulmonary toxicity. In cultured lung vascular endothelial cell monolayers, this drug has been shown to cause cytoskeletal reorganisation and alteration of the intercellular junctions, which was associated with a decrease in the GSH levels and reversed by thiol-redox protectants (Patel et al., 2012). Similar findings have been described in other models of oxidative lung injury, such as the intestinal ischaemia-reperfusion (Zhao et al., 2001) and endotoxin-induced (Ishii et al., 1992) injury models. Previous studies have reported that the loss of GSH increases significantly the susceptibility of cultured endothelial cells to injury by H<sub>2</sub>O<sub>2</sub> (Harlan et al., 1984) and hyperoxia (Suttorp et al., 1991). Bovine pulmonary artery endothelial cells exposed to high doses of H<sub>2</sub>O<sub>2</sub> exhibited a dose-dependent depletion of GSH and ATP, disarrangement of microfilaments into

shortened bundles, cell membrane alteration and the formation of large F actin bundles (Hinshaw et al., 1988; Hinshaw et al., 1986). Loss of GSH in the lung of mice after treatment with a GSH-depleting agent has been shown to cause swelling and decreased numbers of mitochondria in endothelial cells (Owens and Belcher, 1965). Analogously to oxidative damage caused by bleomycin and H<sub>2</sub>O<sub>2</sub>, NR678 may act through this pathway and cause contraction and shape alteration of endothelial cells which result in intercellular gap formation. Swelling of the cytoplasm and the basement membrane, and loss and/or dilation of subcellular organelles have been described in the endothelial cells of NR678-treated rat lung capillaries (see paragraph 3.1.4). However, in contrast to the ultrastructural changes reported in the endothelial cells of rats administered ANTU (Cunningham and Hurley, 1972), no clear evidence of cytoskeletal alteration was detected in NR678 rats.

There is no current explanation for the specific susceptibility of the lungs, and especially of the pulmonary endothelium, to thiourea-induced damage. There are several examples in the literature of drugs which accumulate in the lung, such as amiodarone (Reasor et al., 1990), paraquat and numerous anaesthetics (Boer, 2003; Foth, 1995) to cite but a few. The reason for preferential pulmonary clearance of these compounds, known as “pneumophilic” drugs, has been related to a high grade of diffusion and/or a specific active transport mechanism through the alveolar barrier, which are both favoured by peculiar chemical properties of the aforementioned compounds (Foth, 1995). Most of these drugs in fact are either highly lipophilic compounds or amphiphilic molecules and/or contain amine groups. NR678, however, does not appear to share any of these features. As the drug is absorbed in the gastrointestinal tract and then reaches the systemic circulation, endothelial cells are the first cell type exposed to NR678 effects in the lungs. Interestingly, only the pulmonary endothelium appears to be injured by the test article, as, at least by light microscopy, there was no evidence of morphological or functional impairment of the endothelium in other body compartments. The endothelium lining the alveolar capillaries may represent a direct target of NR678 toxicity due to a peculiar metabolic potential of this cell type or it may be indirectly affected by a reactive metabolite produced nearby that diffuses to endothelial cells.



The first hypothesis would imply that endothelial cells are endowed with higher enzymatic oxidative activity toward NR678 and other thiourea-based molecules, namely with higher levels of FMOs, the enzymes which are mostly responsible for the biotransformation of this class of molecules. RNA-ISH for FMO2 mRNA revealed that this isoform is expressed by several cell types within the lungs, including, but not exclusively, endothelial cells lining the alveolar capillaries (see paragraph 3.3.1). Although not evaluated quantitatively, the distribution and the intensity of the signal for FMO2 mRNA in the lungs was higher than in the other organs examined (brain, kidney and liver) and, interestingly, the cells lining the pulmonary capillaries were the only endothelial cells exhibiting FMO2 expression. Unfortunately, due to technical issues, it was not possible to obtain data concerning the expression of FMO1, the other major FMO isoform in the rat lung, which, in contrast to FMO2, is functionally active in the laboratory rat. The localisation of FMOs and the consequential formation of reactive metabolites within endothelial cells or other alveolar cell types in close proximity with them may partially explain the selective injury to this cell type observed when exposed to small thioureas. On the other hand, endothelial cells may be more susceptible than other pulmonary cells to oxidative injury owing to an intrinsic sensitivity to thiol-redox alterations (ie, GSH depletion) as discussed below, rather than owing to an increased production of intermediate metabolites within the cells or in their vicinity.

#### **4.1.2 NR678 pulmonary toxicity as a model of drug-induced oxidative stress**

The lung is permanently exposed to the environment and is constantly in contact with xenobiotics present in aerosol (Haschek et al., 2009e). Additionally, any compound reaching the blood stream following parenteral administration, ingestion, or skin exposure, necessarily enters the lung, as this organ, differently from any other compartment in the body, receives the entire cardiac output at each pulse. These features enable the pulmonary alveolar-capillary unit to interact with xenobiotics before they reach the systemic circulation yet, at the same time, expose the lungs to toxicologically important consequences (Smith, 1986). Toxic lung damage often results from direct interaction between the parent molecule and its cellular target, as

happens with the inhalation of noxious gases, such as oxygen, ozone, nitric oxide and hydrochloric acid (Haschek et al., 2009e). More commonly, toxicity relies on the metabolic activation of the xenobiotic to a reactive intermediate, in the lung itself or elsewhere in the body; most frequently in the liver. In both cases, reactive intermediates and oxygen metabolites, such as hydroxyl radical, superoxide and hydrogen peroxide, play an integral role in the development of lung injury. In addition, toxic lung damage may be mediated or amplified by a secondary inflammatory response with further release of reactive oxygen and nitrogen species (Smith, 1986).

In order to prevent the risk of oxidative stress on a large surface area constantly exposed to oxygen, the lungs are endowed with integral antioxidant systems (Comhair and Erzurum, 2002; Haschek et al., 2009e). Cells use a plethora of enzymatic antioxidants including catalase, superoxide dismutase (SOD) and, more importantly, glutathione peroxidase (GPx) to remove oxygen intermediates and repair damaged molecules. In addition, intracellular levels of soluble scavengers, such as  $\alpha$ -tocopherol and GSH are crucial components in buffering ROS production and protecting the lung from oxidative insult. Surfactant also appears to have antioxidant properties (Matalon et al., 1990) and the alveolar lining fluid contains GSH levels  $100 \times$  higher than those detected in plasma (Comhair and Erzurum, 2002). When exposed to oxidative stress, the lung may respond to imbalance between physiological antioxidant resources and reactive species by increasing the levels of reducing equivalents. Increased expression of SOD and GPx and altered levels of pulmonary scavengers have been described as a feature of several lung conditions dominated by oxidative stress, such as pulmonary idiopathic fibrosis, acute respiratory distress syndrome and cancer (Rahman et al., 2006). Drugs which upset the oxidant-antioxidant *status quo* through antioxidant enzyme inhibition, consumption of scavengers or reactive oxygen and nitrogen intermediate formation may initiate oxidative stress and lead to damage of major cellular components, such as proteins, DNA and membrane lipids (Haschek et al., 2009e).

Variation in the levels of endogenous GSH in the lung is known to influence the toxic outcome of certain drugs which specifically target this organ and cause

oxidative stress, such as 3-methyl-indole, ipomeanol and naphthalene (Smith, 1986). Pulmonary GSH and sulphhydryl-group depletion has been reported in previously conducted studies in rats administered thiourea (Hollinger et al., 1976), although in other works this drug has been claimed to have opposite effects (Hardwick et al., 1991). When rats were pretreated with GSH-depleting agents such as diethyl maleate, toxicity and/or covalent binding of ANTU and other thiourea-derived molecules in the lung were increased (Hollinger et al., 1976; Tate and Flory, 1993; Tate et al., 1991). Phorone on the other hand causes an initial depletion of GSH in both liver and lungs, followed after 2 d by an elevation of non-protein sulphhydryl levels above the reference levels reported in literature: rats challenged with ANTU 48 h after phorone administration showed decreased lethality and less severe hydrothorax compared to those receiving ANTU alone (Hardwick et al., 1991).

A dose of 5 mg/kg of NR678 administered to rats caused a statistically significant depletion of GSH in lung and liver tissue homogenates (see paragraph 3.2.2.4). Decreases in endogenous GSH levels observed in rats that have been administered NR678 may have been caused by a “futile” redox cycling mechanism, in which the continuous production of an unidentified NR678 reactive intermediate leads to the consumption of antioxidant resources. Accordingly, the depletion of reducing equivalents in the cell impedes further protection from the metabolite, which is therefore able to interact with lung subcellular components and cause irreversible modification of their structure through covalent binding (Smith, 1986). This mechanism has been exemplified for several compounds, including PTU [(Henderson et al., 2004b; Smith and Crespi, 2002), **Figure 4.2**], to which NR678 is structurally similar, and other thiols which are transformed to sulphoxides by monooxygenases via the formation of an intermediate sulfenic acid (Mansuy and Dansette, 2011). The oxidation of thiols to sulfenic acids requires NADPH and O<sub>2</sub> as well and may further progress to generate the corresponding sulfinic acid and then sulfonic acids according to the general formula reported by Mansuy and Dansette (2011):

RSH (thiol) → RSOH (sulfenic acid) → RSO<sub>2</sub>H (sulfinic acid) → RSO<sub>3</sub>H (sulfonic acid)

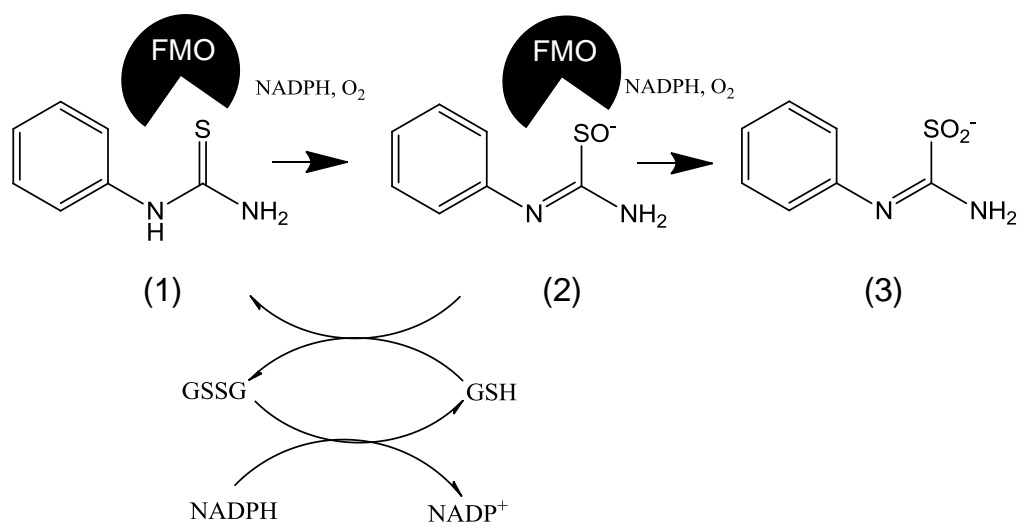


**Figure 4.2.** Scheme of the FMO-mediated S-oxidation of phenylthiourea. Phenylthiourea (1) is transformed into a phenylthiourea sulfenic acid (2) with consumption of NADPH, O<sub>2</sub> and GSH. Further oxidation to sulfinic acid (3) may occur. Redrawn from Smith and Crespi (2002)

Due to their unstable nature, sulfenic acids may react with the parent thiol or with other sulphhydryl groups, including GSH. The reducing scavengers present in the medium revert the sulfenic acid to the parent compound with the formation of mixed disulphides, such as glutathionyl adducts. This cycle ends when all GSH reserve is consumed and the reactive metabolite interacts permanently with constitutive components of the cell (Mansuy and Dansette, 2011). In studies conducted with <sup>35</sup>S- and <sup>14</sup>C-labeled ANTU in rats (Lee et al., 1980), occurrence of covalent binding was demonstrated in lung and liver microsomes. Toxicity and covalent binding were markedly reduced when rats were dosed with  $\alpha$ -naphthylurea (ANU), proving that the sulphur atom contained in ANTU is essential for the toxic manifestations of thiocarbamides and the formation of a reactive metabolite (Boyd and Neal, 1976).

No NR678 sulfenic or sulfinic acids were detected *in vitro* in our microsomal incubations. An attempt to address the lack of an observable NR678 metabolite has been made. Adequacy of the *in vitro* system in use was considered of potential concern and was investigated in the first instance. Liver microsomes were prepared according to a procedure which has been in place for several years in our laboratory (see paragraph 2.4.1); however, quality check of the microsomal homogenates has

always focused on determining whether they possessed adequate CYP rather than FMO activity rates. It has already been mentioned that the contribution of P450 to the metabolism of small thioureas is minor (Onderwater et al., 1999), whilst FMOs appear to be responsible for most of the catalytic turnover for this class of molecules (Ziegler-Skylakakis, 2003). Accordingly, MI assay, as described by Dixit and Roche (1984), was set up to determine the FMO activity of our microsomal preparations. MI S-oxidation activity was observed in both liver and lung microsomal homogenates (see enzyme kinetics parameters in paragraph 3.4.3.1). Although several modifications to the standard incubations (see paragraph 2.4.3) and the HPLC parameters (see paragraph 2.4.4) were introduced, no NR678 metabolite peaks were identified in the chromatograms. Indirect proof of NR678 metabolic turnover occurred in enzyme inhibition experiments (see paragraph 3.4.3.2): when NR678 (500  $\mu$ M) was added to liver and lung microsomal incubations, the activity of FMOs towards MI (500  $\mu$ M) was substantially reduced, suggesting that the compound is metabolised by the *in vitro* system. In addition, a discernible metabolite peak was present in the HPLC chromatogram when PTU, structurally similar to NR678, was incubated using the same conditions (see paragraph 3.1.5). It was concluded that, despite the structural similarity between PTU and NR678, the metabolite/s of the latter could not be observed in an HPLC chromatogram. This is supported by the observation that direct measurement of sulfenic acid kinetics is difficult due to their high reactivity (Mansuy and Dansette, 2011). In most cases, sulfenic acids are not easily detectable as such and trapping agents such as the nucleophilic probe  $\beta$ -dicarbonyl dimedone or different and more sophisticated detection systems, like real time mass spectrometry and x-ray crystallography, have to be employed.

Uneven distribution of GSH in the lung should be taken into consideration when speculating on possible effects of oxidative stress on cell targets. When GSH levels are measured in liver homogenates, it is assumed that hepatocytes contribute most to the actual values, as they comprise approximately 80% of the hepatic volume (Haschek et al., 2009c). The lung has a less homogeneous structure and contains more than 40 different cell types (Haschek et al., 2009e). As such, changes in GSH levels measured from whole lung homogenates need to be carefully examined and always related to the pattern of injury and the cell type mainly affected by the

oxidative insult. Even more caution applies to the interpretation of the GSH measurements presented in this work, as the different texture and water content of the lungs of rats exhibiting pulmonary oedema may have affected the levels of reduced and oxidised glutathione. The herbicide paraquat is an excellent example of a lung toxicant which surprisingly, despite causing oxidative injury via the establishment of a futile redox cycling, does not alter thiol pulmonary levels (Hardwick et al., 1990). A possible explanation for this relies on the selective uptake of paraquat by epithelial cells, which accordingly represent the primary target of the herbicide toxicity. Type I and II pneumocytes comprise only about 20% of pulmonary cell population (Haschek et al., 2009e) and possibly contribute only a small proportion of the total lung GSH (Hardwick et al., 1990). On the other hand, endothelial cells are believed to be one of the main contributors to total pulmonary GSH contents (Hardwick et al., 1990) and it can be hypothesised that oxidative injury to this cell type may result in a more evident decrease in thiol levels. This is thought to be the case with NR678, which targets primarily the pulmonary endothelium and leads to a significant drop in GSH levels in the lungs.

#### **4.1.3 Extra-pulmonary NR678-related effects**

In addition to the lung, NR678-related toxicity was detected also in the liver, where individual necrotic hepatocytes were observed in the centrilobular areas. The morphology of the change (swelling of the hepatocyte cytoplasm with loss of detail of the nucleus) is consistent with necrosis, rather than apoptosis, as confirmed by the lack of positivity using cleaved caspase 3 IH. Hepatocellular necrosis has been described previously with compounds containing a thiourea moiety, such as MI and propylthiouracyl and has been ascribed to the formation of reactive intermediates in the hepatocytes (Woeber, 2002).

Apoptotic lymphocytes were increased in number in the lymphoid organs and tissues of rats that had been given NR678, when compared to vehicle-controls (see paragraph 3.1.3). Some degree of apoptosis is generally expected in control animals and considered within normal limits in tissues such as the lymphoid organs, in which rapid cell turnover occurs (Haschek et al., 2009a). In treated animals, overall numbers of apoptotic lymphocytes were increased, especially in specific lymphoid

compartments such as the thymic cortex and the germinal centres of lymphoid follicles in the spleen, the examined lymph nodes and the gut-associated lymphoid tissue. The lamina propria of the small intestine segments in treated animals also contained scattered apoptotic cells (presumably apoptotic lymphocytes), which are not normally seen as a background change in laboratory rats. Microscopic changes in the lymphoid organs and tissues of treated animals are attributed to NR678, although it can be difficult to make a clear distinction between a direct compound-related immunomodulating effect and a non-specific result of stress/debilitation caused by the test item. A variety of factors and conditions, including background physiological influences, result in decreased cellularity of the lymphoid organs (Pearse, 2006). Normal age-associated decrease in cellularity occurs in the thymus (involution), whereas other factors such as inadequate nutrition, body weight loss and decreased food intake, stress, or toxicity may also cause decreased cellularity in several other lymphoid tissues. Stress in particular, through stimulation of the hypothalamic-pituitary-adrenal gland axis, leads to elevated levels of circulating glucocorticosteroids, which in turn induce lymphocytic apoptosis. Such changes are common following acute debilitating diseases, especially in moribund animals requiring elective euthanasia and can be seen within hours from the onset of the debilitating condition (Greaves, 2007b). These effects are often indistinguishable from immunotoxicity caused by a test article. In some cases, a dose-response relationship may be helpful in deciding whether decreased lymphoid cellularity is a direct or indirect effect of a toxicant. Selective immunomodulating test articles usually show effects on the lymphoid system at low dosages as well, while stress/debilitation-induced lymphoid changes often occur only at the highest dose regimens, where signs of generalised distress are usually well evident (Greaves, 2007b). Decreased lymphoid organ cellularity was seen in rats administered NR678 at high dosages (5 or 10 mg/kg), at which debilitation occurred and was not present in rats given a lower dose such as 0.5 mg/kg (study 3, see paragraph 3.2.2.1.3), supporting the hypothesis of a secondary corticosteroid-induced mechanism as a major contributor to lymphocytic apoptosis. Further investigation of these lymphoid organ changes, needed to clarify this issue, was beyond the aims of the present work.

## **4.2 Morphological characterisation of the adaptive response of the rat lung to sublethal doses of NR678**

In the second part of this work, we assessed the establishment of tachyphylaxis in the lung of rats administered sublethal doses of NR678 and investigated the pulmonary changes that are thought to contribute to the decreased susceptibility of tolerant rats to high, normally lethal doses of this thiourea-derived compound.

### **4.2.1 Onset and duration of tolerance to NR678 in the rat lungs**

Rats develop tachyphylaxis in response to the administration of various thiourea-based molecules, as reported in previous studies where tolerance was induced through the oral or parenteral administration of low doses of thiourea or ANTU, administered up to six times per day or twice weekly for a few weeks (Van Den Brenk et al., 1976). Barton et al. (2000) achieved complete protection from a lethal dose of ANTU (70 mg/kg) in rats administered a low, single dose (5 mg/kg) 24 h before the challenge with the high dose. In order to set up a tolerogenic regimen for NR678 (pilot study 2), a tolerogenic:lethal dose ratio similar to that reported in Barton et al. (2000) was used and the rats were initially dosed with a dose (0.5 mg/kg) of NR678 which was  $10 \times$  lower than the LD<sub>50</sub> (5 mg/kg). We did not expect this dose to induce significant clinical signs, since in previous LD<sub>50</sub> investigations undertaken at BASF, a dose of 2 mg/kg of NR678 was seen to cause only mild transient clinical signs (see **Table 1.1**). Indeed, rats that were administered a dose of 0.5 mg/kg of NR678, followed after 3 h by the high dose, exhibited only mild and transient respiratory distress (see clinical assessment in paragraphs 3.2.1 and 3.2.2.2.1). This is in contrast to the effect of the high dose (5 or 10 mg/kg) of NR678 when administered without prior tolerance induction, which caused severe respiratory clinical signs that required euthanasia of the rats approximately 6 h after dosing (see paragraph 3.1.1). In contrast to previous studies (Barton et al., 2000; Dieke and Richter, 1946; Van Den Brenk et al., 1976), in which rats had been challenged with a lethal dose no less than 24 h after tolerance induction, we found that protection against the NR678 high dose challenge was already effective as early as 3 h after the administration of the tolerogenic dose. This indicates that



tachyphylaxis induced by thiourea-based molecules may represent an extremely effective, timely protective mechanism that develops more rapidly than previously thought.

As expected, the milder clinical signs in tolerant animals were paralleled by macroscopic and microscopic observations that were similar but considerably less severe than those observed in the animals that had received only the lethal dose. In the cohort of rats from group 4 (0.5 mg/kg of NR678, followed by 5 mg/kg after 3 h) euthanased at 24 h post dosing, only one of three rats in this end point exhibited the gross and histological changes consistent with acute toxicity, i.e. hydrothorax and pulmonary hyperaemia and oedema, which occurred though with a mild severity (see paragraphs 3.2.2.2.2-3). The ultrastructural examination of the lungs of the rats euthanased at this time point revealed endothelial injury (endothelial bleb formation, irregular endothelial lining and rare paracellular gap formation), consistent with that observed with the acute toxicity (see paragraph 3.2.2.2.4); however, these ultrastructural findings were scattered rather than present in virtually every alveolar unit, and no evidence of endothelial degeneration or necrosis was observed. This suggests that the mechanism supposedly responsible for the lung injury (gap formation between endothelial cells leading to increased pulmonary vascular permeability) is unaltered during the tolerogenic response, but that the severity of the change is reduced, producing milder effects on the air blood barrier. This was further confirmed by the fact that in rats given the low dose (0.5 mg/kg) of NR678, which had no gross or microscopic observations consistent with altered vascular permeability in the lungs, ultrastructural endothelial cell findings were still observed (see paragraph 3.2.2.1.4), but were less frequent and seen only within a few hours after dosing (at 3 and 6 h), being almost absent at 24 h. Electron microscopical changes at these time points consisted exclusively of blebs within or beneath the endothelial cell cytoplasm, whereas the other endothelial changes that are likely responsible for the increased vascular permeability associated with acute toxicity, such as discontinuous endothelial lining and paracellular gap formation, were not observed in rats receiving the low dose.

In view of the fact that tolerance to the oedematogenic effects of thiourea may represent a possible therapeutic approach against pulmonary conditions characterised by increased permeability and oxidative stress in humans, it seemed of interest to investigate the duration of the protection conferred by a low dose of NR678 in rats. Previous studies have shown that tolerance to molecules containing the thiourea moiety is long lasting. Protection from ANTU in tolerant rats was reported to persist for approximately 3 w after the administration of the high dose (Van Den Brenk et al., 1976). Similarly, Barton et al. (2000) showed that rats were fully protected from the acute toxicity acquired with a low dose of ANTU for approximately 10 d post dosing. Protection, according to these authors, decreased progressively until day 20, when a rechallenge with a high dose led to 100% mortality yet again. Duration of tolerance to NR678 was assessed in study 3, where two cohorts of rats receiving either the low dose (group 3) or the low dose followed by the high dose (group 4) were challenged with the high dose on day 14 (see paragraph 3.2.2.3.1). Confirming the findings reported previously in the literature, partial tolerance to NR678 was possibly still evident on day 14, as demonstrated by the generally decreased incidence and severity of the respiratory clinical signs occurring in these animals when compared to those receiving the high dose only (group 2; see paragraph 3.1.1). However, the degree of hydrothorax and pulmonary oedema in these cohorts (see paragraphs 3.2.2.3.2-3) appeared identical to those of rats from group 2 (paragraphs 3.1.2-3), suggesting that the level of protection conferred by a tolerogenic dose of NR678 may be phasing out after 2 w. Similarly to a previous report (Van Den Brenk et al., 1976), tachyphylaxis to NR678 appeared to be dose-dependent, with a higher dosage (0.5 + 5 mg/kg) of NR678 leading to increased protection compared to a lower one (0.5 mg/kg only, see paragraph 3.2.2.3).

#### **4.2.2 The morphological characterisation of cell proliferation in the lungs of rats tolerant to NR678**

Cell proliferation that followed the administration of the low dose of NR678 was assessed using histology, a combination of different immunohistological markers and ultrastructural examination. Both histology and IH concurred to demonstrate a substantial increase in the number of macrophages and type II pneumocytes in the

lungs of tolerant rats when compared to controls. It is interesting to note the different kinetic behaviour of these cell populations: macrophages free in the alveolar lumen were increased at early time points (3, 6 and 24 h), whilst type II pneumocytes began to increase at 24 h after dosing and reached maximum levels on day 7. This occurred both in rats receiving only the low dose of NR678 (group 3, see **Table 3.5** and **Figures 3.14-16**) and in those challenged 3 h later with the high dose (group 4, see **Table 3.7** and **Figure 3.22**). On day 14, the number of alveolar macrophages and type II pneumocytes had almost completely returned to the levels observed in the controls. The rise in macrophages and type II pneumocytes appeared to be time- rather than dose-dependent, as the increases had similar severity degree in both groups 3 and 4.

To our knowledge, this is the first work to have characterised the pulmonary ultrastructural findings associated with thiourea-induced tachyphylaxis. The ultrastructural examination of type II epithelial cells proliferating at 24 h and 7 d after dosing in both groups 3 and 4 allowed an important distinction: whilst the lungs of the tolerant rats at day 7 were predominantly populated by mature type II epithelial cells exhibiting numerous large lamellar bodies, the alveolar septa of rats euthanased at 6 and 24 h post dosing exhibited numerous immature epithelial cells, with intermediate features between type I and type II pneumocytes (see paragraph 3.2.2.1.4 and **Figure 3.21**). These cells were interpreted as recently divided type II pneumocytes, not fully differentiated yet into type I or type II cells. Although the presence of a specific stem cell population in the lung is still a matter of debate, it is generally accepted that type II pneumocytes are in charge of the dynamic regulation of alveolar epithelial cell regeneration, in virtue of their almost unlimited capacity of renewal (Kasper and Haroske, 1996). During normal cell turnover type II cells divide and differentiate into type I pneumocytes, contributing to the remodelling the alveolar unit and the maintenance of its homeostasis (Fehrenbach, 2001).

The dynamics of type II pneumocyte hyperplasia seen in rats tolerant to NR678 are consistent with the data found in the literature. The patterns of cell renewal following ALI were first investigated in a rat model of pulmonary injury induced by nitrogen dioxide [NO<sub>2</sub>; (Evans et al., 1974)] and then extensively studied in other models of

acute toxic injury (Katzenstein et al., 1990), and were compared with the processes of lung development and alveolar differentiation in the foetus and the newborn rat (Brody and Williams, 1992). Type II cell proliferation has a particularly rapid onset when it is prompted by injury of the alveolar epithelium, developing 3 to 7 d after exposure to the noxious stimulus and persisting for a variable period (Katzenstein et al., 1990). For example, it occurs after 3 d in the lung of mice exposed to hyperoxic injury (Adamson and Bowden, 1974) or following *in vivo* instillation of KGF, which represents a powerful mitogen for type II alveolar cells (Barazzone et al., 1999; Fehrenbach et al., 1999). Evans (Evans et al., 1975), in a pioneer study evaluating the injury to the alveolar epithelium caused by NO<sub>2</sub> in rats, reported an even shorter time frame between inhalation of the gas and the proliferative event: type II pneumocytes began replicating a few hours after exposure, reached the highest extent in the following 2-3 d and decreased to the levels seen in controls by 5 d after exposure. When the same authors examined the levels of incorporation of tritiated-thymidine ([<sup>3</sup>H]-TdR) in the NO<sub>2</sub>-injured rat lung, they found that several cells in the alveolar epithelium were labelled after only 1 h, most of which (approximately 90%) had a morphology consistent with type II pneumocytes; less than 1% were type I pneumocytes and 11.5% had an undetermined morphology (seen to belong to the “intermediate” cell type described above). At 24 h from the inhalation of NO<sub>2</sub>, the number of labelled cells remained constant, while the proportion of type II pneumocytes decreased to approximately 60% of total labelled cells. Concurrently, there was an increase in the proportion (approximately 36%) of intermediate undifferentiated cells labelled with [<sup>3</sup>H]-TdR. The number of labelled type I pneumocytes remained low (approximately 4%). At 48 h after dosing, a substantial increase (to approximately 33%) in the number of type I epithelial cells that had incorporated [<sup>3</sup>H]-TdR was noted: labelled type II pneumocytes and intermediate cells were approximately 46% and 21% of total labelled cells, respectively. The total number of labelled cells and the proportions between the different cell types remained unaltered during the following days, until day 14. Similar results were observed in the lungs of mice exposed to 90% O<sub>2</sub> (Adamson and Bowden, 1974) and using pneumonectomized mice (Brody and Williams, 1992). It is likely that the proliferative event elicited by epithelial injury in the models of ALI mentioned above and in the NR678 experiment resolves with the differentiation of type II

pneumocytes into type I epithelial cells (Fehrenbach et al., 1999) or partly through apoptosis (Bardales et al., 1996) and the restoration of the alveolar epithelial surface. One is tempted to conclude that the proliferation of type II pneumocytes in rats administered NR678 is delayed a few hours when compared to the kinetics of alveolar epithelial cell turnover reported in other types of ALI (Chapman et al., 2002; Evans et al., 1974; Evans et al., 1975; Panos et al., 1995). This is consistent with the fact that traditional models of lung injury usually target the alveolar epithelium, primarily or in combination with the vascular endothelium (Matute-Bello et al., 2008). NR678 instead primarily exerts its toxic effects on the endothelium, with relative sparing of type I pneumocytes (see paragraph 3.1.4). Accordingly, the type II epithelial cell response to thiourea-mediated injury may be delayed compared to other models of lung injury.

#### **4.2.3 An investigation into the mechanisms underlying tolerance to thiourea-based molecules**

As briefly mentioned in the introductory chapter, a considerable amount of literature has been published looking into the defence mechanisms which are supposed to play a role in the adaptive response of the lungs following exposure to sublethal doses of thiourea-based molecules (Barton et al., 2000). Following the observation that administration of KGF to rats attenuated the pulmonary oedema caused by ANTU (Mason et al., 1996), the role of epithelial cell proliferation in the lungs has been investigated as a possible condition underlying tolerance to the rodenticide. Several reports suggested that alveolar epithelial hyperplasia protects rodents from oxidative injury induced by hyperoxia (Panos et al., 1995), bleomycin (Deterding et al., 1997; Sugahara et al., 1998) and hydrogen peroxide (Chapman et al., 2002); however, the mechanism underlying this phenomenon has not been elucidated in these studies. A significant attempt to characterise and interpret the proliferative event occurring in the lungs after the administration of a low dose of ANTU was made by Barton et al. (2000). Similarly to the morphological changes observed with NR678, the authors described an increased number of alveolar macrophages in their tolerant rats, starting at 24 h after dosing and lasting until the end of the study (day 14), but they did not mention the presence of other proliferating cell types, such as type II pneumocytes.

Barton also investigated the levels of proliferation in the lungs of rats administered a low dose of ANTU studying the incorporation of [3H]-TdR and 5-bromo-2'deoxyuridine (BrdU) into the DNA of pulmonary cells. Both labelling systems are used to estimate the proportion of cells in the S phase of the cell cycle (Lin and Allison, 1993). Barton showed that the number of labelled cells in the lungs of tolerant rats increased progressively, beginning at 24 h after administration of the low dose, but did not provide a conclusive identification of the cells incorporating BrdU. The full morphological work-up conducted in rats administered a low dose of NR678 aimed to further characterise the findings reported by Barton and attempted to address how an overall increase in the cells populating the alveolar unit may result in decreased susceptibility to oxidative damage.

Increased cellularity in the alveolus may strengthen the alveolar barrier, enhance the clearance of alveolar fluid (Guery et al., 1997; Sznajder et al., 1998) and/or influence the levels of inflammatory mediators and the oxygen radical scavengers in the lung (Mason et al., 1996). Mason proposed that an increase in the number of type II pneumocytes leads to enhanced synthesis of surfactant and, in turn, to an overall improvement of the antioxidant defences of the lung. KGF was seen to promote the active transport of sodium across the alveolar epithelium, undertaken in part by the Na,K-adenosine triphosphatase (Na,K-ATPase) and, by doing so, to facilitate the clearance of the oedema fluid caused by ANTU (Guery et al., 1997). Macrophages and type II pneumocytes may both cooperate in clearing the alveolar space of the excess of fluid. Type II pneumocytes are equipped with membrane-bound water channels and ion pumps which are thought to control various properties of the alveolar fluid (Fehrenbach, 2001). Alveolar macrophages, despite being cells with a great endocytic capacity and often reported to increase in number in the early stages of pulmonary conditions which alter vascular permeability (Misharin et al., 2011), are not deemed to play a significant role in the clearance of the alveolar fluid accumulated during pulmonary oedema, at least in the first 24-48 h from its onset (Hastings et al., 2004). For example, in a study conducted in sheep administered autologous serum by instillation, the number of alveolar macrophages was dramatically increased by the first 48 h, but the rate of protein clearance remained unaffected and the amount of radio-labelled albumin recovered from the alveolar

macrophages appeared minimal (Berthiaume et al., 1989). However, the same authors provided evidence that the recruitment of macrophages may influence the rate of alveolar fluid reabsorption in a later stage, between 3 and 7 d from the instillation of serum. Accordingly, it has been demonstrated that these cells contribute significantly to the clearance of pulmonary surfactant (Forbes et al., 2007). Our work showed that protection from a lethal dose of NR678 is achieved after only 3 h from the administration of a tolerogenic dose, when there is no morphologic evidence of an increased number of cells in the lungs (see paragraph 3.2.2.1.3). This suggests that clearance of alveolar fluid by increased numbers of alveolar macrophages and type II pneumocytes in the lungs of rats tolerant to NR678 may contribute to the amelioration of the respiratory distress observed after the first few hours, but it is unlikely the primary mechanism associated with the development of tolerance.

With this in mind, we speculated that an increased number of cells in the alveolar unit may have resulted in an enhancement of the antioxidant defense system, which, in turn, may have contributed to the decreased susceptibility of the tolerant lungs to thiourea-induced oxidative injury. It is well known that the lungs are able to upregulate their protective antioxidant scavenging systems when exposed to mild oxidative injury, as occurs for instance in the lungs of chronic smokers (Comhair and Erzurum, 2002). This is usually achieved by increasing the expression of antioxidant enzyme such as SOD or, more frequently, GPx, which leads to higher levels of GSH available to counteract the oxidative insult. This mechanism is unlikely to have an important role in the adaptive process which occurs in NR678-tolerant lungs, as suggested by the fact that GSH levels in tolerant rats at all time points were similar to or lower than those found in the control rats (see paragraph 3.2.2.4).

As discussed in paragraph 1.6.3, several drugs are able to modulate the levels of expression of FMOs in different tissues, either directly or through stimulation of an inflammatory response and production of inflammatory mediators, such as NO. Only very recently, upregulation of FMO3 has been described as a possible factor contributing to the development of resistance to hepatotoxicity caused by paracetamol in mice (O'connor et al., 2013). We thought this could be the case for

NR678 and we hypothesised that tolerance to thioureas might depend on the downregulation of FMO expression in the lungs and consequent decreased levels of the enzymes that are able to catalyse the oxygenation of these molecules to the reactive intermediates responsible for the oxidative injury. Also, we speculated that the pulmonary cells proliferating in response to mild oxidative injury might not possess the same metabolic activity as the corresponding mature type and be unable to metabolise NR678 efficiently. In order to investigate this theory, we analysed the distribution of FMO2 mRNA by RNA-ISH and evaluated the levels of expression of FMO1 and FMO2 in the lungs of tolerant rats. We found that the macrophages and type II pneumocytes in the tolerant rats were strongly positive for FMO2 (paragraph 3.3.2) and that the levels of FMO1 and FMO2 mRNA were significantly increased compared to those observed in the controls (paragraph 3.3.3). According to these results, the decreased susceptibility to oxidative injury which characterises the lungs of tolerant rats does not seem to rely on the downregulation of the enzymes responsible for the metabolism of thiourea-based molecules. It remains to be explored then whether this outcome can be consistent with a mechanism of noncompetitive inhibition of FMOs, according to which the metabolic products of NR678 would have an inhibitory effect on the enzyme, even directly or through the formation of protein adducts or complexes with FMOs, leading to inactivation. Time-dependent inhibition has not been described for FMOs, but it is a well known mechanism which can alter the potency and influence the activity of CYP. It is characterised by irreversible or quasi-irreversible inactivation of the enzymes, which causes lack of function of CYP until new protein is synthesised, typically after several days (Riley et al., 2007). The transient (approximately 14 d) duration of NR678-induced tolerance, coupled with increased synthesis of FMO1 and FMO2 mRNA, may be consistent with time-dependent inhibition of FMOs, which recovers progressively with synthesis of new protein. The possible mechanisms responsible for tolerance to NR678 which were investigated in this work are summarised in **Figure 4.3**.



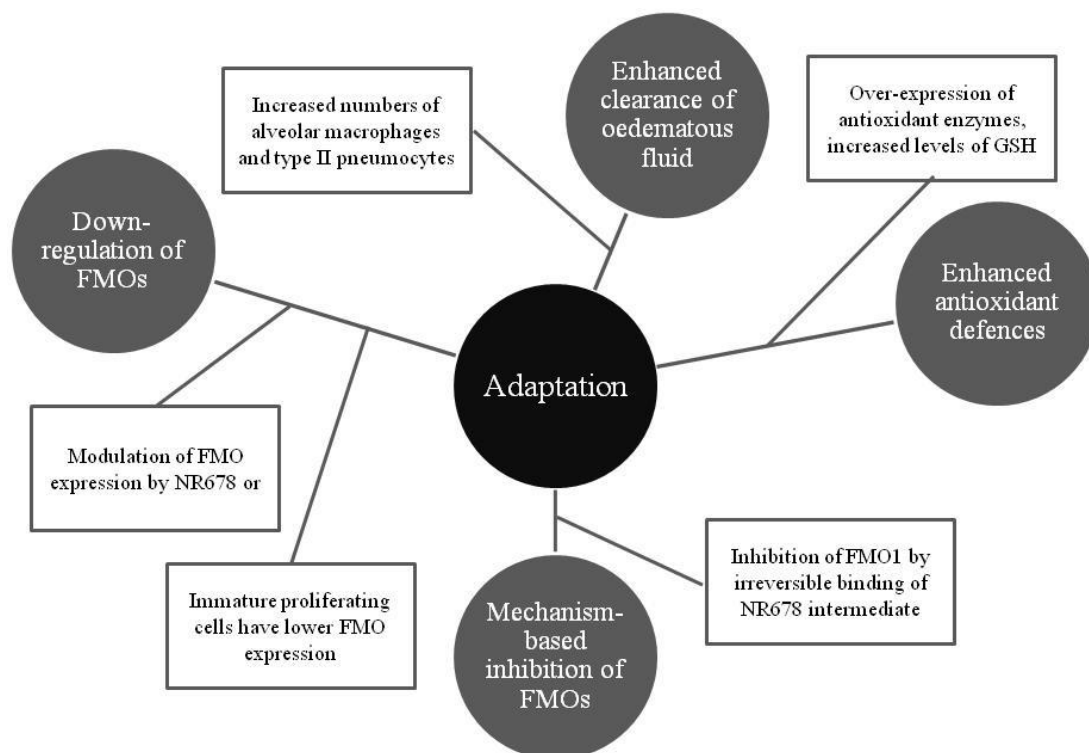


**Figure 4.3.** Possible mechanisms underlying tolerance to NR678.

### **4.3 Assessment of *R. norvegicus* as a suitable animal model to investigate the relationship between FMO2 polymorphism in humans and differences in response to thiourea-based drugs**

The discovery of the genetic variability of *FMO2* dates back to 1998, when Dolphin et al. reported the presence of a premature stop codon in the cDNA of human *FMO2* leading to a truncated and inactive FMO2 enzyme, which is rapidly catabolised (Dolphin et al., 1998). This observation explains the lack of a FMO2 protein in the human lung, whilst in the majority of other species FMO2 is the major FMO pulmonary isoform (Krueger and Williams, 2005). However, a full length *FMO2* was detected by Dolphin et al. (1998) in a few individuals belonging to specific ethnic groups, revealing the existence of a genetic polymorphism. Since the first description, numerous studies have attempted to characterise the allelic frequencies and the ethnic distribution of *FMO2* in humans. Genotyping of a large number of

individuals of different ethnicities showed that the full-length gene, *FMO2\*1*, encoding for the functional protein, is present in approximately 26% of individuals of African descent (Furnes et al., 2003; Whetstine et al., 2000) and 5% of those of Hispanic descent (Krueger et al., 2004; Krueger et al., 2002b). Mutations in the *FMO2* sequence similar to those found in individuals of Caucasian and Asian ethnicities have been described in the laboratory rat, where the *FMO2* expressed in the lungs is truncated and inactive (Lattard et al., 2002b). Wild rats that belong to *R. rattus* species instead possess a full length catalytically active pulmonary *FMO2*. Interestingly, a polymorphism for the *FMO2* gene has been documented in *R. norvegicus* (Hugonnard et al., 2004). The investigation conducted in the last part of this work aimed to characterise the metabolic and toxicological consequences of *FMO2* polymorphism in the rat and to evaluate the relevance of this animal model to man.

The first step of our genotyping analysis, summarised in **Figure 4.4**, aimed to confirm the occurrence of *FMO2* polymorphism in *R. norvegicus* and to determine whether variation existed for a polymorphism in a population of wild rats trapped in the Liverpool urban area. Data available concerning the allelic frequency of *FMO2* in this species are limited to one study (Hugonnard et al., 2004), in which a population of wild rats (*R. norvegicus*) bred in captivity in Lyon, France was genotyped for *FMO2*: according to the authors, the frequency of *FMO2\*1* was comparable to that of the mutant (*FMO2\*2*) form; 48% versus 52%, respectively), and much higher than that described in humans. To our knowledge, our work represents the first study reporting the presence of a polymorphic *FMO2* gene in a wild population of rats and the allelic frequencies expressed by these individuals. The frequency of *FMO2\*1* in these rats was much higher than that detected in humans and in the colony of laboratory-maintained *R. norvegicus* examined by Hugonnard et al. (2004), being approximately 70% (see paragraph 3.4.1). These data may have important implications for the development of rodenticides that are metabolised primarily by FMOs, and specifically those in which the toxicity occurs mainly in the lungs and depends on the bioactivation of the molecule by pulmonary FMOs, such as NR678.

In the second part of our genotyping project, we investigated the allelic frequencies of *FMO2* in two colonies of rats (*R. norvegicus*, Welsh and Berkshire strains) that were available at the BASF facility. These colonies were originally generated by the cross-breeding of wild and laboratory ancestors and they had been maintained under conventional laboratory conditions for several years to be used in studies investigating warfarin-resistance. The number of animals was maintained over the years by brother × sister and parent × offspring mating, with occasional introduction of new wild or laboratory rats. All animals tested (15 out of 37) were homozygous for the allele coding for the functional *FMO2* (see paragraph 3.4.2), suggesting that prolonged inbreeding across these populations had reduced the genetic variability. Despite the lack of genetic polymorphism in the colony, we proceeded to compare the metabolic activity of the microsomal suspensions of lungs homozygous for *FMO2\*1* (Welsh rats) to those homozygous for *FMO2\*2* (Wistar rats) toward MI.

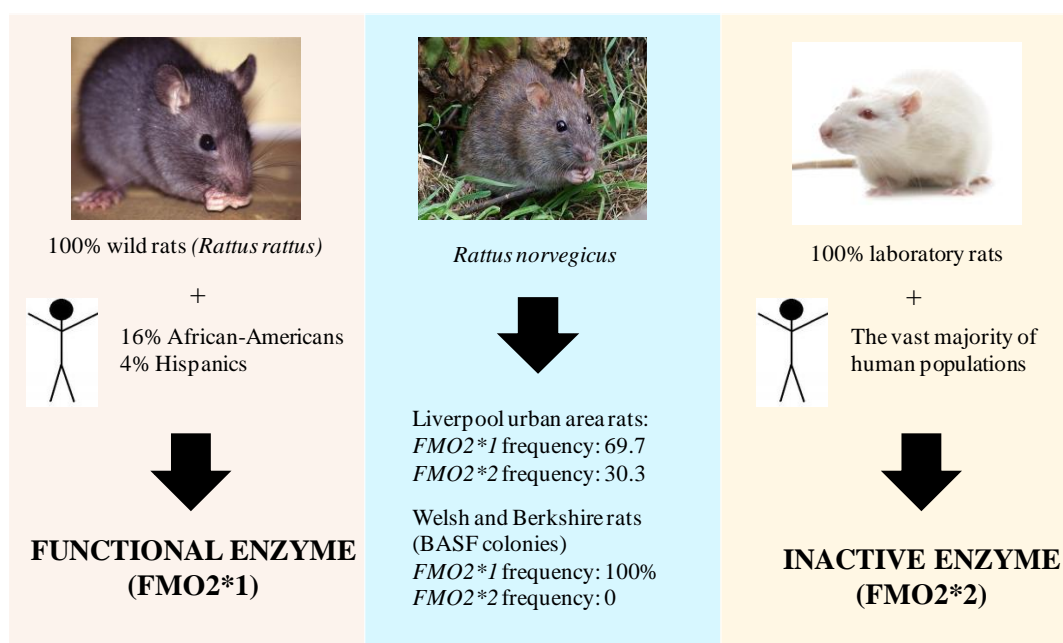


**Figure 4.4.** Summary of *FMO2* genotyping results. Similarly to humans, wild rats trapped in the North West of England exhibit *FMO2* polymorphism, but the frequency of the full length (*FMO2\*1*) allele is much higher compared to humans. Welsh rat colonies housed at BASF, similarly to the black rat (*R. rattus*) were homozygous for *FMO2\*1*.

### 4.3.1 Metabolic consequences of *FMO2* polymorphism

It has already been mentioned that FMO1 and FMO2, the latter only when expressed according to its genetic polymorphism, are the major isoforms detected in the rat lungs using Northern and Western blot analyses (see paragraph 1.5.6.3). The remaining FMO isoforms are either not expressed or found at negligible levels (Hugonnard et al., 2004). Thus, it has been hypothesised that FMO catalytic activity in the lungs may vary considerably in the presence of *FMO2\*1*, which should result in some degree of FMO2-dependent xenobiotic metabolism (Hugonnard et al., 2004). This is supported by numerous studies showing that baculovirus-expressed purified FMO2 catalyses efficiently the oxygenation of a number of xenobiotics, including small thioureas (Henderson et al., 2004b), the thioether insecticides disulfoton and phorate (Henderson et al., 2004a) and the antituberculosis prodrug ethionamide (Henderson et al., 2008).

We compared the catalytic activities of FMOs in different microsomal pools using MI, a highly specific substrate for FMO enzymes (Dixit and Roche, 1984). In our study, the lack of DNTB formation in microsomes that were previously heated at 55°C to inhibit FMO activity confirms that the contribution of P450 to the oxygenation of MI is negligible, if any (see paragraph 3.4.3.1). Published data indicate that the S-oxygenation of MI in hepatic microsomes produced from laboratory rats is represented by a monoenzymatic reaction exhibiting a low  $K_m$  (in the order of 10 to 30  $\mu\text{M}$ ), compatible with either FMO1 or FMO3 kinetic parameters (Lattard et al., 2001; Moroni et al., 1995). Our results show that the  $K_m$  of the enzyme(s) carrying out the oxygenation of MI in Wistar rat liver and lung microsomes fall within the above interval range, suggesting that both FMO1 and FMO3 may be involved in the catabolism of MI in the laboratory rat liver and lung microsomes (see paragraph 3.4.3.1 and **Figure 3.37a,b**). Due to the negligible levels of FMO3 found in the rat lungs (Lattard et al., 2001), it is assumed that the oxygenation of MI is conducted solely by FMO1. This was confirmed by Hugonnard et al. (2004), who showed that the addition of imipramine, a selective inhibitor of FMO1, to the incubations obtained from rat lungs expressing *FMO2\*1* depressed severely the rate of the reaction. In Welsh rat lung microsomes (**Figure 3.37c**), the S-

oxygenation of MI proceeded in two phases. The kinetic parameters of the first component of the reaction were similar to those found in the monoenzymatic reaction carried out by the Wistar rat lungs and were assumed to represent FMO1-mediated oxygenation of MI. The  $K_m$  of the enzyme involved in the second phase was  $6 \times$  higher than that of FMO1 and, based on the lack of other FMO isoforms in the rat lung expressed in significant amounts, certainly corresponds to the functional FMO2. The presence of a functional FMO2 is therefore associated with a substantial increase in the S-oxidative metabolism of MI in the lungs. This was confirmed by monitoring the metabolic rate of a standard concentration of MI in the three different microsomal preparations for several minutes; the change in absorbance during this time was most pronounced in the Welsh rat lung microsomes, slightly smaller in the hepatic microsomes and approximately half the magnitude in the Wistar rat lung microsomes (see paragraph 3.4.3.2). The addition of NR678 to the incubation inhibited the S-oxygenation in all three *in vitro* systems. It needs to be pointed out that our data are based exclusively on the kinetic parameters of the enzymes involved in the S-oxygenation of MI and do not take into account the relative concentrations of FMO1 and FMO2 in the rat lungs, as this information is not available in literature, or FMO substrates different from MI. However, these results suggest that the pulmonary metabolism of MI is enhanced by the presence of a functional FMO2 and it is likely that increased turnover may occur with several other S-containing nucleophilic molecules. Preliminary data describing increased metabolism of the drug ethionamide by human lung microsomes from an individual expressing the functional FMO2 (Henderson et al., 2008) seem to support this statement.

#### **4.3.2 Toxicologic consequences of *FMO2* polymorphism**

The hypothesis that individuals with the *FMO2\*1* allele may carry an increased risk of developing adverse effects to drugs and xenobiotics compared to those lacking a functional FMO2 in the lung has been formulated by several authors (Cashman and Zhang, 2006; Hugonnard et al., 2004; Krueger and Williams, 2005; Philips et al., 2007; Shephard and Phillips, 2010), but never specifically addressed. It has been predicted for instance that the toxicity caused by small thiourea-based molecules may be enhanced in individual possessing a functional pulmonary FMO2 isoform

(Cashman and Zhang, 2006; Krueger et al., 2002b). FMO2 is very active toward bioactivation of thioureas with low molecular weight (see paragraph 1.5.5.2), which are S-oxygenated to highly reactive sulfenic and/or sulfinic acid intermediates capable of GSH oxidation and FMO-dependent redox cycling, resulting in GSH depletion *in vitro* (Henderson et al., 2004b). This is thought to be the mechanism responsible for the pulmonary and hepatic adverse effects observed in patients administered drugs or exposed to environmental molecules which belong to this class of chemical entities (Cashman and Motika, 2010). As another example, investigation into the metabolism of ethionamide, a second-line drug for the treatment of tuberculosis caused by multi-drug resistant mycobacteria, has drawn attention to the importance of understanding the implications of *FMO2* polymorphism on the efficacy and toxicity of xenobiotics (Qian and Ortiz De Montellano, 2006). Ethionamide has numerous side effects, including severe hepatotoxicity and is used in regions of the world where the *FMO2\*1* allele occurs at high frequency [ie, Sub-Saharan Africa, where almost 50% of individuals have at least one *FMO2\*1* allele (Phillips and Shephard, 2008)]. The drug is S-oxygenated to the correspondent S-oxide predominantly by FMOs, and to a lesser extent, by CYP. The rate of this reaction is markedly higher in human lung microsomes obtained from individuals possessing *FMO2\*1* compared to those expressing *FMO2\*2* (Henderson et al., 2008), but the authors have not investigated whether individuals expressing a functional *FMO2* exhibit toxicologically distinct responses to the drug. The presence of the *FMO2\*1* allele has also been predicted to have in certain instances the opposite (protective) effect. This could be the case for thioether-containing organophosphates, such as phorate and disulfoton, which are commonly used pesticides and are excellent substrates of FMOs (Hodgson et al., 1998; Tynes and Hodgson, 1985). S-oxygenation of organophosphates by the flavoenzymes results in detoxification (Kinsler et al., 1988), while the oxon produced by CYP is predominantly responsible for acetylcholinesterase inhibition, the main toxic effect of these compounds (Levi and Hodgson, 1988). In this case, individuals expressing the *FMO2\*1* allele may be more protected from the risk of developing organophosphate toxic effects in the lungs than those expressing the mutant allele.

To our knowledge, the work presented in this thesis represents the first attempt to address this issue. We compared the clinical and post mortem findings obtained in two different populations of rats (Wistar and Welsh rats), administered the same dose (0.5 mg/kg) of NR678 and euthanased at the same time points. The difference in the susceptibility of the two populations to NR678 was pronounced. Rats possessing a mutant pulmonary FMO2 isoform had no clinical signs or gross and histopathological findings consistent with increased vascular permeability, such as pulmonary oedema and hydrothorax, which characterise the acute toxicity of NR678 (see paragraph 3.2.2.1.3). Rats expressing the ancestral gene instead developed transient mild or moderate dyspnoea, which correlated with hydrothorax and pulmonary alveolar and interstitial oedema (see paragraphs 3.4.4.1-3.4.4.3), similar to that observed in Wistar rats that had received a dose of NR678 10 × higher (see paragraphs 3.1.1-3.1.3). These results suggest that the toxicity of the small thiourea-derived molecule NR678 in rats expressing the *FMO2\*1* allele is markedly increased compared to those which lack an active FMO2 enzyme.

#### **4.4 Potential issues and limitations**

Here we list questions, problems and limitations that we have identified in our approach and suggest ways in which the results obtained could be improved and further characterised.

The data collected in the studies conducted in this thesis appeared reasonably uniform between animals within the same group or time point, although a certain level of variability was inevitably observed. This, coupled with the small number of animals/group and/or time point in most of the experiments (most often  $n = 3$ ), complicated at times the interpretation of the results and statistical analyses.

The evaluation of the results obtained using IH was particularly challenging. In recent years, there has been an increasing amount of literature studying the processes involved in the differentiation of pulmonary alveolar epithelial cells, with particular emphasis to the markers which allow their identification (Brody and Williams, 1992; Fehrenbach, 2001). While the list of the potential markers has been growing exponentially, the gold standard for pneumocyte identification appears still to be the

ultrastructural examination (Kasper and Singh, 1995). Some of the immunohistological markers in fact are exclusive to type II pneumocytes, such as SP-C (Kasper et Singh, 1995), while others are shared with different cells in the lung and/or in the body [e.g. lysozyme; (Singh et al., 1988)]. Also, the expression of markers may be influenced by the developmental stage: early in lung embryonic development, epithelial cells express several antigens which are then progressively restricted to specific cell types during the differentiation process (Joyce-Brady and Brody, 1990). For example, SP-C mRNA is present in all epithelial cells in the early development of the rat lung to become uniquely expressed by type II pneumocytes at the end of gestation (Brody and Williams, 1992). Marker expression finally can be influenced by pathogenic processes (Kasper and Singh, 1995). For these reasons, the data obtained from the immunohistological evaluation of NR678 tolerant rat lungs need to be interpreted with caution. The antigen SP-C for example was expressed by approximately 7% of the total alveolar cells in the control rats from the current study (see paragraph 3.2.2.1.3). Data from several sources (Haschek et al., 2009e; Williams, 1990) indicate that type II alveolar epithelial cells represent approximately 14% and 16% of the alveolar cells in the rat and human lung, respectively. The antigen SP-C in the current study therefore appears to be present only in half of the cells that should express it. It needs to be said that, despite the relatively high concentration (1:50) of antibody used in the study, type II pneumocytes expressing SP-C exhibited a generally weak staining intensity, which may have influenced the level of signal detection for the cell counts. The reason for this discrepancy is not known, but might depend on the lower affinity for the rat SP-C protein of the antibody (Santa Cruz), which is raised against the full length human isoform.

Regarding the time-course of the proliferative response occurring in the lungs of tolerant rats, the addition of an intermediate time point between the 24 h and 7 d intervals would probably have been beneficial to fully appreciate the proliferative event, which appears to be only just emergent at the former end point, but already phasing out at the latter. This was particularly evident using immunohistology for PCNA, a multifunctional protein which is essential for progression into the cell cycle (Whitfield et al., 2006). Negligible numbers of proliferating cells were consistently detected at all time points, except in rats from groups 3 and 4 euthanased on day 7,



where a substantial increase in cells expressing PCNA was noted (see paragraphs 3.2.2.1.3 and 3.2.2.2.3). According to the dynamics of type II pneumocyte hyperplasia following oxidative injury that we discussed in paragraph 4.2.2, analysis of a day 2 or 3 time point would have probably registered the highest peak in pneumocyte proliferation and PCNA-positive cells.

We attempted for the first time to characterise the expression of FMO2 in the rat by RNA-ISH. We were particularly interested in the distribution of this isoform within the lungs, to investigate a possible relationship between its expression and the development of NR678 toxicity and tolerance. We also characterised the cellular localisation of FMO2 mRNA in other organs, such as the brain, kidneys and liver. Tissue-specific expression profiles of FMO2 in the rat paralleled those obtained in mice (Janmohamed et al., 2004), but also showed meaningful differences. In the mouse brain, FMO2 is expressed at very low levels and its localisation within this tissue has not been specifically addressed in Janmohamed (2004) work. Although not quantitatively assessed, we detected a moderate to strong hybridisation signal in different areas of the rat brain (cortical and hippocampal neurons and choroid plexus epithelium; see paragraph 3.3.1); this pattern of distribution is similar to that described for other FMO isoforms (FMO1 and 5) in the mouse brain (Janmohamed et al., 2004) and may suggest that cerebral FMO2 mRNA is particularly abundant in the rat. In the rat kidneys, the distribution of FMO2 in proximal and distal tubules and collecting ducts coincided with the results obtained in mice. In the rat liver, FMO2 localised exclusively to the bile duct epithelium (see paragraph 3.3.1). This appears to be an interesting unique feature of the rat, in contrast to the mouse liver where FMO2 is mainly expressed in the periportal hepatocytes (Janmohamed et al., 2004). Similarly to the mouse lung, rat pulmonary FMO2 was mainly expressed in the epithelial lining of terminal bronchioles (mostly in Clara cells) and within the alveolar unit (type II pneumocytes, endothelial cells and alveolar macrophages; see paragraph 3.3.1). The FMO2 ISH signal in the rat lung was widespread and strong, according to the fact that FMO2 is a major pulmonary isoform in this species. This differs from that found in the mouse lung, where FMO2 is expressed at low levels (see **Appendix I**). Of particular interest was the localisation of FMO2 to the endothelium of the pulmonary vessels and capillaries, whilst endothelial cells in

other organs did not show a positive signal. It is difficult to interpret this finding without quantitative data or similar information concerning the localisation of FMO1 in the rat lung; however, the pulmonary endothelium may be endowed with higher levels of FMOs, which can be responsible for its susceptibility to thiourea-induced injury. As a result, this is an area that would need further investigation either in *in vivo* and *in vitro* studies comparing the activity of endothelial cells derived from different tissues toward thiourea-based compounds and their susceptibility to oxidative injury. We originally planned to develop RNA-ISH probes for all five FMO isoforms in order to have a more comprehensive understanding of their distribution in the rat and determine whether this species shares analogies with man and can be used efficiently in reaction phenotyping assessment during drug development. Unfortunately, technical difficulties arose during the design and the preparation of the riboprobes, which, together with time limitations, forced us to concentrate only on the set up of the FMO2 riboprobe. Information on the expression of the other isoforms, especially FMO1 in the lung, would have helped in formulating hypotheses concerning the relationship between FMOs and the development of oxidative injury and/or tolerance to NR678. In addition, we have qualitatively and quantitatively assessed the levels of FMO1 and/or FMO2 mRNA, but we did not explore the expression and distribution of the correspondent proteins. Unfortunately, this was not possible due to the lack of commercial antibodies targeting the rat FMO isoforms. Therefore, differences in the pulmonary expression of FMO1 and FMO2 proteins during thiourea-induced toxicity and tolerance remain to be investigated.

Our genotyping work allowed us to identify a colony of rats (Welsh rats) which expressed a functional FMO2 and to compare the metabolic and toxicological responses of these rats to Wistar rats carrying an inactive *FMO2* gene. We found that the toxicity of NR678 in rats expressing *FMO2\*1* was increased compared to those which lack an active FMO2 enzyme. We believe that the relevance of this animal model to humans is likely to be meaningful, however, we acknowledge that these findings represent only preliminary evidence of this potential increased susceptibility to drug-induced oxidative injury and that this approach requires further experimental investigation. First of all, speculation concerning the translation of these findings to

man should take into consideration the abundance of FMO2 in the rat and human lungs. Unfortunately, quantitative data relative to the concentration of FMOs in the rat lung are not available; however, both humans and rats have similar FMO distribution in the lung, FMO2 being the most abundant FMO isoform, followed by FMO1 (see paragraph 1.5.6.3 and **Appendix 1**) and they both share a naturally occurring *FMO2* polymorphism. It has been proven that human microsomes obtained from the lungs of individuals expressing a functional FMO2 are able to catalyse the oxygenation of FMO-specific substrates more efficiently than those containing an inactive isoform (Henderson et al., 2008). These observations imply that a direct comparison between the two species may still be valid. Another drawback of this approach is that differences in the genetic background other than the mutations of *FMO2*, the health status and the environmental conditions between the two rat populations tested may have influenced the outcome of the study. For example, the presence of pulmonary inflammatory lesions in rats from study 4 (see paragraph 3.4.4.3), which were likely spontaneous in nature and reminiscent of *M. pulmonis* infection, was a major concern for the interpretation of the outcome of the study, as it may have contributed to the increased susceptibility of the Welsh rats to NR678-induced acute lung injury by impairing the physiological pulmonary defences. However, the spontaneous inflammatory lesions were generally limited in distribution and were not recorded in all animals. Also, there were cases in which NR678-induced alveolar and interstitial oedema was observed, in the absence of spontaneous granulomatous inflammation and BALT hyperplasia, which may suggest that the contribution of these incidental findings to the general picture was possibly minor.

During our genotyping analysis, we found that all rats genotyped in the Welsh colony were homozygous for *FMO2\*1*. The presence of *FMO2* polymorphism in these animals would have been ideal for the set up of a toxicity study aimed to compare the toxicological responses to thiourea of rats belonging to the same colony and strain, but with different *FMO2* genotypes. Reintroduction of the mutant *FMO2* allele in the Welsh colony could have been obtained by crossing these rats with Wistar rats, which express *FMO2\*2*; however, this could not have been done without prior monitoring of the colony health status and rederivation. Our experience stresses

once again the imperative need for laboratory animals used in experimental studies to be constantly screened for infectious agents and free of diseases that can cause difficulties in the interpretation of the results.

## 4.5 Concluding remarks

The work presented in this thesis has investigated the morphological and functional aspects of the pulmonary toxicity and tolerance associated with the administration of NR678, a small thiourea-based rodenticide candidate, to rats and has aimed to improve the understanding of *FMO2* polymorphism in rats and humans (**Figure 4.5**). It was found that NR678 was lethal to rats at relatively small doses and caused life-threatening respiratory impairment within a few hours of administration, characterised by extensive hydrothorax and pulmonary oedema. The acute toxicity of NR678 represented an opportunity to elucidate the morphology and cellular targets of oxidative stress, which it is a main injury pathway observed in several models of pulmonary adverse drug reactions and in pulmonary conditions, such as idiopathic fibrosis and ARDS (Comhair and Erzurum, 2002). We have shown that NR678 is metabolised by FMOs, presumably to a highly reactive intermediate, which was not detected by HPLC. We assumed that this reactive compound, similarly to other small thiourea intermediates (Mansuy and Dansette, 2011; Smith and Crespi, 2002), causes a rapid decrease of reducing equivalent levels through a “futile” redox cycling mechanism, as suggested by the decreased levels of hepatic and pulmonary GSH found in our studies and then attacks constitutional components of the cells. Pulmonary endothelial cells are the main target of NR678 oxidative injury and exhibit a reversible impairment of their function, distinguished by a perturbation of vascular permeability through paracellular gap formation. We have concluded that the susceptibility of endothelial cells to NR678-induced injury may represent a specific pathway of this cell type to react to a sudden change in the redox environment and/or may depend on the amount of reactive metabolite produced by FMOs in the endothelial cell cytoplasm or in the adjacent cells. The different susceptibility of pulmonary cells to oxidative injury appears an interesting field of research, which may bring new insight into the understanding of acute lung injury and its prevention. *In vitro* models based on pneumocyte and endothelial cell cultures

may represent a useful tool to study how these cells respond to oxidative stress and how the degree of injury can be modulated by altering the levels of antioxidant resources.

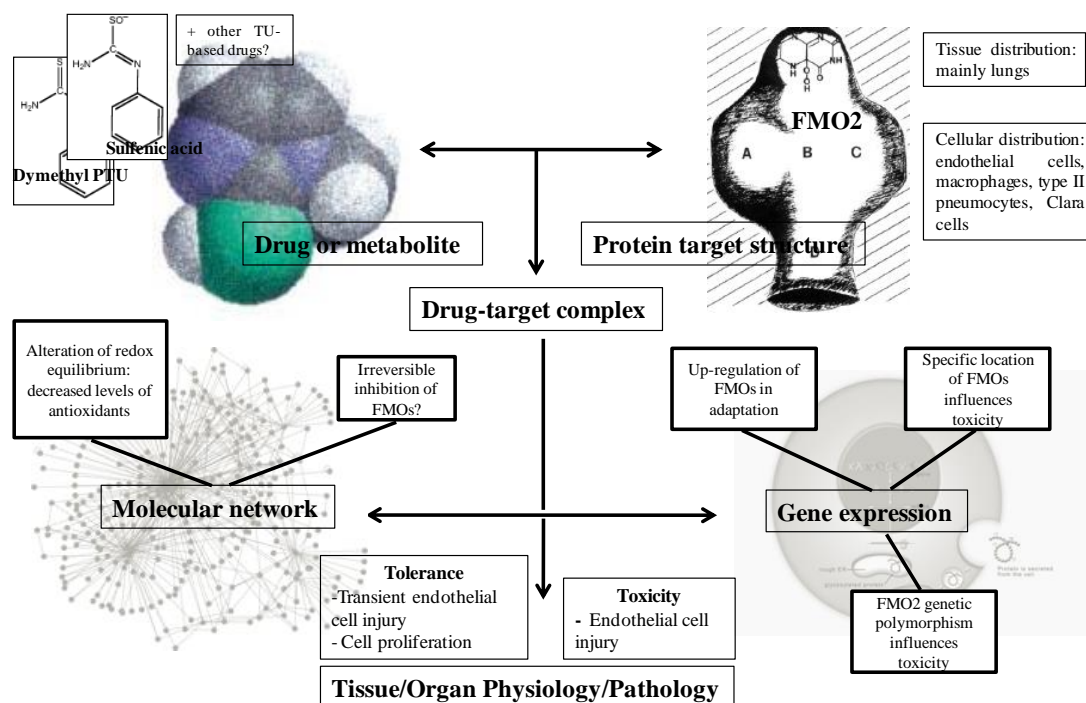


**Figure 4.5.** A system biology approach to the investigation of NR678-induced toxicity and adaptation.

The model of acute lung injury caused by NR678 shares numerous features in common with ARDS, a severe human pulmonary condition characterised by diffuse acute oxidative damage of the alveolar unit, which is not completely understood to date and difficult to treat (Matute-Bello et al., 2008). After we established that rats administered a low dose of NR678 had no clinical respiratory distress and were protected from a normally lethal dose after only 3 h, we were intrigued by the effectiveness and the quick onset of this adaptive response and we proceeded to fully characterise for the first time the morphology of this change, to improve our understanding of the pulmonary defences which are involved in the prevention of lung oxidative injury. In contrast to the animals that had received the high dose only, tolerant rats exhibited mild, infrequent ultrastructural changes in the endothelial cells lining the pulmonary capillaries, which explained the lack of severe gross and microscopic findings consistent with increased vascular permeability. The lungs

reacted to the toxic insult exhibiting at first increased numbers of alveolar macrophages and immature type II pneumocytes, followed by a rise in the number of mature type II pneumocytes one week after dosing. The microscopic changes resolved by the end of the second week, when rats were found to be again susceptible to a lethal dose of NR678. The mechanism involved in the protection of the lungs from oxidative injury remained unclear; however, based on our results, we excluded that tolerance was primarily due to increased clearance of the oedema fluid by macrophages and type II pneumocytes, altered levels of FMO mRNA or GSH. The hypothesis that irreversible inhibition of FMOs may be implicated in the adaptive response of the lungs to NR678 needs further investigation. All available animal models aim to reproduce the mechanisms and consequences of ALI in humans by inducing a significant damage to the alveolar epithelium, which is followed by a reparative process (Matute-Bello et al., 2008). NR678 may represent an interesting and unique model of ALI, where the primary injury affects the endothelial cells rather than the epithelial compartment. Future trials should assess the significance of the responses of the lungs to this type of injury and determine whether they still represent a reparative process or are instead an adaptive reaction, aimed to confer protection to further injury. With this in mind, the investigation of these defence mechanisms may bring new perception into the therapeutic approach of acute lung injury.

To our knowledge, this was the first study to have addressed the possible toxicological consequences associated with a *FMO2\*1* homozygous genotype in rats. We showed that pulmonary microsomes possessing an active FMO2 isoform catalyse the S-oxygenation of MI at a higher rate compared to those homozygous for the inactive form. This correlated in an *in vivo* model with the increased susceptibility of *FMO2\*1* homozygous rats toward NR678 toxicity. We hypothesised that this animal model could be relevant to humans, where similar FMO distribution and *FMO2* polymorphism are observed (Shephard and Phillips, 2010).

An example of future research on the implications of FMO polymorphisms is represented by pyrrolizidine alkaloids, compounds synthesized by several plants belonging to a few Angiosperm families which act as toxins in several domestic

animal species, including ruminants and horses (Cheeke, 1988). The toxic principles in these plants consist of pyrrolic esters, which are derived from bioactivation of the parent compounds by hepatic P450 isoforms CYP3A and CYP2B, whilst FMO catalyses the N-oxygenation, leading to a more soluble, nontoxic N-oxide. Interestingly, susceptibility to PA toxicity varies greatly among vertebrates and differences in the toxic outcome has been ascribed to different expression levels of enzymes involved in the activation and detoxification of the parent compound (Huan et al., 1998a; Huan et al., 1998b). For example, the well-known resistance of guinea pig to PA toxicity has been related to the higher levels of FMO-mediated oxidation. Studying the distribution of hepatic FMOs in the horse for example, whose entire genome has been only recently published (Wade et al., 2009), and investigating the presence of FMO polymorphism in this species may provide significant advances in the prevention of this type of injury.

To conclude, a polymorphism for a specific enzyme, drug transporter or receptor may result in enhanced activity of the protein, decreased activity or no function or may not lead to any change. Research on this field applied to drug metabolism has been the main objective of pharmacogenomic, a branch of pharmacology which aims to investigate the influence of genetic variation on drug response (Ma et al., 2012). The extraordinarily diverse CYP gene family has been the object of countless publications in the last decade due to the prominent role of cytochrome P450 in phase I metabolism. In several cases, the genetic variability documented for numerous xenobiotic metabolising enzymes has been related to increased toxicity and side effects, altered pharmacokinetics and different disease susceptibility (Ginsberg et al., 2010). In recent years there has been a growing amount of literature aiming to characterise the consequences of genetic polymorphism in the FMO enzyme family, especially FMO3 (Cashman and Zhang, 2006). The present study contributes additional evidence that suggests that *FMO2* polymorphism may be relevant to humans and provides an animal model which can be used to study its implications.

## Appendix I – FMO expression in humans and mice

**Table I.1.** Tissue-specific expression of FMOs in humans.

Isoform	Expression	Reference
<b>FMO1</b>	<p>FMO1 is found at extremely low levels in the adult liver. Its expression is detected in the liver of the foetus, but then suppressed 72 hours after birth</p> <p>In the adult, FMO1 is primarily expressed in the kidneys, at a higher concentration than CYP.</p> <p>FMO1 is present, to a minor extent, in the gastrointestinal system and endocrine tissues</p> <p>Similarly to the liver, <i>FMO1</i> gene expression in the human lung and brain is switched off after birth (levels are less than 3% and 1%, respectively, of that in the kidneys)</p>	<p>(Dolphin et al., 1991; Dolphin et al., 1996; Krueger and Williams, 2005; Mccarver and Hines, 2002)</p> <p>(Jakobsson and Cintig, 1973)</p> <p>(Cashman et al., 2008; Dolphin et al., 1991; Dolphin et al., 1996; Phillips et al., 1995)</p> <p>(Cashman and Zhang, 2006; Dolphin et al., 1996)</p>
<b>FMO2</b>	<p>FMO2 is the major form present within the human lung and in most species.</p> <p>FMO2 mRNA is also expressed in the kidneys (<math>7 \times</math> less than the lung), liver, small intestine and brain (<math>50</math> to <math>100 \times</math> less).</p>	<p>(Krueger et al., 2002a)</p> <p>(Zhang and Cashman, 2006)</p>
<b>FMO3</b>	<p>The amount of FMO3 isolated from the adult liver (both sexes) is approximately 65% of that typically obtained for CYP3A4 and approximately equivalent to that of CYP2C9, which in turn represents 20% of total CYP levels in the liver.</p> <p>Levels of FMO3 mRNA in lung, kidney and small intestine are less than 5% of those found in the adult liver. The brain contains less than 1% of the total FMO3 detected in the adult liver.</p>	<p>(Koukouritaki et al., 2002; Shimada et al., 1994)</p> <p>(Zhang and Cashman, 2006)</p>

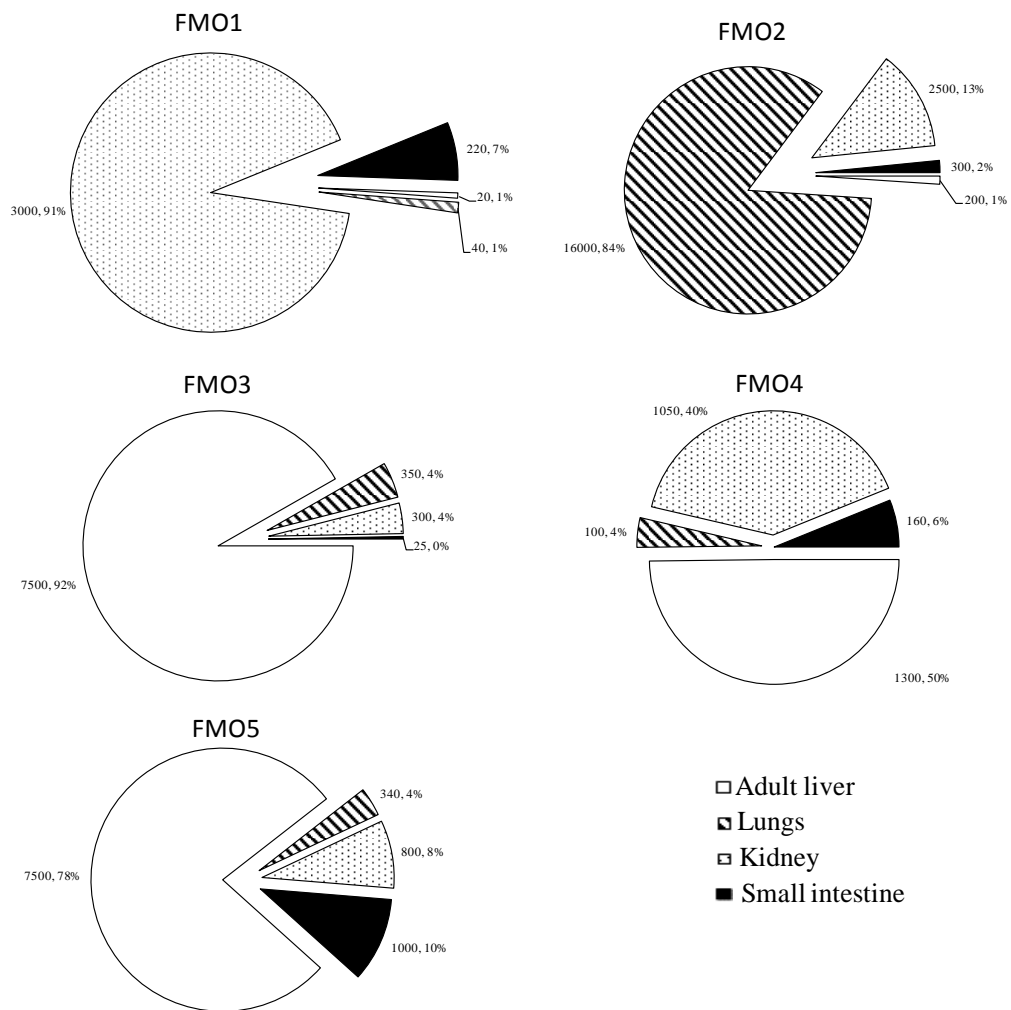


(Cont.)

Isoform	Expression	Reference
<b>FMO4</b>	FMO4 mRNA is present in the liver and the kidney at the same low level	(Dolphin et al., 1996)
	FMO4 contents in the lung, small intestine and foetal liver are approximately 10% of those in the adult liver and the brain contains a much lower amount (1% of adult liver)	(Zhang and Cashman, 2006).
<b>FMO5</b>	FMO5 is present in several foetal and adult tissues in a gender-independent pattern.	(Cashman and Zhang, 2006)
	FMO5 mRNA is the most abundant FMO transcript isolated from the adult human and mouse liver, followed by FMO3.	(Furnes et al., 2003; Janmohamed et al., 2004)
	FMO5 mRNA is present also in the following tissues: foetal liver (approximately 20% of adult liver amounts), small intestine and kidney (approximately 10%), lung (4%) and brain (less than 1%).	(Zhang and Cashman, 2006)
	It has been argued that FMO5 mRNA levels may not correlate well with actual FMO5 protein levels	(Krueger and Williams, 2005)

**Figure I.1** Tissue-dependent FMO mRNA distribution in humans. Abundance and proportion of FMO mRNA are displayed according to the FMO isoform (a) or the tissue considered (b). The values displayed in the data labels refer to the number of copies of the correspondent FMO transcript/ $\mu\text{g}$  mRNA in the different tissues, followed by the percentage distribution of the isoform in the specific tissue. Data are obtained from Zhang and Cashman, 2006.

a)



(b) Cont.

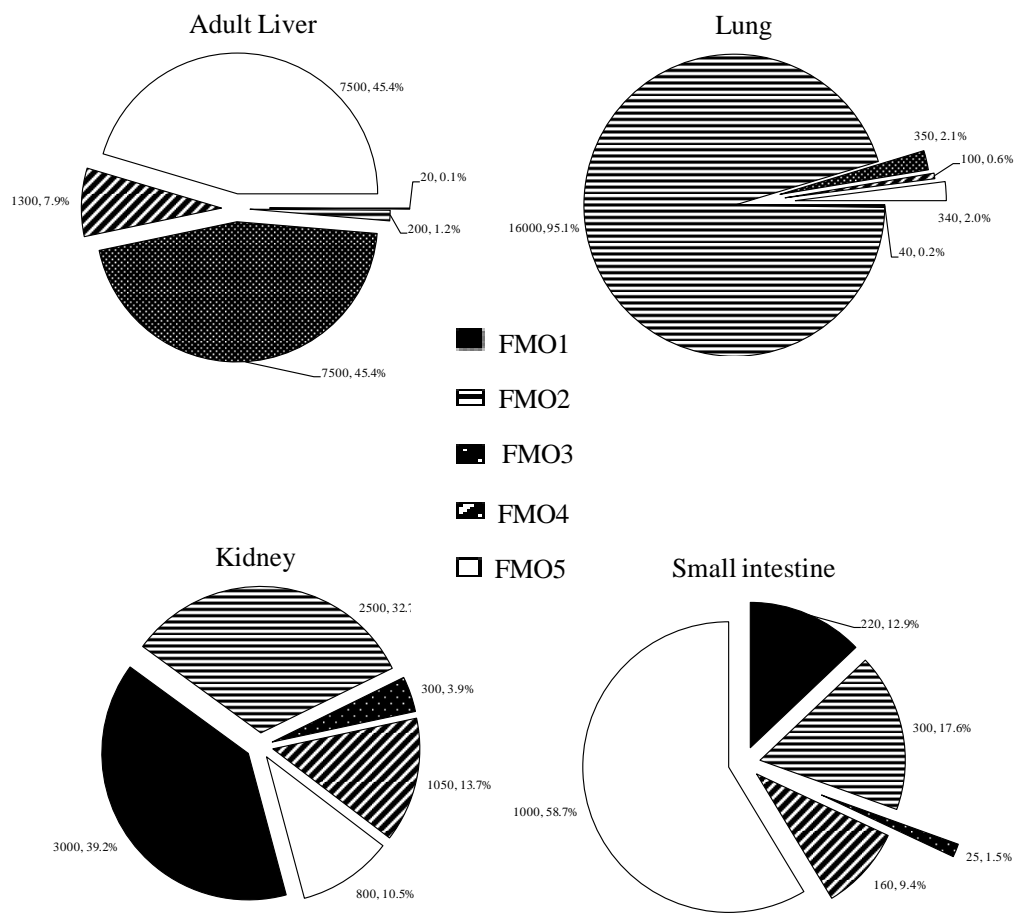
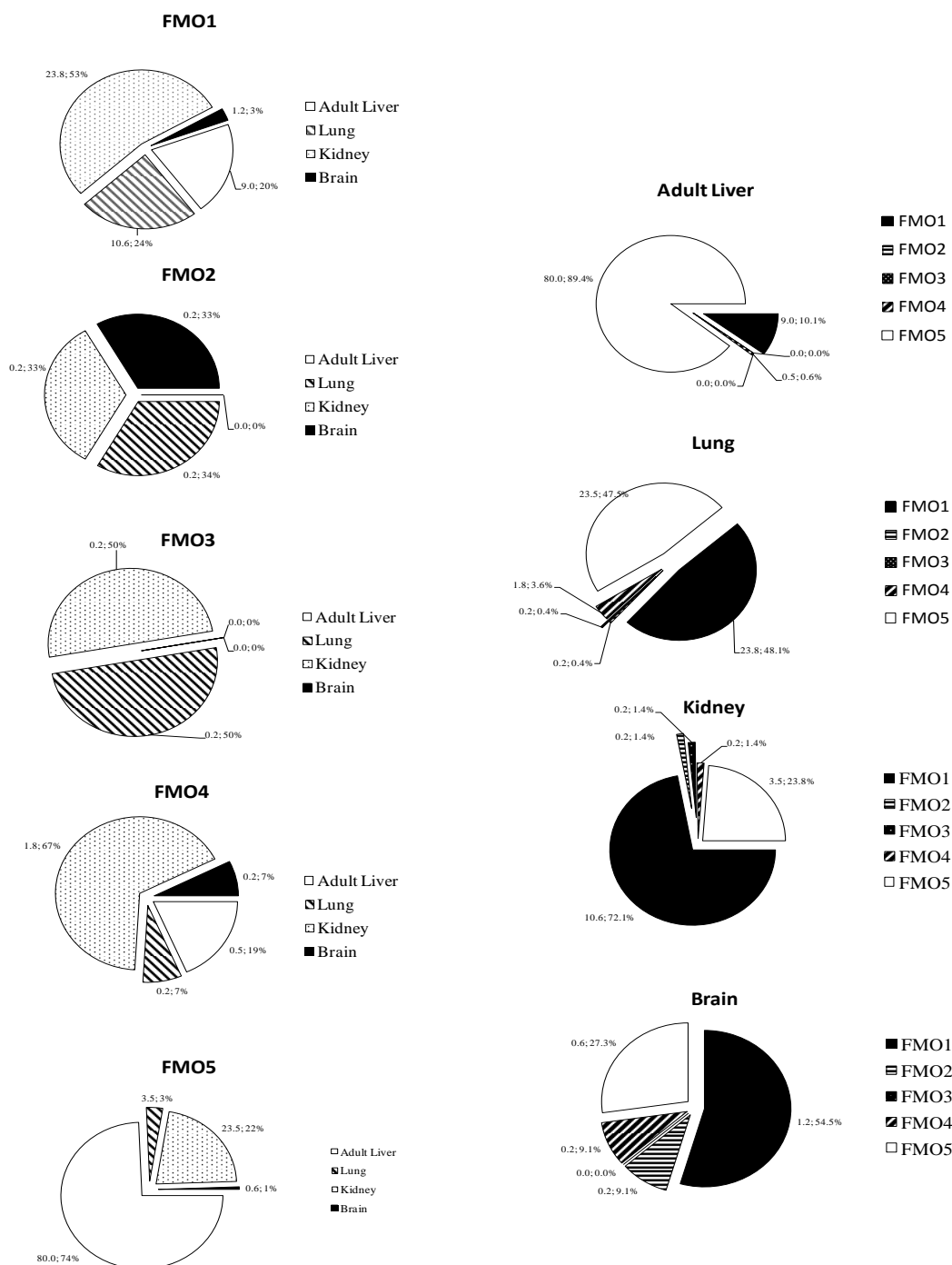
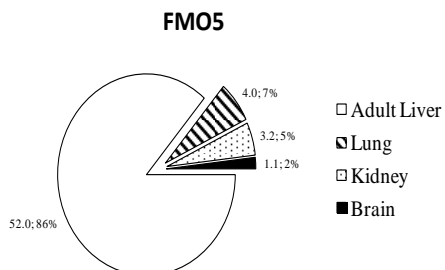
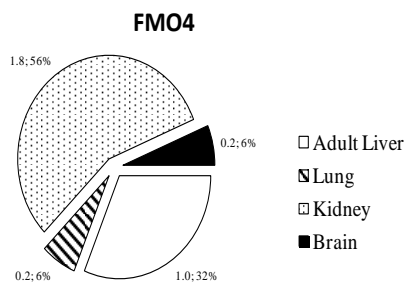
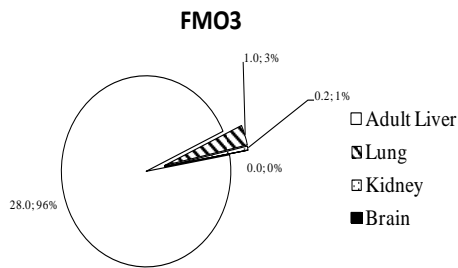
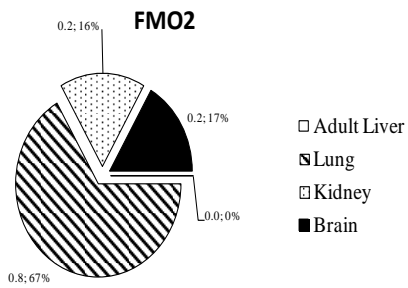
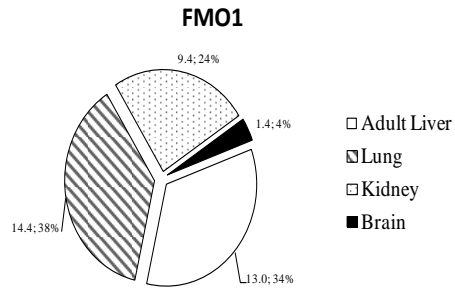


**Figure I.2.** Tissue-dependent *FMO* mRNA distribution in male (a) and female (b) mice. Abundance and proportion of *FMO* mRNA are displayed according to the *FMO* isoform (left) or the tissue considered (right). The values displayed in the data labels refer to the molecules of the correspondent *FMO* transcript/  $\mu\text{g}$  of total mRNA in the cell. Data are obtained from Janmohamed et al. (2004).

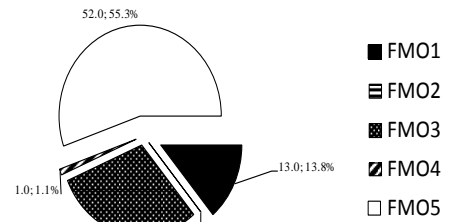
a) Male mice



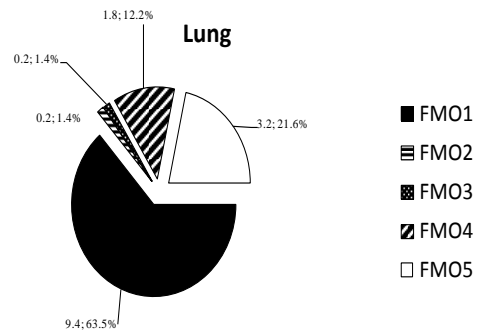
b) Female mice (cont.)



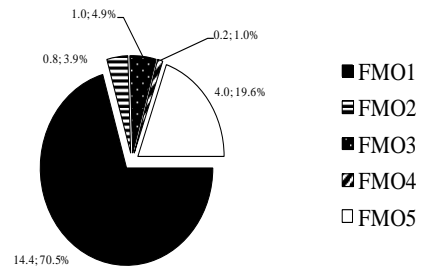
**Adult Liver**



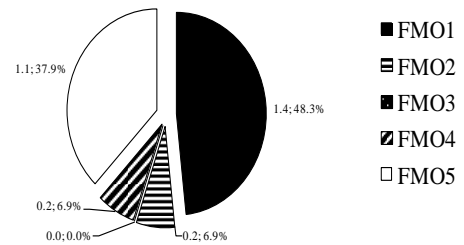
**Lung**



**Kidney**



**Brain**



## Appendix II – Summary of *in vivo* analyses

**Table II.1.** Summary of analyses conducted in each *in vivo* study.

Study	G	NR678 (mg/kg)	End point	HE	Special stains		IH	IH cell counts <sup>a</sup>	TEM	ISH	GSH	qPCR	nPCR	
					MSB, PTAH, LF	MT								
1	1	Control	6 h	F	all	all	AQP-5, FVIII, Cas3 (all)	-	-	-	-	-	-	
	2	10	6 h	F	all	-	AQP-5, FVIII, Cas3 (all)	-	-	-	-	-	-	
3	1	Control	24 h	P	-	all	AQP-5, FVIII, Cas3, SP-C, Lys, PCNA (all)	all	11L-2402	all <sup>b</sup>	all	all	all	
	2	5	6 h	P	-	-	AQP-5, FVIII, Cas3, SP-C, Lys, PCNA (all)	all	11L-2405	all <sup>c</sup>	all	all	-	
	3	3	0.5	3 h	P	-	-	SP-C, Lys, PCNA (all)	all	11L-2420	all <sup>c</sup>	all	all	-
			0.5	6 h	P	-	-	SP-C, Lys, PCNA (all)	all	11L-2424	all <sup>c</sup>	all	all	-
			0.5	24 h	P	-	-	SP-C, Lys, PCNA (all)	all	11L-2427	all <sup>c</sup>	all	all	-
			0.5	7 d	P	-	11L-2430	SP-C, Lys, PCNA (all)	all	11L-2430	all <sup>c</sup>	all	all	-
			0.5	14 d	P	-	11L-2432	SP-C, Lys, PCNA (all)	all	-	all <sup>c</sup>	all	all	-
			0.5 + 5	14 d + 6 h	P	-	-	-	-	-	-	all	-	-
	4	4	0.5 + 5	24 h	P	-	-	SP-C, Lys, PCNA (all)	all	11L-2408	all <sup>c</sup>	all	all	-
			0.5 + 5	7 d	P	-	11L-2411/12	SP-C, Lys, PCNA (all)	all	11L-2411	all <sup>c</sup>	all	all	-
			0.5 + 5	14 d	P	-	11L-2417/18	SP-C, Lys, PCNA (all)	all	-	-	all	all	-
			0.5 + 5 + 5	14 d + 6 h	P	-	-	-	-	-	-	all	-	-
	4	1	Control	24 h	P	-	-	-	-	-	-	-	-	all
		2	0.5, 3h	3 h	P	-	-	-	-	-	-	-	-	all
3		0.5, 6h	6 h	P	-	-	-	-	-	-	-	-	all	
4		0.5, 24h	24 h	P	-	-	-	-	-	-	-	-	all	

G: group. HE: haematoxylin and eosin stain. F: full histopathological examination. P: partial histopathological examination. MSB: Martius Scarlett blue stain. PTAH: Phosphotungstic acid-haematoxylin stain. FL: Fraser Lendrum stain. MT: Masson Trichrome. IH: immunohistology. AQP-5: aquaporin 5. FVIII: factor VIII-related antigen (von Willebrand factor); Cas3: cleaved caspase 3; SP-C: surfactant protein C; Lys: lysozyme; PCNA: proliferating cell nuclear antigen. ISH: *in situ* hybridisation using FMO2 RNA antisense probe. GSH: measurement of glutathione in liver and lung homogenates. qPCR: quantitative polymerase chain reaction for FMO1 and FMO2. nPCR: nested PCR technique for *FMO2* genotyping.

a: cell counts were applied to immunohistological stains for SP-C, Lys and PCNA

b: ISH was evaluated on brain, kidney, liver and lung sections

c: ISH was evaluated on lung sections only.

## Appendix III – Additional reagents and solutions

### Solutions and reagents used for ISH

#### Prehybridisation buffer (PHB-buffer):

6 × SSC, 45% [v/v] deionised formamide, 5 × Denhardt's solution in DEPC-treated water.

Recipe:

20 × SSC (VWR International, Lutterworth, UK): 150 mL

100% formamide, deionised (VWR International): 225 mL

50 × Denhardts solution (VWR International): 50 mL

DEPC (Sigma, Poole, UK) treated water: 70 mL

Stored at –20°C.

Before use, 0.25 mg/mL baker yeast tRNA (Roche, Burgess Hill, UK) and 0.1 mg/mL single strand salmon sperm DNA (Sigma) dissolved in Buffer 4 was added to 50 mL of PHB buffer.

#### Hybridisation buffer (HB-buffer):

60% [v/v] deionised formamide, 6 × Denhardt's solution, 30 mM EDTA [pH 8.0], 30 nM piperazin-N,N'bis(2-ethanesulfate-acid) (PIPES, pH 7.0), 0.9 M NaCl, 0.01% [v/v] Triton X-100, 8000 U heparin.

Recipe :

100% formamide, deionised : 16 mL

20 × hybridisation salts: 8 mL [solution made with EDTA (Sigma) 0.1 M, PIPES (Sigma) pH 7.0, 0.1 M and NaCl (Sigma) 5 M]

50 × Denhardts solution: 3.2 mL

Heparin (20,000 U; VWR International) diluted in 1 mL of distilled water: 400 µL

10% Triton X-100: 320 µL

Aliquoted (696 µL) and stored at –20°C.

Before use, 0.2 mg/mL baker yeast tRNA, 0.25 mg/mL single strand salmon sperm DNA and 62.5 mg/mL dextran sulfate (Fisher, Loughborough, UK) solution (250 mg dextran sulfate dissolved in 400  $\mu$ L distilled water).

**Buffer 1:**

100 mM Tris, 100 mM NaCl, pH 7.5

Recipe:

Tris (Sigma): 12.11 g

NaCl: 8.77 g

Diluted in 1000 mL distilled water

**Buffer 3:**

100 mM Tris, 100 mM NaCl, 50 mM  $\text{MgCl}_2 \cdot 6\text{H}_2\text{O}$ , pH 9.5

Recipe (prepared fresh):

Tris: 2.422 g

NaCl: 1.168 g

$\text{MgCl}_2 + 6\text{H}_2\text{O}$  (add just before use): 2.034 g

Diluted in 200 mL distilled water

**Buffer 4:**

10 mM Tris, 1 mM EDTA, pH 8

Recipe:

Tris: 1.21 g

EDTA: 0.37 g

Diluted in 1000 mL distilled water.

**Solutions and reagents used for qPCR**

SYBRGreen JumpStart Taq ReadyMix (Sigma, Poole, UK)

20 mM Tris-HCl, pH 8.3, 100 mM KCl, 7 mM  $\text{MgCl}_2$ , 0.4 mM each of dNTP [dATP, dCTP, dGTP, TTP], stabilizers, 0.05 unit/mL Taq DNA Polymerase, JumpStart Taq antibody, and SYBR Green I



## **Solutions and reagents used for molecular cloning**

Glucose solution (miniprep)

50 mM glucose, 25 mM Tris-HCl [pH 8.0], 10 mM EDTA and 1 mg/mL lysozyme (Sigma)

Denaturation solution (miniprep) and Buffer P2 (maxiprep)

200 mM NaOH and 1% (w/v) sodium dodecyl sulphate

Neutralisation solution (miniprep)

3 M potassium acetate and 11% (v/v) glacial acetic acid (pH 5.5)

Buffer P1 (maxiprep)

50 mM Tris-Cl, pH 8.0, 10 mM EDTA, 100 ug/mL RNase A

Buffer P3 (maxiprep)

3 M potassium acetate, pH 5.5

Buffer QBT (maxiprep)

750 mM NaCl, 50 mM 3-(N-morpholino) propanesulfonic acid (MOPS), pH 7.0, 15% isopropanol, 0.15% Triton X-100

Buffer QC (maxiprep)

1 M NaCl, 50 mM MOPS, pH 7.0, 15% isopropanol

Buffer QF (maxiprep)

1.25 M NaCl, 50 mM Tris-Cl, pH 8.5, 15% isopropanol

TE Buffer (maxiprep)

10 mM Tris-Cl, pH 8.0, 1 mM EDTA

## References

- Adamson, I.Y. and Bowden, D.H. (1974) The type 2 cell as progenitor of alveolar epithelial regeneration. A cytodynamic study in mice after exposure to oxygen. *Lab Invest.* **30**, 35-42.
- Alberts, B., Johnson A, Lewis J, Raff M, Roberts K and P., W. (2008) Molecular biology of the cell. 5th ed. Garland Science, New York, pp. 477-499.
- Altschul, S.F., Gish, W., Miller, W., Myers, E.W. and Lipman, D.J. (1990) Basic local alignment search tool. *J Mol Biol.* **215**, 403-410.
- Anderson, M.E. (1985) Determination of glutathione and glutathione disulfide in biological samples. *Methods Enzymol.* **113**, 548-555.
- Barazzone, C., Donati, Y.R., Rochat, A.F., Vesin, C., Kan, C.D., Pache, J.C. and Piguet, P.F. (1999) Keratinocyte growth factor protects alveolar epithelium and endothelium from oxygen-induced injury in mice. *Am J Pathol.* **154**, 1479-1487.
- Barber, M., Conrad, M.E., Umbreit, J.N., Barton, J.C. and Moore, E.G. (2000) Abnormalities of flavin monooxygenase as an etiology for sideroblastic anemia. *Am J Hematol.* **65**, 149-153.
- Bardales, R.H., Xie, S.S., Schaefer, R.F. and Hsu, S.M. (1996) Apoptosis is a major pathway responsible for the resolution of type II pneumocytes in acute lung injury. *Am J Pathol.* **149**, 845-852.
- Barton, C.C., Bucci, T.J., Lomax, L.G., Warbritton, A.G. and Mehendale, H.M. (2000) Stimulated pulmonary cell hyperplasia underlies resistance to alpha-naphthylthiourea. *Toxicology.* **143**, 167-181.
- Beers, M.F. and Lomax, C. (1995) Synthesis and processing of hydrophobic surfactant protein C by isolated rat type II cells. *Am J Physiol.* **269**, L744-753.
- Benowitz, N.L., Hukkanen, J. and Jacob, P., 3rd (2009) Nicotine chemistry, metabolism, kinetics and biomarkers. *Handb Exp Pharmacol.* 29-60.
- Berthiaume, Y., Albertine, K.H., Grady, M., Fick, G. and Matthay, M.A. (1989) Protein clearance from the air spaces and lungs of unanesthetized sheep over 144 h. *J Appl Physiol.* **67**, 1887-1897.
- Bhamre, S., Bhagwat, S.V., Shankar, S.K., Boyd, M.R. and Ravindranath, V. (1995) Flavin-containing monooxygenase mediated metabolism of psychoactive drugs by human brain microsomes. *Brain Res.* **672**, 276-280.
- Bhamre, S., Shankar, S.K., Bhagwat, S.V. and Ravindranath, V. (1993) Catalytic activity and immunohistochemical localization of flavin-containing monooxygenase in rat-kidney. *Life Sciences.* **52**, 1601-1607.
- Boer, F. (2003) Drug handling by the lungs. *Br J Anaesth.* **91**, 50-60.
- Boyd, M.R. and Neal, R.A. (1976) Studies on the mechanism of toxicity and of development of tolerance to the pulmonary toxin, alpha-naphthylthiourea (ANTU). *Drug Metab Dispos.* **4**, 314-322.
- Braber, S., Verheijden, K.A., Henricks, P.A., Kraneveld, A.D. and Folkerts, G. (2010) A comparison of fixation methods on lung morphology in a murine model of emphysema. *Am J Physiol Lung Cell Mol Physiol.* **299**, L843-851.
- British Parliament. 1985. Food and Environment Protection Act. Available online: <http://www.legislation.gov.uk/ukpga/1985/48> [Accessed 20-09-2013].

- British Parliament. 1986. Animals Scientific Procedures Act 1986. Available online: <http://www.legislation.gov.uk/ukpga/1986/14/schedule/1> [Accessed 20-09-2013].
- Brody, J.S. and Williams, M.C. (1992) Pulmonary alveolar epithelial cell differentiation. *Annu Rev Physiol.* **54**, 351-371.
- Bustin, S.A., Benes, V., Garson, J.A., Hellems, J., Huggett, J., Kubista, M., Mueller, R., Nolan, T., Pfaffl, M.W., Shipley, G.L., Vandesompele, J. and Wittwer, C.T. (2009) The MIQE guidelines: minimum information for publication of quantitative real-time PCR experiments. *Clin Chem.* **55**, 611-622.
- Cannon, J.G. (2007) Pharmacology for chemists. 2nd ed. American Chemical Society, Washington, D.C., pp. 77-79.
- Cantrell, A.S., Engelhardt, P., Hogberg, M., Jaskunas, S.R., Johansson, N.G., Jordan, C.L., Kangasmetsa, J., Kinnick, M.D., Lind, P., Morin, J.M., Jr., Muesing, M.A., Noreen, R., Oberg, B., Pranc, P., Sahlberg, C., Ternansky, R.J., Vasileff, R.T., Vrang, L., West, S.J. and Zhang, H. (1996) Phenethylthiazolylthiourea (PETT) compounds as a new class of HIV-1 reverse transcriptase inhibitors. 2. Synthesis and further structure-activity relationship studies of PETT analogs. *J Med Chem.* **39**, 4261-4274.
- Cashman, J.R. (1995) Structural and catalytic properties of the mammalian flavin-containing monooxygenase. *Chem Res Toxicol.* **8**, 166-181.
- Cashman, J.R. (2000) Human flavin-containing monooxygenase: substrate specificity and role in drug metabolism. *Curr Drug Metab.* **1**, 181-191.
- Cashman, J.R. (2002) Human flavin-containing monooxygenase (form 3): polymorphisms and variations in chemical metabolism. *Pharmacogenomics.* **3**, 325-339.
- Cashman, J.R. (2004) The implications of polymorphisms in mammalian flavin-containing monooxygenases in drug discovery and development. *Drug Discov Today.* **9**, 574-581.
- Cashman, J.R. (2008) Role of flavin-containing monooxygenase in drug development. *Expert Opin Drug Metab Toxicol.* **4**, 1507-1521.
- Cashman, J.R., Celestial, J.R., Leach, A., Newdell, J. and Park, S.B. (1993a) Tertiary amines related to brompheniramine: preferred conformations for N-oxygenation by the hog liver flavin-containing monooxygenase. *Pharm Res.* **10**, 1097-1105.
- Cashman, J.R. and Motika, M.S. (2010) Monoamine oxidases and flavin-containing monooxygenases. In: McQueen, C.A. Comprehensive toxicology. 2nd ed. Elsevier, Oxford, pp. 95-103.
- Cashman, J.R., Park, S.B., Yang, Z.C., Washington, C.B., Gomez, D.Y., Giacomini, K.M. and Brett, C.M. (1993b) Chemical, enzymatic, and human enantioselective S-oxygenation of cimetidine. *Drug Metab Dispos.* **21**, 587-597.
- Cashman, J.R. and Zhang, J. (2002) Interindividual differences of human flavin-containing monooxygenase 3: genetic polymorphisms and functional variation. *Drug Metab Dispos.* **30**, 1043-1052.
- Cashman, J.R. and Zhang, J. (2006) Human flavin-containing monooxygenases. *Annu Rev Pharmacol.* **46**, 65-100.

- Cashman, J.R., Zhang, J., Nelson, M.R. and Braun, A. (2008) Analysis of flavin-containing monooxygenase 3 genotype data in populations administered the anti-schizophrenia agent olanzapine. *Drug Metab Lett.* **2**, 100-114.
- Cashman, J.R. and Ziegler, D.M. (1986) Contribution of N-oxygenation to the metabolism of MPTP (1-methyl-4-phenyl-1,2,3,6-tetrahydropyridine) by various liver preparations. *Mol Pharmacol.* **29**, 163-167.
- Catucci, G., Gilardi, G., Jeuken, L. and Sadeghi, S.J. (2012) In vitro drug metabolism by C-terminally truncated human flavin-containing monooxygenase 3. *Biochem Pharmacol.* **83**, 551-558.
- Chang, H.K. and Morrison, S.L. (1979) Bone-marrow suppression associated with cimetidine. *Ann Intern Med.* **91**, 580.
- Chapman, K.E., Waters, C.M. and Miller, W.M. (2002) Continuous exposure of airway epithelial cells to hydrogen peroxide: protection by KGF. *J Cell Physiol.* **192**, 71-80.
- Cheeke, P.R. (1988) Toxicity and metabolism of pyrrolizidine alkaloids. *J Anim Sci.* **66**, 2343-2350.
- Cherrington, N.J., Cao, Y., Cherrington, J.W., Rose, R.L. and Hodgson, E. (1998) Physiological factors affecting protein expression of flavin-containing monooxygenases 1, 3 and 5. *Xenobiotica.* **28**, 673-682.
- Chiang, E.T., Wang, T. and Garcia, J.G.N. (2011) Acute lung injury: the injured lung endothelium, therapeutic strategies for barrier protection and vascular biomarkers. In: Yuan, J.X.J., Garcia, J.G.N., West, J.B., Hales, C.A., Rich, S. & Archer, S.L. Textbook of Pulmonary Vascular Disease. Springer, New York, pp. 197-222.
- Chung, W.G., Park, C.S., Roh, H.K. and Cha, Y.N. (1997) Induction of flavin-containing monooxygenase (FMO1) by a polycyclic aromatic hydrocarbon, 3-methylcholanthrene, in rat liver. *Mol Cells.* **7**, 738-741.
- Cinelli, P., Rettich, A., Seifert, B., Burki, K. and Arras, M. (2007) Comparative analysis and physiological impact of different tissue biopsy methodologies used for the genotyping of laboratory mice. *Lab Anim.* **41**, 174-184.
- Clement, B., Lustig, K.L. and Ziegler, D.M. (1993) Oxidation of desmethylpromethazine catalyzed by pig liver flavin-containing monooxygenase. Number and nature of metabolites. *Drug Metab Dispos.* **21**, 24-29.
- Coecke, S., Callaerts, A., Phillips, I.R., Vercruyssen, A., Shephard, E.A. and Rogiers, V. (1998a) Effect of thyroid hormones on flavin-containing monooxygenase activity in co-cultured adult rat hepatocytes. *Toxicol In Vitro.* **12**, 335-341.
- Coecke, S., Debast, G., Phillips, I.R., Vercruyssen, A., Shephard, E.A. and Rogiers, V. (1998b) Hormonal regulation of microsomal flavin-containing monooxygenase activity by sex steroids and growth hormone in co-cultured adult male rat hepatocytes. *Biochem Pharmacol.* **56**, 1047-1051.
- Comhair, S.A. and Erzurum, S.C. (2002) Antioxidant responses to oxidant-mediated lung diseases. *Am J Physiol Lung Cell Mol Physiol.* **283**, L246-255.
- Conkright, J.J., Bridges, J.P., Na, C.L., Voorhout, W.F., Trapnell, B., Glasser, S.W. and Weaver, T.E. (2001) Secretion of surfactant protein C, an integral membrane protein, requires the N-terminal propeptide. *J Biol Chem.* **276**, 14658-14664.

- Cunningham, A.L. and Hurley, J.V. (1972) Alpha-naphthyl-thiourea-induced pulmonary oedema in the rat: a topographical and electron-microscope study. *J Pathol.* **106**, 25-35.
- De Wildt, S.N. (2011) Profound changes in drug metabolism enzymes and possible effects on drug therapy in neonates and children. *Expert Opin Drug Metab Toxicol.* **7**, 935-948.
- Deterding, R.R., Havill, A.M., Yano, T., Middleton, S.C., Jacoby, C.R., Shannon, J.M., Simonet, W.S. and Mason, R.J. (1997) Prevention of bleomycin-induced lung injury in rats by keratinocyte growth factor. *Proc Assoc Am Physicians.* **109**, 254-268.
- Dieke, S.H., Allen, G.S. and Richter, C.P. (1947) The acute toxicity of thioureas and related compounds to wild and domestic Norway rats. *J Pharmacol Exp Ther.* **90**, 260-270.
- Dieke, S.H. and Richter, C.P. (1946) Age and species variation in the acute toxicity of alphanaphthyl thiourea. *Proc Soc Exp Biol Med.* **62**, 22-25.
- Dixit, A. and Roche, T.E. (1984) Spectrophotometric assay of the flavin-containing monooxygenase and changes in its activity in female mouse liver with nutritional and diurnal conditions. *Arch Biochem Biophys.* **233**, 50-63.
- Dolphin, C., Shephard, E.A., Povey, S., Palmer, C.N., Ziegler, D.M., Ayesh, R., Smith, R.L. and Phillips, I.R. (1991) Cloning, primary sequence, and chromosomal mapping of a human flavin-containing monooxygenase (FMO1). *J Biol Chem.* **266**, 12379-12385.
- Dolphin, C.T., Beckett, D.J., Janmohamed, A., Cullingford, T.E., Smith, R.L., Shephard, E.A. and Phillips, I.R. (1998) The flavin-containing monooxygenase 2 gene (FMO2) of humans, but not of other primates, encodes a truncated, nonfunctional protein. *J Biol Chem.* **273**, 30599-30607.
- Dolphin, C.T., Cullingford, T.E., Shephard, E.A., Smith, R.L. and Phillips, I.R. (1996) Differential developmental and tissue-specific regulation of expression of the genes encoding three members of the flavin-containing monooxygenase family of man, FMO1, FMO3 and FMO4. *Eur J Biochem.* **235**, 683-689.
- Eaton, D.L. and Gilbert, G.S. (2008) Principles of toxicology. In: Casarett, L.J., Doull, J. & Klaassen, C.D. Casarett and Doull's toxicology: the basic science of poisons. 7th ed. McGraw-Hill, New York, pp. 29-31.
- Eswaramoorthy, S., Bonanno, J.B., Burley, S.K. and Swaminathan, S. (2006) Mechanism of action of a flavin-containing monooxygenase. *Proc Natl Acad Sci U S A.* **103**, 9832-9837.
- European Parliament and European Council. 1998. Directive 98/8/EC of the European Parliament and of the Council of 16 February 1998 concerning the placing of biocidal products on the market. Available online: <http://eur-lex.europa.eu/LexUriServ/LexUriServ.do?uri=OJ:L:1998:123:0001:0063:EN:PDF> [Accessed 21-09-2013].
- Evans, M.J., Cabral, L.C., Stephens, R.J. and Freeman, G. (1974) Acute kinetic response and renewal of the alveolar epithelium following injury by nitrogen dioxide. *Chest.* **65**, Suppl:62S-65S.
- Evans, M.J., Cabral, L.J., Stephens, R.J. and Freeman, G. (1975) Transformation of alveolar type 2 cells to type 1 cells following exposure to NO<sub>2</sub>. *Exp Mol Pathol.* **22**, 142-150.

- Eyer, P., Worek, F., Kiderlen, D., Sinko, G., Stuglin, A., Simeon-Rudolf, V. and Reiner, E. (2003) Molar absorption coefficients for the reduced Ellman reagent: reassessment. *Analyt Biochem.* **312**, 224-227.
- Falls, J.G., Ryu, D.Y., Cao, Y., Levi, P.E. and Hodgson, E. (1997) Regulation of mouse liver flavin-containing monooxygenases 1 and 3 by sex steroids. *Arch Biochem Biophys.* **342**, 212-223.
- Farid, N.R. (2004) Molecular basis of thyroid cancer. Kluwer Academic, Boston, pp. 277-278.
- Fehrenbach, H. (2001) Alveolar epithelial type II cell: defender of the alveolus revisited. *Respir Res.* **2**, 33-46.
- Fehrenbach, H., Kasper, M., Tschernig, T., Pan, T., Schuh, D., Shannon, J.M., Muller, M. and Mason, R.J. (1999) Keratinocyte growth factor-induced hyperplasia of rat alveolar type II cells in vivo is resolved by differentiation into type I cells and by apoptosis. *Eur Respir J.* **14**, 534-544.
- Food and Drug Administration. 2001. U.S. Department of Health and Human Services. Guidance for industry. Bioanalytical method validation. Available online: <http://www.fda.gov/downloads/Drugs/Guidances/ucm070107.pdf> [Accessed 25-09-2013].
- Forbes, A., Pickell, M., Foroughian, M., Yao, L.J., Lewis, J. and Veldhuizen, R. (2007) Alveolar macrophage depletion is associated with increased surfactant pool sizes in adult rats. *J Appl Physiol.* **103**, 637-645.
- Forrest, J.A., Shearman, D.J., Spence, R. and Celestin, L.R. (1975) Letter: neutropenia associated with metiamide. *Lancet.* **1**, 392-393.
- Foth, H. (1995) Role of the lung in accumulation and metabolism of xenobiotic compounds-implications for chemically induced toxicity. *Crit Rev Toxicol.* **25**, 165-205.
- Franklyn, J.A. (2009) Thyroid gland: Antithyroid therapy--best choice of drug and dose. *Nat Rev Endocrinol.* **5**, 592-594.
- Furnes, B., Feng, J., Sommer, S.S. and Schlenk, D. (2003) Identification of novel variants of the flavin-containing monooxygenase gene family in African Americans. *Drug Metab Dispos.* **31**, 187-193.
- Furnes, B. and Schlenk, D. (2005) Extrahepatic metabolism of carbamate and organophosphate thioether compounds by the flavin-containing monooxygenase and cytochrome P450 systems. *Drug Metab Dispos.* **33**, 214-218.
- Gagliardi, S., Ogliari, P., Davin, A., Corato, M., Cova, E., Abel, K., Cashman, J.R., Ceroni, M. and Cereda, C. (2011) Flavin-containing monooxygenase mRNA levels are up-regulated in als brain areas in SOD1-mutant mice. *Neurotox Res.* **20**, 150-158.
- Gibson, K.F. and Phadke, S. (1994) Intracellular distribution of lysozyme in rat alveolar type II epithelial cells. *Exp Lung Res.* **20**, 595-611.
- Gil, J. (2011) Microcirculation of the Lung: Functional and Anatomic Aspects. In: Yuan, J.X.-J., Garcia, J.G.N., Hales, C.A., Rich, S., Archer, S.L. & West, J.B. Textbook of pulmonary vascular disease. 1st. ed. Springer, New York, pp. 13-24.
- Gill, H.J., Tingle, M.D. and Park, B.K. (1995) N-Hydroxylation of dapsone by multiple enzymes of cytochrome P450: implications for inhibition of haemotoxicity. *Br J Clin Pharmacol.* **40**, 531-538.

- Ginsberg, G., Guyton, K., Johns, D., Schimek, J., Angle, K. and Sonawane, B. (2010) Genetic polymorphism in metabolism and host defense enzymes: implications for human health risk assessment. *Crit Rev Toxicol.* **40**, 575-619.
- Giri, S.N., Hollinger, M.A. and Rice, S.A. (1991a) Effects of thiourea on pulmonary vascular permeability and on lung and plasma histamine levels in rats. *Toxicol Lett.* **57**, 283-290.
- Giri, S.N., Hollinger, M.A. and Rice, S.A. (1991b) Effects of thiourea tolerance on plasma histamine, and lung vascular permeability. *Arch Toxicol.* **65**, 603-605.
- Greaves, P. (2007a) Endocrine glands. *In: Greaves, P. Histopathology of preclinical toxicity studies : interpretation and relevance in drug safety evaluation.* 3rd ed. Elsevier/AP, Boston, pp. 827-836.
- Greaves, P. (2007b) Haemopoietic and lymphatic systems. *In: Greaves, P. Histopathology of preclinical toxicity studies : interpretation and relevance in drug safety evaluation.* 3rd ed. Elsevier/AP, Boston, pp. 126-127.
- Greaves, P. (2007c) Male genital tract. *In: Greaves, P. Histopathology of preclinical toxicity studies : interpretation and relevance in drug safety evaluation.* 3rd ed. Elsevier/AP, Boston, pp. 661-668.
- Greaves, P. (2007d) Respiratory tract. *In: Greaves, P. Histopathology of preclinical toxicity studies : interpretation and relevance in drug safety evaluation.* 3rd ed. Elsevier/AP, Boston, pp. 233.
- Guengerich, F.P. (2001) Common and uncommon cytochrome P450 reactions related to metabolism and chemical toxicity. *Chem Res Toxicol.* **14**, 611-650.
- Guengerich, F.P. (2003) Cytochromes P450, drugs, and diseases. *Mol Interv.* **3**, 194-204.
- Guery, B.P., Mason, C.M., Dobard, E.P., Beaucaire, G., Summer, W.R. and Nelson, S. (1997) Keratinocyte growth factor increases transalveolar sodium reabsorption in normal and injured rat lungs. *Am J Respir Crit Care Med.* **155**, 1777-1784.
- Guo, W.X., Poulsen, L.L. and Ziegler, D.M. (1992) Use of thiocarbamides as selective substrate probes for isoforms of flavin-containing monooxygenases. *Biochem Pharmacol.* **44**, 2029-2037.
- Hardwick, S.J., Adam, A., Smith, L.L. and Cohen, G.M. (1990) Potentiation of the cell specific toxicity of paraquat by 1,3-bis(2-chloroethyl)-1-nitrosourea (BCNU). Implications for the heterogeneous distribution of glutathione (GSH) in rat lung. *Biochem Pharm.* **39**, 581-589.
- Hardwick, S.J., Skamarauskas, J.T., Smith, L.L., Upshall, D.G. and Cohen, G.M. (1991) Protection of rats against the effects of alpha-naphthylthiourea (ANTU) by elevation of non-protein sulphhydryl levels. *Biochem Pharm.* **42**, 1203-1208.
- Harlan, J.M., Levine, J.D., Callahan, K.S., Schwartz, B.R. and Harker, L.A. (1984) Glutathione redox cycle protects cultured endothelial cells against lysis by extracellularly generated hydrogen peroxide. *J Clin Invest.* **73**, 706-713.
- Harper, T.W. and Brassil, P.J. (2008) Reaction phenotyping: Current industry efforts to identify enzymes responsible for metabolizing drug candidates. *Aaps Journal.* **10**, 200-207.
- Haschek, W.M., Wallig, M.A. and Rousseaux, C.G. (2009a) The Immune system. *In: Haschek, W.M., Wallig, M.A. & Rousseaux, C.G. Fundamentals of toxicologic pathology.* 2nd ed. Elsevier, London, pp. 451-489.



- Haschek, W.M., Wallig, M.A. and Rousseaux, C.G. (2009b) Kidney and lower urinary tract. *In: Haschek, W.M., Wallig, M.A. & Rousseaux, C.G. Fundamentals of toxicologic pathology.* 2nd ed. Elsevier, London, pp. 261-318.
- Haschek, W.M., Wallig, M.A. and Rousseaux, C.G. (2009c) The liver. *In: Haschek, W.M., Wallig, M.A. & Rousseaux, C.G. Fundamentals of toxicologic pathology.* 2nd ed. Academic, London, pp. 198.
- Haschek, W.M., Wallig, M.A. and Rousseaux, C.G. (2009d) Principles of toxicology. *In: Haschek, W.M., Wallig, M.A. & Rousseaux, C.G. Fundamentals of toxicologic pathology.* 2nd ed. Elsevier Inc., London, pp. 1-8.
- Haschek, W.M., Wallig, M.A. and Rousseaux, C.G. (2009e) The respiratory tract. *In: Haschek, W.M., Wallig, M.A. & Rousseaux, C.G. Fundamentals of toxicologic pathology.* 2nd ed. Elsevier, London, pp. 93-133.
- Hastings, R.H., Folkesson, H.G. and Matthay, M.A. (2004) Mechanisms of alveolar protein clearance in the intact lung. *Am J Physiol Lung Cell Mol Physiol.* **286**, L679-689.
- Health and Safety Executive. 2012. Pesticides Law. Available online: <http://www.pesticides.gov.uk/guidance/industries/pesticides/topics/pesticide-approvals/legislation> [Accessed 21-092013].
- Heidari, R., Babaei, H. and Eghbal, M. (2013) Mechanisms of methimazole cytotoxicity in isolated rat hepatocytes. *Drug Chem Toxicol.* **36**, 403-411.
- Hemminki, K., Rajaniemi, H., Lindahl, B. and Moberger, B. (1996) Tamoxifen-induced DNA adducts in endometrial samples from breast cancer patients. *Cancer Res.* **56**, 4374-4377.
- Henderson, M.C., Krueger, S.K., Siddens, L.K., Stevens, J.F. and Williams, D.E. (2004a) S-oxygenation of the thioether organophosphate insecticides phorate and disulfoton by human lung flavin-containing monooxygenase 2. *Biochem Pharmacol.* **68**, 959-967.
- Henderson, M.C., Krueger, S.K., Stevens, J.F. and Williams, D.E. (2004b) Human flavin-containing monooxygenase form 2 S-oxygenation: sulfenic acid formation from thioureas and oxidation of glutathione. *Chem Res Toxicol.* **17**, 633-640.
- Henderson, M.C., Siddens, L.K., Morr e, J.T., Krueger, S.K. and Williams, D.E. (2008) Metabolism of the anti-tuberculosis drug ethionamide by mouse and human FMO1, FMO2 and FMO3 and mouse and human lung microsomes. *Toxicol Appl Pharm.* **233**, 420-427.
- Hernandez, D., Janmohamed, A., Chandan, P., Omar, B.A., Phillips, I.R. and Shephard, E.A. (2009) Deletion of the mouse FMO1 gene results in enhanced pharmacological behavioural responses to imipramine. *Pharmacogenet Genom.* **19**, 289-299.
- Hernandez, D., Janmohamed, A., Chandan, P., Phillips, I.R. and Shephard, E.A. (2004) Organization and evolution of the flavin-containing monooxygenase genes of human and mouse: Identification of novel gene and pseudogene clusters. *Pharmacogenetics.* **14**, 117-130.
- Hinrichs, A.L., Murphy, S.E., Wang, J.C., Saccone, S., Saccone, N., Steinbach, J.H., Goate, A., Stevens, V.L. and Bierut, L.J. (2011) Common polymorphisms in FMO1 are associated with nicotine dependence. *Pharmacogenet Genom.* **21**, 397-402.



- Hinshaw, D.B., Armstrong, B.C., Beals, T.F. and Hyslop, P.A. (1988) A cellular model of endothelial cell ischemia. *J Surg Res.* **44**, 527-537.
- Hinshaw, D.B., Sklar, L.A., Bohl, B., Schraufstatter, I.U., Hyslop, P.A., Rossi, M.W., Spragg, R.G. and Cochrane, C.G. (1986) Cytoskeletal and morphologic impact of cellular oxidant injury. *Am J Pathol.* **123**, 454-464.
- Hodgson, E., Cherrington, N., Coleman, S.C., Liu, S.M., Falls, J.G., Cao, Y., Goldstein, J.E. and Rose, R.L. (1998) Flavin-containing monooxygenase and cytochrome P450 mediated metabolism of pesticides: from mouse to human. *Rev Pest T.* 231-243.
- Hodgson, E. and Levi, P.E. (2001) Metabolism of pesticides. *In: Krieger, R.I. & Krieger, W.C. Handbook of pesticide toxicology. Vol. 1, Principles.* 2nd ed. / edited by Robert I. Krieger. ed. Academic, San Diego, California; London, pp. 531-562.
- Hollinger, M.A., Giri, S.N. and Budd, E. (1976) A pharmacodynamic study of (14C) thiourea toxicity in mature, immature, tolerant, and nontolerant rats. *Toxicol Appl Pharm.* **37**, 545-556.
- Huan, J.Y., Miranda, C.L., Buhler, D.R. and Cheeke, P.R. (1998a) The roles of CYP3A and CYP2B isoforms in hepatic bioactivation and detoxification of the pyrrolizidine alkaloid senecionine in sheep and hamsters. *Toxicol Appl Pharm.* **151**, 229-235.
- Huan, J.Y., Miranda, C.L., Buhler, D.R. and Cheeke, P.R. (1998b) Species differences in the hepatic microsomal enzyme metabolism of the pyrrolizidine alkaloids. *Toxicol Letters.* **99**, 127-137.
- Hugonnard, M., Benoit, E., Longin-Sauvageon, C. and Lattard, V. (2004) Identification and characterization of the FMO2 gene in *Rattus norvegicus*: a good model to study metabolic and toxicological consequences of the FMO2 polymorphism. *Pharmacogenetics.* **14**, 647-655.
- Hurley, J.V. (1978) Current views on the mechanisms of pulmonary oedema. *J Pathol.* **125**, 59-79.
- Ishii, Y., Partridge, C.A., Del Vecchio, P.J. and Malik, A.B. (1992) Tumor necrosis factor-alpha-mediated decrease in glutathione increases the sensitivity of pulmonary vascular endothelial cells to H<sub>2</sub>O<sub>2</sub>. *J Clin Invest.* **89**, 794-802.
- Ishizuka, M., Tanikawa, T., Tanaka, K.D., Heewon, M., Okajima, F., Sakamoto, K.Q. and Fujita, S. (2008) Pesticide resistance in wild mammals--mechanisms of anticoagulant resistance in wild rodents. *J Toxicol Sci.* **33**, 283-291.
- Itagaki, K., Carver, G.T. and Philpot, R.M. (1996) Expression and characterization of a modified flavin-containing monooxygenase 4 from humans. *J Biol Chem.* **271**, 20102-20107.
- Jakobsson, S.V. and Cintig, D.L. (1973) Studies on the cytochrome P-450-containing mono-oxygenase system in human kidney cortex microsomes. *J Pharmacol Exp Ther.* **185**, 226-234.
- Janmohamed, A., Hernandez, D., Phillips, I.R. and Shephard, E.A. (2004) Cell-, tissue-, sex- and developmental stage-specific expression of mouse flavin-containing monooxygenases (FMOs). *Biochem Pharmacol.* **68**, 73-83.
- Jeffery, P.K. and Reid, L. (1975) New observations of rat airway epithelium: a quantitative and electron microscopic study. *J Anat.* **120**, 295-320.
- Jeitner, T.M. and Lawrence, D.A. (2001) Mechanisms for the cytotoxicity of cysteamine. *Toxicol Sci.* **63**, 57-64.

- Joyce-Brady, M.F. and Brody, J.S. (1990) Ontogeny of pulmonary alveolar epithelial markers of differentiation. *Dev Biol.* **137**, 331-348.
- Kaderlik, K.R., Poulsen, L.L. and Ziegler, D.M. (1991) Studies on the mechanism for the thermal inactivation of hog liver flavin-containing monooxygenase. *Pr Pharm Cl.* **8**, 85-94.
- Kajita, J., Inano, K., Fuse, E., Kuwabara, T. and Kobayashi, H. (2002) Effects of olopatadine, a new antiallergic agent, on human liver microsomal cytochrome P450 activities. *Drug Metab Dispos.* **30**, 1504-1511.
- Kalgutkar, A.S., Gardner, I., Obach, R.S., Shaffer, C.L., Callegari, E., Henne, K.R., Mutlib, A.E., Dalvie, D.K., Lee, J.S., Nakai, Y., O'donnell, J.P., Boer, J. and Harriman, S.P. (2005) A comprehensive listing of bioactivation pathways of organic functional groups. *Curr Drug Metab.* **6**, 161-225.
- Kasper, M. and Haroske, G. (1996) Alterations in the alveolar epithelium after injury leading to pulmonary fibrosis. *Histol Histopathol.* **11**, 463-483.
- Kasper, M. and Singh, G. (1995) Epithelial lung cell marker: current tools for cell typing. *Histol Histopathol.* **10**, 155-169.
- Katzenstein, A.-L.A., Askin, F.B. and Bennington, J.L. (1990) Acute lung injury patterns: diffuse alveolar damage and bronchiolitis obliterans-organizing pneumonia. In: Katzenstein, A.-L.A. Katzenstein and Askin's surgical pathology of non-neoplastic lung disease. 4th ed. Saunders, Philadelphia, pp. 9-57.
- Kawaji, A., Miki, T. and Takabatake, E. (1995) Partial purification and substrate specificity of flavin-containing monooxygenase from rat brain microsomes. *Biol Pharm Bull.* **18**, 1657-1659.
- Kawaji, A., Ohara, K. and Takabatake, E. (1994) Determination of flavin-containing monooxygenase activity in rat brain microsomes with benzydamine N-oxidation. *Biol Pharm Bull.* **17**, 603-606.
- Keiner, C. (2005) Wartime rat control, rodent ecology, and the rise and fall of chemical rodenticides. *Endeavour.* **29**, 119-125.
- Kim, Y.H., Lim, D.S., Lee, J.H., Shim, W.J., Ro, Y.M., Park, G.H., Becker, K.G., Cho-Chung, Y.S. and Kim, M.K. (2003) Gene expression profiling of oxidative stress on atrial fibrillation in humans. *Exp Mol Med.* **35**, 336-349.
- Kim, Y.M. and Ziegler, D.M. (2000) Size limits of thiocarbamides accepted as substrates by human flavin-containing monooxygenase 1. *Drug Metab Dispos.* **28**, 1003-1006.
- Kimura, T., Kodama, M. and Nagata, C. (1983) Purification of mixed-function amine oxidase from rat liver microsomes. *Biochem Bioph Res Co.* **110**, 640-645.
- Kinsler, S., Levi, P.E. and Hodgson, E. (1988) Hepatic and extrahepatic microsomal oxidation of phorate by the cytochrome-P450 and FAD-containing monooxygenase systems in the mouse. *Pest Biochem Physiol.* **31**, 54-60.
- Kipar, A., Bellmann, S., Kremendahl, J., Kohler, K. and Reinacher, M. (1998) Cellular composition, coronavirus antigen expression and production of specific antibodies in lesions in feline infectious peritonitis. *Vet Immunol Immunopathol.* **65**, 243-257.
- Klick, D.E. and Hines, R.N. (2007) Mechanisms regulating human FMO3 transcription. *Drug Metab Rev.* **39**, 419-442.
- Klockars, M. and Osserman, E.F. (1974) Localization of lysozyme in normal rat tissues by an immunoperoxidase method. *J Histochem Cytochem.* **22**, 139-146.

- Kohn, M.H., Pelz, H.J. and Wayne, R.K. (2003) Locus-specific genetic differentiation at R<sub>w</sub> among warfarin-resistant rat (*Rattus norvegicus*) populations. *Genetics*. **164**, 1055-1070.
- Koukouritaki, S.B., Simpson, P., Yeung, C.K., Rettie, A.E. and Hines, R.N. (2002) Human hepatic flavin-containing monooxygenases 1 (FMO1) and 3 (FMO3) developmental expression. *Pediatr Res*. **51**, 236-243.
- Krueger, S.K., Henderson, M.C., Siddens, L.K., Vandyke, J.E., Benninghoff, A.D., Karplus, P.A., Furnes, B., Schlenk, D. and Williams, D.E. (2009) Characterization of sulfoxxygenation and structural implications of human flavin-containing monooxygenase isoform 2 (FMO2.1) variants S195L and N413K. *Drug Metab Dispos*. **37**, 1785-1791.
- Krueger, S.K., Martin, S.R., Yueh, M.-F., Pereira, C.B. and Williams, D.E. (2002a) Identification of active flavin-containing monooxygenase isoform 2 in human lung and characterization of expressed protein. *Drug Metab & Dispos*. **30**, 34-41.
- Krueger, S.K., Siddens, L.K., Martin, S.R., Yu, Z., Pereira, C.B., Cabacungan, E.T., Hines, R.N., Ardlie, K.G., Raucy, J.L. and Williams, D.E. (2004) Differences in FMO2\*1 allelic frequency between Hispanics of Puerto Rican and Mexican descent. *Drug Metab Dispos*. **32**, 1337-1340.
- Krueger, S.K., Vandyke, J.E., Williams, D.E. and Hines, R.N. (2006) The role of flavin-containing monooxygenase (FMO) in the metabolism of tamoxifen and other tertiary amines. *Drug Metab Rev*. **38**, 139-147.
- Krueger, S.K. and Williams, D.E. (2005) Mammalian flavin-containing monooxygenases: structure/function, genetic polymorphisms and role in drug metabolism. *Pharmacol Therapeut*. **106**, 357-387.
- Krueger, S.K., Williams, D.E., Yueh, M.-F., Martin, S.R., Hines, R.N., Raucy, J.L., Dolphin, C.T., Shephard, E.A. and Phillips, I.R. (2002b) Genetic polymorphisms of flavin-containing monooxygenase (FMO). *Drug Metab Rev*. **34**, 523-532.
- Lambert, D.M., Mamer, O.A., Akerman, B.R., Choiniere, L., Gaudet, D., Hamet, P. and Treacy, E.P. (2001) In vivo variability of TMA oxidation is partially mediated by polymorphisms of the FMO3 gene. *Mol Genet Metab*. **73**, 224-229.
- Lattard, V., Buronfosse, T., Lachuer, J., Longin-Sauvageon, C., Moulin, C. and Benoit, E. (2001) Cloning, sequencing, tissue distribution, and heterologous expression of rat flavin-containing monooxygenase 3. *Arch Biochem Biophys*. **391**, 30-40.
- Lattard, V., Lachuer, J., Buronfosse, T., Garnier, F. and Benoit, E. (2002a) Physiological factors affecting the expression of FMO1 and FMO3 in the rat liver and kidney. *Biochem Pharmacol*. **63**, 1453-1464.
- Lattard, V., Longin-Sauvageon, C. and Benoit, E. (2003) Cloning, sequencing and tissue distribution of rat flavin-containing monooxygenase 4: two different forms are produced by tissue-specific alternative splicing. *Mol Pharmacol*. **63**, 253-261.
- Lattard, V., Longin-Sauvageon, C., Krueger, S.K., Williams, D.E. and Benoit, E. (2002b) The FMO2 gene of laboratory rats, as in most humans, encodes a truncated protein. *Biochem Biophys Res Co*. **292**, 558-563.
- Lattard, V., Longin-Sauvageon, C., Lachuer, J., Delatour, P. and Benoit, E. (2002c) Cloning, sequencing, and tissue-dependent expression of flavin-containing

- monooxygenase (FMO) 1 and FMO3 in the dog. *Drug Metab Dispos.* **30**, 119-128.
- Lawton, M.P., Cashman, J.R., Cresteil, T., Dolphin, C.T., Elfarra, A.A., Hines, R.N., Hodgson, E., Kimura, T., Ozols, J., Phillips, I.R., Philpot, R.M., Poulsen, L.L., Rettie, A.E., Shephard, E.A., Williams, D.E. and Ziegler, D.M. (1994) A nomenclature for the mammalian flavin-containing monooxygenase gene family based on amino-acid-sequence identities. *Arch Biochem Biophys.* **308**, 254-257.
- Lawton, M.P., Kronbach, T., Johnson, E.F. and Philpot, R.M. (1991) Properties of expressed and native flavin-containing monooxygenases: evidence of multiple forms in rabbit liver and lung. *Mol Pharmacol.* **40**, 692-698.
- Lee, M.Y., Clark, J.E. and Williams, D.E. (1993) Induction of flavin-containing monooxygenase (FMO B) in rabbit lung and kidney by sex steroids and glucocorticoids. *Arch Biochem Pharmacol.* **302**, 332-336.
- Lee, P.W., Arnau, T. and Neal, R.A. (1980) Metabolism of alpha-naphthylthiourea by rat liver and rat lung microsomes. *Toxicol Appl Pharm.* **53**, 164-173.
- Lee, S.K., Kang, M.J., Jin, C., In, M.K., Kim, D.H. and Yoo, H.H. (2009) Flavin-containing monooxygenase 1-catalysed N,N-dimethylamphetamine N-oxidation. *Xenobiotica.* **39**, 680-686.
- Lemoine, A., Williams, D.E., Cresteil, T. and Leroux, J.P. (1991) Hormonal regulation of microsomal flavin-containing monooxygenase: tissue-dependent expression and substrate specificity. *Mol Pharmacol.* **40**, 211-217.
- Leoni, C., Buratti, F.M. and Testai, E. (2008) The participation of human hepatic P450 isoforms, flavin-containing monooxygenases and aldehyde oxidase in the biotransformation of the insecticide fenthion. *Toxicol Appl Pharm.* **233**, 343-352.
- Levi, P.E. and Hodgson, E. (1988) Stereospecificity in the oxidation of phorate and phorate sulfoxide by purified FAD-containing mono-oxygenase and cytochrome-P450 isozymes. *Xenobiotica.* **18**, 29-39.
- Li, M., Al-Sarraf, A., Sinclair, G. and Frohlich, J. (2011) Fish odour syndrome. *Can Med Assoc J* **183**, 929-931.
- Lickteig, A.J., Riley, R., Melton, R.J., Reitz, B.A., Fischer, H.D. and Stevens, J.C. (2009) Expression and characterization of functional dog flavin-containing monooxygenase 3. *Drug Metab Dispos.* **37**, 1987-1990.
- Lin, J. and Cashman, J.R. (1997) Detoxication of tyramine by the flavin-containing monooxygenase: stereoselective formation of the trans oxime. *Chem Res Toxicol.* **10**, 842-852.
- Lin, P. and Allison, D.C. (1993) Measurement of DNA content and of tritiated thymidine and bromodeoxyuridine incorporation by the same cells. *J Histochem Cytochem.* **41**, 1435-1439.
- Lock, E.A. and Reed, C.J. (1998) Xenobiotic metabolizing enzymes of the kidney. *Toxicol Pathol.* **26**, 18-25.
- Lopez, A., Prior, M., Lillie, L.E., Gulayets, C. and Atwal, O.S. (1988) Histologic and ultrastructural alterations in lungs of rats exposed to sub-lethal concentrations of hydrogen sulfide. *Vet Pathol.* **25**, 376-384.
- Lowry, O.H., Rosebrough, N.J., Farr, A.L. and Randall, R.J. (1951) Protein measurement with the Folin phenol reagent. *J Biol Chem.* **193**, 265-275.
- Lum, H. and Malik, A.B. (1994) Regulation of vascular endothelial barrier function. *Am J Physiol.* **267**, L223-241.

- Lunden, A., Marklund, S., Gustafsson, V. and Andersson, L. (2002) A nonsense mutation in the FMO3 gene underlies fishy off-flavor in cow's milk. *Genome Res.* **12**, 1885-1888.
- Ma, J.D., Lee, K.C. and Kuo, G.M. (2012) Clinical application of pharmacogenomics. *J Pharm Pract.* **25**, 417-427.
- Mackenzie, C.G. and Mackenzie, J.B. (1943) Effect of sulfonamides and thioureas on the thyroid gland and basal metabolism. *Endocrinology* **32**, 185-209.
- Mansuy, D. and Dansette, P.M. (2011) Sulfenic acids as reactive intermediates in xenobiotic metabolism. *Arch Biochem Biophys.* **507**, 174-185.
- Martin, T.R., Hagimoto, N., Nakamura, M. and Matute-Bello, G. (2005) Apoptosis and epithelial injury in the lungs. *Proc Am Thorac Soc.* **2**, 214-220.
- Mason, C.M., Guery, B.P., Summer, W.R. and Nelson, S. (1996) Keratinocyte growth factor attenuates lung leak induced by alpha-naphthylthiourea in rats. *Crit Care Med.* **24**, 925-931.
- Matalon, S., Holm, B.A., Baker, R.R., Whitfield, M.K. and Freeman, B.A. (1990) Characterization of antioxidant activities of pulmonary surfactant mixtures. *Biochim Biophys Acta.* **1035**, 121-127.
- Matute-Bello, G., Frevert, C.W. and Martin, T.R. (2008) Animal models of acute lung injury. *Am J Physiol Lung Cell Mol Physiol.* **295**, L379-399.
- Mccarver, D.G. and Hines, R.N. (2002) The ontogeny of human drug-metabolizing enzymes: phase II conjugation enzymes and regulatory mechanisms. *J Pharmac Exp Ther.* **300**, 361-366.
- Meyrick, B., Miller, J. and Reid, L. (1972) Pulmonary oedema induced by ANTU, or by high or low oxygen concentrations in rat-an electron microscopic study. *Br J Exp Pathol.* **53**, 347-358.
- Meyrick, B.O. (1990) Structure of the Normal Pulmonary Vasculature and Changes with Disease. *In: Meyrick, B.O. Electron microscopy of the lung.* M. Dekker, New York, pp. 215-255.
- Minister of Agriculture. 1997. The Control of Pesticides Regulations. . Available online: <http://www.legislation.gov.uk/ukxi/1997/188/body/made> [Accessed 21-09-2013].
- Mirza, S.H., Mirza, M.K. and Malik, A.B. (2011) Animal models of increased lung vascular permeability. *In: Yuan, J.X.-J., Garcia, J.G.N., Hales, C.A., Rich, S., Archer, S.L. & West, J.B. Textbook of pulmonary vascular disease.* 1st. ed. Springer, New York, pp. 471-484.
- Misharin, A.V., Scott Budinger, G.R. and Perlman, H. (2011) The lung macrophage: a Jack of all trades. *Am J Respir Crit Care Med.* **184**, 497-498.
- Mitchell, R.N. and Cotran, R.S. (2007a) Acute and chronic inflammation. *In: Kumar, V., Cotran, R.S. & Robbins, S.L. Robbins basic pathology.* 8th ed. Saunders/Elsevier, Philadelphia, PA, pp. 31-58.
- Mitchell, R.N. and Cotran, R.S. (2007b) Cell injury, cell death and adaptations. *In: Kumar, N.M., Cotran, R.S. & Robbins, S.L. Robbins basic pathology.* 8th ed. Saunders/Elsevier, Philadelphia, PA, pp. 1-30.
- Moroni, P., Longin-Sauvageon, C. and Benoit, E. (1995) The flavin-containing monooxygenases in rat liver: evidence for the expression of a second form different from FMO1. *Biochem Bioph Res Co.* **212**, 820-826.
- Motika, M.S., Zhang, J., Ralph, E.C., Dwyer, M.A. and Cashman, J.R. (2012) pH dependence on functional activity of human and mouse flavin-containing monooxygenase 5. *Biochem Pharmacol.* **83**, 962-968.

- Mushiroda, T., Douya, R., Takahara, E. and Nagata, O. (2000) The involvement of flavin-containing monooxygenase but not CYP3A4 in metabolism of itopride hydrochloride, a gastroprokinetic agent: comparison with cisapride and mosapride citrate. *Drug Metab Dispos.* **28**, 1231-1237.
- Myers, A.L., Hassan, H.E., Lee, I.J. and Eddington, N.D. (2010) Repeated administration of oxycodone modifies the gene expression of several drug metabolising enzymes in the hepatic tissue of male Sprague-Dawley rats, including glutathione S-transferase A-5 (rGSTA5) and CYP3A2. *J Pharm Pharmacol.* **62**, 189-196.
- Nace, C.G., Genter, M.B., Sayre, L.M. and Crofton, K.M. (1997) Effect of methimazole, an FMO substrate and competitive inhibitor, on the neurotoxicity of 3,3'-iminodipropionitrile in male rats. *Fundam Appl Toxicol.* **37**, 131-140.
- Nagata, T., Williams, D.E. and Ziegler, D.M. (1990) Substrate specificities of rabbit lung and porcine liver flavin-containing monooxygenases: differences due to substrate size. *Chem Res Toxicol.* **3**, 372-376.
- Neu-Yilik, G., Amthor, B., Gehring, N.H., Bahri, S., Paidassi, H., Hentze, M.W. and Kulozik, A.E. (2011) Mechanism of escape from nonsense-mediated mRNA decay of human beta-globin transcripts with nonsense mutations in the first exon. *RNA.* **17**, 843-854.
- Niwa, T., Murayama, N., Umeyama, H., Shimizu, M. and Yamazaki, H. (2011) Human liver enzymes responsible for metabolic elimination of tyramine; a vasopressor agent from daily food. *Drug Metab Lett.* **5**, 216-219.
- Novick, R.M., Mitzey, A.M., Brownfield, M.S. and Elfarra, A.A. (2009) Differential localization of flavin-containing monooxygenase (FMO) isoforms 1, 3, and 4 in rat liver and kidney and evidence for expression of FMO4 in mouse, rat, and human liver and kidney microsomes. *J Pharmac Exp Ther.* **329**, 1148-1155.
- Novick, R.M., Vezina, C.M. and Elfarra, A.A. (2010) Isoform distinct time-, dose-, and castration-dependent alterations in flavin-containing monooxygenase expression in mouse liver after 2,3,7,8-tetrachlorodibenzo-p-dioxin treatment. *Biochem Pharmacol.* **79**, 1345-1351.
- O'Connor, M.A., Koza-Taylor, P., Campion, S.N., Aleksunes, L.M., Gu, X., Enayetallah, A.E., Lawton, M.P. and Manautou, J.E. (2013) Analysis of changes in hepatic gene expression in a murine model of tolerance to acetaminophen hepatotoxicity (autoprotection). *Toxicol Appl Pharm.* [Epub ahead of print: Epub date: 16-10-2013].
- Omura, T. and Sato, R. (1964) The carbon monoxide-binding pigment of liver microsomes. II. Solubilization, purification, and properties. *J Biol Chem.* **239**, 2379-2385.
- Onderwater, R.C., Commandeur, J.N., Groot, E.J., Sitters, A., Menge, W.M. and Vermeulen, N.P. (1998) Cytotoxicity of a series of mono- and di-substituted thiourea in freshly isolated rat hepatocytes: a preliminary structure-toxicity relationship study. *Toxicology.* **125**, 117-129.
- Onderwater, R.C., Commandeur, J.N., Menge, W.M. and Vermeulen, N.P. (1999) Activation of microsomal glutathione S-transferase and inhibition of cytochrome P450 1A1 activity as a model system for detecting protein alkylation by thiourea-containing compounds in rat liver microsomes. *Chem Res Toxicol.* **12**, 396-402.

- Overby, L.H., Carver, G.C. and Philpot, R.M. (1997) Quantitation and kinetic properties of hepatic microsomal and recombinant flavin-containing monooxygenases 3 and 5 from humans. *Chem-Biol Interact.* **106**, 29-45.
- Owens, C.W. and Belcher, R.V. (1965) A Colorimetric Micro-Method for the Determination of Glutathione. *Biochem J.* **94**, 705-711.
- Panos, R.J., Bak, P.M., Simonet, W.S., Rubin, J.S. and Smith, L.J. (1995) Intratracheal instillation of keratinocyte growth factor decreases hyperoxia-induced mortality in rats. *J Clin Invest.* **96**, 2026-2033.
- Park, C.S., Baek, H.M., Chung, W.G., Lee, K.H., Ryu, S.D. and Cha, Y.N. (1999) Suppression of flavin-containing monooxygenase by overproduced nitric oxide in rat liver. *Mol Pharmacol.* **56**, 507-514.
- Parkinson, A. and Ogilvie, B.W. (2008) Biotransformation of Xenobiotics *In: Klaassen, C.D. Casarett and Doull's toxicology: the basic science of poisons.* 7th ed. McGraw-Hill, New York, pp. 161-304.
- Parte, P. and Kupfer, D. (2005) Oxidation of tamoxifen by human flavin-containing monooxygenase (FMO) 1 and FMO3 to tamoxifen-N-oxide and its novel reduction back to tamoxifen by human cytochromes P450 and hemoglobin. *Drug Metab Dispos.* **33**, 1446-1452.
- Patel, R.B., Kotha, S.R., Sauers, L.A., Malireddy, S., Gurney, T.O., Gupta, N.N., Elton, T.S., Magalang, U.J., Marsh, C.B., Haley, B.E. and Parinandi, N.L. (2012) Thiol-redox antioxidants protect against lung vascular endothelial cytoskeletal alterations caused by pulmonary fibrosis inducer, bleomycin: comparison between classical thiol-protectant, N-acetyl-L-cysteine, and novel thiol antioxidant, N,N'-bis-2-mercaptoethyl isophthalamide. *Toxicol Mech Methods.* **22**, 383-396.
- Pearse, G. (2006) Histopathology of the thymus. *Toxicol Pathol.* **34**, 515-547.
- Percy, D.H. and Barthold, S.W. (2007) Pathology of laboratory rodents and rabbits. 3rd ed. Blackwell, Ames, Iowa., pp. 138-155.
- Pettit, F.H., Orme-Johnson, W. and Ziegler, D.M. (1964) The requirement for flavin adenine dinucleotide by a liver microsomal oxygenase catalyzing the oxidation of alkylaryl amines. *Biochem Biophys Res Co.* **16**, 444-448.
- Pfaffl, M.W. (2001) A new mathematical model for relative quantification in real-time RT-PCR. *Nucleic Acids Res.* **29**, e45.
- Phillips, I.R., Francois, A.A. and Shephard, E.A. (2007) The flavin-containing monooxygenases (FMOs): genetic variation and its consequences for the metabolism of therapeutic drugs. *Current Pharmacogenomics.* **5**, 292-313.
- Phillips, I.R., Dolphin, C.T., Clair, P., Hadley, M.R., Hutt, A.J., McCombie, R.R., Smith, R.L. and Shephard, E.A. (1995) The molecular biology of the flavin-containing monooxygenases of man. *Chem Biol Interact.* **96**, 17-32.
- Phillips, I.R. and Shephard, E.A. (2008) Flavin-containing monooxygenases: mutations, disease and drug response. *Trends Pharmacol Sci.* **29**, 294-301.
- Philpot, R.M., Arinc, E. and Fouts, J.R. (1975) Reconstitution of the rabbit pulmonary microsomal mixed-function oxidase system from solubilized components. *Drug Metab Dispos.* **3**, 118-126.
- Qian, L. and Ortiz De Montellano, P.R. (2006) Oxidative activation of thiacetazone by the Mycobacterium tuberculosis flavin monooxygenase EtaA and human FMO1 and FMO3. *Chem Res Toxicol.* **19**, 443-449.
- Rae, J.M., Johnson, M.D., Lippman, M.E. and Flockhart, D.A. (2001) Rifampin is a selective, pleiotropic inducer of drug metabolism genes in human

- hepatocytes: studies with cDNA and oligonucleotide expression arrays. *J Pharmac Exp Ther.* **299**, 849-857.
- Rahman, I., Kode, A. and Biswas, S.K. (2006) Assay for quantitative determination of glutathione and glutathione disulfide levels using enzymatic recycling method. *Nat Protoc.* **1**, 3159-3165.
- Raina, S., Preston, G.M., Guggino, W.B. and Agre, P. (1995) Molecular cloning and characterization of an aquaporin cDNA from salivary, lacrimal, and respiratory tissues. *J Biol Chem.* **270**, 1908-1912.
- Reasor, M.J., Ogle, C.L. and Miles, P.R. (1990) Response of rat lungs to amiodarone: preferential accumulation of amiodarone and desethylamiodarone in alveolar macrophages. *Exp Lung Res.* **16**, 577-591.
- Renne, R., Fouillet, X., Maurer, J., Assaad, A., Morgan, K., Ha, F., Nikula, K., Gillet, N. and Copley, M. (2001) Recommendation of optimal method for formalin fixation of rodent lungs in routine toxicology studies. *Toxicol Pathol.* **29**, 587-589.
- Richter, C.P. (1945) The development and use of alpha-naphthyl thiourea (ANTU) as a rat poison. *J Am Med Assoc.* **129**, 927-931.
- Richter, C.P. (1946) Biological factors involved in poisoning rats with alpha-naphthyl thiourea (ANTU). *Proc Soc Exp Biol Med.* **63**, 364-372.
- Richter, C.P. (1952) The physiology and cytology of pulmonary edema and pleural effusion produced in rats by alpha-naphthyl thiourea (ANTU). *J Thorac Surg.* **23**, 66-91.
- Riley, R.J., Grime, K. and Weaver, R. (2007) Time-dependent CYP inhibition. *Expert Opin Drug Metab Toxicol.* **3**, 51-66.
- Ripp, S.L., Itagaki, K., Philpot, R.M. and Elfarra, A.A. (1999) Species and sex differences in expression of flavin-containing monooxygenase form 3 in liver and kidney microsomes. *Drug Metab Dispos.* **27**, 46-52.
- Rodriguez-Fuentes, G., Coburn, C., Curras-Collazo, M., Guillen, G. and Schlenk, D. (2009) Effect of hyperosmotic conditions on flavin-containing monooxygenase activity, protein and mRNA expression in rat kidney. *Toxicol Letters.* **187**, 115-118.
- Rodriguez, R.J. and Buckholz, C.J. (2003) Hepatotoxicity of ketoconazole in Sprague-Dawley rats: glutathione depletion, flavin-containing monooxygenases-mediated bioactivation and hepatic covalent binding. *Xenobiotica.* **33**, 429-441.
- Rodriguez, R.J. and Miranda, C.L. (2000) Isoform specificity of N-deacetyl ketoconazole by human and rabbit flavin-containing monooxygenases. *Drug Met Dispos.* **28**, 1083-1086.
- Rouer, E., Lemoine, A., Cresteil, T., Rouet, P. and Leroux, J.P. (1987) Effects of genetic or chemically induced diabetes on imipramine metabolism. Respective involvement of flavin monooxygenase and cytochrome P-450-dependent monooxygenases. *Drug Metab Dispos.* **15**, 524-528.
- Rozen, S. and Skaletsky, H. (2000) Primer3 on the WWW for general users and for biologist programmers. *Method Mol Cell Biol.* **132**, 365-386.
- Rutili, G., Kvietys, P., Martin, D., Parker, J.C. and Taylor, A.E. (1982) Increased pulmonary microvascular permeability induced by alpha-naphthylthiourea. *J Appl Physiol.* **52**, 1316-1323.



- Schlenk, D., Erickson, D.A., Lech, J.J. and Buhler, D.R. (1992) The distribution, elimination, and in vivo biotransformation of aldicarb in the rainbow trout (*Oncorhynchus mykiss*). *Fundam Appl Toxicol.* **18**, 131-136.
- Schoeb, T.R., Mcconnell, E.E., Juliana, M.M., Davis, J.K., Davidson, M.K. and Lindsey, J.R. (2009) Mycoplasma pulmonis and lymphoma in bioassays in rats. *Vet Pathol.* **46**, 952-959.
- Scott, A.M., Powell, G.M., Upshall, D.G. and Curtis, C.G. (1990) Pulmonary toxicity of thioureas in the rat. *Environ Health Perspect.* **85**, 43-50.
- Shephard, E.A., Chandan, P., Stevanovic-Walker, M., Edwards, M. and Phillips, I.R. (2007) Alternative promoters and repetitive DNA elements define the species-dependent tissue-specific expression of the FMO1 genes of human and mouse. *Biochem J.* **406**, 491-499.
- Shephard, E.A. and Phillips, I.R. (2010) The potential of knockout mouse lines in defining the role of flavin-containing monooxygenases in drug metabolism. *Expert Opin Drug Metab Toxicol.* **6**, 1083-1094.
- Shephard, E.A., Treacy, E.P. and Phillips, I.R. (2012) Clinical utility gene card for: trimethylaminuria. *Eur J Hum Genet.* **20**.
- Shimada, T., Yamazaki, H., Mimura, M., Inui, Y. and Guengerich, F.P. (1994) Interindividual variations in human liver cytochrome P-450 enzymes involved in the oxidation of drugs, carcinogens and toxic chemicals: studies with liver microsomes of 30 Japanese and 30 Caucasians. *J Pharmac Exp Ther.* **270**, 414-423.
- Shinegene Molecular Biotech, I. 2012. Housekeeping gene primers for RT-PCR. Available online: <http://www.synthesisgene.com/tools/Housekeeping-Gene-Primers.pdf> [Accessed 15-08-2012].
- Siddens, L.K., Henderson, M.C., Vandyke, J.E., Williams, D.E. and Krueger, S.K. (2008) Characterization of mouse flavin-containing monooxygenase transcript levels in lung and liver, and activity of expressed isoforms. *Biochem Pharmacol.* **75**, 570-579.
- Singh, D., Kashyap, A., Pandey, R.V. and Saini, K.S. (2011) Novel advances in cytochrome P450 research. *Drug Discov Today.* **16**, 793-799.
- Singh, G., Katyal, S.L., Brown, W.E., Collins, D.L. and Mason, R.J. (1988) Pulmonary lysozyme-a secretory protein of type II pneumocytes in the rat. *Am Rev Respir Dis.* **138**, 1261-1267.
- Smith, L.L. (1986) The response of the lung to foreign compounds that produce free radicals. *Annu Rev Physiol.* **48**, 681-692.
- Smith, P.B. and Crespi, C. (2002) Thiourea toxicity in mouse C3H/10T1/2 cells expressing human flavin-dependent monooxygenase 3. *Biochem Pharm.* **63**, 1941-1948.
- Stormer, E., Roots, I. and Brockmoller, J. (2000) Benzydamine N-oxidation as an index reaction reflecting FMO activity in human liver microsomes and impact of FMO3 polymorphisms on enzyme activity. *Br J Clin Pharmacol.* **50**, 553-561.
- Sugahara, K., Iyama, K., Kuroda, M.J. and Sano, K. (1998) Double intratracheal instillation of keratinocyte growth factor prevents bleomycin-induced lung fibrosis in rats. *J Pathol.* **186**, 90-98.
- Suttorp, N., Kastle, S. and Neuhof, H. (1991) Glutathione redox cycle is an important defense system of endothelial cells against chronic hyperoxia. *Lung.* **169**, 203-214.

- Sznajder, J.I., Ridge, K.M., Yeates, D.B., Ileki, J. and Olivera, W. (1998) Epidermal growth factor increases lung liquid clearance in rat lungs. *J Appl Physiol.* **85**, 1004-1010.
- Tate, T.M. and Flory, W. (1993) Effect of 2-thiothiazone (TTZ) on hepatic and pulmonary glutathione (GSH) concentrations in rats. *Bull Environ Contam Toxicol.* **50**, 554-560.
- Tate, T.M., Henk, W. and Flory, W. (1991) Acute toxicity of 2-thiothiazone in rats. *Arch Environ Contam Toxicol.* **20**, 380-384.
- Teunissen, S.F., Rosing, H., Schinkel, A.H., Schellens, J.H. and Beijnen, J.H. (2010) Bioanalytical methods for determination of tamoxifen and its phase I metabolites: a review. *Anal Chim Acta.* **683**, 21-37.
- Tijet, N., Boutros, P.C., Moffat, I.D., Okey, A.B., Tuomisto, J. and Pohjanvirta, R. (2006) Aryl hydrocarbon receptor regulates distinct dioxin-dependent and dioxin-independent gene batteries. *Mol Pharmacol.* **69**, 140-153.
- Tynes, R.E. and Hodgson, E. (1985) Magnitude of involvement of the mammalian flavin-containing monooxygenase in the microsomal oxidation of pesticides. *J Agr Food Chem.* **33**, 471-479.
- Tynes, R.E., Sabourin, P.J. and Hodgson, E. (1985) Identification of distinct hepatic and pulmonary forms of microsomal flavin-containing monooxygenase in the mouse and rabbit. *Biochem Bioph Res Co.* **126**, 1069-1075.
- Van Den Brenk, H.A., Kelly, H. and Stone, M.G. (1976) Innate and drug-induced resistance to acute lung damage caused in rats by alpha-naphthyl thiourea (ANTU) and related compounds. *Br J Exp Pathol.* **57**, 621-636.
- Vandeputte, C., Guizon, I., Genestie-Denis, I., Vannier, B. and Lorenzon, G. (1994) A microtiter plate assay for total glutathione and glutathione disulfide contents in cultured/isolated cells: performance study of a new miniaturized protocol. *Cell Biol Toxicol.* **10**, 415-421.
- Veeramah, K.R., Thomas, M.G., Weale, M.E., Zeitlyn, D., Tarekegn, A., Bekele, E., Mendell, N.R., Shephard, E.A., Bradman, N. and Phillips, I.R. (2008) The potentially deleterious functional variant flavin-containing monooxygenase 2\*1 is at high frequency throughout sub-Saharan Africa. *Pharmacogen Genom.* **18**, 877-886.
- Vineis, P. and Pirastu, R. (1997) Aromatic amines and cancer. *Cancer Causes Control.* **8**, 346-355.
- Virkel, G., Lifschitz, A., Sallovitz, J., Pis, A. and Lanusse, C. (2004) Comparative hepatic and extrahepatic enantioselective sulfoxidation of albendazole and fenbendazole in sheep and cattle. *Drug Metab Dispos.* **32**, 536-544.
- Vivet, P., Brun-Pascaud, M., Mansour, H. and Pocardalo, J.J. (1983) Non-hypoxaemic pulmonary oedema induced by alpha-naphthyl thiourea in the rat. *Br J Exp Pathol.* **64**, 361-366.
- Vollinga, R.C., Menge, W.M., Leurs, R. and Timmerman, H. (1995) New analogs of burimamide as potent and selective histamine H3 receptor antagonists: the effect of chain length variation of the alkyl spacer and modifications of the N-thiourea substituent. *J Med Chem.* **38**, 2244-2250.
- Wade, C.M., Giulotto, E., Sigurdsson, S., Zoli, M., Gnerre, S., Imsland, F., Lear, T.L., Adelson, D.L., Bailey, E., Bellone, R.R., Blocker, H., Distl, O., Edgar, R.C., Garber, M., Leeb, T., Mauceli, E., Macleod, J.N., Penedo, M.C., Raison, J.M., Sharpe, T., Vogel, J., Andersson, L., Antczak, D.F., Biagi, T., Binns, M.M., Chowdhary, B.P., Coleman, S.J., Della Valle, G., Fryc, S.,

- Guerin, G., Hasegawa, T., Hill, E.W., Jurka, J., Kiialainen, A., Lindgren, G., Liu, J., Magnani, E., Mickelson, J.R., Murray, J., Nergadze, S.G., Onofrio, R., Pedroni, S., Piras, M.F., Raudsepp, T., Rocchi, M., Roed, K.H., Ryder, O.A., Searle, S., Skow, L., Swinburne, J.E., Syvanen, A.C., Tozaki, T., Valberg, S.J., Vaudin, M., White, J.R., Zody, M.C., Lander, E.S. and Lindblad-Toh, K. (2009) Genome sequence, comparative analysis, and population genetics of the domestic horse. *Science*. **326**, 865-867.
- Wang, T., Fontenot, R.D., Soni, M.G., Bucci, T.J. and Mehendale, H.M. (2000) Enhanced hepatotoxicity and toxic outcome of thioacetamide in streptozotocin-induced diabetic rats. *Toxicol App Pharmacol*. **166**, 92-100.
- Wang, Z., Klipfell, E., Bennett, B.J., Koeth, R., Levison, B.S., Dugar, B., Feldstein, A.E., Britt, E.B., Fu, X., Chung, Y.M., Wu, Y., Schauer, P., Smith, J.D., Allayee, H., Tang, W.H., Didonato, J.A., Lusis, A.J. and Hazen, S.L. (2011) Gut flora metabolism of phosphatidylcholine promotes cardiovascular disease. *Nature*. **472**, 57-63.
- Ward, A.K., Classen, H.L. and Buchanan, F.C. (2009) Fishy-egg tainting is recessively inherited when brown-shelled layers are fed canola meal. *Poult Sci*. **88**, 714-721.
- Watt, B.E., Proudfoot, A.T., Bradberry, S.M. and Vale, J.A. (2005) Anticoagulant rodenticides. *Toxicol Rev*. **24**, 259-269.
- Whetstone, J.R., Yueh, M.F., Mccarver, D.G., Williams, D.E., Park, C.S., Kang, J.H., Cha, Y.N., Dolphin, C.T., Shephard, E.A., Phillips, I.R. and Hines, R.N. (2000) Ethnic differences in human flavin-containing monooxygenase 2 (FMO2) polymorphisms: detection of expressed protein in African-Americans. *Toxicol App Pharmacol*. **168**, 216-224.
- Whitfield, M.L., George, L.K., Grant, G.D. and Perou, C.M. (2006) Common markers of proliferation. *Nat Rev Cancer*. **6**, 99-106.
- Williams, C.M. (1990) The alveolar epithelium: structure and study by immunocytochemistry. In: Schraufnagel, D.E. Electron microscopy of the lung. 2nd ed. M. Dekker, New York, pp. 121-147.
- Williams, D.E., Ziegler, D.M. and Nordin, D.J. (1984) Rabbit lung flavin-containing monooxygenase is immunochemically and catalytically distinct from the liver enzyme. *Biochem Bioph Res Co*. **125**, 116-122.
- Witter, M.P. and Amaral, D.G. (2004) The hippocampal formation. In: Paxinos, G. The rat nervous system. 3rd ed. Elsevier, London, pp. 637-658.
- Woeber, K.A. (2002) Methimazole-induced hepatotoxicity. *Endocr Pract*. **8**, 222-224.
- Wu, R.F., Liao, C.X., Tomita, S., Ichikawa, Y. and Terada, L.S. (2004) Porcine FAD-containing monooxygenase metabolizes lidocaine, bupivacaine and propranolol in vitro. *Life Sciences*. **75**, 1011-1019.
- Xie, G., Wong, C.C., Cheng, K.W., Huang, L., Constantinides, P.P. and Rigas, B. (2012) Regioselective oxidation of phospho-NSAIDs by human cytochrome P450 and flavin monooxygenase isoforms: implications for their pharmacokinetic properties and safety. *Br J Pharmacol*. **167**, 222-232.
- Yanni, S.B., Annaert, P.P., Augustijns, P., Bridges, A., Gao, Y., Benjamin, D.K., Jr. and Thakker, D.R. (2008) Role of flavin-containing monooxygenase in oxidative metabolism of voriconazole by human liver microsomes. *Drug Metab Dispos*. **36**, 1119-1125.

- Young, G.A. and Vincent, P.C. (1980) Drug-induced agranulocytosis. *Clin Haematol.* **9**, 483-504.
- Zhang, J. and Cashman, J.R. (2006) Quantitative analysis of FMO gene mRNA levels in human tissues. *Drug Metab Dispos.* **34**, 19-26.
- Zhang, J., Chaluvadi, M.R., Reddy, R., Motika, M.S., Richardson, T.A., Cashman, J.R. and Morgan, E.T. (2009) Hepatic flavin-containing monooxygenase gene regulation in different mouse inflammation models. *Drug Metab Dispos.* **37**, 462-468.
- Zhang, J., Defelice, A.F., Hanig, J.P. and Colatsky, T. (2010) Biomarkers of endothelial cell activation serve as potential surrogate markers for drug-induced vascular injury. *Toxicol Pathol.* **38**, 856-871.
- Zhao, X., Alexander, J.S., Zhang, S., Zhu, Y., Sieber, N.J., Aw, T.Y. and Carden, D.L. (2001) Redox regulation of endothelial barrier integrity. *Am J Physiol Lung Cell Mol Physiol.* **281**, L879-886.
- Zhou, J. and Shephard, E.A. (2006) Mutation, polymorphism and perspectives for the future of human flavin-containing monooxygenase 3. *Mutat Res.* **612**, 165-171.
- Ziegler-Skylakakis, K. (2003) Thiourea. Concise International Chemical Assessment Document. No. 49. World Health Organization, Geneva, pp. 1-37.
- Ziegler, D.M. (1978) Intermediate metabolites of thiocarbamides, thioureylenes and thioamides: mechanism of formation and reactivity. *Biochem Soc Trans.* **6**, 94-96.
- Ziegler, D.M. (1990) Flavin-containing monooxygenases - enzymes adapted for multisubstrate specificity. *Trends Pharmacol Sci.* **11**, 321-324.
- Ziegler, D.M. (1991) Bioactivation of xenobiotics by flavin-containing monooxygenases. *Adv Exp Med Biol.* **283**, 41-50.
- Ziegler, D.M. (2002) An overview of the mechanism, substrate specificities, and structure of FMOs. *Drug Metab Rev.* **34**, 503-511.
- Ziegler, D.M., Duffel, M.W. and Poulsen, L.L. (1979) Studies on the nature and regulation of the cellular thio:disulphide potential. *Ciba Found Symp.* **72**, 191-204.
- Ziegler, D.M. and Mitchell, C.H. (1972) Microsomal oxidase. IV. Properties of a mixed-function amine oxidase isolated from pig liver microsomes. *Arch Biochem Biophys.* **150**, 116-125.
- Ziegler, D.M. and Poulsen, L.L. (1978) Hepatic microsomal mixed-function amine oxidase. *Methods in enzymology.* **52**, 142-151.